Università Politecnica delle Marche
Scuola di Dottorato di Ricerca in Scienze dell'Ingegneria
Corso di Dottorato in Ingegneria Industriale

Thermodynamic and fluid-dynamic challenges associated with the transport of CO_2 via pipelines

Ph.D. Dissertation of:
Matteo Vitali

Supervisor:
Prof. Francesco Corvaro

Assistant Supervisor:
Prof. Barbara Marchetti

XX Edition - new series

Università Politecnica delle Marche
Scuola di Dottorato di Ricerca in Scienze dell'Ingegneria
Corso di Dottorato in Ingegneria Industriale

Thermodynamic and fluid-dynamic challenges associated with the transport of CO_2 via pipelines

Ph.D. Dissertation of:
Matteo Vitali

Supervisor:
Prof. Francesco Corvaro

Assistant Supervisor:
Prof. Barbara Marchetti

XX Edition - new series

Università Politecnica delle Marche
Dipartimento di Ingegneria Industriale e Scienze Matematiche (DIISM)
Via Brecce Bianche – 60131 Ancona (AN), Italy

To my family

Acknowledgments

This thesis is the result of a doctoral project funded under the European-Regional Program POR Marche FSE 2014/2020 - Project "EUREKA" - Doctoral Scholarships for innovation 2018. I would like to give sincere gratitude to the project partners: Università Politecnica delle Marche, Enereco S.p.A. and Regione Marche for this opportunity.

I wish to thank the following people who have contributed a lot in many ways to the development of this thesis. The first big thanks go to my academic supervisors Prof. Francesco Corvaro and Prof. Barbara Marchetti as well as my industry supervisor Nicola Rovelli for giving me the unique opportunity to enhance my skills with trust and leadership. Moreover, I would like to acknowledge the invaluable support from Mariella Leporini, PhD and from the Saipem S.p.A. FLOW group during the development of some parts of this work.

To my former colleagues at the Enereco offices: special thanks to Giacomo Bonci for his constant mentorship, for the technical tips but also for teaching me a pragmatic and effective approach to problem-solving; I am also grateful for the support and the helpful advices from Valerio, Daniele, Ugo, Milena, Luca, Matteo and the other people from the Process Department of Enereco S.p.A. during the years spent together.

To my fellow researchers at DIISM: Giovanni, Lingkang, Nicola, Gianluca, Sara, Sebastiano, Giulio, Serena and the others. You made these last few years interesting and also funny.

I would like to thank my northern colleagues from NTNU and SINTEF offices for the great time spent together and for the opportunity they gave me. A sincere thanks to Francesco Finotti and Prof. Pierluigi Salvo Rossi for their trust and support. I've also enjoyed and learned a lot during the experimental work done with Martin, Markus, Ingeborg, Jacob, and the other members of the SINTEF Energy Research Thermodynamic team.

The final acknowledgements are to the most important people in my life, to my family and friends of a lifetime for the support in everyday life, especially during these tough times. And finally, to Silvia, thank you for pushing me and staying by my side no matter what or where. I love you.

Ancona, January 2022

Matteo Vitali

Abstract

The emissions related to the human activities that led to greenhouse effect can be related, but not limited to, the carbon dioxide emissions. Carbon Capture Utilization and Storage (CCUS) is claimed as a solid climate mitigation strategy in particular for the most challenging missions. The development of an international CO_2 transportation network is considered a necessary cross-cutting topic in the Carbon Capture and Storage sector. Indeed, the development of large-scale CCUS projects will require the management and transport of CO_2 in the presence of impurities and with lower costs. The accuracy of modelling CO_2 in the presence of other components needs to be further assessed and lots of thermodynamic aspects of CO_2 management are still object of debate and research. In this work the thermodynamic and fluid-dynamic challenges associated with the transport of CO_2 via pipelines have been investigated. A complete and critical review of the main thermodynamics aspects involved during the transport of CO_2 at high-pressure has been presented. The aspects related to risk and safety of CO_2 pipelines have been deeply analysed with specific focus on the modelling of accidental releases with computational fluid dynamic and simplified models. Furthermore, an assessment of the most suitable equations of state for the accurate modelling of CO_2 in presence of impurities is also proposed with quantitative and qualitative conclusions. Moreover, the transient transport phenomena involved for the transport of dense-phase CO_2 have been analysed experimentally and numerically. Horizontal depressurization behaviour have been modelled with numerical thermofluid-dynamic simulations and validated against experimental data obtained from high-resolution measurements on a state-of-the-art large scale laboratory. This work includes also some experimental activity performed for the study of vertical flows in CO_2 pipes for injection and the development of a data extraction and processing tool. Finally, the simulation of running shear fracture and its implication in CO_2 have been also discussed and a tool for the simulation of decompression in CO_2-rich mixtures has been developed and validated.

Contents

List of Figures

List of Tables

Chapter 1.

Introduction

"We are in danger of destroying ourselves by our greed and stupidity. We cannot remain looking inwards at ourselves on a small and increasingly polluted and overcrowded planet."

Stephen Hawking.

These is one of the most impacting quotes regarding climate change that have been ever pronounced. Climate change is a fact, and it has been proven from years. The constantly increasing of CO_2 and other pollutant emission are strictly related to the human activities on earth. The industrialization and the rapid growth of both population, goods and energy demand are the most important driving factors of greenhouse effects. The global primary energy consumption from the industrialization in 1800 started thanks to the utilization of traditional biomass and coal (end of 1800) as a primary source for the steam production. The world energy needs increased following the two world wars and the then exploded with the economic boom. The energy mix started with the golden years for the oil and gas industry and then after the studies conducted on nuclear weapons, nuclear power plants became a reality in most of the industrialized countries (see Figure 1.1). The renewable sources such as wind, solar and hydro are considered the energy sources of the future due to the low environmental impact during the lifetime and the democratic origin of the primary power source. Indeed, wind and solar energy are available nearly everywhere, depending on environmental conditions, while oil, gas and coal are strictly related to the availability of specific regions and countries. It should be considered that for natural gas, notably thanks to Iran and Qatar, the Middle East holds 43 % of the global reserves. However, the high volatility of the renewable sources as well as oil and gas interests of major investment companies, slowed the market with renewable energy sources limiting their diffusion due to economical and political strategies. The world energy mix scenarios of these days is clearly dominated by fossil fuels, mainly oil, gas and coal (see Figure 1.2). The Paris Agreements to limit the climate changes associated to human activities and emissions, lies strongly in the implementation of renewable energy sources for 2050. However, since the total decommissioning of all the oil and gas platforms and power plants is not close, optimization and emission limitation strategies must be adopted. To better understand the role of the human

needs in the energy mix implication and the relation between sustainable growth and zero-emission strategies, models can be developed.

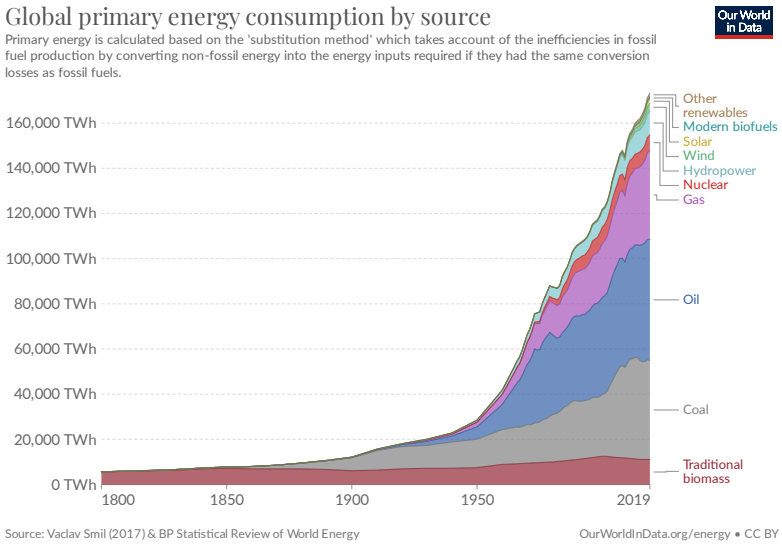

Figure 1.1.: World energy mix evolution trough from 1800 to 2019.

An equation that linked this factors is the Kaya identity developed by Japanese energy economist Yoichi Kaya in the 1989 [39]. The Kaya identity is an identity stating that the total emission level of the greenhouse gas carbon dioxide can be expressed as the product of four factors: human population, GDP per capita, energy intensity (per unit of GDP), and carbon intensity (emissions per unit of energy consumed). The Kaya equation (1.1) is a mathematically more consistent variation of Ehrlich & Holdren's [40] formula that describes the factors of environmental impact.

$$F = P \cdot \frac{G}{P} \cdot \frac{E}{G} \cdot \frac{F}{E} \tag{1.1}$$

where: F is global CO_2 emissions from human sources, P is global population, G is world GDP, E is global energy consumption and G/P is the GDP per capita, E/G is the energy intensity of the GDP, F/E is the carbon footprint of energy.

In Figure 1.3 a prospects of the Kaya Identity with drivers of CO_2 emissions in the World is presented. It can be clearly noted how the CO_2 emissions are increasing rapidly from the 60s as well as population growth and GDP. Indeed, the population growth in the last decades as well as the rapid development of emerging Asian countries increased the unbalancing of the identity. In 1961 the global population was around 3.07 billions while in 2020 the total population was estimated around 7.75 billions. In 2013, coal use accounted for 44% of global CO_2 emissions; and since

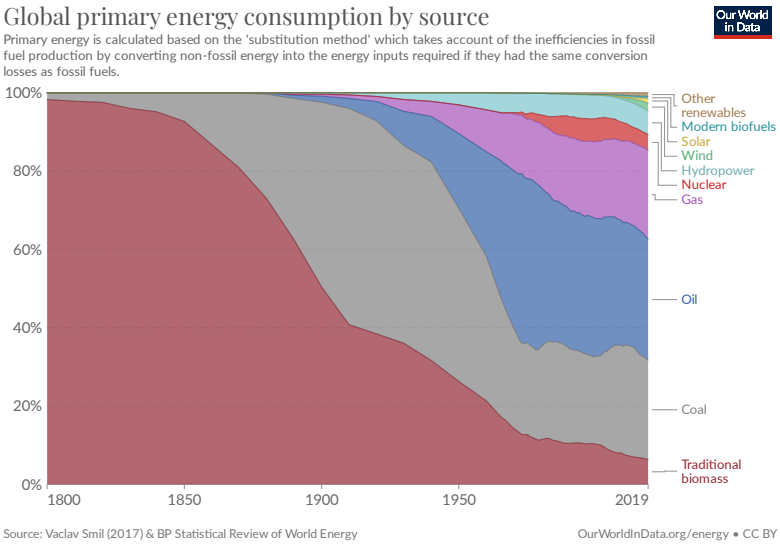

Figure 1.2.: World energy mix distribution (%).

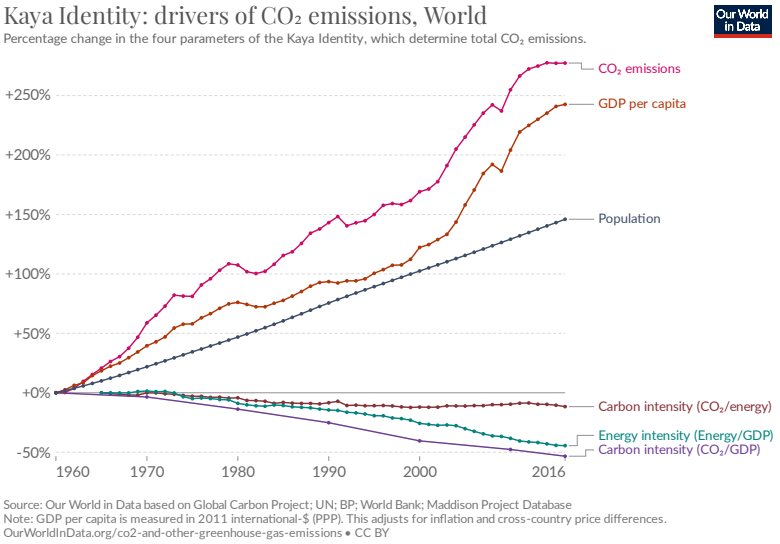

Figure 1.3.: Percentage change in the four parameters of the Kaya Identity, which determine total CO_2 emissions [1].

2000, global coal consumption has grown by 73%. China has absorbed 70% of that growth because of its rapid economic development [41].
Emission related to the human activities that led to greenhouse effect can be related, but not limited to, the carbon dioxide emissions. CO_2 content in the atmosphere is now around 418 ppm, moreover, according to Mauna Loa Observatory as reported in Figure 1.4, the trend was constantly increasing over the last 60 years [2].

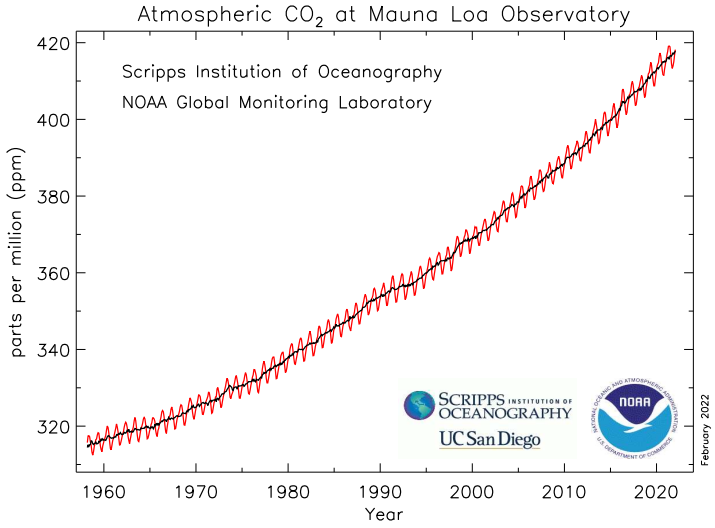

Figure 1.4.: Monthly mean carbon dioxide measured at Mauna Loa Observatory, Hawaii (2022) [2].

Heavy industries are responsible for 20% of global emissions today, more than 50 % of which are related to steel and cement industries (see Figure 1.5). Electricity production generates the second-largest share of greenhouse gas emissions. In the United States, more than 60% of electricity comes from burning fossil fuels, mainly coal and natural gas [42].

Carbon Capture Utilization and Storage (CCUS) is claimed as a solid climate mitigation strategy in particular for the most challenging missions. Most greenhouse gas emissions in the atmosphere over the last 150 years are addressable to human activities [43]. CCUS involves three major steps; capturing CO_2 at the source, compressing it for transportation and then injecting it deep into a rock formation at a carefully selected and safe site, where it is permanently stored [3].

- Capture: The separation of CO_2 from other gases produced at large industrial process facilities such as coal and natural-gas-fired power plants, steel mills, cement plants and refineries.
- Transport: Once separated, the CO_2 is compressed and transported via pipelines, trucks, ships or other methods to a suitable site for geological

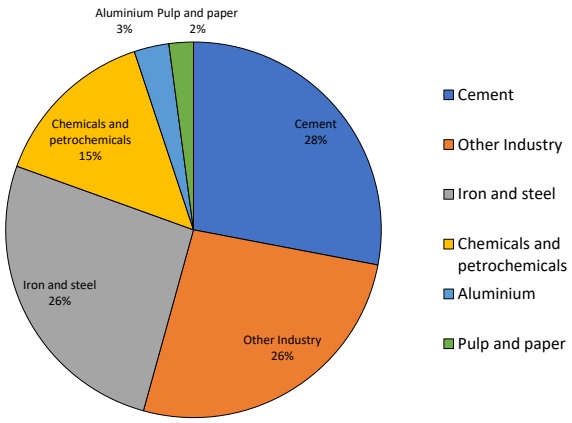

Figure 1.5.: Heavy industries global emissions (reproduced from[3]).

storage.

- Storage: CO_2 is injected into deep underground rock formations, usually at depths of one kilometre or more.

In the International Energy Agency (IEA) Sustainable Development Scenarios (SDS), carbon capture utilization and storage (CCUS) accounts for 9% of the cumulative emissions reductions needed globally by 2050 [44]. Thus, CCUS is not the solution to climate change, but a part of a big plan to decarbonize and reduce the environmental impact of heavy industries. Application of Direct Air Capture on the other hand can reduce CO_2 from the athmosphere directly if developed at scale with a correct LCA of the plant (see Carbfix [45]). Plans for more than 30 commercial CCUS facilities have been announced in the last three years, mainly in Europe and the United States, but also in Australia, the People's Republic of China, Korea, the Middle East and New Zealand. Projects now nearing a final investment decision represent an estimated potential investment of around USD 27 billion, more than double the investment planned in 2017 [44]. Moreover, since hydrogen is considered the fuel of the future, the interest in its development has increased during the last years. The production of hydrogen is called "green" when entirely produced from renewable energy sources and "blue" when it is obtained with steam methane reforming (SMR) associated with CCS [46, 47]. Hence, due to the low cost of blue hydrogen, if compared with green hydrogen [48], in the near term, CCS will play an essential role in the development of blue hydrogen production since SMR is an assessed and reliable technology. However, the high costs of the CCS

technologies have lowered commercial development [49]. The key aspects for the development of CCUS projects are related to costs, incentives, and public perceptions [50, 51]. The introduction of the Utilization term in the CCUS notation, it include all the possible uses for the CO_2 from waste to high-value product. The possible uses of CO_2 can be mainly divided in direct-use of it or the conversion to products. According to the IEA [44] the possible utilization include the conversion of CO_2 into fuel such as methanol, chemical products such as polymers or building materials (aggregates, cement). The direct-use of CO_2 include the utilization as a heat transfer fluid for refrigeration, supercritical power cycles (see Allam cycle [52]), yield boosting, Enhanced Oil Recovery and uses in the food, fertilizers and beverages industries.
Handling, management and feasibility are the focus of the overall processes required for the CO_2 market development. In the last decades, the atmospheric venting of excess gases such as CO_2 was economically convenient for companies and no strict regulations have been imposed. However, in the last years, a more conscious approach to the emission gases including but not limited to CO_2 have been proposed as part of a new Green Deal, especially in Europe. The management of the CO_2 was technically feasible, even if lot of uncertainties and optimization are still matter of research and study. Despite that, the utilization of the CO_2 or the permanent storage started to became feasible from an economic perspective since the CO_2-price increased over the last years. Trading Economics Carbon Emissions Allowances Prices are sourced from the European Union Emissions Trading System (EU ETS), the world's largest cap and trade greenhouse gas emissions market. Allowances for carbon emissions are first allocated considering EU directives for the maximum amount of greenhouse gases that can be emitted. Allowances for carbon emissions are then auctioned and traded. A record 98.50 € CO_2 EU-ETS has been reached on February 2022, a huge increase if compared with average value of 22.02 € registered in 2008 [53].
Once the economical feasibility is assessed, several technical challenges remains for the safe and reliable management of the CO_2-value chain. Firstly, the captured CO_2 should be controlled in term of purity, thermodynamic conditions also impact the equipment required for the processing. Than it could be necessary to transport CO_2 over great and small distances, this can be achieved with the utilization of pressurized vessels or pipelines. The CO_2 can be transported by ship, truck and potentially rail. In this work, the challenges associated with thermo-fluid dynamic of CO_2 has been investigated from different aspects. The research focused mainly on the challenges involved during the transport of CO_2 via pipeline. In the second chapter (2) a critical review of the most important thermodynamic aspects has been presented, while the third chapter (3) analyze all the risk and safety related aspects. Indeed, the accidental release modelling have been assessed in term of techniques and most appropriate approaches, both with computational fluid dynamic and simplified models. In Chapter 4, the uncertainties of vapour-liquid-equilibrium (VLE) description as well as density prediction have been analysed trough the evaluation of several equation of state. The main scope was to identify and optimize the selection of the most

appropriate equation of state for the description of both VLE and density specifically for CO_2-rich mixtures. The work has been developed with cubic equation of states, high-accuracy models and trough the validation with experimental data. Finally, in Chapter 5, the transient phenomena associated with the flow assurance of CO_2 pipelines have been investigated. The chapter is divided in three main categories: the horizontal flow depressurization analysis, the experimental activities performed on an advanced CO_2 facility with the development of data extraction and analysis tool; the calculation of the expansion wave velocity for CO_2-rich mixtures trough a novel algorithm for the calculation and consequent validation with experimental data. Conclusions of the work have been presented for each chapter, in order to better present the results achieved, identify the lack of knowledge and the further development.

Chapter 2.

CO_2 pipelines design challenges

2.1. Introduction

The development of an international CO_2 transportation network is considered a necessary cross-cutting topic in the Carbon Capture and Storage sector. CO_2 pipeline development is an important aspect for the realization of most decarbonization CCS projects (see 1). The captured CO_2 for large CCS projects can be transported mainly by pipeline or by ship [54–56] even if it would be technically feasible the transportation by road or railway. The captured CO_2 needs to be stored in depleted oil fields or saline aquifer; in Europe, prosperous and secure CO_2 storage related to EOR activities has been carried out since 1997 in Norway [57]. CO_2 pipelines can be divided offshore and onshore; despite natural gas pipelines are nowadays distributed for more than 500000 km in the U.S. [58], carbon dioxide pipelines only reached 8000 km in 2013. According to the PHMSA database [59], onshore pipelines in the U.S. have been constructed since the 1970s for EOR operations. The U.S. experience reports that transporting pure CO_2 (>99%) in dry conditions does not present specific issues. However, the development of large-scale CCS projects will require the management and transport of CO_2 in the presence of impurities and with lower costs. The accuracy of modelling carbon dioxide in the presence of other components needs to be further assessed. Lots of thermodynamic aspects of CO_2 management are still object of debate and research. Recent advances in processing simulations and construction materials can potentially lower costs and increase safety and accuracy during the development of CO_2 pipelines. Since lot of practical issues and cost-driver can be attributed to the uncertainties of simulations, in this chapter the main issues related to flow assurance and process simulation of CO_2-rich pipelines investigated are summarized [60].

2.2. The presence of impurities

The presence of impurities combined with potentially long-distance transportation of CO_2 could lead to challenging engineering and flow assurance issues. In particular, the water content in the pipeline may result in corrosion, ice and gas hydrate formation, and pipeline blockage, so the fluid system should meet specific dehydration

requirements. Furthermore, the gaseous CO_2-rich stream is generally compressed to be transported as a liquid or dense-phase state to avoid two-phase flow and increase process fluid density. The presence of impurities such as N_2, O_2, H_2, CH_4, SO_2, CO, H_2S, and Ar will also change the properties of the stream, the system's bubble point pressure, and viscosity, hence affecting the compression performance [4]. In this section, the impact of impurities on the thermodynamic behaviour of the CO_2 stream has been analyzed. Several aspects are included, such as the impact on flow properties and pipeline system operating envelope for stable operation. The effect of water as impurity has been extensively discussed in section 2.3 due to its high importance in carbon dioxide transport via pipeline, also related to corrosion effects. However, free water cross-chemical reaction could also affect other impurities and impact the thermodynamic of the process. The impurities that can occur in CO_2 streams are crucial for low-cost CO_2 pipeline and ship transportation. Many aspects of the transportation chain, from design to operations, is dependent on the presence of the impurities such as operating pressure and temperature and the quantity of CO_2 that can be transported as well as ductile fracture propagation, health and safety, operative parameters, corrosion control, and dispersion modelling too [61]. The impurities influence the thermodynamic properties relevant to CO_2 pipeline transport, including the density of the stream, the specific pressure drop, and the critical point. Consequently, the pipeline design parameters such as diameter, wall thickness, inlet pressure, minimum allowable operational pressure, and the distance between booster stations are potentially subject to change. The amount of the impurities and the type, that can be found in the stream, depends on the fuels used and the capture technology adopted. In 2.1, a summary of concentration ranges of impurities in the captured CO_2 based on available experimental data reported by other authors is resumed. There are no solid technical barriers hindering the production of high purity CO_2 from the flue gas of fossil fuel-fired power plants. However, high purity requirements are likely to induce additional costs and energy requirements resulting in a high loss of power plant efficiency [62].

The most common capture methods reported in literature and industry are Post-Combustion, Pre-Combustion, and Oxy-Combustion. The capturing process adopted affects the purity of the CO_2-rich stream and its related range of impurities. In Table 2.2, a detailed summary of capture methods and related potential components range has been reported. According to Anheden et al. [63], the critical impurities in the CO_2 stream that are of most concerns for pipelines are H_2, N_2, SO_X, NO_X, H_2O, H_2S, Ar, O_2, and CH_4. As reported in 2.2, the oxyfuel stream shows more significant quantities of the non-condensable gases like O_2, N_2, Ar, and H_2, which have the tendency to alter the phase of CO_2 and the oxide impurities like SO_X, NO_X, and H_2O, which have a propensity for corrosion and hydrate formations. These phenomena have adverse impacts on CO_2 transport, injection, and storage [29]. Moreover, for the transient transport processes, other properties, including the speed of sound, Joule-Thomson effect (J-T), and diffusivity, should be considered [24]. In literature,

Component	Min mol%	Max mol%
CO_2	75	99
N_2	0.02	10
O_2	0.04	5
H_2	0.06	4
CH_4	0.7	4
Ar	0.005	3.5
SO_2	<0.0001	1.5
H_2S+COS	0.01	1.5
NO_X	0.0002	0.3
CO	0.0001	0.2
H_2O	<0.0001	0.1

Table 2.1.: Possible concentration ranges of the impurities in the captured CO_2 streams (Reproduced from [27, 28]).

there are experimental studies on some typical interactions such as CO_2/Ar, CO_2/CO, CO_2/H_2O, CO_2/SO_2, CO_2/N_2O_4, CO_2/COS, CO_2/NH_3, and others including more than one substance in the addiction of the main component (CO_2) [4, 15, 64, 64–71]. The experimental datasets available in the literature, however, do not include all possible interactions.

Components	Unit	Post-Combustion	Pre-Combustion	Oxy-Combustion
CO_2	vol%	99.7 – 99.9	95.0 – 99.7	74.8 – 99.95
O_2	vol%	0.0035 – 0.03	0.03 – 1.3	0.001 – 6.0
N_2	vol%	0.01 – 0.29	0.0195 – 1.3	0.01 – 16.6
Ar	vol%	0.0011 – 0.045	0.0001 – 1.3	0.01 – 5.0
H_2	vol%	Trace	0.002 – 3.0	Trace
H_2O	ppmv	100 – 640	0.1 – 600	0 – 1000
NO_X	ppmv	20 – 50	400	0 – 2500
SO_X	ppmv	0 – 100	25	0.1 – 25000
CO	ppmv	1.2 – 20	300 – 4000	0 – 162
H_2S	ppmv	Trace – 170	100 – 3400025	Trace

Table 2.2.: Fluid composition and potential range for three different capture processes (Reproduced from [29]).

In general terms, impurities in the CO_2 stream affect pressure and temperature drop with respect to pure CO_2 behaviour. An increase in pressure drop leads to a decrease of CO_2 mixture density along the pipeline, while the opposite happens with an increase in temperature drop. At given pT conditions, fluid density affects pipeline capacity and pump performances. Thus, impurities in the CO_2 stream can cause an increase or a decrease in pipeline costs. A relevant selection of current theoretical studies on pVT properties for a mixture of CO_2 and impurities is detailed below. Tan Y. et al. [72] studied the impact of fluid pVT properties on the performance

of CO_2 pipeline transport. The study mainly focused on density, viscosity, heat capacity, and thermal conductivity. The results of the sensitivity study conducted showed that over-estimate density and viscosity increase frictional pressure losses while an under-estimation of density and viscosity decreases it. The results are quite predictable; in fact, increasing density and heat capacity will lead to a lower temperature drop, while a decrease will result in a higher temperature drop. Peletiri et al. [73] analyzed the impact of impurities in the transportation of CCUS operations. Results show that N_2 has the highest impact while H_2S has the lowest one in terms of CO_2 transportation performances (pressure loss, density, and critical pressure). The research was conducted on commercial software Aspen HYSYS, and the Peng-Robinson (PR) equation of state was considered for the thermodynamic properties of CO_2 mixture. The effect of impurities on phase envelope behaviour has been investigated by Wetenhall et al. [61] for a binary combination of CO_2 with 2% of other compounds such as H_2, H_2S, NO_2. Simulations have been performed using PR equation of state (EoS).

The maximum amount of each component has been defined in several projects and detailed in Table 2.3. In some cases, design limits were included to address specific potential issues common to many compounds. Due to the low critical temperature, N_2, CH_4, and H_2 could require increased pipe strength to minimize ductile fracture potential, moreover non-condensable impurities (N_2, O_2, Ar, CH_4, H_2) should be limited to reduce the compression work required [30, 31]. NETL report [30] states that: *"total non-condensable impurities should be limited to less than 4 % vol. "*, mainly because their presence decreases the density of the mixture. Some recommendations are based on the toxicity of the component (CO, H_2S) as a standard requirement often included for other fluid mixture transportation (i.e., natural gas).

Component	Unit	NETL Recommendations
H_2O	ppmv	500
H_2S	vol %	0.01
CO	ppmv	35
O_2	vol %	0.001
NO_X	ppmv	100
SO_X	ppmv	100
Ar	vol %	4
N_2	vol %	4
CH_4	vol %	4
H_2	vol %	4
NH_3	ppmv	50

Table 2.3.: CO_2 specifications and recommendations for maximum impurity concentrations (Reproduced from [30]).

Only the main components have been listed in Table 3, but other components

such as COS, C_2H_6, HCL, HF, HCN, Hg could be present in trace or limited to 1 % vol. Jensen et al. [74] reported that discontinuous CO_2 supplies, historically, "have not impacted in-field distribution pipeline networks, wellbore integrity, or reservoir conditions". The U.S. experience has demonstrated that it is possible to overcome the discontinuity in CO_2 supply related to EOR operations through the correct operation adaptability of the pipeline and storage site. However, since the EOR operations could differ from CCS operations, the composition can potentially affect several design parameters of the pipeline. Some impurities such as NO_2, SO_2, and H_2S may result in a lower pressure drop than pure CO_2 and may help reduce the cost of the pipeline [75, 76]. Craig and Butler [76] reported that 2 mol % of various impurities would change the density from pure CO_2 by less than 50 kg/m^3 for a given temperature; however, the density deviation can be very different depending on pressure and close to the critical point. Al-Siyabi et al. [4] investigated the effects of impurities on the CO_2 transport density. The density of six different binary CO_2-rich mixtures (at liquid phase) have been tested. The measurements were performed at a pressure up to 50 MPa in the temperature range of 283 K to 301 K. Measurement on a multi-components CO_2-rich mixture has been included. In Figure 2.1, the density reduction for four different types of binary mixture has been reproduced. It should be noted that H_2 has the most decisive impact on density reduction at 283 K, while Ar has the most negligible impact.

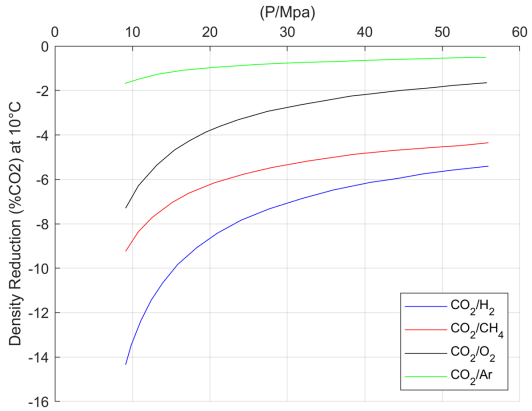

Figure 2.1.: Density reduction trend in liquid CO_2 for different combinations of mixtures. (Reproduced from Al-Siyabi et al. [4]).

Further analyses on impurity effects were performed in the testing program CO2PIPETRANS Joint Industry Project (JIP) during the second phase [77, 78]. The experiments were carried out at the two different temperatures of 4 °C and 50 °C, at a pressure of approximately 10 MPa. Water concentration in the range of 50 and 500 ppmv has been tested in addiction with other components (i.e., O_2, SO_2, H_2S, NO_2) in several. Results derived from the project have been included in the recommended practice DNV-GL-RP-F104 [78], with some suggestions for the management of impurities in CO_2 streams for pipeline transport. An investigation

on the effect of impurities on CO_2 pipeline failure was conducted by Brown et al. [79] via a sensitivity analysis. The utilization of a generalized polynomial chaos (gpC) expansion with sparse grids has been compared with other standard techniques. The work shows that N_2 has the highest effect of all the other impurities on the flowrate released during a simulated pipeline failure event. An experimental analysis of the impact of impurities, namely O_2, Ar, N_2, and H_2O, and their implications on thermo-physical and phase behaviour of CO_2 in the CCS chain was conducted by Chapoy et al. [15]. SRK-EoS model was used to predict phase envelope, while the density of CO_2 was predicted using MBWR (Modified Benedict-Webb-Rubin) equation. The viscosity model from Pedersen et al. [80] was modified to reproduce CO_2 behaviour better. Results show that the mixture can have 10-30 % less dissolved water than pure CO_2; furthermore, density can be 35 % lower if compared with pure CO_2. As reported in the previous sections, the density reduction will impact the efficiency and the costs of compression and pumping. Finally, the density reduction in the presence of impurities should be managed wisely, with regards to related costs and purity requirements for the final user of CO_2 or storage site requisites.

2.3. Water content and corrosion

Control of carbon steel CO_2 corrosion in pipelines is a central issue in the industry since it affects the costs of materials and maintenance. Main corrosion scenarios are uniform or localized corrosion (such as pitting), erosion-corrosion, corrosion at welds, sulfide stress corrosion cracking, stress corrosion cracking related to the simultaneous presence of CO, CO_2, and water. The corrosion management usually adopts two strategies for onshore CO_2 pipelines, depending on 'dry conditions' or 'wet conditions' of the pipeline, which affect composition control and the consequent transport conditions. The control of water content in dry conditions (99 % CO_2) impacts the costs for dewatering operations; on the other side, the wet conditions should be clearly studied and designed with respect to free-water formation and pH control. If the utilization of corrosion allowance or inhibitors is common practice, the utilization of internal coating designed to control corrosion is not applied, even if the research at laboratory scale is ongoing [81–84]. Internal coating, as well as innovative materials, can be an innovative viable corrosion management technology.

2.3.1. Water content

Water plays an essential role because carbon steel pipelines are subjected to corrosion deterioration due to the presence of water, which is a significant threat to pipeline integrity. Based on best practices, corrosion should be very limited in CO_2 transport pipelines when the water content is abundantly below the water solubility limit [85]. However, it is important to remark that water solubility depends on process conditions such as temperature and pressure and is related to cross chemical reactions

and interactions with other fluid components present in the mixture. Field experience and lab data indicate that the corrosion rate of carbon steel for dense phase CO_2 (near 100 %) is quite insignificant if no free water is present [86]. According to the U.S. experience related to enahanced oil recovery [87], the issues related to corrosion resulted near to zero due to the very dry carbon dioxide utilized in the systems. The results from a testing campaign of an American oil company in the 1970s reported that corrosion rates were less than 5×10^{-4} *mm/year*. The water content in those experiments was 1000 ppmv, the H_2S concentration 800 ppmv, and the temperature between 3 and 23 °C. However, it is still unclear what the water concentration should be, especially when the impurities such as CH_4, O_2, H_2S, SO_2, NO_2 are considered together [88], in Annex A of ISO 27913:2016 [89], it is stated that: *"since the maximum concentration of a single impurity will depend on the concentration of the other impurities, it is not possible, due to lack of data and current understanding, to state a fixed maximum concentration of a single impurity when other impurities are, or maybe, present"*. The standard, therefore, recommends consulting the most up-to-date research during pipeline design. The definition of a maximum water content value is strictly related to water solubility and consequently related to temperature conditions. Commissioning of a CO_2 pipeline and blowdown scenarios have been discussed in the CO_2 Europipe project [88]. Since an accidental blowdown can led to a drastic temperature drop in the pipeline, it was suggested to investigate the relation between the the water content and CO_2 during controlled depressurization linked to maintenance activities or safety issues. Salari et al. [90] presented a model and procedure to calculate the water content of carbon dioxide; the water content estimated was then validated with available experimental tests. The authors also proposed charts and algorithms that can be applied to standard simulation tools. Carroll [91] proposed the utilization of the models included in AQUAlibrium for calculating equilibrium in sour gas systems where water can be present, the work included the binary mixture CO_2-H_2O. To characterize the humidity content thresholds for CO_2 pipeline transport in supercritical conditions a methodology was presented by Xiang et al. [92]. Premium grade quality steel API 5L X70 operating with high-pressure CO_2 mixtures containing SO_2 has been tested; corrosion levels observed by the study supported the recommended humidity content level proposed by DYNAMIS Project [28]. The superior limit of humidity content can be identified through the method established in the study. Furthermore, in [30], it has been underlined that the limit value of 500 ppmv has been selected as a compromise among the multiple sources within 20 ppmv and 650 ppmv. However, should be considered that the type and the concentration of the impurities can be specific to the analyzed stream. A careful approach should be adopted to compounds that can potentially form acids in the presence of water humidity content. However, minimal reliable experimental data are available in the literature on the vapour/liquid-liquid equilibria for the CO_2-water system. A rigorous comparison with experimental data was presented from Chapoy et al. [5] to predict the phase

behaviour, hydrate dissociation pressures, and the dehydration requirements of CO_2-rich gases (Figure 2.2). A statistical thermodynamic approach, with the Cubic-Plus-Association equation of state, was employed to model the phase equilibria. The hydrate-forming conditions have been modelled by the solid solution theory of van der Waals and Platteeuw.

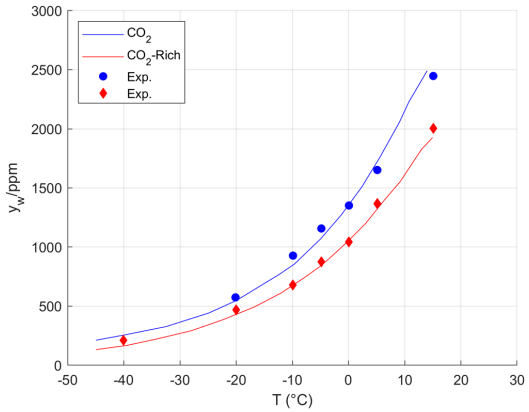

Figure 2.2.: Experimental water content data (markers) and predictions (lines) for the water content at 13.8 MPa. (Reproduced from Chapoy et al. [5]. Copyright© 2014 American Chemical Society).

According to Figure 2.2, more water can be dissolved in the pure CO_2 and CO_2-rich streams compared to pure CH_4; hence the dehydration requirement for this type of fluids could be more stringent. The estimated experimental accuracy of water content is ± 5 ppm mole. The water solubility in CO_2-rich streams in standard pipeline operation conditions in the temperature range of 5 - 35 °C and the pressure range of 9 - 15 MPa has been investigated in [66]. A comparison between experimental data and equations of state has been performed; the GERG-2008 and the EoS-CG were considered for the comparison. The authors noted that in the range of pressure and temperature studied, the water solubility increased with the increase of temperature or pressure. Moreover, the experimental data showed a drop in the water solubility limit of 75 ppm and down to 200 ppm with the presence of 2.5 % of any of N_2, O_2, or CH_4 in CO_2. The hydrate formation curve for CO_2 (pure element) in the presence of free water has been fitted from experimental data by Uilhoorn [93]. The simulations have been carried out for soil clay ranges from low (around 4 %) to high moisture content (more than 20 %). The results have shown that, when the CO_2 is in a supercritical state (pressure above 7.38 MPa at 40 °C) at the pipe inlet, the CO_2 stream might operate outside the hydrate stability region, even if water is present. During a controlled transient condition such as a shut-in or a startup procedure, the risk of hydrates formation is limited if the water content of the CO_2 stream is kept below 250 ppm (at 40°C). It should be noted that in the case of pure-CO_2 hydrate cannot exist above 22°C, so it is unlikely to form at 40°C if water is not present. However, the risk still exist for low temperature, thus, in situations of extremely

rapid depressurization, even a low water content level could not be sufficient to avoid hydrates formation.

2.3.2. Corrosion risk

Brown [41] pointed out that the specifications proposed in the DYNAMIS project cannot be considered safe enough for normal operative conditions (low margin), indeed the allowable water limit of 500 ppmv is too high for the risk of corrosion or solid formation. In the work developed by Foltran et al. [94], the solubility of water in CO_2-N_2 binary mixtures has been investigated at 25 and 40°C in the pressure range between 8 and 18 MPa. The study reports that the presence of N_2 can lower the water concentration in CO_2 by up to 42 % in the studied conditions. In the experiments performed by Choi et al. [95], carbon steel samples were exposed to water-saturated CO_2 and CO_2-saturated water in the CO_2 pressure range of 4 - 8 MPa at 50° C. The corrosion rate is very low when the water content is considerably under the solubility limit. However, the study previously performed by Choi et al. [96] reported that corrosion took place also in the water-saturated CO_2 phase under supercritical conditions when no free water is present. Experimental tests of CO_2 in presence of impurities (O_2 and SO_2) at 8 MPa CO_2 and 50°C were performed for carbon steel. The aim of the study was to evaluate the corrosion formation under a CO_2-saturated water phase and water-saturated CO_2 phase. The addition of O_2 increases the corrosion rate of carbon steel under supercritical CO_2 environments. However, the corrosion rates do not increase with increasing O_2 content; instead, the corrosion rate reaches a maximum of 1 mm/y with 4 % of O_2. The addition of 0.8 bar SO_2 (1 %) in the gas phase dramatically increased the corrosion rate of carbon steel from 0.38 to 5.6 mm/y. The effects of impurities such as O_2 and H_2S have been investigated by Sun et al. [97] in term of steel corrosion. A severe corrosion has been observed when O_2 (2000 ppmv) and H_2S (2000 ppmv) were both present, up to 0.3396 mm/y, while if considered separately, the effect that can be attributed to H_2S is eight time higher if compared with O2 impact. Similarly, He et al. [98] simulated the combined effect of CO_2, H_2S and Cl^- on the corrosion of stainless steel 316L. Dugstad et al. [85] noted that corrosion rate > 1 mm/y can be reached in presence of NO_2, this means that NO_2 (NO_X and SO_X) can have a great impact at water concentrations lower than solubility limit. The study performed by Dugstad et al. [86] supported that corrosion does not take place in pure CO_2 or CO_2+O_2 when the water content is far below the reported water solubility limit for pure CO_2 (500 ppm). However, corrosion occurred at a very low water concentration (200 ppm) when the system was contaminated with SO_2. The formation of sulphuric acid (H_2SO_4) can occur in presence of SO_2, water, and O_2. The authors also pointed out that, below the critical temperature, CO_2 depressurization to a pressure below the critical pressure will results in a biphasic system; Thus, should be considered that impurities could be present between the two phases (not proportionally). Indeed, the concentration

of several impurities will increase in the remaining liquid CO_2 phase. Then, in liquid phase, the risk of corrosion formation originated by the presence of water and other impurities must be considered if water concentration exceed the solubility threshold [85, 86]. Laboratory experiments with dense phase CO_2 were also performed by Dugstad et al. [32], water concentration up to 300 ppmv has been considered jointly with the presence of other compounds. The inspection was realized on carbon steel (10 MPa, 298 – 318 K) and corrosion has been observed. The formation of sulfuric acid, nitric acid, and elemental sulfur was also detected. Several CO_2 specifications and recommendations for maximum impurity concentrations have been published; a summary is reported hereafter in Table 2.4 with a specific focus on water content recommendations. It should be noted that when the specifications/recommendations were published, most of them had not been experimentally verified.

Reference	H_2O (ppmv)
Canyon Reef carriers	122
Central Basin Pipeline	630
Cortez Pipeline	630
Weyburn Pipeline	20
DYNAMIS Project (2008)	500
NETL Recommendations (2012-2013)	730 / 500
Carbonet (2016)	100
Institute for Energy Technology (IFE)	300
Goldeneye/Peterhead (2014-2016)	50
Northern Lights Project (2019)	30
Literature review	20-730

Table 2.4.: CO_2 specifications and recommendations for maximum water concentrations [28–35].

A great range of values for water concentration has been proposed over the years. Literature review reports a minimum allowable water content of 20 ppmv and a maximum around 730 ppmv. A review performed by Halseid et al. [99] reported that corrosion experiments for dense phase CO_2 containing impurities are not regulated by any normative. In the tests performed by Sim et al. [100], steel coupons were exposed to a supercritical CO_2 environment, the water content in the range from 100 ppmw to 50000 ppmw. Weight-loss tests have shown that the mass-loss results from 100 ppmw to 1500 ppmw were not too dissimilar. The difference in mass loss was more evident in the >1500 ppmw region, where a maximum mass loss of 1.6 mg/cm^2 has been recorded at 1500 ppmw. According to experiments conducted by the authors [100], the water content limit could potentially be increased to approx. 1000 ppmw. However, this increase in water concentration limit assumes that pressure and temperature for both processes are identical. Hua et al. [101] conducted autoclave experiments at 8 MPa and temperatures within 35°C and 50°C; CO_2 was either saturated or under-saturated with water, depending on testing conditions. During the

under-saturated tests (at 50°C), corrosion was not observed with water content below 1600 ppm; a small level of corrosion was recorded with 300 ppm of water present at 35°C. The influence of SO_2 on the tolerable water content to avoid corrosion during the transportation of supercritical CO_2 has been investigated by Hua et al. [102]. Corrosion experiments have been performed on carbon steel in autoclaves containing CO_2 at 8 MPa and 35°C in the presence of 0, 50, and 100 ppm SO_2. Results indicated that minimization of water content is a better strategy compared to reducing SO_2 content to reduce general and localized corrosion. Hence, corrosion can occur if the water content is well below the solubility limit of water in supercritical CO_2 (300 ppm) when SO_2 is present (up to 100 ppm). In the work developed by Sun et al. [6], a thermodynamic model was utilized to investigate the effects of impurities on the water precipitation and water chemistry characteristics (Figure 2.3). Water content from 200 ppm to 4333 ppm (saturated solubility of H_2O in CO_2 at 10 MPa and 50 °C) has been tested in a CO_2-rich mixture. As reported in Figure 3, results show how the corrosion rate trend rapidly increases for a water content within >1500 ppmv.

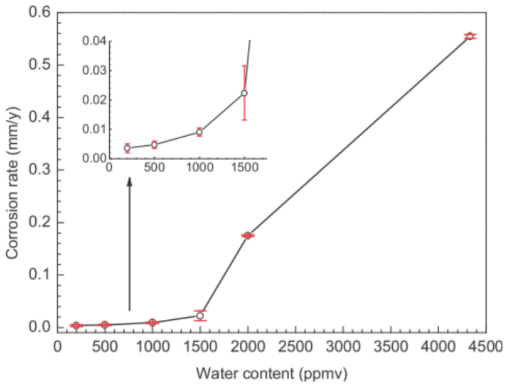

Figure 2.3.: Variations of corrosion rate with water content exposed to supercritical CO_2-rich mixture environment at 50°C and 10 MPa for 72 hours (Reproduced from Sun et al. [6]).

In order to identify the safe operating window for CO_2 transport, several reviews of leading causes and experiments related to internal corrosion in the CO_2 pipeline for CCS activities have been proposed during the years [32, 103]. Lack of corrosion data from both laboratory experiments and the field where anthropogenic CO_2 is transported makes accurate corrosion prediction challenging. Furthermore, corrosion experiments in dense phase CO_2 in presence of impurities are not regulated by standard procedures. The consensus among the difficulties introduced by the water content seems to be globally recognized. The philosophy of controlling water content in the CO_2 stream to control corrosion is an important parameter and must be assessed during the design phase. Alternative to dry conditions can be adopted with specific approaches such as the correct quantification of corrosion allowance accounting for corrosion and erosion as well as the utilization of inhibitors and coatings. The corrosion challenges present several solutions that should be evaluated

for each project. Such solutions have different costs and operative requirements that should be considered.

2.4. Low temperature and dry-ice formation

The transport of CO_2 in dense phase presents low-temperature risks during depressurization of pipelines. During the decompression, very low temperatures near -56°C may happen; thus, an uncontrolled depressurization presents a risk of brittle fracture and ductile fracture propagation. Therefore, pipeline materials need to have specific characteristics as suitable low-temperature toughness and resistance to ductile fracture propagation, or process control measures need to be introduced to avoid rapid depressurization [104]. According to the thermodynamic, liquid or supercritical phase, CO_2, when depressurised, may change phase to be: pure vapour, two-phase liquid and vapour mixture, two-phase solid and vapour mixture or, if the final pressure is at the triple point pressure, three phases solid, liquid and vapour. At the end of a depressurisation to atmospheric pressure, the CO_2 can only be a vapour or a solid, or a mixture of both. CO_2 cannot exist at atmospheric pressure in its liquid phase [36]. There are two cooling effects associated with the blowdown: the Joule-Thomson effect that occurs on the pressure reducing element and the mass reduction within a fixed volume inside the pipeline; in fact, due to the adiabatic expansion of the pipeline inventory, fluid temperature decreases. Typically, the temperature inside the pipeline should be monitored to control the rate of depressurization to avoid shallow temperatures that may pose a threat to the integrity of the pipeline. Moreover, solid CO_2 formation inside the pipeline might be dangerous as well, either for its very low temperature that makes the construction material rigid and for the possible over-pressure caused by solid CO_2 during the restart of the line [105]. Low-temperature scenarios should be investigated with respect to pipeline dips during depressurization, solid formation in vent systems, depressurization control and vent stack configurations. It should be noted that complete venting (depressurization) of a CO_2 pipeline should be an infrequent event and would mainly be required for safety reasons. Venting large volumes of high concentration and pressure CO_2 into the atmosphere has health, safety, and environmental implications, which impacts the engineering design. Furthermore, during the design and the location of vent stacks, it should be considered that CO_2 is heavier than air at atmospheric conditions [106]. Terenzi et al. [107] investigated the thermophysical behaviour of several High Vapour Pressure fluids (HVP), including liquified petroleum gas (LPG), natural gas liquified (NGL), methane-rich mixtures, CO_2-rich mixtures. The physical behaviour during blowdown of pipeline sections of typical lengths within 20-40 km is similar. However, CO_2 introduces complex thermodynamic behaviour such as physical properties that are not accurately predicted by standard equation of state, a narrow phase envelope and the potential formation of solid phases during depressurization. Since the transport of CO_2 in dense phase presents characteristic low-temperature risks when

depressurising pipelines and piping, the depressurization behaviour of CO_2 pipelines has been investigated for both summer and winter conditions, either numerically and through experimental tests.

2.4.1. Depressurization

According to the Flow Assurance report from the White Rose CCS project [106], during the depressurization of long CO_2-rich dense phase pipelines, several phenomena will take place. Pressure reduction will cause the boiling of CO_2 with consequent temperature reduction of pipeline metal the CO_2 absorbs the heat from the surrounding environment. Joule-Thomson cooling will occur as the CO_2-rich gas expands and the pipeline inventory is reduced through venting. Moreover, due to the terrain profile, gas pockets will be trapped between liquid columns, causing pressure differences on both sides of the high elevation points. The trapped liquid CO_2 will continue to boil until pressure on the side closest to the vent is low enough for the gas to sweep the trapped liquid. In this situation, additional J-T cooling could take place. It has also been predicted that the minimum temperature does not always occur at a single location. The minimum temperature moves in the liquid phase along the pipeline as the liquid is vaporized because the gas-liquid interface moves as more liquid CO_2 is vaporized. During depressurization, particularly around the peak elevation point, the presence of localized cold metal temperatures as the liquid CO_2 boils and vaporizes should be considered. The HLP fluid behaviour in pipeline dips has been included in the work of Terenzi et al. [107]; it was also found out that for a given fluid composition and flow discharge system configuration, the most impacting parameters are the soil thermal properties and the depth of the deepest dip in the elevation profile. Dall'Acqua et al. [108] developed a tool for the blowdown simulation of CO_2-rich mixtures based on the Peng-Robinson equation of state, called PRDECOM. Results for tested mixtures report good accuracy compared with experimental tests, in particular in the plateau zone. A two-phase flow model to simulate the transient flow of CO_2-rich mixtures in pipes has been adopted from Munkejord and Hammer [109]. The results suggest the necessity of taking into account the heat capacity of the pipe. The homogeneous equilibrium model and a more complex two-fluid model, in which the interphasic friction is explicitly modelled, have been compared. The thermodynamic properties were calculated using the Peng–Robinson equation of state (classical van der Waals mixing rule). However, in some cases, the GERG-2008 equation of state showed significant differences compared to the Peng-Robinson in key parameters, such as density, speed of sound and phase envelope. A review of model and data for CO_2 transport has been reported by Munkejord et al. [110], where a depressurization case study expansion-tube data has been included, as well as considerations on transient conditions that involve speed of sound and non-equilibrium models. Generally, a good agreement for fluid pressure has been observed in the model proposed by Munkejord and Hammer, although with

a tendency towards underprediction, particularly near the outlet in the first part of the depressurization.

2.4.2. Dry-ice formation

Several authors addressed the possibility of low temperature experimentally during depressurizations both inside pipeline and vent systems [10, 19, 109, 111–113]. A large-scale experiment has been conducted by Cao et al. [114] in order to measure the cross-sectional temperature, phase evolution and density distribution during the release of dense CO_2. The decrease in velocity of the dense phase CO_2 temperature observed was faster than that of gas-liquid phase CO_2. The possible formation of dry ice was observed and confirmed since the CO_2 reached the triple point on the bottom of the cross-section at 162 m and 108.8 m from the release end. Experimental and numerical studies on hydrate and solid formations in carbon dioxide have been conducted by several authors [5, 85, 114–121]. The thermodynamic properties of the liquid and vapour phases have been calculated by Martynov et al. [115] using the GERG 2004 equation of state, while the solid and vapour properties along the sublimation line are predicted using an extended Peng Robinson EoS. According to the results, the homogeneous equilibrium model (HEM) assumption produces a reasonably accurate estimation of the liquid-phase temperature. The temperature in the liquid phase was found to be as much as 60 °C lower than that in the vapour phase. However, solid CO_2 volume predicted, based on the flow model, was found to be significantly lower than that observed experimentally. An experimental system for CO_2 pipeline leakage study has been designed in the study by Xie et al. [119]. The formation/sublimation of massive dry ice clogs and the dispersion of CO_2 cloud, which should be significant for actual leakage conditions, was difficult to observe or measure. Vianello et al. [120] investigated the dynamic and thermal fluid dynamic behaviour of a dry ice particle deposition after an expansion to atmospheric conditions. The analytical model proposed proves that the effects related to solar radiation are negligible since they do not considerably affect the quick process of sublimation of dry ice particles. Dry-ice and solid formations could also affect the vent configurations and their maintenance: if solid CO_2 formation is possible, the vent design should minimize the potential for blockage. According to Pipeline Hazardous Material Safety Administration (PHMSA) [59], more than 43 % of the incidents reported on CO_2 pipelines in the United States are related to "equipment failure" that includes mainly "malfunction of control/relief equipment". In the recommended practice DNV-GL-RP-F104 [78], each onshore vent station should have the capacity to depressurize the entire volume between the block valves; the integrity of the pipeline and safety considerations related to the release of CO_2 should also be guaranteed. Consideration should be given in the design of the vent system to the potential for very low temperatures downstream of the control valve due to the expansion and possibility for solid CO_2. Several authors proposed preliminary design as well as guidelines on

vent systems and CO_2 venting philosophy [36, 76, 104, 106, 122–126]. In the work performed by Feliu et al. [126], the software VMGSim has been utilized for the quantitative determination of the dry-ice formation. The study highlighted that the use of the cooling medium in compressors increases the amount of dry ice formed as it cools down the section holdup at the beginning, while an increase in the initial blowdown temperature helps to reduce the amount of dry ice formed downstream of the blowdown valves. Finally, a heating medium that could keep the surroundings of the restriction orifice at a hot temperature could also help to reduce the solid CO_2 formation.

2.5. Conclusions

In this chapter, the main challenges and uncertainties associated with CO_2 pipeline transportation and their impact on properties, design, operations have been identified and discussed. Since cost is one of the significant concerns on the development of CO_2 pipelines for large CCS projects, optimization of design parameters should be pursued. Even if at present the main driving force for CCS projects is related to EOR, the recent growing interest in blue hydrogen production could lead to significant investments in CCS projects. For large-scale CCS projects, pipeline transport is more suitable than road or railway if the capture plant is far from the storage site. Since the anthropogenic carbon dioxide is likely to contain several other components, the CO_2 stream should theoretically be purified up to 99 % in order to manage it effectively. However, the purification costs, such as the cryogenic technique, are notably very expensive and strongly affect the CAPEX during the feasibility of the overall project. Thus, the effect of the impurities has been studied over the years in order to comprehend better the thermodynamic behaviour of CO_2-rich streams and how to deal with them. This chapter also highlighted how the availability of experimental results is poor and limited to binary or ternary mixtures. Consequently, the modelling of CO_2-rich streams is far from a well-known practice. For this reason, an extensive testing and validation of EoSs has been conducted and is reported in Chapter 4. During the years, it has been proved that the presence of impurities such as N_2, O_2, H_2, CH_4, SO_2, CO, H_2S, and Ar will change the physical properties of the stream, such as density and viscosity, hence affecting the compression performance. Several guidelines have been reported in recent literature about the maximum allowed concentration of each impurity in a CO_2-rich mixture stream. Results in literature, show that N_2 has the highest impact while H_2S has the lowest on density, pressure loss, and critical pressure, even if stringent limitations have to be imposed on H_2S content for toxicity issues. Non-condensable components such as N_2, O_2, Ar, CH_4, H_2 should be limited to reduce the amount of compression work. Specific attention should be reserved, during the design phase, to water content and corrosion-related issues. Corrosion can be significantly lower in CO_2 transport pipelines if the water content is maintained under the water solubility value; however, it is not easy to

define a unique maximum allowable water content for pipeline design due to several variables that must be taken into account. Water solubility depends on process conditions such as temperature and pressure, as well as the related to cross-chemical reactions and interactions with other fluid components present in the mixture. The DYNAMIS project and NETL reported a value limit of 500 ppmv for a carbon steel pipeline design; however, this could be applicable in normal operating conditions. Transient conditions and accidental depressurization could lead to corrosion and hydrate formation problems. Hence, the water solubility drastic drop-off during transient phenomena with associated problems. Moreover, in the case of rapid depressurization, even a low water content level might not be sufficient to avoid hydrates. Other aspects that are challenging from a process point of view are low temperatures. In this work, the focus has been reserved to depressurizations and solid formations. Some authors noted that the minimum temperature inside the pipeline does not occur at a single location but moves in the liquid phase along the pipeline as the liquid is vaporized. The lowest temperatures are localized in low points of the pipeline, where liquid tends to pool. The formation of solids could occur inside the cross-section of the pipeline during the blowdown process, as well as invents and blowdown valves. Some authors pointed out that the solid CO_2 volume predicted based on common flow models was found to be significantly smaller than what has been observed experimentally. Therefore, further research on solid formations modelling, especially during fast transient, should be perused too.

Chapter 3.

Risk and safety of CO_2 pipelines

3.1. Introduction

The safe transport of carbon dioxide via pipelines is an important aspect for developing large-scale CCUS projects. CO_2 is usually transported in dense phase or liquid state, in high-pressure pipelines for economic reasons [127–132]. Even if tons of CO_2 are transported every day in the U.S., most of the pipelines are located in not densely populated areas [74]. In the near future, CCUS projects, in Europe and other countries, might be developed to cross densely populated areas; an accurate risk assessment is therefore required. Since CO_2 is toxic at certain concentrations, the accidental release of large inventories can pose an asphyxiation risk to human and other biologic life forms that needs to be assessed and prevented or mitigated (i.e., Lake Nyos disaster in 1986 [133, 134]). A detailed risk analysis can be required to develop and route a CO_2 pipeline [135, 136]. Vianello et al. [137] performed a risk assessment of a CO_2 pipeline network case study in the UK, an heavy gas integral model have been used in the work. The results noted that in proximity of the pipeline network the population can be exposed at serious injuries; however, the authors identified some gaps in the consequence analysis. An accidental release study should be included to determine the safety distances from the pipeline [136]. Mazzoldi et al. [138] investigated with integral models and CFD the safety distances related to CCS projects, the authors highlights that the over estimation provided by Gaussian models can potentially compromise entire project development. Since CO_2 is considerably different from natural gas (i.e., CO_2 density is higher than air density), the most used simplified dispersion models could be not suitable for the correct simulation of the release. To obtain an accurate prediction of CO_2 dispersion behavior, a computational fluid dynamics (CFD) approach could be required for the most challenging scenarios when the topography is complex, and hills are presents. In this chapter it has been evaluated which tools are suitable for the accurate estimation and simulations of risk related to CO_2 pipelines; risks for humans and assessment methodologies are reported. A complete review of the main aspects related to release modeling for CO_2 from a pipeline rupture scenario has been also analyzed and discussed in this work.

3.2. Risk analysis workflow

The risk management framework for CCS project shall be the same as for other projects as outlined in ISO 31000 [7, 8, 36]. It should be recognized that CO_2 pipelines at the scale that will be associated with CCS projects are novel to many countries and this should be reflected in the risk management strategy adopted. In Figure 3.1 a schematization of the risk management process as per ISO 31000 is reported.

Figure 3.1.: Graphical representation of the Risk Management Process [7]

A number of publications [8, 20, 78, 123, 137, 139–146] and research projects such as CO2EUROPIPE, CO_2PipeHaz, CO2RISKMAN, COOLTRANS, INTEG-RISK have addressed this matter. CO2Europipe recommends the use of formal QRA methods to determine the HSE risks of CO_2 pipeline transport. A quantitative risk assessment (QRA) usually includes the determination of failure scenarios with a certain probability. These failure scenarios have a certain probability attributed to them based on expert judgment or heuristics; in this case experience with pipeline operation and failure [147].The CO2Europipe project highlighted a limited experience on pipeline failure frequencies and dose-effect relationship especially for human health. The differences in safety risk policies between EU state members were identified as a weakness during the design process. The major accident hazard potential associated with the CO_2 stream is likely to be from a loss of containment event. It is important that each CCS project and operation undertake a rigorous process of hazard identification, to ensure that all reasonably foreseeable major accident hazards are identified [8]. According to Vianello et al. [137, 145], in order to assess risk, several aspects need to be defined and quantified:

- Identification of hazards;
- Frequency of occurrence of hazards;
- Consequences of hazard occurring.

In case of loss of containment scenario, the identification and accurate prediction of an accidental release is a crucial parameter. Some aspects of CO_2 transportation

should be adequately considered within the selection of the worst case scenarios (leak size, location of the leak, orientation, etc.) to include in the assessment [8]. In addition to the standard potential initiating causes addressed in an HAZID studies, it should be considered that ground topography may have a significant influence on the movement of a large CO_2 release as it will be a heavier-than-air cloud, also features that may reduce the release momentum and air entrainment/mixing as well as features that contain or channel a release and the ones that may reduce the air flow in the vicinity of a CO_2 release.

Consequence Assessment	Scenarios modelled Hole sizes Crater modelling Discharge rates Topography Computational Fluid Dynamics (CFD) Weather data
Vulnerability modelling	Level of harm Harm criteria Escape modelling Population data
Risk criteria	Hazard or consequence criteria Individual risk Societal risk Risk matrix approaches ALARP

Table 3.1.: Pipeline risk assessment methodologies and criteria.

In Table 3.1 a summary of the main aspects related to a pipeline risk assessment methods and criteria is reported. There are lot of other causes that should be included in the hazard identification that can evolve to accident or potential risk for health and/or equipment. For a CO_2 pipeline in particular, there is a risk of temperature, due to embrittlement of containment envelope due to rapid depressurization of a liquid phase CO_2 inventory, or due to CO_2 stream flow expansion (J-T). Moreover, internal corrosion and mechanical failure as well as over-pressure due to rapid sublimation of solid CO_2 can be relevant causes too. The escalation of the cause can be immediate (BLEVE, crack propagation) or delayed, such as loss of containment, leakage, exposure to a build-up of toxic and/or harmful substances at location of release. The potential consequences are schematized in Figure 3.2 and should be carefully considered.

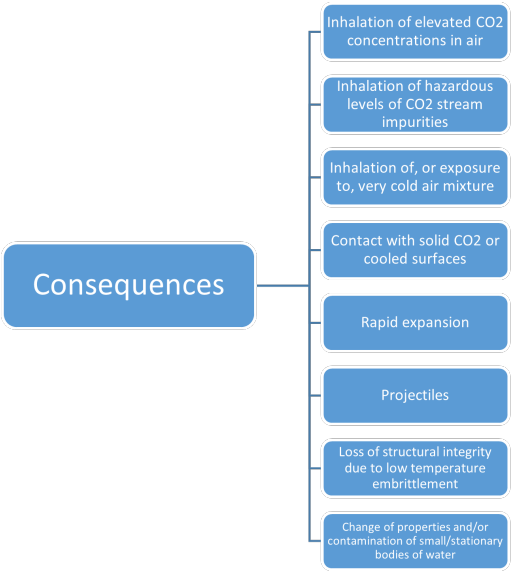

Figure 3.2.: Potential consequences of cause events for CO_2 pipelines [8].

3.3. Health effects and probit function

Carbon dioxide at atmospheric pressure and temperature is a colorless, odorless gas, which is about 1.5 times heavier than air. The CO_2 molecule is composed of two oxygen atoms covalently bonded to a single carbon atom ($O{=}C{=}O$), reported also in Figure 3.3. Since it is fully oxidized, it is not very reactive and not flammable.

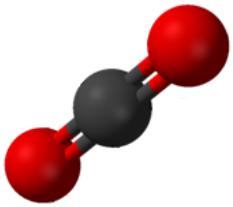

Figure 3.3.: Carbon dioxide chemical structure

In humans, CO_2 is a normal component of blood gases at low concentrations, however if inhaled at high levels it is lethal. Humans are very sensitive to changes in CO_2 concentrations. Indeed, in addition to the hazard of asphyxiation due to CO_2 displacing oxygen in the air, the inhalation of elevated concentrations of CO_2 can increase the acidity of the blood triggering adverse effects on the respiratory, cardiovascular and central nervous systems [36].

The risk management strategy should be based on relevant industry good practice which focuses on inherent safety and the prevention of incidents with the potential to endanger people, the environment, or properties. Compared to natural gas, there are less companies with relevant experience in full-scale CCS projects development and few projects has been completed so far [148]. Thus, great care should be taken

Property	Unit	Value
Molecular Weight	g/mol	44.009
Triple Point Temperature	°C	-56.558
Triple Point Pressure	bara	5.18
Boiling Point	°C	-78.464
Critical Temperature	°C	31.1
Critical Pressure	bara	73.8
Standard density (gas)	kg/m^3	1.98
Density (critical point)	kg/m^3	467
Density (liquid/dense phase)	kg/m^3	740-800
Density (solid phase, freezing point)	kg/m^3	1562
Viscosity (liquid/dense phase)	cSt	0.08
Heat Capacity (C_p) gas phase@15 °C	J/(mol K)	36.61

Table 3.2.: Main properties of Carbon Dioxide ([36–38])

during hazard identification and management when dealing with CCS projects. The growing interests from energy companies in CCS will lead to the development of new generation CO_2 pipeline systems that will require thorough risk assessments and to be design within acceptable risk levels as required by DNV-GL [78]. Since the fluid is usually transported in dense phase, there is the potential for large inventories of CO_2 being released in the atmosphere which could reach populated areas with hazardous concentrations. For this purpose, both the content of the pipeline and the human activity around the pipeline need to be categorized. As reported in Table 3.3 according to ISO 13623 [89] and DNV-GL-RP-F104 [78], CO_2 is categorized as a category C fluid. However, there is a guidance note stating that it is recommended that CO_2 is categorized by category E unless long operational experience exists. This will requires higher safety factors in the design. To properly assess the risk of an installation, it is necessary to evaluate the potential consequence of an accidental release. The complex thermodynamic of the phenomena and the limited experience in handling CO_2 are points of concern that need further investigation for a proper assessment.

As reported in Table 3.4, concentration and exposure time to toxic gases such as CO_2 has a certain impact on human health. The normal concentration of CO_2 in air is low (below 1 Vol %, around 0.041 Vol %). Acute exposure to 1 % and 1.5 % CO_2 is tolerated quite comfortably with very little noticeable respiratory stimulation occurring until the inspired CO_2 concentration exceeds about 2 %. While Exposure of humans to CO_2 concentrations ranging from 17 - 30 % will quickly (i.e. within 1 minute) result in loss of controlled and purposeful activity, unconsciousness, coma, convulsions, and death.

According to McGillivray et al. [139] there are a number of different methods available to calculate levels of harm such as: dangerous toxic load, probit functions and concentration. The dangerous toxic load and probit methods are based on

Category	Description
A	Typically non-flammable water-based fluids.
B	Flammable and/or toxic fluids which are liquids at ambient temperature and at atmospheric pressure conditions (i.e. methanol).
C	Non-flammable fluids which are non-toxic gases at ambient temperature and atmospheric pressure conditions (i.e. nitrogen, carbon dioxide, argon, air).
D	Non-toxic, single-phase natural gas.
E	Flammable and/or toxic fluids which are gases at temperature and atmospheric pressure conditions and are conveyed as gases and/or liquids (i.e. hydrogen, natural gas, ethane, ethylene, LPG, ammonia and chlorine).

Table 3.3.: Fluids categorization according to ISO13623 and DNVGL-ST-F101

fatality whereas concentration is usually used as a measure of injury or harm, for example, work place exposure limits. Another approach has been reported from the Energy Institute [36], a correlation between CO_2 concentration and effects on health was proposed. The levels and consequences found good agreement with the one reported lately from CO2RISKMAN [8, 36]. Since the threshold concentration method appears not very suitable and precise for engineering application such as a detailed pipeline risk analysis, statistical methods are often suggested from authors. Probit analysis can be used as part of estimating the frequency of fatality [149]. For an individual release, the following relation can be applied:

$$\text{Frequency of Fatality} = RF \times POF \tag{3.1}$$

where RF is the frequency of the release and POF is the probability of fatality due to exposure to release. The frequency of release may be obtained from data for frequency of failure using event trees, fault trees or both. The probability of fatality may be obtained using a probit expression. Probit equations provide a means of relating the intensity of the toxic exposure to the degree or percentage response of the objects being exposed. A probit function takes the form:

$$Probit = a + b \log (dose) \tag{3.2}$$

where a, b are constants characteristic of the gas (or any other agent). The *dose* variable is a function of the factor that causes injury or damage to the vulnerable resource. The usual form when applied to toxic exposure situations is:

$$Probit = a + b \ln(C^n \times t) \tag{3.3}$$

Note that C is the concentration of carbon dioxide in air (usually reported in

CO_2 concentration in the air (% v/v)	Exposure	Effects on humans
2	Several hours	Headache, difficult breathing upon mild exertion
3	1 hour	Mild headache, sweating, and difficult brathing at rest
4-5	Within a few minutes	Headache, dizziness, increased blood pressure, unconfortable breathing
6	1-2 minutes <16 minutes Several hours	Hearing and visual disturbances Headache, difficult breathing (dyspnea) Tremors
7 - 10	Few minutes 1.5 minutes to 1 hour	Unconsciousness, near consciousness Headache, increased heart rate, shortness of breath, dizziness, sweating, rapid breathing
>10 - 15	1 minutes to several minutes	Dizziness, drowsiness, severe muscle twitching, unconsciousness
17 - 30	Within 1 minute	Loss of controlled and purposeful activity, unconsciousness, convulsions, coma, death

Table 3.4.: Acute health effects of high concentrations of CO_2 asphyxiation from elevated CO_2 concentrations [36].

ppmv or mg/m^3 or kg/m^3), while t is the exposure time in minutes or seconds. Most common probit function are formulated with C in ppm while t in minutes. The constant n is typically set to toxic value, namely 8 or 9. The Probit variable is normally distributed between 2 (zero probability) and 8 (100 % probability of outcome) with a mean value of 5, and a standard deviation of 1. Several Probit functions have been reported in literature for CO_2 [139, 147, 149–151], especially designed for QRA risk analysis during pipeline design phase. A collection of the most relevant ones is reported in the Table 3.5.

Author	a	b	n	Units
			Toxic Value	[C,t]
HSL [149]	-89.80	1	8	[ppm, min]
Tebodin [150]	-98.81	1	9	[ppm, min]
McGillivray [139]	-90.80	1	5.2	[ppm, min]
Molag/Koorneef [147]	4.45	1	5.2	[kg/m^3, s]
DSB [151]	-90.80	1.01	8	[ppm, min]

Table 3.5.: Probit Function parameters by author and associated units.

In order to identify a dose-effect relationship, the utilization of probit functions have been observed. The main aspects related to CO_2 toxicity are reported, either in term of asphyxiation due to CO_2 displacing oxygen in the air and the increase of blood acidity, triggering adverse effects on the respiratory, cardiovascular and central nervous systems. According to current version of ISO 13623 and DNVGL-ST-F101, CO_2 is categorized as a category C fluid; however, fluid category for CO_2 is expected to be modified in the next revision of ISO 13623 possibly as category E fluid. A release of CO_2 would increase the level of CO_2 in the air and proportionately decrease the other air components, this can cause asphyxiation in human beings. An approach based on threshold limits have been reported from multiple sources in this analysis. However, since the concentration method appears not very suitable and precise for engineering application such as a detailed pipeline risk analysis, statistical methods are usually suggested from authors. Several statistical model (probit function) for assessing the dose-response relationship for a generalized typical population have been evaluated. The absence of a dose-effect relationship as well as internationally standardized exposure thresholds for CO_2 for use in QRAs has been recognized as an uncertainty. A large difference between the probit function evaluated has been noted, for this reason it is still not easy to identify a single specific function that accurately describe the dose-effect relationship. The relation appeared to be non-linear and described by an asymptotic function.

3.4. Failure frequency applicability to onshore CO_2 pipelines

3.4.1. Introduction

During a QRA, failure is usually assessed with the use of statistical/historical data. However, for CO_2 handling systems the operating experience is limited compared to hydrocarbon transporting systems and, for this reason, hydrocarbon pipeline statistics are normally used as a proxy. The only database that contains statistics on CO_2 pipelines is the PHMSA since in the U.S. several CO_2 pipelines have been constructed since the 1970's, essentially for Enhanced Oil Recovery operations. However, there is limited statistical data available compared to the hydrocarbon pipelines experience and care should be taken when undertaking the frequency analysis. In this section an analysis of incidents data related to the onshore CO_2 pipelines in the U.S. between 1985 and 2020 reported by the Pipeline Hazardous Material Safety Administration (PHMSA) of the U.S. Department of Transportation is presented. In this section it has been analysed the incident scenarios, the causes and the consequences so as to provide an estimate of a specific CO_2 pipeline failure rate to be used in quantitative risk assessments.
The objective of the frequency analysis is to examine the initiating events identified, assess the probability/frequency and potential outcomes of the accidental event. Frequency is defined as "the number of events or outcomes per defined unit of time"

[7] and can be applied to past events or to potential future events, where it can be used as a measure of likelihood/probability. Historical data for relevant gaseous/dense phase CO_2 service systems and components is significantly less robust than for other mature industries. In literature, the most commonly used databases, which account for incidents related to pipelines are: the European Gas Pipeline Incident Data Group (EGIG), the UK Pipeline Operators Association (UKOPA) and the Conservation of Clean Air and Water in Europe (CONCAWE) and the Pipeline and Hazardous Material Administration in the US (PHMSA). However, the only one that contains statistics on CO_2 pipelines incidents is the PHMSA. In some instances, failure rates of natural gas pipelines have been used [152], while in other cases an estimation of the failure rate from the PHMSA database has been proposed [128, 139, 147, 153]. Gale and Davison [128] in their study, reported that CO_2 pipelines in U.S. have a frequency of incident of 0.32 events per 1000 km per year, whereas natural gas and hazardous liquid pipelines have an incident frequency of 0.17 and 0.82 events per 1000 km per year respectively. According to Koornneef et al. [147], cumulative failure rates (puncture plus rupture) assumed within studies on risks of CO_2 pipelines show a range within one order of magnitude, i.e. from 1.2×10^{-4} to 6.1×10^{-4} km^{-1} year. According to the PHMSA more than 8000 km of onshore CO_2 pipelines have been installed in the U.S. from 1968 to 2020, mostly for enhanced oil recovery (EOR) applications. Most of the incidents reported in PHMSA database are related to small leaks, malfunctions, and minor incidents. Due to the limited mileage of CO_2 pipelines, most of the incidents reported, did not represent serious or critical injuries or even deaths. According to current regulation, title 49 of the Code of Federal Regulations, the pipeline operator should submit an incident report within 30 days of a pipeline incident. The PHMSA defines as significant incidents those that:

- involve fatalities or injuries requiring in-patient hospitalizations
- have $ 50,000 or more in total costs (including loss to the operators or the others, but excluding cost of gas lost,
- results in release of 50 barrels or more of product,
- result in an unintentional fire or explosion.

3.4.2. Data analysis

This study focused on analyzing the PHMSA incident data related to CO_2 pipelines operating in the US from 1994 to 2020. The database collects incidents data related to Hazardous Liquid pipeline systems, where carbon dioxide is included, starting from 1968. However, no incident related to carbon dioxide commodity has been reported before 1994. More than 30 CO_2 pipelines are operating in the U.S., with six crossing provincial/state boundaries and one crossing an international border into Canada. In the incident reports, pipelines from 7 states of the U.S. have been included,

namely located in Texas, Oklahoma, Utah, North Dakota, Mississippi, Louisiana and Alabama. Pipeline failure rates are usually defined based on kilometers of installed pipeline; this provides an indication of the operating experience and the size of the data sample. Incident statistics are more reliable when are based on large data samples. If compared to hydrocarbon pipelines, operational experience and pipeline exposure is limited and updated incident data is scarce for CO_2 pipelines. The number of kilometers of CO_2 pipelines is approx. 8000 km while more than 550000 km of hydrocarbon pipelines are operational. In Figure 3.4 the evolution of total mileage of CO_2 pipeline in the U.S. from 2004 to 2020 has been reported in km (U.S. Department of Transportation., 2020). In the U.S. the first pipelines constructed to transport CO_2 date back to 1963, however the majority of the infrastructure was built between 1980-1990. The graph starts from 2004 as yearly detailed data for previous period cannot be retrieved from the database.

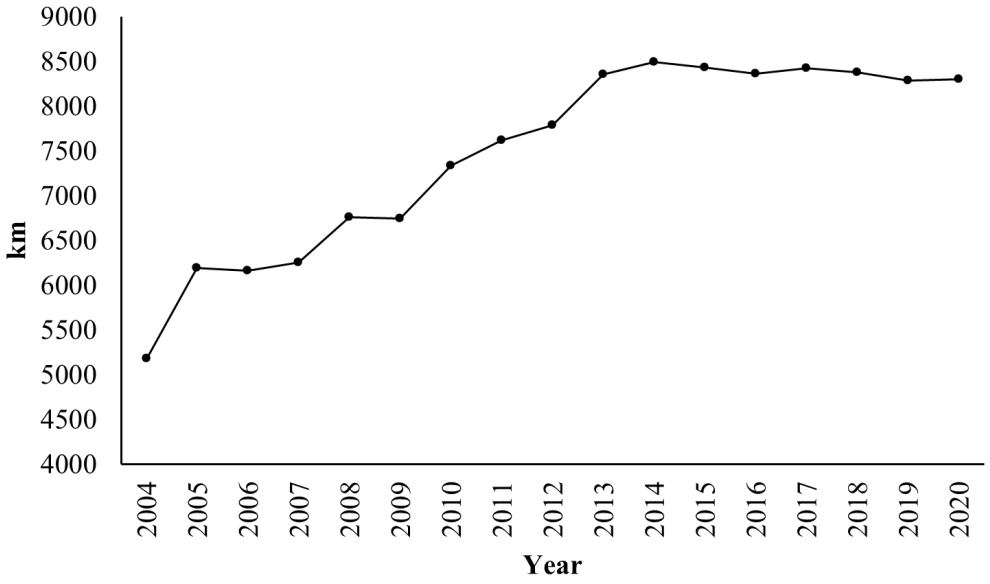

Figure 3.4.: Evolution of total kilometers of CO_2 pipeline in the USA from 2004 to 2020.

The evolution of the mileage of carbon dioxide pipeline in the US generally shows an increasing trend from 2004 to 2014, with a maximum of 8490 km of pipeline. The development after 2014 shows an almost constant value with a local maximum of 8434 km in 2015 and a local minimum of 8283 km in 2019. Policies and economic interest were the main driving factor in the development of CO_2 pipelines, since most of the operating pipelines in the united states are related to enhanced oil recovery (EOR) activities. The total length of installed pipeline is fundamental to calculate the exposure. Exposure calculated as the length of installed pipeline multiplied by its exposed duration and is expressed in kilometers-years. Considering the uncertainty on the installed pipeline length, the pipeline operating experience (expressed in

km-year) to be used for the failure frequency calculation is estimated starting from 1985. The exposure evolution during the last 16 years is reported in Figure 3.5.

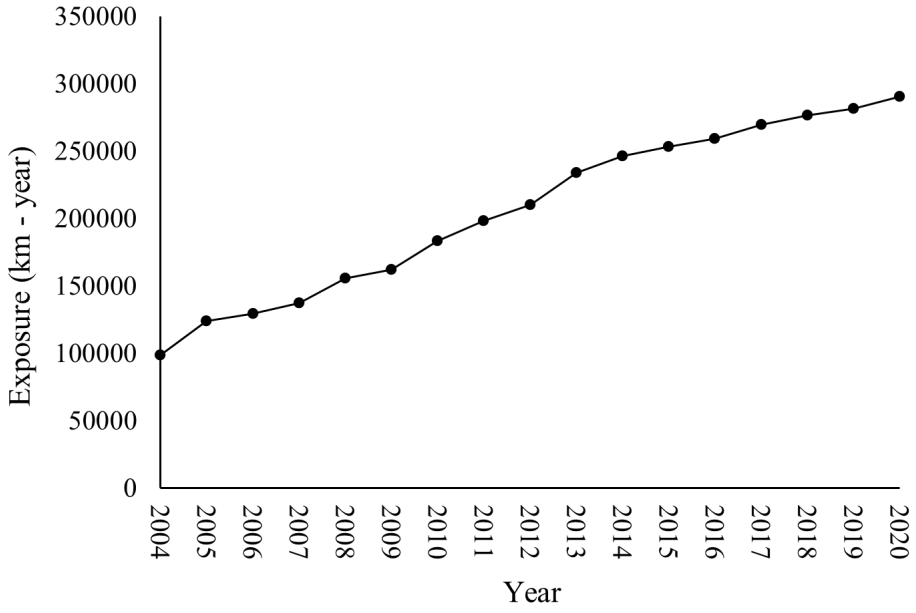

Figure 3.5.: Exposure evolution CO_2 pipeline in the USA from 2004 to 2020.

With regards to the recorded incidents involving CO_2 pipelines, between 1994 and 2020, a total of 106 incidents related to onshore CO_2 transmission pipelines were reported to PHMSA database. Figure 3.6 shows the number of incidents recorded for CO_2 pipeline in the period 1994-2020. Incident database indicates date and place of each reported incident by the pipeline's operators. It should be outlined that, since the database was accessed in October 2020, a percentage of incidents that could potentially have been reported in the remaining months of the year 2020 are not included in this analysis.

Since PHMSA reports no incidents before 1994, Figure 3.6 shows the recorded incidents for CO_2 pipeline operating in the U.S.A. from 1994 to 2020. No incidents were recorded in 1998 and 1999, the maximum number of incidents has been recorded in 2016 and 2017 with a total of 9 incidents for each year. The minimum (non-zero) number of incidents were recorded in 1995,1997, 2000 and 2001 with a single occurrence for each year. The average number of incidents reported for each year from 2004 and 2020 is 3.93 incident/year. None of the recorded incidents resulted in fatalities. Only one incident resulted in an injury. This is an important difference with respect to accidental scenarios involving hydrocarbon pipeline releases.
Amongst the information reported in the incident form, there is the incident cause, sub-cause and incident description which is of paramount importance to further analyze the data and identify the major categories of failures. As reported by [152], the incident form has changed over the years as well as the number of fields required.

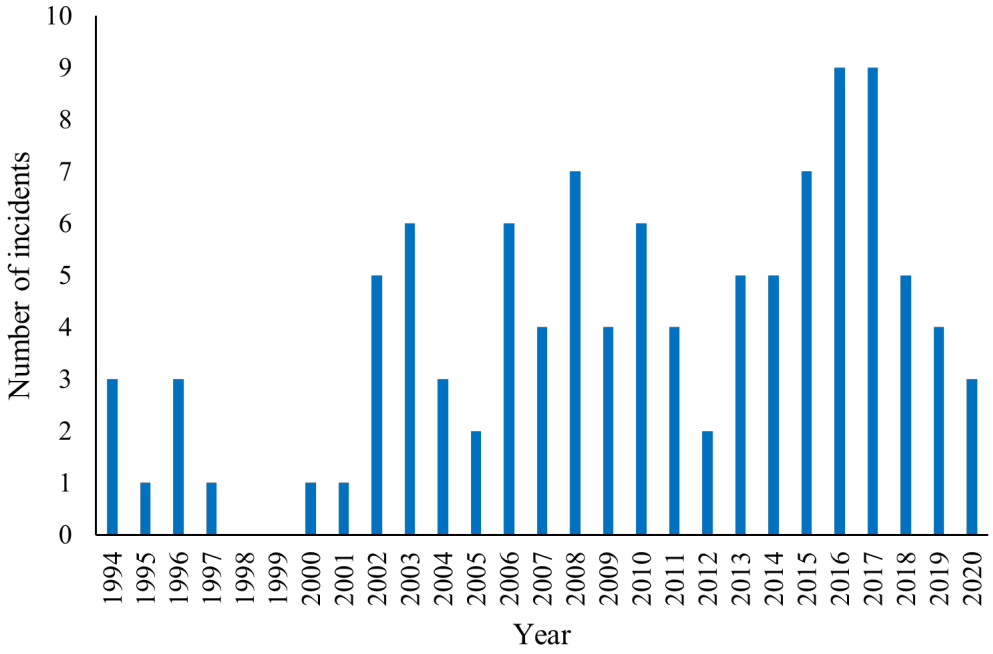

Figure 3.6.: Number of incidents recorded for CO_2 pipelines in the U.S.A. (1994-2020) from PHMSA.

In the latest form, in use since 2010, 8 incident causes can be selected, while several sub-causes can be added to better describe the incidents. The main causes available are: corrosion, natural force damage, excavation damage, other outside force damage, material failure of pipe or weld, equipment failure, incorrect operation, other accident cause. Based on the analysis of the 106 recorded incidents involving CO_2 pipelines in the period 1994-2020 the incident cause distribution reported in Table 3.6 and Figure 3.7 has been found.

Incident Cause	No. of incidents	Percentage of the total (%)
Equipment failure	46	43.40
Material Failure of Pipe or Weld	22	20.75
Corrosion	12	11.32
Other accident cause	11	10.38
Incorrect operation	10	9.43
Excavation damage	2	1.89
Other outside force damage	2	1.89
Natural force damage	1	0.94

Table 3.6.: Number of incidents causes between 1994 and 2020 for CO_2 pipelines reported in PHMSA.

"*Equipment failure*" has been identified as the most frequent incident cause reported in database, with 46 occurrences, accounting for 43.40 % of the total events. 22

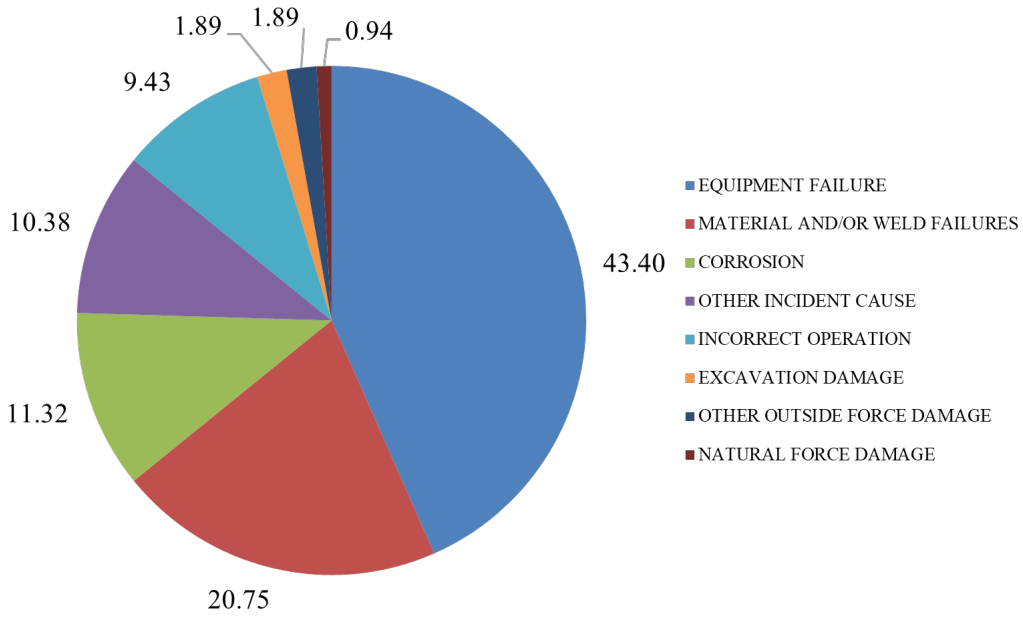

Figure 3.7.: Distribution of incidents causes between 1994 and 2020 reported in PHMSA.

incidents have been attributed to "*material failure of pipe or weld*", that constitute 20.75 % of the total. "*Corrosion*", that include internal corrosion as well as external, counts 12 reported incidents (11.32 %), followed by "*other accident cause*" (10.38 %), "*incorrect operations*" (9.43 %), "*excavation damage*" (1.89 %), "*other outside force damage*" (1.89 %) and "*natural force damage*" (0.94 %). In Figure 4 the incident causes have been reported with respect of percentage of the total events reported. The ones classified as "*corrosion*" were 12, 9 of which have been attributed to "*external corrosion*", while no information has been reported for the remaining 3 incidents. A total of 46 incidents have been classified as "*equipment failure*", 30.43 % of the equipment failure has been attributed to the "*malfunction of control/relief equipment*", while 28.26 % to "*non-threated connection failure*". A single case has been reported as "*icing of relief valve*". It should be noted that for 8 cases, the sub-cause was not reported. Another significant information that can be extracted from the database is whether the incident required a shutdown of the facility and how long this has lasted. On a total of 106 events registered, 43 required the pipeline shutdown, in 43 more no shutdown was necessary and for the remaining 20 cases the information are not available.

3.4.3. Frequency failure calculation

In the U.S. the first pipelines-built to transport CO_2 date back to 1963, however the majority of the infrastructure was built between 1980-1990. Considering all the recorded incidents in the PHMSA database and the calculated operating experience

(km year) it is possible to evaluate the CO_2 pipeline incident frequency. Figure 3.8 reports the variation of the calculated incident frequency in the period 2004 – 2020 between a lower bound and an upper range estimated considering different pipeline operating experience time-frame. The upper bound is based on pipeline operating experience since 1990, while the lower bound on operating experience since 1968. According to this data the incident frequency can vary between 2.5×10^{-4} event/year (lower bound) and 4.2×10^{-4} event/year (upper bound) with an average value of 3.6×10^{-4} event/year. This is in line with values reported in previous studies [29, 58, 147].

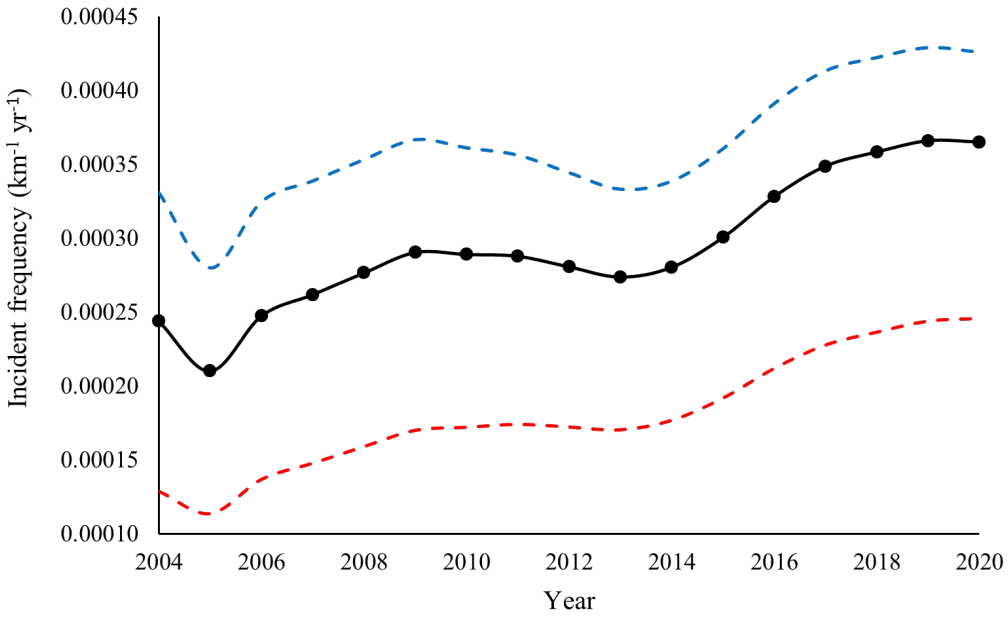

Figure 3.8.: Incident frequency trend (2004-2020) for CO_2 pipelines in the U.S.A. based on PHMSA.

The black line reported in Figure 3.8 has been based on pipeline operating experience since 1985 with a total of 290500 km year, the upper blue dashed line is based on pipeline operating experience since 1990 with 249000 km year, while the lower red dashed line is based on pipeline operating experience since 1968 with 431600 km year.

3.4.4. Discussion and conclusions

In this section, the failure frequency associated to gaseous/dense-phase onshore CO_2 pipelines have been analyzed. The main uncertainties associated to a failure frequency analysis for CO_2 transportation systems are the availability of historical failure data for CO_2 and the assessment of possible outcomes and incident development. The only

recognized database that contains statistics on CO_2 pipeline incidents is the Pipeline and Hazardous Materials Safety Administration (PHMSA) from U.S. Department of Transportation. However, the limited operating experience, if compared with the database available for other hydrocarbon services such as natural gas, suggested to adopt a cautious approach in the use of this specific data. In fact, CO_2 pipelines operating in the U.S. are approx. 2 % of the overall pipeline network. A total of 106 incidents are reported from 1986 to 2020 for CO_2 services. Approx. 45 % of incidents registered, occurred due to causes related to equipment malfunction, more than 30 % of these cases are associated with pressure or thermal relief valves relieving in unwanted conditions. The remaining incidents from equipment failure are associated with the failure of small components that lead to minor releases. The second main cause is material related defects, in fact, mostly of the failures occurred at a weld and resulted in minor releases. However, in some cases the failure occurred in a pipe segment and resulted in more significant releases. The third contribution is related to corrosion, since in all incidents reported external corrosion originated the failure. According to the analyzed data, the incident frequency can vary between a lower bound of 2.5×10^{-4} event/year and an upper bound of 4.2×10^{-4} event/year with an average value of 3.6×10^{-4} event/year. The utilization of data contained in PHMSA and other databases should be treated very carefully, however, the accurate reporting of accidents during the years can highlight the weakest aspects of the system. Finally, due to the limited data available on the PHMSA database related to onshore CO_2 pipeline, its applicability is not indicated (as it is) for a failure frequency estimation.

3.5. CO_2 accidental releases

3.5.1. Experimental release tests

Experimental release tests can be very expensive and usually are not affordable for small-medium laboratories, especially for large-scale scenarios. Several experimental works have been reported in the literature; these can be classified in large-scale and small scale experiments. Furthermore, the aim of the studies can be considered to be an additional parameter for the categorization. Most of the experimental work analyzed can be divided between far-field and near-field modeling. Studying the behavior and thermodynamics evolution in the near field is typically carried out in small scale set up or laboratory scale. During a release, the monitoring of far-field evolution has been developed in large-scale or full-scale outdoor experiments. Since the costs and infrastructure necessary for a large-scale set up are not easily sustainable by a single research center or university, several Joint Industry Projects (JIP) and Research Projects (RP) have been developed over the years. The most important JIPs and RPs are reported in Table 3.7 with the associated period, scale, and objectives.

In this section a literature review of the most important experimental studies

Table 3.7.: Relevant CO_2 pipeline related JIPs and RPs programs during the years [9].

JIP/RP Name	Years/Period	Scale	Objectives and Scope
CO2SAFEARREST	2016 - 2019	Full-scale	Burst tests research program. Two full-scale tests with buried pipeline (CO_2-N_2 mixture), 24 inches.
COSHER	2011 - 2015	Large-Scale	Obtain data to support the development of models to determine safety zones/consequence distances.
CO2PIPETRANS	2009 - 2015	Medium-Scale Large-Scale	Fill the knowledge gap identified in the DNV-RP-J202. Results of the project were included in DNVGL-RP-F104 (2017).
COOLTRANS	2011 - 2015	Large-Scale	Identify and propose solutions to key issues relating to the safe routing, design, construction and operation of onshore CO_2 pipelines in the UK.
CO2PIPEHAZ	2009 - 2013	Small Scale Large-Scale	Improve the understanding of the hazards represented by CO_2 releases.
CO2QUEST	2013 - 2016	Small Scale Medium-Scale	Study the impact of the quality of CO_2 on storage and transport.
CATO	2004–2008 2010 - 2014 2015-ongoing	N/A	A national program, which includes complete studies in all aspects of CCS.
CO2EUROPIPE	2009 - 2011	N/A	Outline guidance to elements of the European plan to develop large-scale EU CO_2 infrastructure.
CO2RISKMAN	2010 - 2013	N/A	Development of industry guideline to assist the designer and projects on the emerging CCS industry. Potential hazards associated with handling CCS CO_2 streams are discussed.

related to CO_2 release and dispersion is reported. Particular attention has been paid to large-scale tests for accuracy and readiness to develop validation and comparison studies by reducing the scale-up errors compared to operating pipelines. To highlight the main aspects related to a CO_2 release, a schematic diagram has been reported in Figure 3.9. The release can be divided in near-field (phase change, expansion, air-mixing and solid formation) and far-field zone, where the atmospheric dispersion of the heavy CO_2 cloud continues at large distances start.

The analysis focused first on near-field experiments that highlighted important release aspects. Since near-field modeling can strongly impact the far-field modeling and the definition of safety distances, particular attention should be reserved to these aspects. Pursell [154] presented some results from laboratory scale release tests performed in Health and Safety Laboratory (UK). The experiments were performed both for liquid and gas phase of CO_2 from release orifices of 2 and 4 mm (diameter), the set up was connected to a pressurized vessel containing CO_2 at pressure from 40 to 55 barg. The rapid expansion of the fluid downstream the orifice occurs approx. following an isenthalpic expansion to atmospheric pressure, then the CO_2 jet continues to expand as it entrains and mixes with the surrounding air. Guo et al. [155] studied the near-field characteristics and dispersion behaviour of supercritical [113], gaseous, and dense-phase CO_2 experimentally. A large-scale pipeline set up

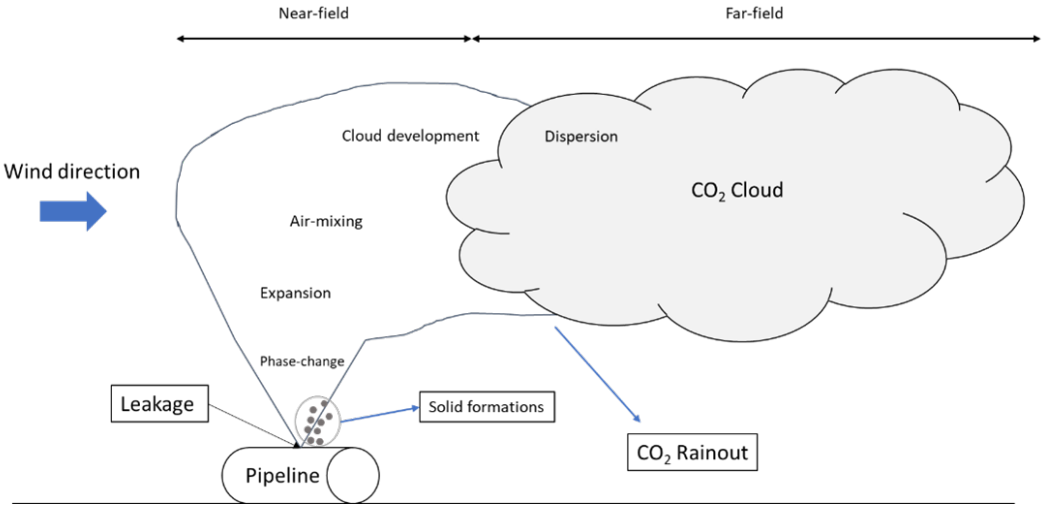

Figure 3.9.: Schematization of a CO_2 release from an onshore pipeline [9].

with an internal diameter of 233 mm and a total length of 258 m was constructed during the CO2QUEST project. Six tests have been performed, and several orifice diameters have been tested from 15 mm to full-bore rupture. The near-field behavior and the under-expanded jet flow structure have been analyzed; solid phase formation was observed. The sublimation of solid CO_2 removes heat from the gas phase with a consequent temperature reduction. The formation of solid CO_2 can impact the properties and the shape of the cloud. Based on the experimental data performed by Guo et al. [155], the development of the visible cloud can be divided into three stages: a "rapid expansion", a "metastable stage", and a "slow attenuation stage". The distance of the 50,000 ppm concentration contour for three orifice diameters was determined in all the experiments. The maximum safety distance of 160 m has been measured for the full-bore rupture at the initial condition of 9.1 Mpa at 21.6 °C (dense phase). Safety distances measured for dense phase were consistently greater than gas phase tests. An experimental study of supercritical CO_2 leakage has been reported by Fan et al. [156]. The pressure and temperature conditions analyzed varied from 81 to 110 bar and 34.9 °C to 100.9 °C. The authors noted how the mass flow rate decreases with the increase of upstream temperature and length-diameter ratio and increases with the increase of upstream pressure. However, the effect of upstream temperature variation (at approx. 100 bar) on the jet structure was not so evident in the range between 37.6 °C and 40.1 °C. An experiment with various measurement methods was developed by Teng et al. [157] to carry out controllable CO_2 release from a high-pressure vessel. Pure liquid CO_2 has been used for the experiments, orifice diameter of 1 and 2 mm. Initial pressure varies from 80 bar to 100 bar, while temperature from 301 K to 313 K. The lowest temperatures measured were -41.9 °C (1 mm diameter) and -45 °C (2 mm diameter). The maximum velocity along the jet centreline was 250 m/s. The results suggest that for a supercritical CO_2 leakage, dry ice particles with size between 1 and 3 μm can be formed. The initial

temperature shows limited impact on the size of dry ice particles, while a wider size distribution can be addressed to a higher initial pressure. Li et al. [112] developed a reduced scale facility with dry supercritical CO_2 to analyse the jet plume's early stage flow characteristics in the near-field. Initial pressure was set up to 8.02 MPa; the velocity in the centreline of jet plume was measured from different leakage sizes (0.5, 1, 3, 5 mm), showing a correlation with the depressurization process during the leakage. Ahmad [10] reported the results based on COSHER JIP; a large-scale rupture test was conducted on a loop test built in Spadeadam (UK). A 219 mm diameter pipeline buried underground filled with dense phase CO_2 has been used. Temperature, pressure, concentration distribution and dispersion cloud have been considered with low wind conditions 1.9 m/s. Approximately 136 ton of CO_2 were released in 204 s. The maximum height of the plume was registered at 60 m from the ground while the maximum horizontal extension at 400 m, the minimum temperature registered during the release was -78 °C. The test has been conducted at approx. 150 bar and the average temperature of the fluid in the reservoir was around 13 °C. In Figure 3.10 the visible cloud formed after the rupture is reported at subsequent times; images have been captured from a video.

Figure 3.10.: The visible cloud behavior after the rupture; from left to right, at 10, 30 and 120 s from the break (From Ahmad et al. [10], Copyright Elsevier, 2015).

In 2017, other tests were carried out in Spadeadam (UK); two full-scale burst tests were performed during CO2SafeArrest JIP to evaluate the fracture propagation and arrest characteristics and CO_2 dispersion in the atmosphere [11, 158]. The outer diameter of the test section was a steel pipe 610 mm, 85 m long, connected to approx. 120 m long reservoirs at both ends. A mixture of 91% CO_2 and N_2 pressurized to about 15 MPa was adopted. The pipeline rupture was induced by initiating the crack with explosives; several sensors (temperature, pressure, oxygen cells) have been positioned over a pattern terrain in the vicinity of the crack. Two burst tests have been conducted; for the first test, all the pipe test section was buried under a 1 m deep soil cover, while in the second test, only half the length of the pipe test section was buried. The resulting crack propagated in both directions as the pipe wall was torn open sideways. The CO_2 cloud reached an altitude peak of 250 m, as well as the debris thrown out of the crater formed. As reported in the schematization of Figure 3.11, the crater extension measured approx. 45 m in the horizontal (pipe direction) while the perpendicular extension varied between 5.8 m and 9 m. The average width

of the crater is about 7.4 m, which is 12 times of the outer pipe diameter.

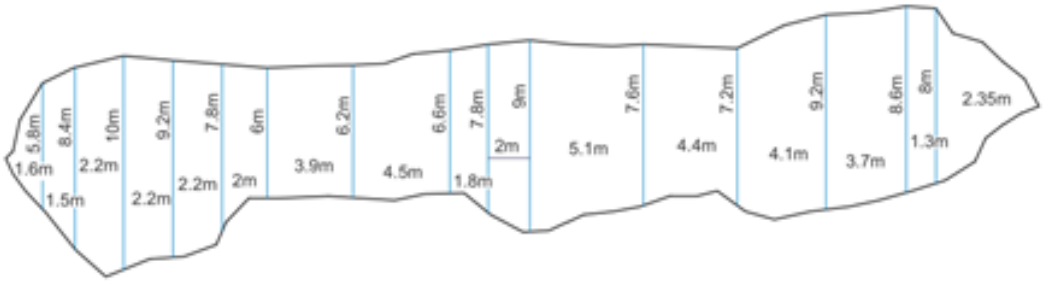

Figure 3.11.: Crater outline and length measured after the rupture test (From Applied Energy, Liu et al. [11], Copyright: Elsevier, 2019).

3.5.2. Model methods and development

Modeling a release of a CO_2 pipeline requires the assessment of some important aspects, such as transient conditions, multi-phase jet, as well as the dispersion behavior. A rapid pressure drop will follow the release of CO_2 from a pipeline; the pressure and temperature reduction a phase transition from liquid-vapor is expected. Moreover, for lower temperature the formation of solids is also a possibility. The phase transition can impact the flow conditions within the pipeline and the properties of the fluid. The precise simulation of transient depressurization, with regards of flow rate and thermodynamic properties of CO_2 during the release, will impact the accuracy of the cloud dispersion prediction. Specific focus must be reserved to phase transition and density prediction of the CO_2 during transient operations in order to better predict solid formations. Release and dispersion studies are required for risk evaluations [9]. Three main steps can be identified in dispersion modeling:

- Outflow calculations
- Expansion to atmospheric pressure (near-field)
- Far-field dispersion

Some specific difficulties for modeling CO_2 releases can be highlighted, which may constitute a limitation in developing accurate simulations, in particular: the selection of an Equation of State for an accurate description of the thermodynamic properties throughout the release process, the modeling of phase changing (from dense phase to gaseous), prediction of solid phase formation, the validity of homogeneous equilibrium (HEM) assumption. Another aspect to be considered is the very limited experience in CO_2 pipeline modeling; for this reason, most codes and simplified models need to be assessed and validated with experimental tests data. Two main approaches are available to model an accidental release:

- Simplified models

- CFD models

The simplified models usually require very low CPU usage compared to CFD models; hence they are faster and optimized for risk analysis. However, a simplified model, such as an integral model, is based on several assumptions and simplifications to the physics of the phenomena; for these reasons they need to be extensively validated with real case data, experimental tests. CFD models can provide a very detailed description of the physics and the behavior of a CO_2 release; this kind of approach is required when a complex topography, specific environment conditions or presence of buildings or other obstructions in the nearby area. These models require high experience and specific knowledge from the user to be set up and executed, compared to simplified integral models. Moreover, the uncertainties specific to CO_2 related to limited experience and optimization often require custom-made inputs and user-defined functions to be implemented in commercial CFD software. The flowchart reported in Figure 3.12 represents a modeling strategy based on the one proposed by Woolley et al. [146] about the needs to create a link between the near-field and the far-field modeling. Moreover, the thermodynamic modeling of the main properties from the flow models needs to be inputted correctly during the near-field model.

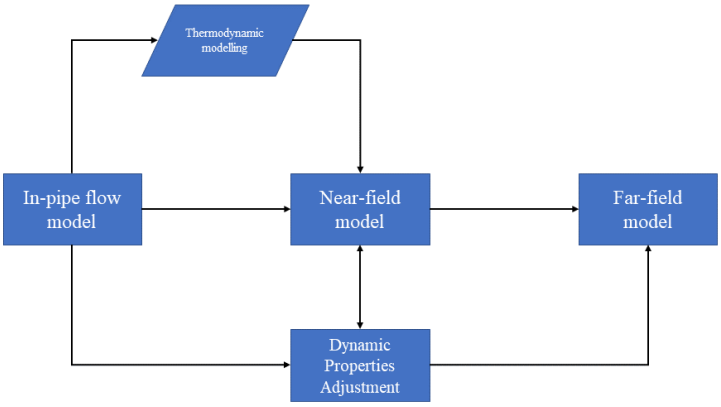

Figure 3.12.: Integrated thermo-physical modeling strategy.

3.5.3. Simplified models

The most commonly available simplified models are the integral models implemented in existing commercially available software. The most relevant studies related to CO_2 modeling through integral models have been reported. Since most risks in the oil and gas industry come from flammable liquids or gases, none of them was originally

designed to take into account inert gas such as CO_2. The main models identified during the literature review are:

- FRED
- PHAST
- ALOHA
- EFFECTS

FRED is an integral model developed from Shell, it adopts a semi-empirical jet model for the first part of the release and a similarity model for the dense gas dispersion. FRED assumes the homogeneous equilibrium model (HEM) between the CO_2 phases. The dispersion of CO_2 is calculated through the model AEROPLUME, the model HEGADAS can be then invoked for develop the simulation starting from AEROPLUME results. It should be noted that AEROPLUME is intended to predict the near-source behavior. Then, far from the source, the dispersion is better modeled by a far-field model. For this purpose, either HEGADAS or another model PGPLUME are invoked to finish the calculations. Indeed, Shell program HEGADAS is a dense gas model specifically developed to account for the restricted mixing of dense gas clouds [159–161]. PHAST (by DNV) is a hazard assessment software package for modeling atmospheric releases of flammable or toxic chemicals. The Unified Dispersion Model (UDM) included in PHAST, can simulate unpressurized and pressurized releases, time-dependent releases, complex thermodynamic behavior and different atmospheric conditions. The HEM is used for the two-phase flow jet. Finally, solid particles deposition on the ground is not considered in version 6.7 [162]. The Gaussian model ALOHA can handle several hazardous scenarios such as toxic gas dispersion, fires, and explosions. The aerial dispersion model included in ALOHA can estimate the movement and dispersion of chemical gas clouds; both the Gaussian and heavy gas model are also available. The Gaussian model is used for the dispersion prediction for gases which buoyancy is close to air, namely the gases that have the same density as air [163]. The heavy gas dispersion calculations implemented in ALOHA are based on those used in the DEGADIS model [164]. The simplified model EFFECTS contains a series of models from the Yellow Book [165] that allows detailed modeling and quantitative assessment of gas releases, liquid or pressurized liquefied gas, two-phase, and spray release. The model applied for the gas release from a long pipeline (Wilson model) is suitable for total rupture of a long gas pipeline. Heavy gas dispersion models are available for rapid gas release, pool evaporation, horizontal or vertical jet. Liquefied gas from long pipeline is modeled with the Morrow model. The model can be used to calculate the behavior of expanding pressurized liquid in a pipeline after a rupture [166]. To investigate the capability of the simplified models reported, identify the weakness and the most suitable models for carbon dioxide modeling, importance has been reserved to validation and comparison studies.

Several studies related to CO_2 accidental release modeling have been conducted. Comparison between experimental data and integral models is considered more relevant; however, the comparison with CFD models has also been considered. Dixon et al. [159] compared the integral model FRED with two CFD models (OpenFOAM and ANSYS-CFX) and experimental data. The horizontal releases tests conducted by Shell at Spadeadam (UK) test facility were considered (orifice diameter up to 25.4 mm). The thermodynamics library employed by FRED usually cannot account for solid CO_2, the liquid-vapor saturation line was instead derived to atm. pressure. The concentration and plume width predicted from the FRED model produced slightly better agreement with the data than both CFD models. Despite the prediction of solid particles, the FRED model overall reproduced well the hazard distances. Mazzoldi et al. [167] performed a comparison against experimental data reported by Hanna et al. [168] with the Gaussian model ALOHA and presented an evaluation of the atmospheric dispersion CFD tool Fluidyn-PANACHE. The author noted that for CO_2, the application of threat zones modeled with Gaussian methods to population densities were over-conservative. Hazards identification resulting from releases of high-pressure CO_2 was also part of the review performed from HSL [169]. According to the authors, to overcome the high computational costs, a practical alternative could be the creation of a statistical model of the results based on many consequence model calculations results. A hundred PHAST simulations performed with PHAST have been used to run a sensitivity analysis with a Gaussian emulator. The releases consisted of above ground, steady-state horizontal, diameter from 12.7 to 50.8 mm of dense phase CO_2 (100–150 bar, approx. at ambient temperature). A Bayesian analysis has been performed rapidly using PHAST outputs. In the analysis of Gant et al. [162] developed with PHAST, seven model inputs have been considered to highlight the most sensitive parameter during the modeling scenario for CO_2 releases. These scenarios were mainly relevant, in scale, to leaks from large diameter onshore vessels or non-buried pipes. The main factor that have been varied for the sensitivity analysis were the temperature and pressure, the wind speed, the outer diameter and humidity. In the range evaluated (pressure range within 100 and 150 bar), the greatest influence on the dispersion distance can be addressed to release point height and orifice diameter. Simulation results from an integral model and two different CFD models have been compared to data experiments conducted by INERIS [169]. The integral model PHAST adopted produced similar results to the ANSYS-CFX model, particularly the centerline temperatures were under-predicted by up to 20 °C, while an over-prediction of the centerline concentrations by up to 8 % v/v has been registered. Witlox et al. [170] performed a validation of the experimental data from CO2PIPETRANS with the consequence-modelling package included in PHAST 6.7. The results from the tests performed by BP and Shell during the JIP between 2006 and 2010 have been considered for high-pressure releases. A total of nine tests from BP and eight tests from Shell have been considered for the validation procedure. Several orifice diameters from 6.3 mm to 25.62 mm are reported for the

validation; the minimum release duration of 40 s was registered for the biggest orifice, namely 25.62 mm, while a maximum release duration >700 s for the 6.3 mm orifice diameter. Two different models available in PHAST have been used for the simulation of steady-state liquid release (DISK model) and time-varying releases (TVDI model). The metastable assumption was not implemented first, but flashing was allowed in correspondence to the orifice; to have more precise concentrations prediction, conservation of momentum was considered for the expansion from orifice. The global accuracy of PHAST in the near-field was not affected by wind direction deviation, while the far-field accuracy has been impacted. Compared to British Petrol (BP) data, in the near field, the averaged concentration output from PHAST seems to match with good accuracy. A larger effect of averaging was observed downstream (at 20 m and 40 m) with more deviation compared to experimental data. Generally, the estimation provided by PHAST resulted conservative in terms of averaged concentrations. Shell experiments results were generally under-predicted by PHAST. However, a better accuracy for the steady-state has been registered if compared with BP experimental data. For time-varying releases, the Peng-Robinson EOS produces the most accurate results, especially for the flow rate predictions since the equation provides accurate density values. According to the results, the PHAST discharge and dispersion models predicted the release rates and concentrations accurately. The EFFECTS model was used in some works [147, 171] to estimate the dispersion from a CO_2 pipeline. EFFECTS models are sensitive to initial pressure, temperature, composition and orifice size [165]. Due to the different models included, such model seems well suited to modeling CO_2 releases. However, no publicly available detailed validation with CO_2 release experimental tests has been found in this literature review.

3.5.4. CFD models

The most relevant studies related to CO_2 modeling with CFD have been reported. Specific attention has been reserved to commercially available software and their capability to handle CO_2 releases. The main CFD codes identified during the literature review are:

- ANSYS FLUENT
- ANSYS-CFX
- FLACS
- OpenFOAM
- FLUIDYN PANACHE

To have an understanding of the main weaknesses and identify the most suitable models, great attention has been given to validation and comparison studies. Validation against experimental data are considered fundamental; however, comparison

with other CFD models has been taken into account too. Considering that due to computational costs it is not feasible to model the entire phenomenon (from outflow to far-field dispersion) in a single simulation, each study focused either on the outflow and near field or on the far field; some publications presented an integrated approach in subsequent steps. The integration of near-field and far-field models is complex and time consuming, thus it is considered feasible only for specific situations. The work of Fiates et al. [172] focused on the customization of a computational tool for handling gas dispersion of heavy gases, such as LNG and CO_2. The hybrid switch model (HSM) addresses the deficiencies of the HEM approach when applied to CO_2 releases and considers equilibrium, non-equilibrium, solid formation and phase change. The model has been implemented in OpenFOAM. Experimental tests of British Petroleum and Shell reported by Witlox et al. [173] were used to validate the HSM to estimate the discharge leak rate and properties. A comparison with HEM and frozen model shows the better results of the new model. During CO2SafeArrest JIP, full-scale burst tests of CO_2 pipeline were performed in 2017–2018. Godbole et al. [158] described the numerical and experimental investigation of the dispersion of CO_2 in the atmosphere following its release in the burst tests. The maximum CO_2 concentration was reasonably well predicted in the simulations done with CFX. The time of arrival of the CO_2 cloud was overestimated compared to measurements, especially at more distant locations. This could be due to the impact of average wind speed assumed in the simulations. More recently, Liu et al. [11] performed numerical simulations of CO_2 release from a full-scale pipeline. ANSYS Fluent was used for CFD simulation of the release, the species transport model was employed to predict the fraction of each species and the turbulence was modeled with the k-ω SST model. The authors highlight that the wind direction as well as the pipe orientation, can affect the calculated consequence distance especially for high speed wind conditions. The major consequence distance (more than 1500 m) calculated for 50000 ppm envelope was reached from an 800 mm (ID) at wind speed of 10 km/h. In general, it was observed that the consequence distance increases with the wind speed; however, for large releases, even at lower wind speed it can reach long distances. Another experiment (Wen et al. [174]) was used to compare the dispersion process. The analysis indicates good agreement with experimental data. However, the author recommended further investigating the influence of the atmospheric boundary layer. Mack et al. [175] presented CFD calculation of heavy gas dispersion based on experimental results and extrapolated them to a representative full-bore rupture scenario of a CO_2 pipeline. Several full-scale CO_2 pipeline release scenarios have been simulated, including a representative terrain topology. The OpenFOAM software, 7×105 nodes, k-ϵ turbulence model has been used to simulate a pipeline rupture scenario in a representative terrain of 2.4×2.4 km. From the results presented, it is clear how terrain plays a significant role at lower wind speeds. According to author, large CFD modeling becomes fundamental especially in the vicinity of depression because it can overcome the limitations of simple models. Liu B. et al.

[176] performed several simulations with ANSYS FLUENT to investigate the effect of CO_2 dispersion over two different topographies: a flat terrain with an axisymmetric hill and a simplified model of an urban area with buildings. The approach has been validated through an experimental scaled model in a partially enclosed box-shaped space. According to the results, the CFD model slightly underestimated the CO_2 concentration in the near-field region close to the source. In the hilly terrain case, CO_2 tends to disperse around the hill, while in the urban scenario, most of the CO_2 was trapped in the street downwind of the source with less significant lateral spread. The work presented by Gant et al. [169] tested the ANSYS-CFX and FLACS codes to model far-field CO_2 dispersion employing the same source conditions for the CO_2 jet. A Lagrangian particle-tracking model was used in CFX code, heat transfer between the gaseous phase and dry ice was simulated using the Ranze-Marshall correlation, while the k-ω SST turbulence model has been selected. In FLACS, a two-phase RANS with Lagrangian method has been used, the standard k-ϵ model for turbulence and a cartesian grid was adopted. The CFX code was sensitive to the source condition, while FLACS was sensitive to solid CO_2 particle size. Liu et al. [177] presented a CFD model to predict the atmospheric dispersion of CO_2 over complex terrains. ANSYS Fluent was used to carry out the simulations. Based on the RANS approach, turbulence was modeled using the k-ϵ model. The wind velocity profile was described through an atmospheric boundary layer (ABL) using a power-law correlation. Mazzoldi et al. [178] performed dispersion simulations with the CFD code Fluidyn-PANACHE, the Peng-Robinson EOS has been used together with a k-ϵ approach for the turbulence. The author noted how the version of the software (4.0724) could not account for the presence of a solid phase within a gas flow. Liu et al. [179] presented a two-stage CFD model using real gas EOS developed in ANSYS FLUENT. A standard RANS approach while a User-Defined Real Gas Model for CO_2 properties has been created following Peng-Robinson EOS. Both k-ϵ and k-ω SST models for turbulence have been evaluated and compared with acceptable results; the k-ω SST model was employed in the work. A more complex approach is the integrated approach described by Woolley et al. [146] that couples the near-field modeling with the far field. As described in Figure 3.12, this approach can be adopted in order to obtain a higher level of accuracy if compared with conventional modeling strategies. The integration of output from the near-field model as input for the far field model will also require some adjustment of the most relevant thermodynamic properties. The disadvantages of this approach are the CPU requirements as well as the complexity of the thermodynamic calculations involved. Few examples are available in the literature of successful applications of this modeling strategy. The near-field multi-phase modeling of a CO_2 release has been reported by Woolley et al. [180]. A second-order accurate upwind finite volume solution scheme and the k-ϵ model for turbulence were employed while the properties have been derived from a composite EOS. The gas phase properties were calculated with the Peng–Robinson EOS, while the dense phase and saturation pressure were

derived from tabular data generated with the Span and Wagner EOS. An adaptive finite volume grid algorithm has been applied with 3D rectangular mesh and the homogeneous relaxation model (HRM) has been implemented to consider the delay in vaporization during the decompression process. Far-field dispersion modeling was undertaken using two different CFD codes, namely FLACS and ANSYS-CFX, in both cases the Eularian-Lagrangian formulation was used. The input for the far-field calculation is derived from the near-field simulation. In CFX, heat transfer between gas and solid phases was modeled using the Ranz–Marshall correlation while turbulence effects were simulated with the k-ω SST formulation. In FLACS, two-phase CO_2 dispersion are modeled using an Euler–Lagrangian method; a RANS approach was employed, while turbulence is modeled using a standard k-ϵ model. Particle deposition and interaction with obstacles was modeled, while collisions, breakup and coalescence between particles have been neglected. A two-phase gas-solid CO_2 stream was considered at the crater outlet. FLACS and ANSYS-CFX have been applied also for dispersion calculations in realistic terrain. A domain size of 10 km $\times$ 5 km with a height of 1 km has been considered in the FLACS simulation, accounting 2.7 million nodes thanks to multi-block Cartesian mesh. Same terrain modeling required more than three million nodes in CFX for a very smaller area even with an unstructured mesh. All the particles sublimated in the air in the simulations performed with CFX due to smaller size of particles assumed (20 μm), on the other hand the larger particles diameter adopted in the FLACS (300 μm) simulations led to some solid CO_2 rain out to the terrain. The results suggest that banks of solid could formed with particle size in the order of 300 μm or larger. Near-field and far-field models have been coupled with the thermophysical property with an integrate approach. The resources required were found to be significant (weeks) in terms of computing time.

3.6. Conclusions

In the previous sections of this chapter, the most common and commercially available simplified models and CFD models have been analyzed. Comparison based on a literature review of experimental and numerical works has been included.
The most relevant and detailed data were referred to the validation performed with PHAST and FRED packages. Some works reported using the Gaussian model ALOHA; however, this is deemed unsuitable due to the considerable over-prediction. Some work addressed the use of EFFECTS, but no validation data have been reported so far. Based on the literature analyzed, the commercial software available that include the possibility to account for solid CO_2 formation and several source terms are PHAST and FRED. Moreover, PHAST and FRED have been compared with large-scale CO_2 release experiments (Shell and BP data included in CO2PIPETRANS). According to recent research and development reports, good performance for both FRED and PHAST have been reported. The results presented a good agreement

in concentration prediction and temperature over distances, for both PHAST and FRED, compared with experimental tests. Thus, these integral models are suggested when the topography does not present significant complexity or great variations. During the review of CFD models, specific importance has been given to the works that included a validation between experimental tests and simulations. A total of five commercially available codes have been reviewed as described in the previous sections. The overall CFD codes review for CO_2 modeling was divided between the near-field analysis and the far-field dispersion. In most works, a RANS approach with an Eulerian-Lagrangian formulation was adopted, with the k-ϵ turbulence model. In some cases, the k-ω SST has been preferred. Particle-tracking methods to account for solid phase formation were proposed by some authors with considerable computational efforts. Good results have been obtained for the three-phase simulation, even if this strategy is not easy to implement and manage for standard users. The particles size of CO_2 is an important input; a comparative study reported a complete sublimation of the particles in the air in the simulations performed with CFX (20 μm), while the larger particles diameter adopted in the FLACS simulations (300 μm) led to some solid CO_2 rain out.

Chapter 4.

Fluid characterization for CO_2-rich mixtures

4.1. Introduction

Carbon dioxide management is becoming a major argument of interest in these evolving industries, and the design of related CCUS equipment (process, shipping and pipelines) will require deep knowledge in order to optimize the entire CCUS systems in terms of technological robustness, safety and costs. Among other factors, such an optimization depends on accurate and robust models for the characterization of the fluids involved. Equations of State are the most important models providing all thermodynamic properties of pure components or mixtures of components, like their phase behaviour and density. Currently, it is well established that the Span-Wagner [181, 182] is the most accurate Equation of State (EoS) to characterize pure-CO_2. However, some concerns and open-points are present if the CO_2 is not pure and contains impurities such as hydrocarbons and other components that can be produced by common capture processes [15, 183] such as non-condensable gases. Since the presence of impurities considerably alters the thermodynamic properties of the CO_2, an accurate prediction of the latter by means of proper Equations of State is needed. In the present work, 6 EoSs are tested against experimental data found in literature in order to numerically quantify their uncertainties in predicting the Vapor-Liquid Equilibria (VLE) data and the density of different CO_2 multicomponent mixtures. In fact, the correct prediction of both the VLE data and the density of CO_2-rich mixtures are of vital importance to proper design a pipeline to transport anthropogenic CO_2: the accurate estimation of the density allows a correct prediction not only of the pressure drops (and therefore of the pipeline size), but also of the mixture speed of sound which in turn determines a the proper estimation of the decompression wave speed and the required material toughness necessary to mitigate possible ductile fracture propagation. In addition, the saturation pressure (included in the VLE) is another thermodynamic parameter important in determining the decompression wave speed and therefore the minimum material toughness needed to arrest the propagation of a running shear fracture. As a prerequisite step for investigating the performance of the selected EoSs, an extensive literature analysis has performed

and here presented with focus on the selection of high-quality experimental data operative ranges related to flow assurance of CCS CO_2-rich mixtures.

4.2. Experimental datasets

In order to assess the accuracy of VLE and density prediction of the selected thermodynamic models, an extensive literature review on suitable experimental data has been conducted. Results of this analysis highlighted several high-resolution datasets that were useful for the EoSs validation process. Several datasets have been also discarded since they were not suitable for the current analysis for many reasons such as low percentage of CO_2, lack of accuracy, few data points, and aged non-digitizable data. Further refinement on the available dataset has been performed to limit the range to the scope of this work, namely the typical pressure (0 - 20 MPa) and temperature (253.15 - 313.15 K) ranges that can normally occur during CO_2 transport via pipeline. Finally, a total of 7 papers [13, 14, 16, 23, 24, 64, 184] have been selected for VLE data validation, including 20 different mixtures in terms of composition. Moreover, density prediction validation against experimental data included 7 high-quality papers, covering 27 different mixtures composition. In Table 4.1 a summary of the experimental data utilized for both VLE and density validation is reported.

In 1988, Yokohama et al. [13] performed bubble-points measurements for ternary mixtures containing H_2-CO-CO_2 from 253.15 to 303.15 K and for a pressure up to 9 MPa. The experimental procedure described by Arai et al. [186] was adopted, data have been then compared with PR EoS and Redlich-Kwong (RK). Ely et al. [184] conducted isochoric measurement of VLE for binary mixture (CO_2-N_2), temperatures from 250 to 330 K, and pressures to 34 MPa have been considered. Densities of CO_2-H_2 mixtures have been measured by Abadio and McElroy [185] in 1993 in the temperature range between 303.15 K and 343.15 K and for pressure up to 12.7 MPa; the main scope of the work was to obtain second and third virial coefficients starting from experimental results. Sanchez-Vicente et al. [17] also performed density measurements on CO_2-H_2 binary mixtures using a high-pressure vibrating-tube densitometer. Al-Siyabi [4] in his analysis on the effect of impurities, reports lot of experimental datasets including binary and ternary mixtures specifically oriented to CCUS lookalike. However, a wider range of both temperature and pressure was analysed. The effect of impurities such as O_2, N_2, Ar, CH_4 on CO_2 stream captured from power plants has been investigated by Ahmad et al. [23] through the experimental testing of binary CO_2-rich mixtures. Binary and ternary CO_2-rich mixtures have been tested by Tenorio et al. [14] in order to assess the uncertainties related to some CCS modeling processes; the study included N_2 and H_2 as impurities at different concentrations. Vapor-phase behaviour and virial coefficients have been analysed starting from density measurements by Ben Souissi et al. for CO_2-Ar [25] and CO_2-H_2 [26] binary systems. Ke et al. [24] measured VLE and densities in

Table 4.1.: Experimental datasets utilized for VLE and density validation

Authors	Year	Data type	Mixtures	Temperature range (K)	Pressure range (MPa)	Uncertainties
Yokohama et al. [13]	1988	VLE	$CO_2/H_2/CO$	253.15 - 303.15	<9	N/A
Ely et al. [184]	1989	VLE	CO_2/CH_4, CO_2/N_2	250 - 330	2.3-32	P:±0.01% T:±0.001 K
Abadio & McElroy [185]	1993	Density	CO_2/H_2	303.15 - 343.15	0.600 - 12.700	N/A
Sanchez-Vicente et al. [17]	2013	Density	CO_2/H_2	288.15 - 333.15	<23.000	T:±0.05 K; P:±0.0035 MPa
Al-Siyabi [4]	2013	Density	CO_2/N_2, CO_2/O_2, CO_2/Ar, CO_2/CO, CO_2/H_2, CO_2/CH_4	283.15 - 423.15	<50	T:±0.01 K
Ahmad et al. [23]	2014	VLE	CO_2/O_2, CO_2/N_2, CO_2/Ar, CO_2/CH_4	277.35 - 302.15	4.100–7.930	N/A
Tenorio et al. [14]	2015	VLE	CO_2/N_2, CO_2/H_2	252 - 304		N/A
Ben Souissi et al. [25]	2017	Density	CO_2/Ar	273.15 - 323.15	0.500 - 9.100	T:±0.0025 K; P:±0.0035%
Ben Souissi et al. [26]	2017	Density	CO_2/H_2	273.15 - 323.15	0.510 - 5.990	T:±0.0025 K; P:±0.0035%
Ke et al. [24]	2017	VLE and density	CO_2/Ar/N_2, CO_2/Ar/H_2 $CO_2/CH_4/N_2/H_2/O_2$/Ar/CO,	268.00 - 333.00	3.100 - 23.000	T: 0.02 K; P: 0.007 MPa
Nazeri et al. [64]	2017	VLE and density	$CO_2/N_2/O_2$/Ar, $CO_2/CH_4/C_2H_6/C_3H_8/C_4H_{10}$	273.00 - 423.00	1.000 - 126.000	T: ±0.02 K; P: ±0.02 MPa
Gimeno et al. [16]	2018	VLE and density	CO_2/SO_2	263.00 - 423.00	0.100 - 70.000	T: 0.006 K; P: 0.018 MPa

ternary mixtures, using a fibre-optic phase equilibrium analyser, two ternary systems relevant for CCS industry have been included (CO_2-Ar-N_2 and CO_2-Ar-H_2). Three multi-component CO2-rich mixtures have been tested by Nazeri et al. [64], density has been measured using an Anton Paar DMA-HPM densitometer. Compared to the other datasets, a considerable number of components, especially hydrocarbons, have been included in this study. Finally, the most accurate study on the VLE behaviour of the binary mixture CO_2-SO_2 reported in literature, has been developed by Gimeno et al. [16]. Five different concentrations have been tested in the study and accurate experimental data has been published both for VLE and density.

4.3. Thermodynamic models

4.3.1. Cubic equations of state

The most diffuse equations of state for properties prediction are classified as cubic equations of state. The cubic family of EoSs are based on a cubic dependence on the volume with two parameters, a and b; and a temperature-dependent function which can be correlated to experimental data (Vapour Pressure) [183]. In this work two cubic EoS have been considered for the analysis: the Peng-Robinson Advanced (including Peneloux volume correction) and the CPA-Infochem. SuperTRAPP model [187] has been utilized to predict the thermo-physical properties such as viscosity and thermal conductivity. Surface tension has been described with the linear gradient model theory to interfacial tension between liquid-gas and liquid-liquid phases [188]. The EoSs have been utilized as implemented in the licensed software Multiflash 7.2 by KBC. The PR EoS has been introduced in 1976 [189] as a two constant cubic equation of state, improvement with volume correction have been then introduced by other authors [189, 190]. The classic form of PR EoS is reported in Eq. (4.1) for pure compound while for mixtures, binary interaction parameters are described, k_{ij} is a symmetric binary interaction parameter that is generally a constant.

$$P = \frac{RT}{(\nu - b)} - \frac{a\ \alpha(\omega, T_R)}{(\nu(\nu + b) + b(\nu - b)} \tag{4.1}$$

$$a = \frac{(0.45724\ R^2\ T_C^2)}{P_C} \tag{4.2}$$

$$b = \frac{(0.07780\ R\ T_C)}{P_C} \tag{4.3}$$

The volume correction introduced by Peneloux [191] is useful for evaluating the liquid density where the original EoS were least successful. In addiction the PRA utilized in this work is optimized to match stored values for the liquid density and the saturated vapour pressure, and a choice of mixing rule [192]. The (Cubic-Plus-Association) CPA EoS has been presented in 1996 as results of a project financed by

Shell starting from 1995, the CPA is based on a combination of the Soave-Redlich-Kwong (SRK) equation with the association term of the Wertheim theory [193]. This equation has been included due to its large relevance and utilization in the oil and gas industry especially for fluid characterization oriented to flow assurance simulations [194]. The typical formulation of CPA for pure compounds as introduced by Kontogeorgis et al. [195] is reported in Eq. (4.4) as follow:

$$P = \frac{RT}{(\nu - b)} - \frac{a}{\nu(\nu + b)} + \frac{RT}{\nu}\rho \sum_{A} \left[\frac{1}{X^A} - \frac{1}{2}\right] \frac{\partial X^A}{\partial_\rho} \tag{4.4}$$

the mole fraction X^A of molecules not bonded at site A can be defined as per Eq. (4.5):

$$X^A = \left(1 + \rho \Sigma_B \; X^B \; \Delta^{AB}\right)^{-1} \tag{4.5}$$

The CPA EoS reported in Eq. (4.4) has five pure compound parameters, three from the physical part and two association-based parameters.

4.3.2. Non-Cubic equations of state

Non-cubic models and Equations of State have been also included in the validation process since can be relevant and led to more accurate results in some cases. The Multi-reference fluid corresponding states (CSMA), GERG-2008 (Infochem) and REFPROP® 10.0 fluid database [196] from National Institute of Standard (NIST) have been selected for this analysis. SuperTRAPP model [187] has been utilized to predict the thermo-physical properties such as viscosity and thermal conductivity. The Macleod-Sugden surface tension model [80] has been adopted for CSMA and GERG-2008 (Infochem). REFPROP 10.0 is based on the most accurate pure fluid and mixture models available in literature. Mixture calculations performed employ a model that applies mixing rules to the Helmholtz energy of the mixture components; it uses a departure function to account for the departure from ideal mixing [196, 197]. The GERG EoS was created mainly for natural gas mixtures, due to its industrial importance, a consortium of European gas companies financed the project for the development of GERG [198]. Further developments led to the GERG-2004 [199] and then to GERG-2008 [200] which is the model utilized in this work. The GERG-2008 (Infochem) EoS as implemented in the Multiflash 7.2 from KBC has been utilized for more stability. GERG-2008 (Infochem) has been extended to provide a pseudo-reference EoS for petroleum fractions or components where high-accuracy EoS are not available. With this extension, the model can be used for modelling the fluid phase behavior of light condensates containing small amounts of residuals or a mixture with some components that the high accuracy EoS are not available [192, 201]. The CSMA model is a multi-reference fluid corresponding states that also includes the GERG-2004/2008 natural gas model. This is an industry-standard high-accuracy model for mixtures of natural gas components: including hydrocarbons, but also CH_4, N_2, CO_2, Ar, O2, H_2, CO, H_2O, He, H_2S. The model includes appropriate

binary interaction parameters (BIPs) for all components available [26,34].

4.4. Vapour-Liquid equilibrium

Depending on the characteristics of the capture technology, on the type of fuel and oxidant that are used, captured CO_2 streams may contain different types and amounts of impurities [67]. As described in Section 2.2, the presence of impurities may strongly impact the thermo-physical properties of the captured CO_2 stream as well as the VLE and the density. The overall efficiency of the CCUS value chain can be impacted from the presence of certain impurities, since purification processes can be required to achieve operative condition. As widely reported in Chapter 2, corrosion and hydrate formation are real problem that should be considered during the transport of CO_2 via pipeline. The presence of other chemical compound, with different concentrations, can impact the thermo-fluid dynamic of the entire system. Moreover, while the accurate description of CO_2 properties is almost fully covered by the Span-Wagner EoS [181], for CO_2-rich mixtures, more uncertainties can be noted. VLE and density are the main aspects investigated in this chapter since their impact is strong and can affect the pipeline design, including safe operating condition definition, corrosion risk, running ductile fracture, pipeline thickness and both CAPEX and OPEX. Vapour-Liquid-Equilibrium is usually measured trough experimental activities with an equilibrium cell. A common experimental setup usually includes an equilibrium cell, one or more thermostatic baths, pressure and temperature transducer, a gas-chromatograph is connected to the samplers for the sample analysis.

The setup reported in Figure 4.1, described by Westman et al. [12] was built as part of the CO_2Mix project, is a typical configuration of a VLE measurement apparatus. In the experiment conducted, the VLE has been measured using an isothermal analytical method with a variable-volume cell, the control of the setup is ensured trough a LabView control panel.

In this work, the accuracy of VLE prediction as calculated by the tested models have been assessed through a direct comparison of the results. Since the dew-point line prediction was generally good for all the tested models, a specific focus has been reserved to bubble-point line prediction. Indeed, the bubble-point line is notably a more important parameter for the design of CO_2 pipelines since it can be considered one of the driving parameters for the running shear fracture prediction. Experimental datasets have been compared with EoS prediction through a series of simulations performed both with Multiflash 7.2 and REFPROP. Differences in density prediction as well as VLE description have been highlighted, results have been analyzed numerically. Phase-envelope in p-T diagrams have been plotted, continuous lines are relative to EoS predictions while scatters are relative to experimental data available measured at different points. Since a high number of similar compositions at different concentrations have been analyzed for VLE, the most important results

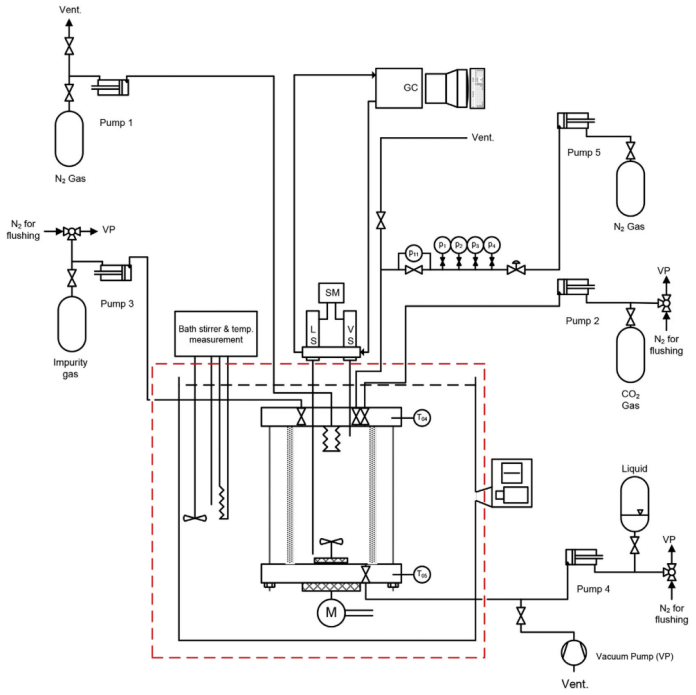

Figure 4.1.: Principal diagram of cell apparatus for the VLE measurement built for the CO_2mix project (Reproduced from [12])

have been reported graphically in this section (Figure 4.2-4.7), while in the complete collection of the results has been reported in Appendix A.

To numerically define the deviation of the prediction from the experimental datasets, an interpolation analysis has been done. Since pressure is the main parameter of interest for the bubble point accuracy prediction, isotherm have been assumed for each point and the relative deviation from the experimental measured point has been calculated. As reported in Table 4.2, this analysis was useful to estimate which prediction led to over-estimation of measured bubble points or under-estimation of them. The Average Deviation (AD - %) parameter has been calculated on bubble point pressure as indicated in Eq. (4.6) for each point at fixed temperature:

$$AD\ (\%) = \frac{p_{model} - p_{exp}}{p_{model}} \times 100 \tag{4.6}$$

Since the results are not absolute values, it can be clearly observed that negative values correspond to under-estimation of experimental data while positive values to an over-estimation of them. Dew point line is generally well predicted in most cases from all tested EoSs while bubble points line prediction seems to be more sensitive to composition and concentrations of other compounds. Based on results reported in Table 4.2 it should be noted that the highest AD ($\geq \pm 10\%$) occurred for GERG-2008 model were in presence of O_2, while for CPA EoS when H_2 was present. An AD $\geq \pm 10\%$ occurs more frequently on GERG and CPA, while an AD between $\pm$ 5% and $\pm$ 10% occurs most frequently for REFPROP and PRA. Finally, based on

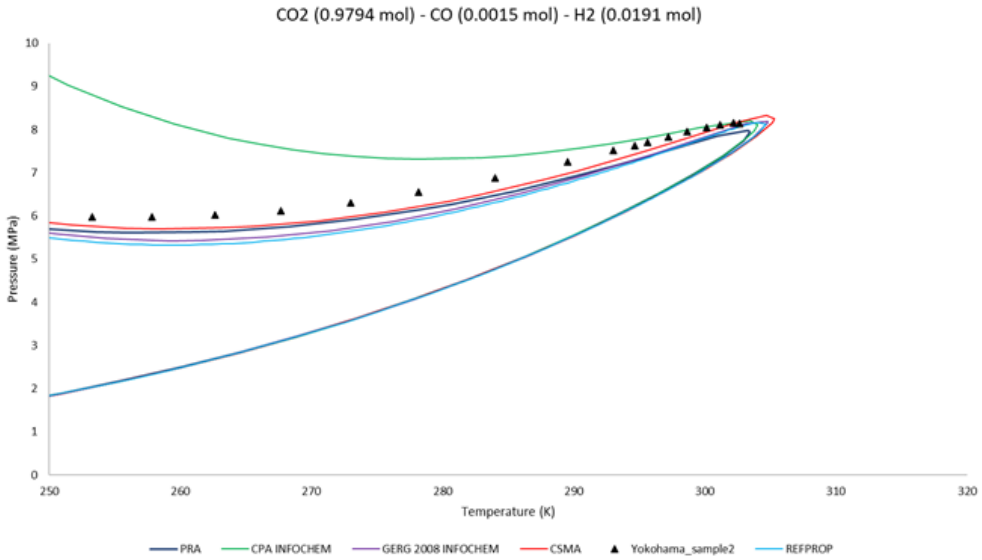

Figure 4.2.: Phase envelope for CO_2-CO-H_2 ternary mixture, experimental data from Yokohama et al. [13] vs models.

the analysed cases, an AD $\leq \pm$ 5% occurred mostly for CSMA model. Indeed, on 73% of cases, the AD was $\leq \pm$ 5% showing a more accurate bubble point prediction.

An unweighted mean value (UM) of the calculated AD, reported in Table 4.2, has been calculated. The results shows that PRA and REFPROP give an avg. under-estimation of respectively 2.6% and 1.2%. An avg. over-estimation has been registered for CPA-Infochem, GERG-2008 Infochem and CMSA of respectively 2.4%, 0.8% and 1.2%. However, it should be noted that the number of data points can impact the averaged values. For this reason, a weighted average mean (WAM) value has been calculated with the Eq. (4.7) based on the results.

$$UM = \frac{\sum_{i=1}^{n} x_i}{n} \tag{4.7}$$

$$WAM = \frac{\sum_{i=1}^{n} w_i x_i}{\sum_{i=1}^{n} w_i} \tag{4.8}$$

where for each of "i" case from 1 to "n": w_i = weight (number of experimental points), x_i = AD (%).

As expected, the WAM gives different results since the datasets were very different in term of number of datapoints. In Table 4.3 the calculated value for UM and WAM are reported. It can be highlighted that GERG-2008 (Infochem) and CSMA show a different outcome, the WAM values are negative, it means there is a tendency to under-estimation. The WAM also increase the uncertainties of the over-estimation addressed to PRA and CPA-Infochem models. As a major conclusion it could be again noted that the CSMA model led to the most accurate results for UM value and even better if WAM if considered.

Table 4.2.: VLE deviation from measured experimental datasets, mean AD (%) considered.

			Bubble point exp. data	AD (%)				
Author	CO_2 content	Other components	n° exp. points	PRA	CPA INFOCHEM	GERG INFOCHEM	CSMA	REFPROP
Yokohama et al. [13]	98.96%	CO (0.07%)+H_2 (0.97%)	20	-3.57	4.34	-4.28	-2.69	-4.82
Ke et al. [24]	98.00%	Ar (1%)+N_2 (1%)	13	-3.09	-3.17	-0.03	N/A	0.22
Ahmad et al. [23]	98.00%	CH_4 (2%)	6	0.40	0.20	1.34	1.29	N/A
Tenorio et al. [14]	97.99%	N_2 (2.01%)	8	-0.40	-0.59	1.45	0.31	1.46
Yokohama et al. [13]	97.94%	CO (0.15%)+H_2 (1.91%)	17	-5.05	8.50	-5.95	-3.13	-7.02
Ahmad et al. [23]	97.50%	Ar (2.50%)	6	-0.39	-0.34	4.51	5.64	N/A
Ahmad et al. [23]	97.50%	O_2 (2.5%)	6	-0.28	-0.24	10.31	5.77	5.19
Ahmad et al. [23]	97.50%	N_2 (2.5%)	5	7.10	6.81	9.52	8.46	9.54
Tenorio et al. [14]	97.00%	H_2 (3%)	18	-6.00	12.40	-7.92	-4.23	-8.35
Yokohama et al. [13]	96.55%	CO (0.25%)+H_2 (3.20%)	15	-5.91	12.11	-6.62	-3.07	-7.98
Tenorio et al. [14]	96.01%	N_2 (3.99%)	19	-1.46	-1.60	1.15	0.26	1.19
Gimeno et al. [16]	95.32%	SO_2 (4.68%)	4	0.09	0.20	0.47	0.15	0.15
Tenorio et al. [14]	95.01%	H_2 (4.99%)	19	-7.38	14.49	-9.08	-4.16	-9.82
Tenorio et al. [14]	95.00%	N_2 (2%)+H_2 (3%)	19	-4.89	6.70	-5.46	-1.80	-5.68
Ke et al. [24]	95.00%	Ar (2%)+H_2 (3%)	12	-9.09	6.10	-7.68	-3.27	-8.40
Ahmad et al. [23]	95.00%	CH_4 (5%)	5	1.22	0.83	2.78	2.69	N/A
Ahmad et al. [23]	95.00%	O_2 (5%)	5	-6.07	-5.98	11.94	4.61	3.36
Ahmad et al. [23]	94.50%	Ar (5.50%)	6	-6.41	-6.30	3.26	5.40	N/A
Ahmad et al. [23]	94.50%	N_2 (5.5%)	5	2.94	2.72	4.89	6.32	4.75
Tenorio et al. [14]	93.00%	N_2 (4%)+H_2 (3%)	17	-4.42	10.63	-5.38	-1.73	-5.68
Ke et al.	90.00%	Ar (5%)+N_2 (5%)	11	-6.90	-6.87	1.06	N/A	-0.31
Chapoy et al. [15]	89.83%	O_2 (5.05%)+Ar (2.05%)+N_2 (3.07%)	5	-0.49	-0.06	18.64	12.93	10.41
Gimeno et al. [16]	89.69%	SO_2 (10.31%)	4	-1.04	-0.83	-0.30	-1.01	-1.07
Gimeno et al. [16]	80.29%	SO_2 (19.71%)	4	-1.81	-1.40	-0.22	-1.75	-1.55

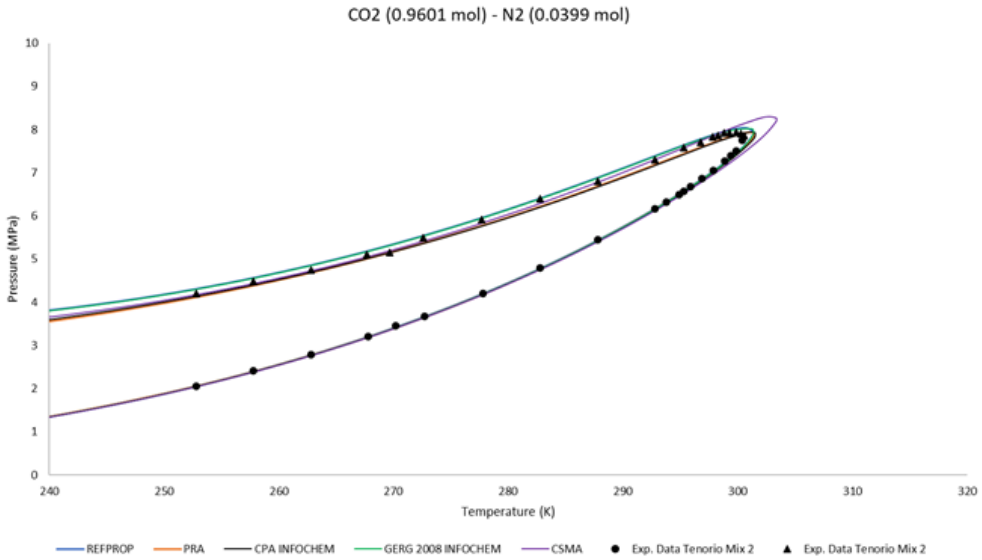

Figure 4.3.: Phase envelope for CO_2-N_2 binary mixture, experimental data from Tenorio et al. [14] vs models.

Table 4.3.: UM and WAM calculated on Table 4.2 results.

	PRA	CPA-Infochem	GERG-2008 (Infochem)	CSMA	REFPROP
UM	2.6%	2.4%	0.8%	1.2%	-1.2%
WAM	3.8%	4.5%	-2.0%	-0.5%	-3.1%

4.5. Density

Density prediction results of tested models have been summarized in this subsection. As already described for VLE, a similar procedure has been adopted, experimental datasets have been validated with models results for each measured point available. This has been achieved through multi-flash p-T simulations at given conditions. Composition, concentrations, pressure, and temperature from the experimental datasets were utilized as input parameters, density calculated value were considered as main output results. A visual representation of the location of measured points from datasets have been also provided in comparison with VLE prediction of each tested model. This was useful to assess if the prediction deviation was originated by a model lack of accuracy or if the phase was wrongly predicted due to major deviation in VLE prediction.

An example of wrong density prediction that can be addressed to bad VLE description can be found in Figure 4.8. Indeed, the phase-envelope of both CPA-Infochem and REFPROP near the critical point, include many densities measured points inside the two-phase fluid zone, this according to Table 4.5, will results in a major AAD of 6.55 % and 11.02 % respectively. Moreover, since the problem do not seem evident for smaller concentration of H_2 (see Figure 4.9 and Figure 4.10),

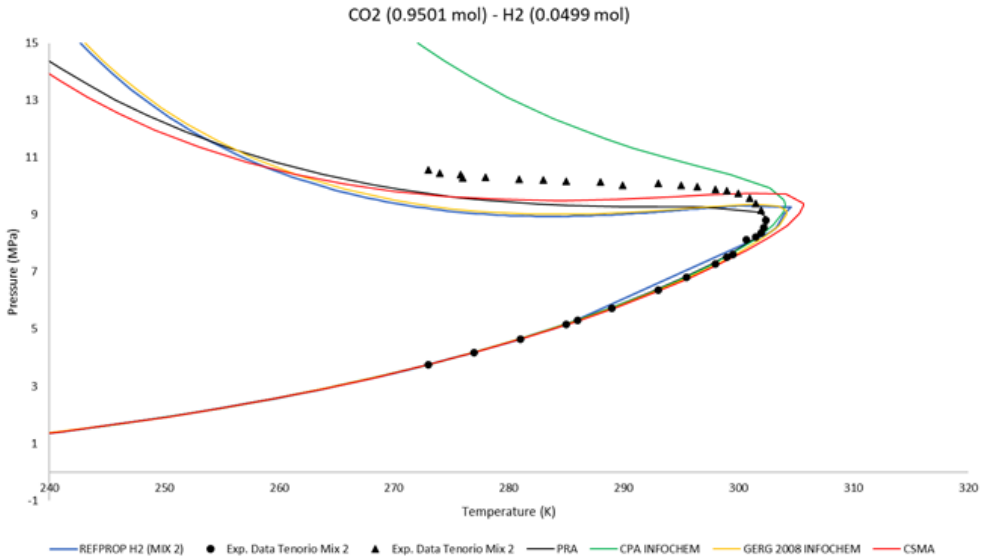

Figure 4.4.: Phase envelope for CO_2-H_2 binary mixture, experimental data from Tenorio et al. [14] vs models.

a less accurate density prediction can be expected if the hydrogen concentration increases for that models. Following the simulation of every point of the datasets, an analysis has been conducted in term of Average Absolute Deviation (AAD - %) in order to analytically define the accuracy of each tested model. The AAD have been calculated as described in Eq. (4.9):

$$AAD\ (\%) = \frac{\rho_{exp} - \rho_{model}}{\rho_{exp}} \times 100 \tag{4.9}$$

Table 4.4.: UM and WAM calculated on Table 4.5 results.

	CSMA	GERG-2008 (Infochem)	PRA	CPA-Infochem	REFPROP
UM	1.32	1.08	2.32	3.18	2.60
WAM	1.38	1.18	2.57	3.82	3.03

In Table 4.4, the results from the AAD analysis have been summarized, the mean value of AAD calculated for each dataset have been reported. However, it should be noted that the number of data points and the different ranges of experimental datasets in term of pressure and temperature can impact the averaged values. Thanks to this analysis is still possible to obtain some indications of which model perform generally better than others in density prediction giving p-T values as input.

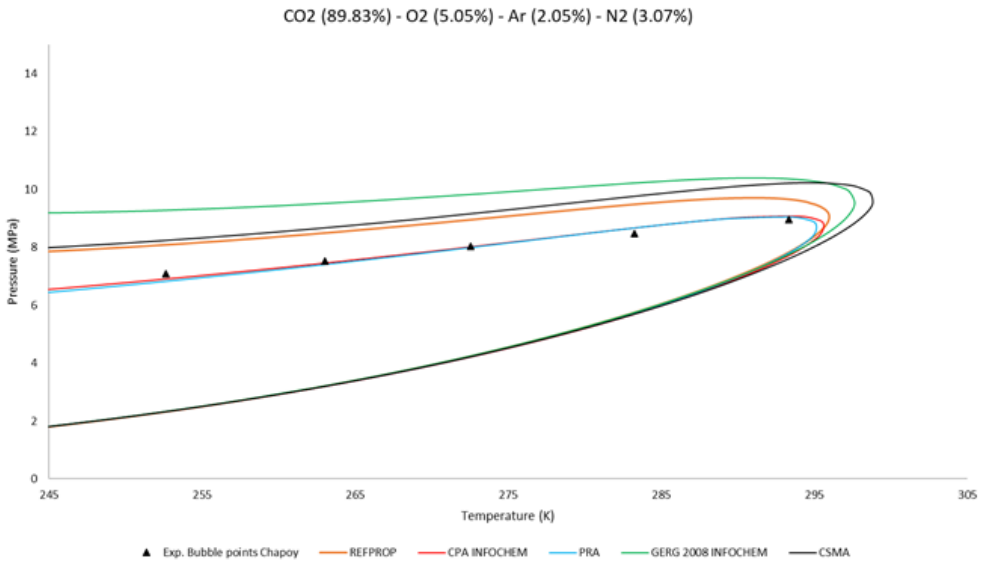

Figure 4.5.: Phase envelope for 4-elements mixture, experimental data from Chapoy et al. [15] vs models.

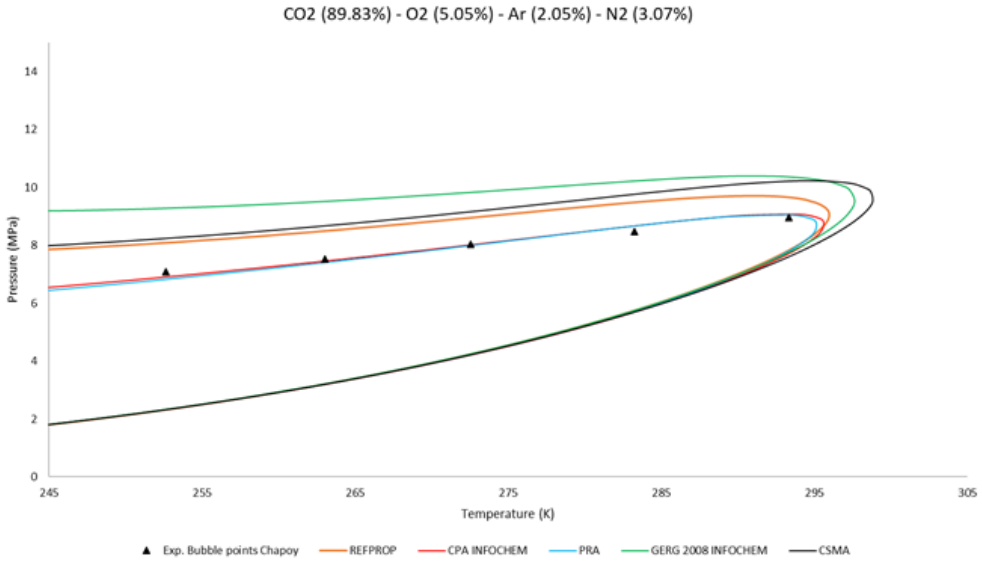

Figure 4.6.: Phase envelope for CO_2-N_2-H_2 ternary mixture, experimental data from Tenorio et al. [14] vs models.

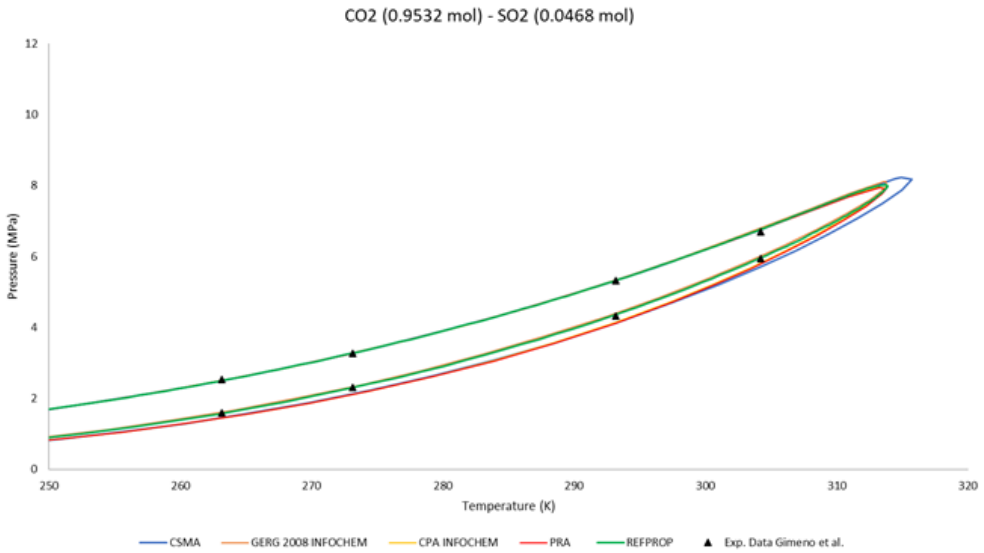

Figure 4.7.: Phase envelope for CO_2-SO_2 binary mixture, experimental data from Gimeno et al. [16] vs models.

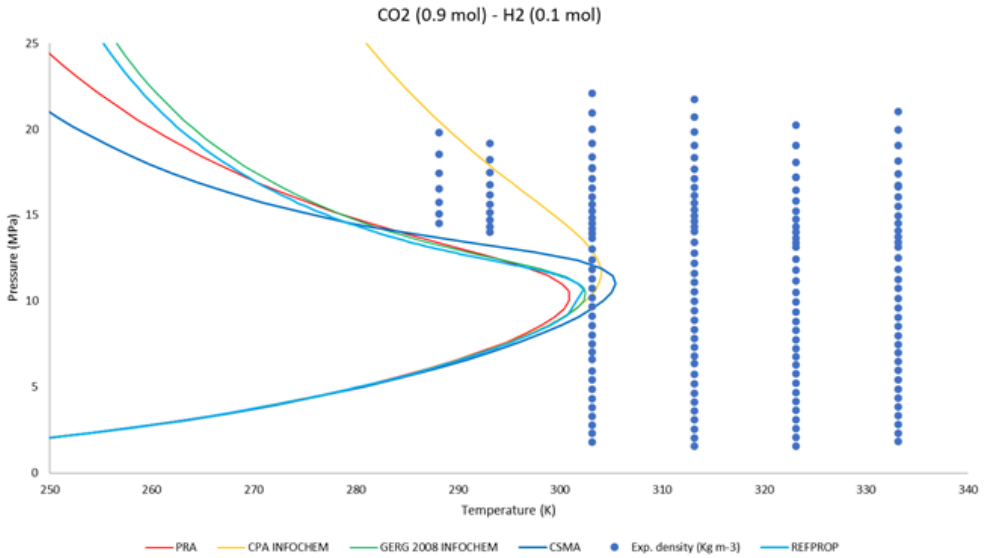

Figure 4.8.: VLE prediction and measured density p-T coordinates from Sanchez-Vicente et al. [17] for CO_2-H_2 binary mixture.

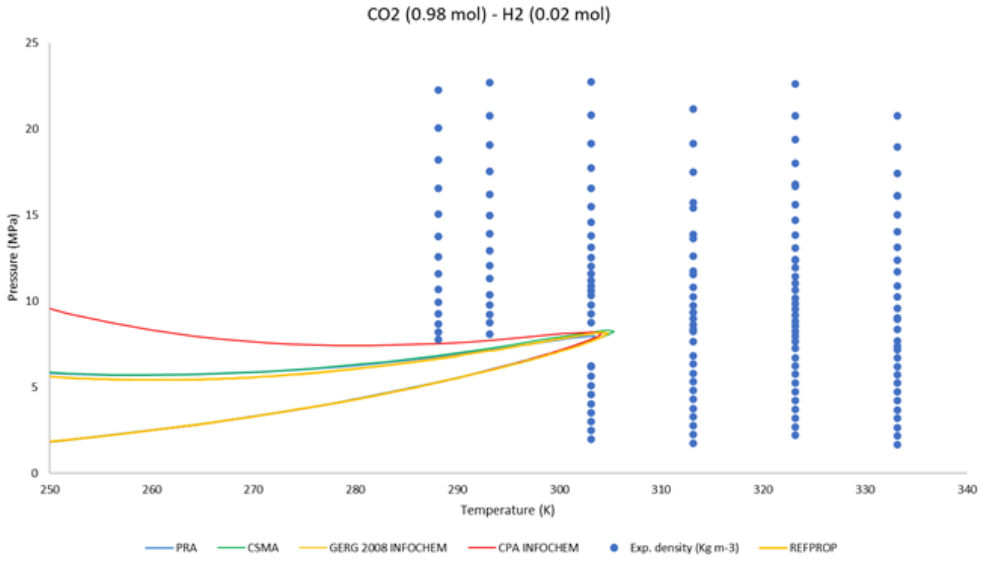

Figure 4.9.: VLE prediction and measured density p-T coordinates from Sanchez-Vicente et al. [17] for CO_2-H_2 binary mixture.

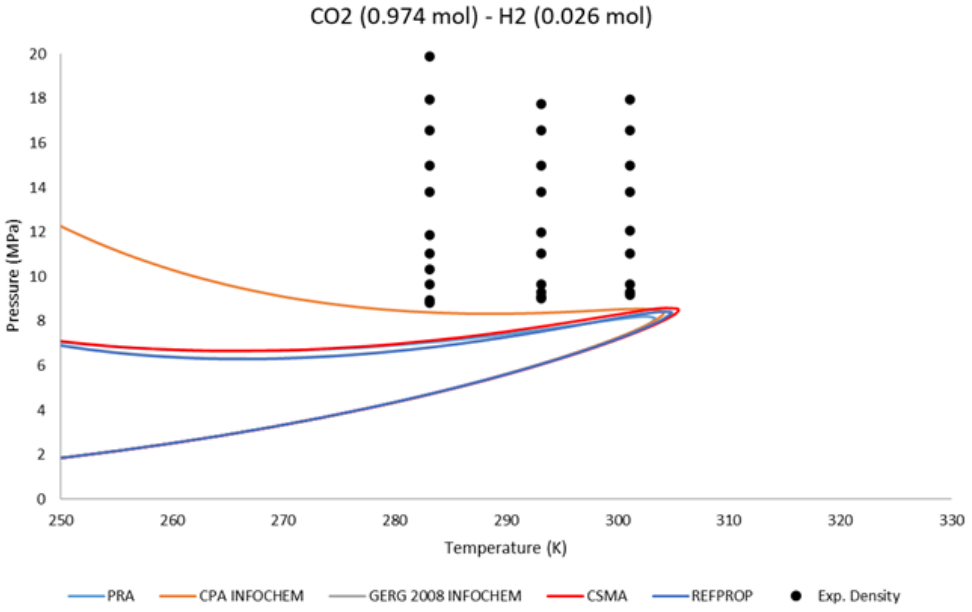

Figure 4.10.: VLE prediction and measured density p-T coordinates from Al-Siyabi for CO_2-H_2 [4] binary mixture

Ref.	Year	Mixture	n°points	Mean AAD %				
				CSMA	GERG2008 (INFOCHEM)	PRA	CPA-INFOCHEM	REFPROP
[185]	**1993**	CO_2 (0.5093) + H_2 (0.4903) + N_2 (0.0002)	13	0.76	0.19	1.16	1.48	0.19
		CO_2 (0.5672) + H_2 (0.4324) + N_2 (0.0002)	11	0.82	0.09	1.19	1.66	0.10
		CO_2 (0.6181) + H_2 (0.3813) + N_2 (0.0002) + O_2 (0.0001)	11	0.78	0.23	1.24	1.41	0.26
		CO_2 (0.6005) + H_2 (0.3991) + N_2 (0.0002)	9	1.14	0.28	1.57	1.83	0.31
		CO_2 (0.6446) + H_2 (0.3550) + N_2 (0.0002)	9	0.93	0.31	1.47	1.61	0.34
[4]	**2013**	CO_2 (0.941) + CH_4 (0.059)	50	1.44	1.92	3.38	4.54	1.93
		CO_2 (0.954) + N_2 (0.046)	45	0.46	0.08	2.00	2.73	0.07
		CO_2 (0.950) + Ar (0.050)	71	1.19	1.20	2.67	3.60	1.53
		CO_2 (0.941) + CO (0.059)	49	2.86	2.91	2.89	4.00	2.06
		CO_2 (0.950) + O_2 (0.050)	72	1.01	0.67	1.78	2.23	0.95
		CO_2 (0.974) + H_2 (0.026)	30	3.93	2.59	1.05	4.23	2.59
		CO_2 (0.950) + H_2 (0.05)	66	2.27	3.67	3.51	5.95	3.65
		CO_2 (0.956) + CH_4 (0.0067) + H_2 (0.0082) + N_2 (0.0141) + CO (0.0021) + Ar (0.0121) + O_2 (0.0008)	55	1.20	1.08	2.02	2.79	31.01
[17]	**2014**	CO_2 (0.9) + H_2 (0.1)	165	2.55	1.82	3.20	6.55	11.02
		CO_2 (0.925) + H_2 (0.075)	169	2.25	1.69	3.17	5.98	2.74
		CO_2 (0.98) + H_2 (0.02)	154	0.59	0.56	3.75	5.32	0.57
[25]	**2017**	CO_2 (0.5) + Ar (0.5)	21	0.34	0.08	1.96	0.82	0.01
		CO_2 (0.75) + Ar (0.25)	36	1.04	0.60	2.40	1.02	0.08
[26]	**2017**	CO_2 (0.94638) + H_2 (0.05362)	19	0.14	0.09	0.93	0.25	0.10
[24]	**2017**	CO_2 (0.9) + N_2 (0.05) + Ar (0.05)	143	1.30	0.59	2.21	3.18	0.55
		CO2 (0.9045) + N2 (0.0955)	32	1.14	0.69	3.27	4.20	0.69
[64]	**2017**	CO_2 (0.956437) + CH_4 (0.006261) + N_2 (0.0141) + H_2 (0.008175) + O_2 (0.0008) + Ar (0.0121) + CO (0.002127)	63	1.44	1.46	3.17	3.88	1.43
		CO_2 (0.8983) + N_2 (0.0505) + O_2 (0.0307) + Ar (0.0205)	43	1.40	1.45	3.15	4.20	1.47
		CO_2 (0.6999) + CH_4 (0.2002) + ETHANE (0.06612) + PROPANE (0.0258) + N-BUTANE (0.003997) + I-BUTANE (0.003998)	49	1.63	2.24	3.36	4.04	2.23
[16]	**2018**	CO_2 (0.8029) + SO_2 (0.1971)	200	1.83	1.40	1.86	1.88	2.37
		CO_2 (0.9532) + SO_2 (0.0468)	200	0.76	0.87	2.00	3.15	1.52
		CO_2 (0.9931) + SO_2 (0.0069)	200	0.30	0.29	2.34	3.43	0.39

Table 4.5.: Density deviation from measured experimental datasets, mean AAD (%) considered.

According to the results reported in table, the maximum mean values of AAD have been registered for the binary mixture containing 0.1 mol of H_2. The major deviation of AAD = 31.01 % reported for REFPROP in a 7-elements mixture can be mainly addressed to bad convergence of the software, therefore the VLE was wrongly described, with a direct impact on phase prediction and consequently density calculation. A mean AAD $\geq$ 5% was registered for CPA and REFPROP models only, while mean AAD values $\leq$ 1% were more frequent in GERG 2008, REFPROP and CSMA respectively. It can be stated that, based on the analysed data, most of mean AAD values for cubic equations (CPA and PRA) were between 1 and 2%. Following the same methodology reported for the VLE analysis, the UM and WAM have been calculated with Eq. (4.7) and (4.8). Results from the UM and WAM calculation shows how the PRA and CPA-Infochem give in general more accurate results in density prediction, based on the analysed datasets. Difference between UM and WAM is not as large as the VLE analysis since the datasets considered for density are in general denser, with the only exception of old data from 1993 from Abadio and McElroy [185].

4.6. Conclusions

The EoSs accuracy is a matter of great interest in the CCS industry and for CO_2 processing, particularly for VLE and density predictions. A large deviation between experimental and prediction can lead to high uncertainties on the design and sizing of pipelines, separators, vessels with great impact on costs too. In this chapter, several EoSs have been tested against high-quality experimental data published in literature. Density measurements have been considered as well as VLE including bubble point and dew point measurements. The accuracy of the tested EoSs has been assessed through the evaluation of quantitative parameters such as AD and WAM for density and bubble point prediction. Results show that CSMA and GERG-2008 (Infochem) gave in general more accurate results in density prediction, the WAM for CSMA and GERG-2008 (Infochem) were both around 1%. However, it should be considered that not all experimental datasets included measurements in the supercritical phase. Results for bubble points validation shows how large differences can be highlighted based on CO_2 and impurities concentrations. Notably, as reported in Section 4.3, larger uncertainties have been found when H_2 was present. The best average performances for bubble point predictions have been registered for CSMA and GERG-2008 (Infochem) models, with an average under-estimation. More conservative results have been obtained for Cubic EoSs such as PRA and CPA with an average over-estimation up to 4.5%. This chapter provides quantitative data on the accuracy for CCS applications of existing EoSs commonly utilized in the energy industry. The presented results provide the indication of main bias, uncertainties and trends related to the accuracy of different EoSs in estimating the VLE and the density of rich-CO_2 mixtures. Of course, further experimental measurements for

both VLE and density are needed since there are not enough data to fully validate thermodynamic models with CO_2 mixtures with a number of components equal or higher than 5.

Chapter 5.

Transient Flow-Assurance modelling of CO_2

5.1. Introduction

Flow Assurance plays a key role in both design and operation of pipelines for anthropogenic CO_2 transport to Carbon Capture & Storage (CCS) injection wells. Proper modelling of thermodynamic properties of CO_2 streams containing impurities, as well as of the relevant fluid dynamics, are of vital importance for a safe, reliable, and cost-effective design and for a flexible operation of CCS pipelines as they significantly affect the operating conditions to assure a single-phase flow and to handle varying amounts and quality of CO_2 produced by different sources, water solubility, corrosion, ductile fracture propagation and integrity, safety, processing, hydrates formation, and metallurgical issues. In general, existing flow models and tools were developed for other fluids, and may not be accurate for CO_2 and CO_2-rich mixtures. In this chapter, the transportation via pipeline of CO_2 has been deeply analysed in both horizontal and vertical conditions. The horizontal depressurization phenomena has been studied trough the analysis of experimental data available in literature, then numerical models have been utilized for the validation and the simulation of the transient of the phenomena. Furthermore, the vertical transport has been studied trough an experimental campaign performed in a high-quality laboratory based in Norway. Finally, a new code for the simulation of transient decompression of mixtures, specifically designed for CO_2-rich mixtures has been presented in section 5.4.

5.2. Horizontal depressurization

Transient operations in Flow Assurance are notably the most interesting and hard to predict phenomena. Since steady-state conditions involve an equilibrium state where most of the equation can be directly solved with an exact solution, for transient events, this assumption is not always verified. As reported in the previous chapters (see 2 and 4) the accurate prediction of CO_2 properties is not easy to reach, especially in presence of impurities. When considering transient operation, such as depressurization, start-

up, emergency blow-down, the uncertainties in the prediction of the thermo-physical properties are even higher. In this section the horizontal depressurization of a CO_2 pipeline has been studied trough the analysis of high-accuracy experimental data and with a commercial numerical code. In the scenarios analysed, pure-CO_2 has been considered since plus a reference case with pure N_2. The main focuses in the horizontal depressurization test are the pressure-wave propagation and the low temperatures reached. These experiments are relevant for the prediction of running-ductile fracture (RDF), where a defect in the pipeline develops into a crack running along the pipeline. As reported in Chapter 3 the results of this rupture can be dangerous, both for people nearby and for gas release. The fracture can run for hundreds meters before it stops, if that happen, the release can be very rapid and lot of CO_2 in gaseous form is released in the atmosphere (see 3.10 and 3.11). The depressurization implication on the expansion wave and the ductile fracture propagation has been discussed more in section 5.4. When dealing with horizontal pipes the fluid regime should be accurately considered, indeed a two-phase fluid can form and it can have different characteristics. These can severely impact the measurements of sensors and the accuracy of the models. In Figure 5.1 the most common type of horizontal flows are reported, the stratified flow has the strongest tendency to occur in downhill or horizontal flow with relatively small gas and liquid flow rates. The depressurization process studied in this work start with single-phase fluid, however the possibility to have two-phase fluid transient condition during the process should be taken into account. Indeed, this can cause wrong measurements from temperature sensors and also introduce uncertainties during validation.

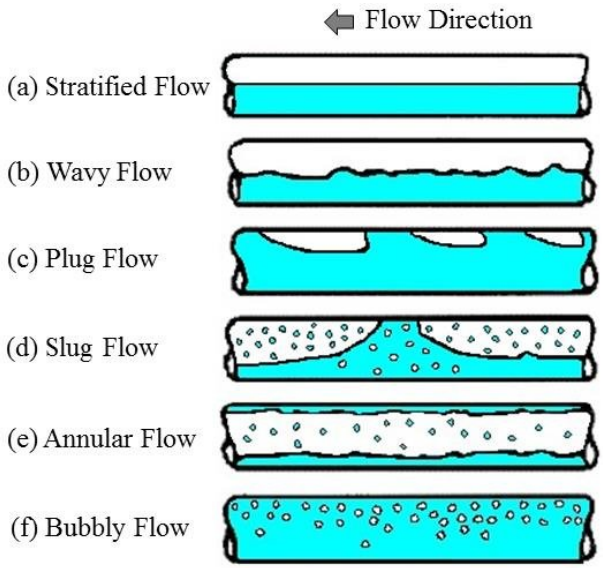

Figure 5.1.: Gas-liquid flow regimes in horizontal pipes [18].

5.2.1. Experimental data

In order to validate and compare model against experimental data, the accuracy of the measurement should be ensured. A literature review trough the existing databases has been conducted in order to identify the most suitable, updated and accurate data for the purpose. Main scope of this chapter as previously outlined, is the numerical modelling of transient operations involving high-pressure CO_2 in pipeline. In this section the horizontal depressurization of a CO_2 pipeline has been investigated. There are not so many data-sets available in literature so far, moreover it is very difficult to obtain accurate data from full-scale operating pipelines. The main reason is the few number of CO_2 pipeline currently operating, furthermore, to obtain accurate and high-resolution data it is necessary to equip the pipe with lot of instruments such as pressure and temperature sensors. Since the transient behaviour can be very different depending on starting conditions, multiple cases should be analysed. In particular, depressurization from gas phase and dense-phase can be strongly different from each other, with more uncertainties for the modelling. The experimental data published from Munkejord et al. [19] in 2020, has been utilized for the horizontal depressurization. The experimental campaign has been conducted in the ECCSEL ERIC depressurization facility in Trondheim (NO) by SINTEF Energy Research. The facility was specifically built for experiments related to CO_2 and CO_2-rich depressurization, the pipe is 61.67 m long with an inner diameter of 40.8 mm and outer diameter of 48.3 mm. The main construction details relevant for this analysis are reported in Table 5.1.

Table 5.1.: Specifications of ECCSEL ERIC Depress test section [19].

Parameter	Value
Pipe inner diameter	40.8 mm
Pipe outer diameter	48.3 mm
Pipe length at 25 °C	61.668 m
Pipe material	SS316, EN 1.4401 Properties at 20°C: density 8000 kg m^{-3}, thermal conductivity 15 W m^{-1} K^{-1} , specific heat 500 J kg^{-1} K^{-1}
Pipe surface roughness	Ra 0.2–0.3 μm
Insulation layer thickness	60 mm
Insulation layer material	Glass wool Properties: density 75 kg m^{-3}, thermal conductivity 0.032 W m^{-1} K^{-1} , specific heat 840 J kg^{-1} K^{-1}

The facility is composed by a test section with heat tracing, a rupture disk, a gas supply system, two-stage compression with a cooling aggregate, and a heater. The ECCSEL ERIC process scheme including the main equipment is reported in

Figure 5.2. The test section is fully instrumented with 16 fast-response pressure transducers Kulite CTL-190(M) type, while for temperature measurements: 23 Type E thermocouples are installed for the measurement of the fluid temperature, 11 are placed at axial positions together with pressure sensors on opposite sides of the pipe and 12 are installed at the top, bottom and side of the pipe at four locations in order to capture any stratification of the flow as described by Munkejord et al. [19]. In Figure 5.3 a sketch of the test section with the instrumentation and their relative position is reported. The rupture disk is positioned on the left end of the 61.67 m long pipe, the number of sensor is denser around the outlet while it become sparser far from there. This because the first section is the most challenging to measure during a depressurization experiment, indeed the decompression is very rapid as well as the pressure drop, especially in the first 1-2 seconds.

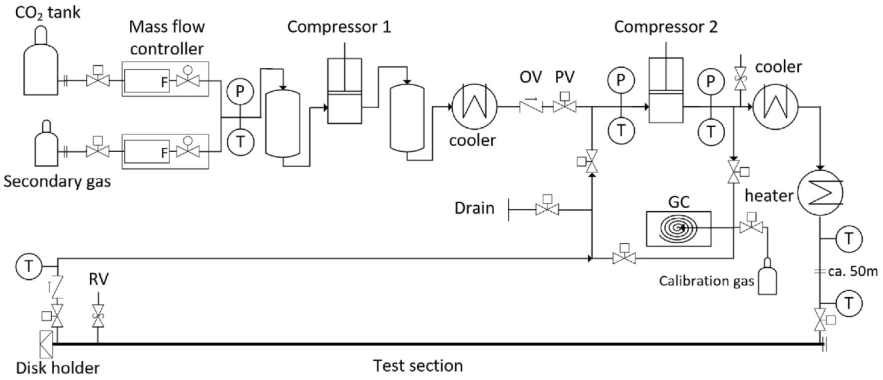

Figure 5.2.: ECCSEL ERIC Depress facility [19].

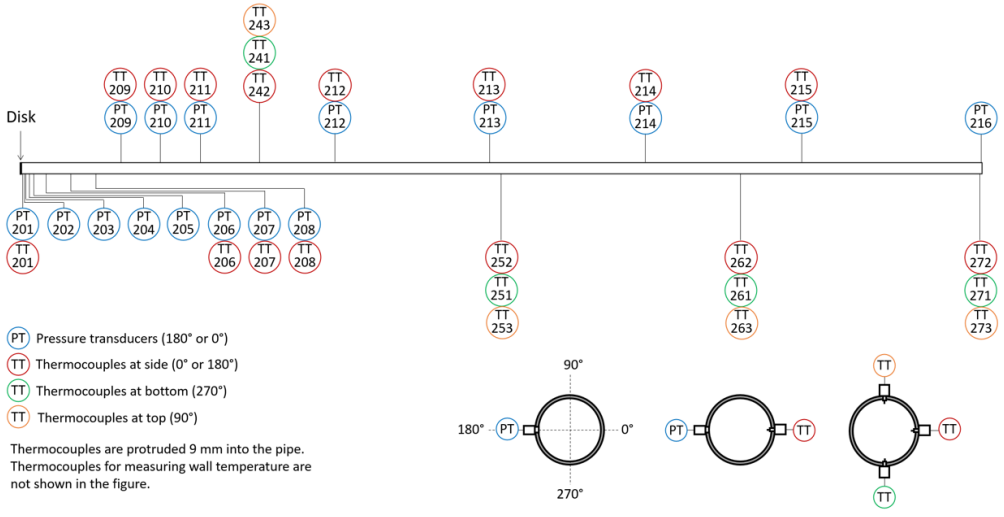

Figure 5.3.: ECCSEL ERIC Depress - test section with instrumentation [19].

In the work considered as reported so far, a total of 5 different tests have been reported. In Table 5.2 a summary of the tests considered is presented. Four tests

have been performed with pure CO_2 at different steady-state conditions in term of temperature and pressure, while a single test has been performed with N_2, the authors outlined that it was performed as a reference case to test another simulation code. The first four tests, namely number 3, 4, 6, 8 have been designed similarly, the main difference lays in the steady-state (starting) pressure. Test 4 and 8 have been conducted at very similar conditions for repeatability of the measurements. Indeed, minor differences can be found in temperature, while pressure drives the starting phase condition of the CO_2. Test 3 start from a relatively low pressure of 4.05 Mpa (40.4 bar) and a temperature of 283.35 K (10.2 °C), which means that the CO_2 is in gas phase. The other tests (4, 6, 8) are executed starting from a dense-phase (liquid CO_2), at different conditions. This because the phase transition from liquid to gas during a rapid transient is the most important and challenging part to correctly predict with a simulator. For this reason the focus of the experimental campaign was reserved to dense-phase decompression scenarios and only a single test has been performed starting from gas phase. As reported in Table 5.2 the highest pressure tested is for the test 4, while the highest temperature is reported for test 6. The ambient temperature should have a limited impact on the phenomena for two main reasons: the process is very rapid and the good insulation of the pipe, the temperature impact should be limited but not negligible.

Table 5.2.: Tests considered and main experimental conditions [19].

Test no.	Fluid	Pressure (MPa)	Temperature (°C)	T_{amb} (°C)
3	CO_2	4.04	10.2	4
4	CO_2	12.54	21.1	22
6	CO_2	10.4	40	6
8	CO_2	12.22	24.6	9
11	N_2	5.13	10	9

For this experiments, the author equipped the test pipe with a rupture disk in order to simulate the sudden rupture at a fixed pressure. The disk type Fike SCRD-BT-FSR was utilized for these tests. The burst tolerance was ensured within $\leq$5% from the vendor. The experimental campaign procedure for each test is mainly composed from few steps. Once the rupture disk is equipped on the test section, pressurization of the system with CO_2 starts. When the pressure reach a value of 70% of the test pressure (see Table 5.2), re-circulation start in order to achieve a precise and stable value of pressure. Temperature and pressure near the target are controlled trough bypass and heater/cooler, in order to obtain stable values. When the pressure reach the target, the rupture disk is triggered and the sudden depressurization of the test section starts. When the depressurization starts, two pneumatic valves automatically close to stop re-circulation.

Results obtained from the measurements of thermocouples and pressure transducers have been published with a high-resolution. An elaboration of this data have been

Table 5.3.: Density and thermal properties of the test section materials.

	Density (kg m^{-3})	Thermal Conductivity (W m^{-1} K^{-1})	Specific Heat (J kg^{-1} K^{-1})
Pipe steel	8000	15	500
Insulation layer	75	0.032	840

conducted and the plot of main sensors is presented in this section. Starting from Test 3 (see Table 5.2), the results obtained from thermocouples are presented in Figure 5.4 for the sensors close to the outlet for the first 20 s.

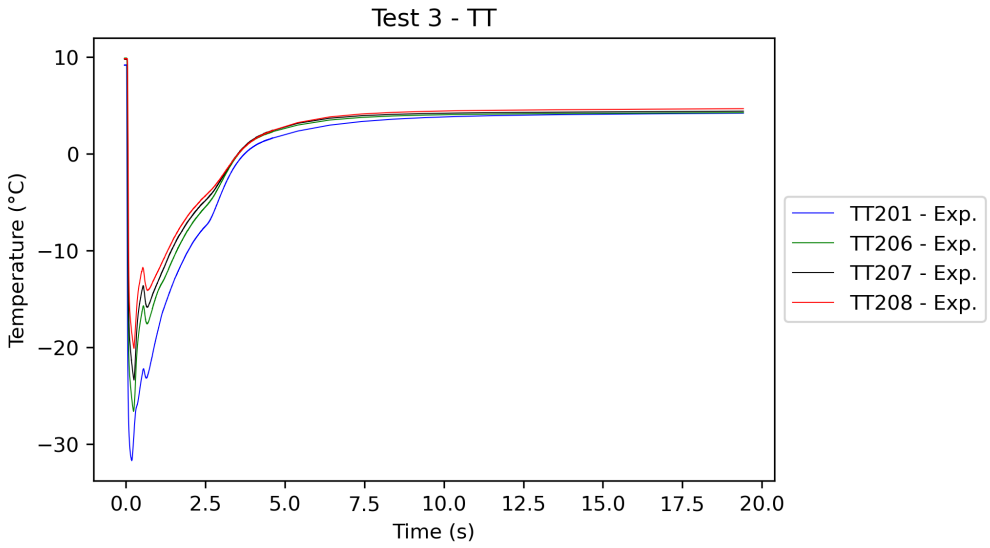

Figure 5.4.: Test 3 - Experimental data for TT sensors close to the outlet.

In Figure 5.4 it is clearly visible how the temperature rapidly decrease due to decompression and consequent expansion of the gas. A minimum temperature close to -30 °C is recorded for the sensor TT201 while the temperature decrease effect is notably lower for the other sensors far from the rupture disk. The temperature reach than the equilibrium after 10 s from the disk opening. Munkejord et al. [19] noted that the results from sensors close to the outlet (PT201, TT201) passes and deviates from the liquid-gas saturation curve in the first 0.06 s. It can be stated that a high uncertainties can be registered in the first few seconds due to non-equilibrium transient conditions. This is true especially for the sensors close to the outlet. Indeed, also in this case, that was initially in a gaseous phase (Test 3) a phase transition during decompression has been observed, accoring to results.

Test 4 has been conducted starting from a higher pressure (12.54 Mpa) at 21.1 °C, at this conditions, the CO_2 is in dense-phase, meaning that it looks like a liquid phase also in term of density, but its viscosity is closer to a gas-phase condition. As expected, starting from this conditions, the decompression phenomena is stronger and

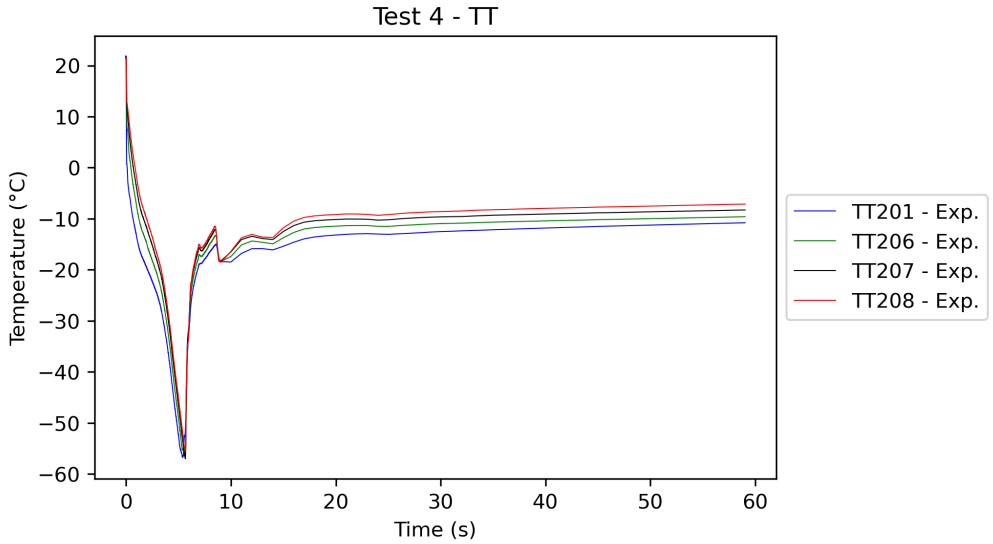

Figure 5.5.: Test 4 - Experimental data for TT sensors close to the outlet.

a lowest temperature has been registered. All the sensor close to the outlet registered a minimum temperature of -55 °C within the first 10 seconds from the release start. The behaviour registered from sensors TT201, TT206, TT207, TT208 is reporeted in Figure 5.5. The temperature rapidly decrease in the first 5 seconds, then it start to rise and start stabilizing after around 20 seconds. Since the low temperature can form solid-phase CO_2 (also called dry-ice) and initiate brittle fractures, the minimum value of temperature is relevant during the simulations and temperature predictions. In Test 4, the minimum value has been registered from the sensor at the opposite side of the outlet (61.3 m from the outlet), sensor TT271 positioned at the bottom of the test section pipe.

A focus on this has been reported in Figure 5.6, measurements from thermocouples TT201 (at the outlet) and TT261 (46 m from the outlet) have been also included. It can be observed that a minimum temperature of -73.5 °C has been registered, since is close to -78 °C (gas to solid deposition temperature), there was a risk of solid formations at 61.3 m from the outlet. Solid formation could also impact the measurement of temperature. Authors also observed that dry-out occurs later at the farther position, and a larger difference between the sensors at this point may indicate a larger degree of flow stratification. This aspect should be further investigated as well as the accuracy of the solid phase prediction with numerical codes. A similar behaviour has been observed also for Tests 6 and 8, which were realized at similar starting conditions. The minimum temperature also in this case has been registered far from the outlet, in sensor TT271, and was -73.58 °C for Test 6 and -74.00 °C for Test 8 as reported in Figure 5.7 and 5.8.

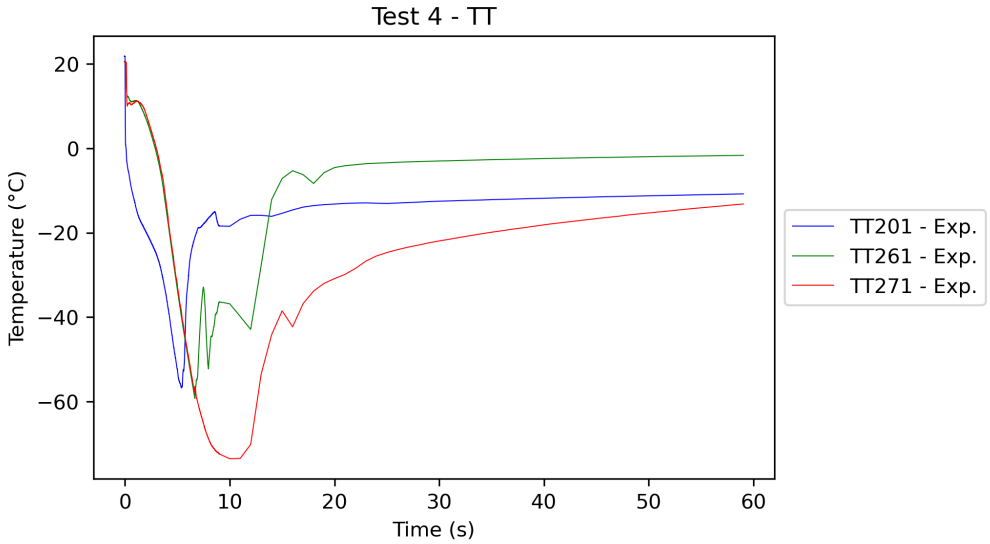

Figure 5.6.: Test 4 - Experimental data for TT far from the outlet.

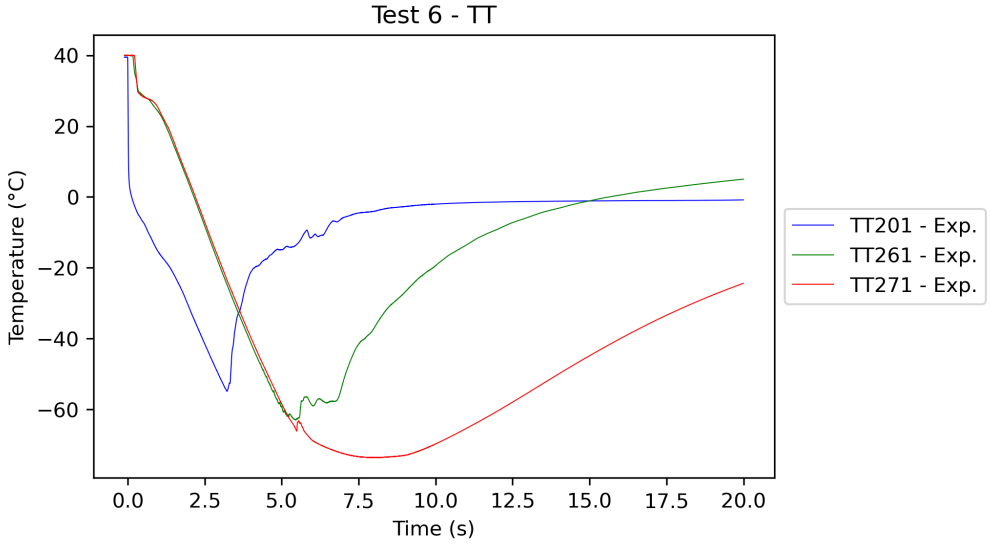

Figure 5.7.: Test 6 - Experimental data for TT far from the outlet.

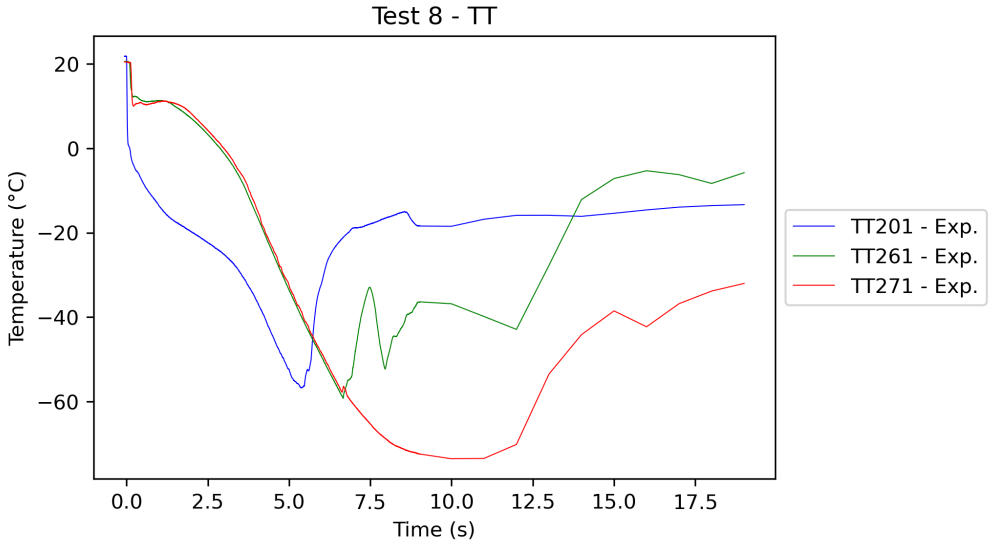

Figure 5.8.: Test 8 - Experimental data for TT far from the outlet.

Pressure transducers has been utilized for the measurements of pressure, as previously stated, the transient phenomena of depressurization is very rapid especially at the very first end of the pipe. Indeed, as reported in Figure 5.3, the location of sensor is denser around the outlet orifice in order to better capture the pressure behaviour. Starting from Test 3, the depressurization behaviour have been plotted in Figure 5.9, in order to describe the main differences between a gas-phase decompression and a dense-phase one. Note that the edges in the pressure traces after about 0.18 s in Figure 5.9 are due to the reflection at the closed end of the pipe. For Test 3 the reflection of the pressure wave is slightly visible, while this is more evident in dense-phase tests such as 4, 6 and 8.

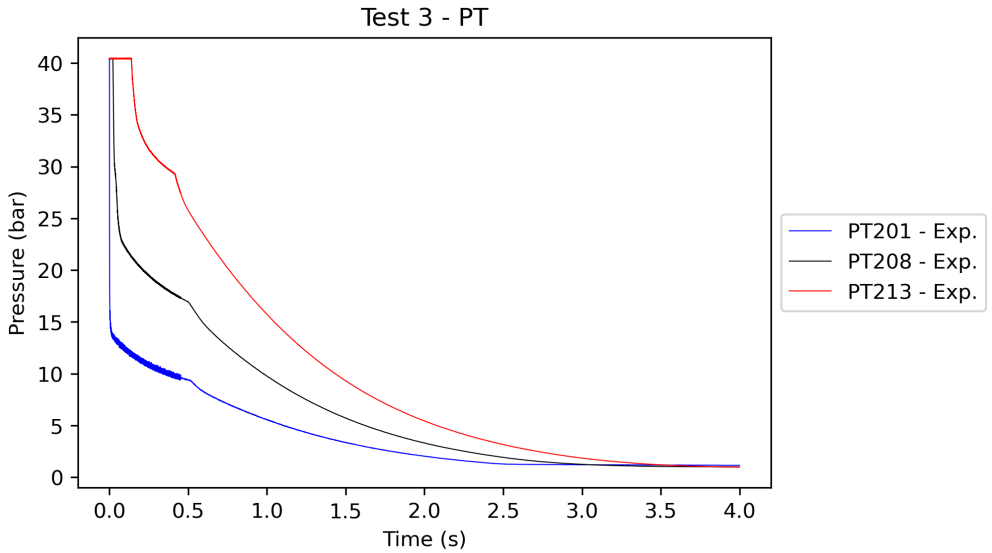

Figure 5.9.: Test 3 - Experimental data for PT close to the outlet.

In Figure 5.10 the results from the Test 4 are reported for the first 4 seconds, while a focus on the very first second from the rupture disk opening for the same test has been reported in Figure 5.11. It is clearly visible how the pressure decrease from 12.54 Mpa (125 bar) and reach a local minimum peak of 3.3 Mpa (33 bar) for PT201 in nearly 0.01 seconds. In Table 5.4, the minimum pressure values measured for the PT201 are reported as well as the pressure difference registered from starting pressure. Note that the accuracy in the first sensor for the few milliseconds could be lower due to noise and the velocity of the phenomena.

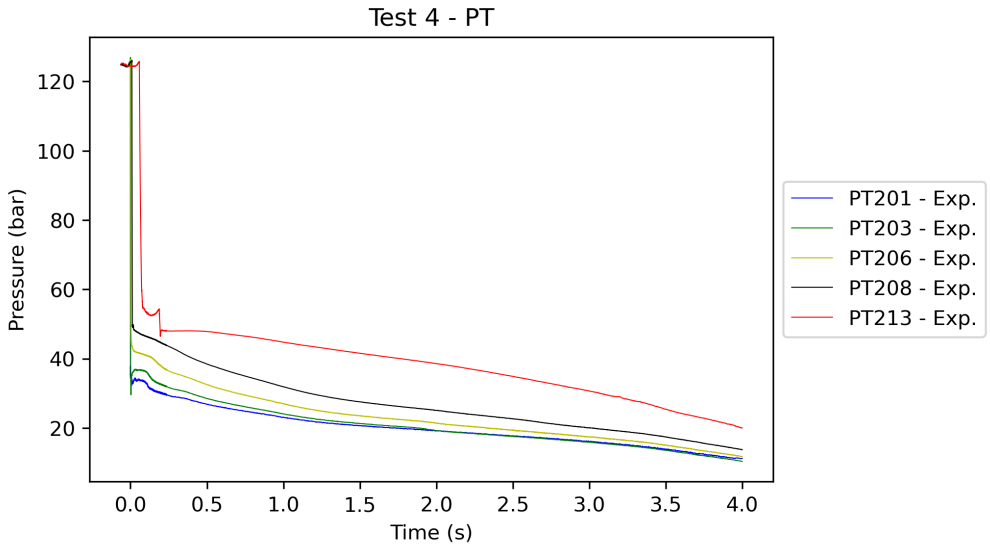

Figure 5.10.: Test 4 - Experimental data for PT close to the outlet.

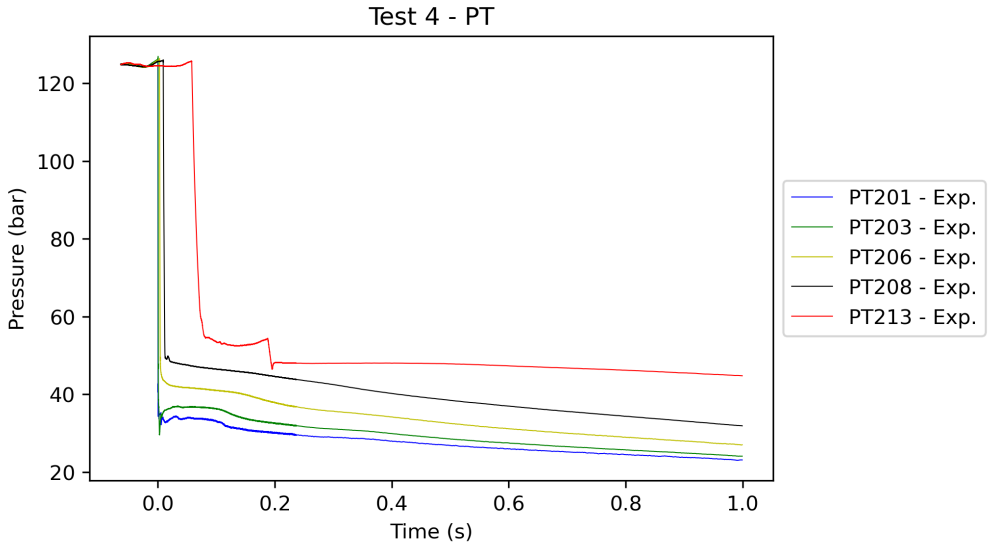

Figure 5.11.: Test 4 - Experimental data for PT close to the outlet (focus).

In the dense-phase region, the pressure waves are fast, while they are much slower

Table 5.4.: Pressure sudden drop on PT201 in the first milliseconds ($\leq$ 0.1 s).

Test no.	P $_{start}$ (MPa)	P $_{min}$ (MPa)	ΔP (MPa)
3	4.04	1.35	2.69
4	12.54	3.45	9.09
6	10.40	4.25	6.15
8	12.22	2.80	9.42

in the two-phase region, below the critical pressure of 7.38 MPa. Indeed, the pressure wave propagates faster in liquids and slower when gas-phase is present. Following a single pressure trace, it can be observed that upon arrival of the first pressure wave, the pressure drops fast from about 10 MPa down to a 'plateau' pressure, close to the critical pressure. Depending on the position, the pressure remains at the plateau for a while, after which it continues to decrease. One can observe that close to the outlet, the pressure drops fast also in the two-phase region [19]. This is also visible in Figure 5.12.

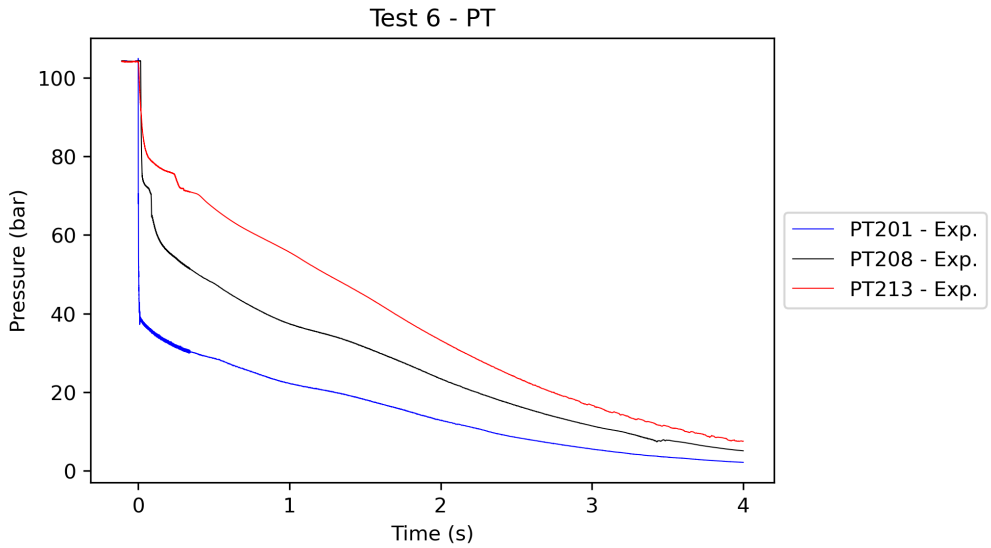

Figure 5.12.: Test 6 - Experimental data for PT (plateau).

5.2.2. Numerical model

In this work, the code used for thermo-hydraulic analysis is OLGA Dynamic Multi-phase flow simulator from Schlumberger. OLGA was originally developed as a dynamic one dimensional modified two fluid model for two-phase hydrocarbon flow in pipelines and pipeline networks, with processing equipment included. Later, a water option was included which treats water as a separate liquid phase. OLGA was originally based on the computer program OLGA 83, developed by IFE in 1983 for the Norwegian State Oil Company, Statoil. Since 1984, OLGA has been improved

continuously due to the experimental database from the large scale two-phase flow at SINTEF Multi-phase laboratory and extensive use and numerical testing at IFE and in the oil companies involved [202]. In the later years, more two-phase and three-phase field data have become available for the testing of OLGA [203].
OLGA is capable of dynamic simulation of pipeline networks with process equipment such as compressors, pumps, heat exchangers, separators, check-valves, controllers and mass sources/sinks. OLGA has full network capability, that is, it handles both diverging and converging networks. Computing a transient multiphase flow situation with a dynamic model requires increased CPU-time expenditure compared with ordinary steady state models. The additional time dimension also increases the amount of output produced by the code. The dynamic feature of the program imposes additional requirements on the user, compared with steady state models, but the results of the transient program are significantly more useful in design of the pipeline and its attendant facilities than steady state methods. OLGA is a modified two-fluid model, i. e. separate continuity equations for the gas, liquid bulk and liquid droplets are applied; these may be coupled through interfacial mass transfer. Only two momentum equations are used; one for the continuous liquid phase and one for the combination of gas and possible liquid droplets. The velocity of any entrained liquid droplets in the gas phase is given by a slip relation. One mixture energy equation is applied; both phases are at the same temperature. This yields six conservation equations to be solved: three for mass, two for momentum, and one for energy. To close the system of equations, boundary and initial conditions are required. The specification of initial conditions is a fundamental difference between transient and steady state model where these are not required. In this work, the restart capability has been used to start with data saved from a previous (steady-state) simulation. When two phases flow simultaneously in pipes, the flow regime, pressure- and velocity fields are strongly connected. The phases tend to separate because of differences in density. Perhaps the most distinguishing aspect of multiphase flow is the variation in the physical distribution of the phases in the pipe, a characteristic known as flow regime. During two-phase flow in pipes, the flow pattern that exists depends on the relative magnitudes of the forces that act on the fluid. In OLGA two basic flow regimes are distinct. Distributed that contains bubble and slug flow and separated, which contains stratified and annular mist flow (see Figure 5.1). Two basic flow regime classes are applied; distributed and separated flow. The former contains bubble and slug flow, the latter stratified and annular mist flow. Transition between the regime classes is determined by the program on the basis of a minimum slip concept combined with additional criteria.
The two-phase model equations implemented in OLGA, as reported in the first releases [202, 203] is hereafter summarized. Separate continuity equations are applied for gas, liquid bulk and liquid droplets, which may be coupled through inter-phasic mass transfer. Conservation of mass for the gas phase (5.1), the liquid phase at the wall (5.2) and the liquid droplets (5.3):

$$\frac{\partial}{\partial t}\left(V_g \cdot \rho_g\right) = -\frac{1}{A}\frac{\partial}{\partial z}\left(A \cdot u_g \cdot V_g \cdot \rho_g\right) + \Psi_g + M_g \tag{5.1}$$

$$\frac{\partial}{\partial t}\left(V_l \cdot \rho_l\right) = -\frac{1}{A}\frac{\partial}{\partial z}\left(A \cdot u_l \cdot V_l \cdot \rho_l\right) - \Psi_g \frac{V_l}{V_l + V_d} - \Psi_e + \Psi_d + M_l \tag{5.2}$$

$$\frac{\partial}{\partial t}\left(V_d \cdot \rho_l\right) = -\frac{1}{A}\frac{\partial}{\partial z}\left(A \cdot u_d \cdot V_d \cdot \rho_l\right) - \Psi_g \frac{V_d}{V_l + V_d} + \Psi_e + \Psi_d + M_d \tag{5.3}$$

In the equations above V_g, V_l, V_d denote volume fractions of gas, liquid-film and liquid-droplets respectively. A is the pipe cross-section area, Ψ_g is the mass transfer rate between the phases, the Ψ_e and Ψ_d is the entrainment and deposition rates. A possible mass source of phase f is given as M_f. Subscripts g, l, d and i denote gas, liquid, droplets and interphase. Conservation of momentum is expressed for the gas, possible liquid droplets and liquid bulk or film in (5.4) (5.5) (5.6).

$$\begin{aligned}\frac{\partial}{\partial t}\left(V_g \cdot \rho_g \cdot u_g\right) = -V_g\frac{\partial p}{\partial z} - \frac{1}{A}\frac{\partial}{\partial z}\left(A \cdot u_g^2 \cdot V_g \cdot \rho_g\right) - \Psi_g \frac{V_d}{V_l + V_d} + \\ - \lambda_g \frac{1}{2} \cdot \rho_g \cdot \mid u_g \mid \cdot u_g \cdot \frac{P_g}{4A} + \lambda_i \frac{1}{2} \cdot \rho_g \cdot \mid u_r \mid \cdot u_r \cdot \frac{P_i}{4A} + V_g \cdot \rho_g \cdot g \cdot \cos\vartheta + \Psi_g \cdot u_a - F_d\end{aligned} \tag{5.4}$$

$$\begin{aligned}\frac{\partial}{\partial t}\left(V_d \cdot \rho_l \cdot u_d\right) = -V_d\frac{\partial p}{\partial z} - \frac{1}{A}\frac{\partial p}{\partial z}\left(A \cdot u_d^2 \cdot V_d \cdot \rho_l\right) + V_d \cdot \rho_l \cdot g \cdot \cos\vartheta + \\ - \Psi_g \frac{V_d}{V_l + V_d} u_a + \Psi_e \cdot u_i - \Psi_d \cdot u_d + F_d\end{aligned} \tag{5.5}$$

$$\begin{aligned}\frac{\partial}{\partial t}\left(V_l \cdot \rho_l \cdot u_l\right) = -V_l\frac{\partial p}{\partial z} - \frac{1}{A}\frac{\partial}{\partial z}\left(A \cdot u_l^2 \cdot V_l \cdot \rho_l\right) - \lambda_l \frac{1}{2} \cdot \rho_l \cdot \mid u_l \mid \cdot u_l \cdot \frac{P_l}{4A} + \\ + \lambda_i \frac{1}{2} \cdot \rho_g \cdot \mid u_r \mid \cdot u_r \cdot \frac{P_i}{4A} + V_l \cdot \rho_l \cdot g \cdot \cos\vartheta + \Psi_g \frac{V_l}{V_l + V_d} u_a - \Psi_e \cdot u_i + \\ + \Psi_d \cdot u_d - V_l\left(\rho_l - \rho_g\right) \cdot g \cdot \frac{\partial V_l}{\partial z}\sin\vartheta\end{aligned} \tag{5.6}$$

p is the pressure, ϑ is the pipe inclination from the vertical, the Pf is the wetted perimeter of the given phase f. The internal source M is assumed to enter a 90° angle to the pipe wall thus carrying no net momentum. When $\Psi > 0$ the evaporation from the liquid film gives $v_a = v_l$, and evaporation from the liquid droplets gives $v_a = v_d$. For $\Psi < 0$ the condensation gives $v_a = v_g$. The conservation equations can be applied to all possible flow regime, (5.7) defines the relative velocity, v_r:

$$u_g = k \cdot (u_l + u_r) \tag{5.7}$$

A similar definition for the droplet velocity is defined by u_{0d}, which is the fall velocity of the droplets (5.8).

$$u_d = k \cdot (u_g + u_{0d}) \tag{5.8}$$

OLGA reformulates the problem before discretisizing the differential equations to obtain a pressure equation. The conservation of mass equations (from (5.4) to (5.6)) may be expanded with regards to pressure, temperature and composition. This assumes that the densities are given as (5.9).

$$\rho_f = \rho\,(p, T, x) \tag{5.9}$$

After inserting the conservation of mass equations and applying (5.10).

$$V_g + V_l + V_d = 1 \tag{5.10}$$

then a single equation for the pressure and phase fluxes appears (5.11).

$$\begin{aligned}\left[\frac{V_g}{\rho_g}\left(\frac{\partial \rho_g}{\partial p}\right)_{T,x} + \frac{1-V_g}{\rho_l}\left(\frac{\partial \rho_l}{\partial p}\right)_{T,x}\right]\frac{\partial p}{\partial t} = &-\frac{1}{A\rho_g}\frac{\partial}{\partial z}\left(A \cdot u_g \cdot V_g \cdot \rho_g\right) + \\ &- \frac{1}{A\rho_l}\frac{\partial}{\partial z}\left(A \cdot u_l \cdot V_l \cdot \rho_l\right) - \frac{1}{A\rho_d}\frac{\partial}{\partial z}\left(A \cdot u_d \cdot V_d \cdot \rho_d\right) + \\ &+ \Psi_g\left(\frac{1}{\rho_g} - \frac{1}{\rho_l}\right) + M_g \cdot \frac{1}{\rho_g} + M_l \cdot \frac{1}{\rho_l} + M_d \cdot \frac{1}{\rho_d}\end{aligned} \tag{5.11}$$

The energy conservation of the mixture is expressed by the following equation (5.12):

$$\begin{aligned}\frac{\partial}{\partial t}\left[m_g\left(e_g + \frac{1}{2}u_g^2 + gL\right) + m_l\left(e_l + \frac{1}{2}u_l^2 + gL\right) + m_d\left(e_d + \frac{1}{2}u_d^2 + gL\right)\right] = \\ = -\frac{\partial}{\partial z}\left[m_g \cdot u_g\left(H_g + \frac{1}{2}u_g^2 + gL\right) + m_l \cdot u_l\left(H_l + \frac{1}{2}u_l^2 + gL\right) + \right. \\ \left. + m_d \cdot u_d\left(H_d + \frac{1}{2}u_d^2 + gL\right) + H_s + U\right.\end{aligned} \tag{5.12}$$

Where m_f is a product of $V_f \rho_f$, e is the internal energy per unit mass, the elevation is given with L, H_s is the enthalpy from the mass sources and U is the heat transfer from the pipe walls.
The latest releases available of the software have been utilized in this work, namely the OLGA 2020.2 and the OLGA 2021.1. In this releases several improvement have been introduced to handle CO_2 processing and improve the numerical stability. In

the first patch release of the 2020.2 code, the numerical robustness of the code has been improved, and the functionality for the management of pure CO_2 has been enhanced. To improve calculation accuracy, the CO_2 viscosity model is replaced with more accurate published experimental data references. For simulations of pure CO_2 with the SINGLECOMPONENT option, OLGA 2020.2 includes an option to use predefined pressure and temperature ranges when generating the PVT table. Indeed, when dealing with rapid changes trough valves and other equipment, a wide range of pressure and temperature value can be encountered, therefore, custom grid can be required to optimize the iterations. The OLGA single component module is used for steam pipeline system analysis. The single component module allows the tracking of a single component, (i.e. H_2O or CO_2) that crosses the saturation line in time or space in a pipeline. The standard OLGA cannot deal with single component systems if the saturation line is crossed due to the explicit coupling between volume balance and energy balance equations and the lack of a two phase region (two phase envelope). Numerical stability has been improved trough a new calculations steps in the pre-processor. OLGA 2021.1 release included the updates from the NORSOK M506 standard, the utilization of Pressure-Enthalpy (PH) table instead of Pressure-Temperature (PT) table has been improved for speed and stability. The possibility to use OLGA PH table for two-phase single component simulation of CO_2 has been included. Moreover, the possibility to import data from Multiflash 7.2 (as utilized in Chapter 4) with its powerful capabilities to describe VLE and density is available. Finally, the accuracy of OLGA for simulation points that lays around the critical point has been enhanced specifically for pure CO_2. The accurate modelling of pure CO_2 with the single component is based on the Span-Wagner EoS [181], since is the most acknowledged for pure CO_2 processing (see Chapter 4).

5.2.3. Model validation

The main scope of this section is the estimation of the capabilities of existing numerical simulator to predict thermo-fluid dynamic changes of CO_2 when transported in high-pressure pipeline. This objective has been obtained trough the validation of the experimental data with OLGA codes 2020.2 and 2021.1 and the evaluation of the results. The experimental data utilized in this part of the work have been described in Subsection 5.2.1 based on the experimental activities performed and published by Munkejord et al. [19]. The numerical model utilized has been described in Subsection 5.2.2 and it's based on the OLGA multi-phase dynamic simulator software by Schlumberger. The results from cases reported in the experimental data (see Table 5.2) has been collected and analysed as reported in the previous Subsections 5.2.1 and 5.2.2.
The OLGA model for the validation has been built (see Figure 5.13) in order to replicate as much accurately as possible the test section described in Figure 5.2. The

details reported in Table 5.1 has been utilized for the material properties and the insulation layering of the numerical model. This aspects has been revised accurately since it has an impact on the temperature calculation. The simulated rig test section has been reproduced in OLGA and several sensitivities have been conducted in order to identify the optimized number of cells for the pipe mesh. A non-regular 1-D mesh has been selected at the end, with 100 sections, the elements were not equally spaced since a dense mesh has been created near the pipe outlet (rupture disk). Grid-sensitivity has been conducted from 30 to 1000 elements, a good agreement in term of computational time and quality of the results resulted in a 100 elements mesh grid.

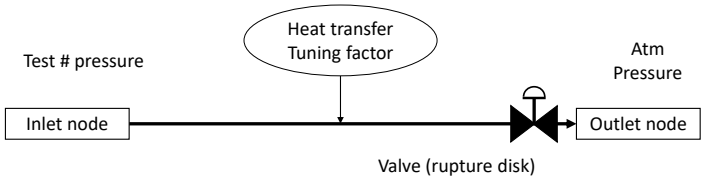

Figure 5.13.: OLGA model of the test section of ERIC DEPRESS facility.

The single component option for CO_2 has been called for the simulation of the phenomena. The improved PH interpolation has been utilized instead of the classic PT method, and the auto-range table generation optimized for CO_2 has been selected (see Subsection 5.2.2). The inlet of the pipe has been simulated as a closed mass node, while the end as an atmospheric pressure driven node. The rupture disk has been simulated trough a rapid valve with an opening time of 0.001 s. Sensitivities has been conducted between 0.5 and 0.00001 and it has been found that 0.001 was the plateau in term of results improvements against CPU-time. Indeed, the opening time has an impact on the pressure prediction if compared to experimental data, that cannot be neglected. The valve model has been also selected trough a sensitivity analysis and the Henry-Faskue Model was selected as the better solution among the available models if compared with experimental data results.
The workflow of the entire simulation process adopted for each simulation is reported in the scheme reported in Figure 5.14. Each simulation has been set based on the

fluid condition and boundary conditions defined in the experimental data as reported in Table 5.2. Then the steady-state simulation is initialized and run for a fictional time in order to reach convergence and a stable steady-state condition with the valve closed. The stability and the output are checked, if the results are satisfactory, a .rsw file is written. The transient simulation start from reading the steady-state simulation as an input, and the valve opening is set as well as the numerical parameter for the convergence of the simulation. Transient simulation is run and results are evaluated firstly in term of stability, convergence and physics, later-on against experimental data. Sensitivities has been run in term of:

- Mesh size and grid
- Valve model
- Integration coefficient
- Tuning factors

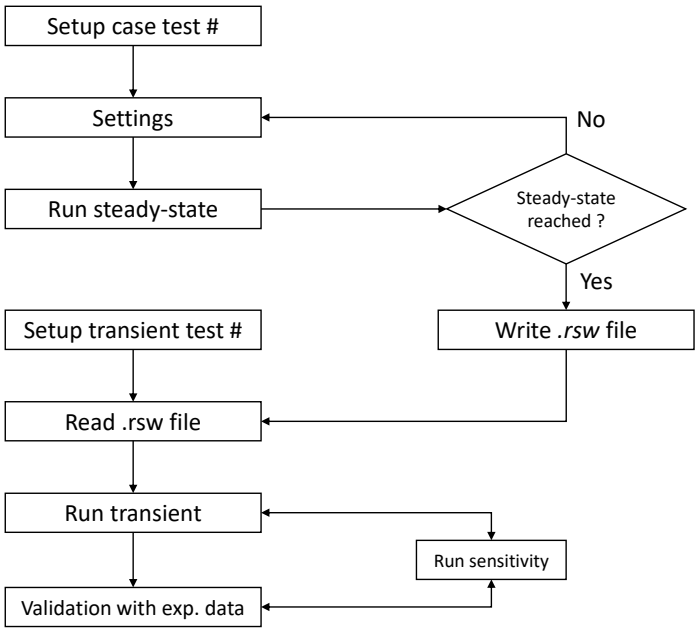

Figure 5.14.: Simulations flowchart for experimental data validation.

According to Table 5.2 the first case that has been tested was the nitrogen test 11. Indeed, in order to consider the capabilities for the simulation of CO_2 and validate them against experimental data, a comparison with standard gas has been performed. The nitrogen tables has been generated trough Multiflash 7.2 and the results have been passed to OLGA as an input composition file. Since no-phase change is expected

at this condition for N_2, the results should be generally more accurate and easy to simulate. In Figure 5.15 the results of the simulation compared with experimental data have been reported for five pressure sensors, namely PT201, PT203, PT206, PT208 and PT213. Results from the first 5 seconds after the disk rupture opening of the simulation show a good agreement in term of trend and time-to-steady-state. While an over-estimation resulted from the simulations for the very first seconds for the sensors close to the outlet (see Figure 5.16 for focus). In Figure 5.15 and 5.16 can also be noted how the pressure trend has an edge at $t < 0.5$ s, this is probably due to the reflection of the pressure wave on the bottom of the pipe since it is closed on one end as also reported in Subsection 5.2.1.

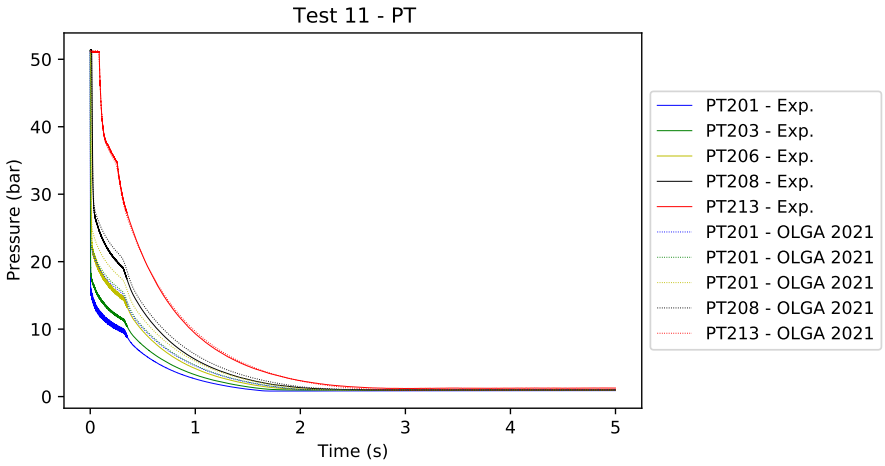

Figure 5.15.: Test 11 - Validation of experimental data vs OLGA model (I).

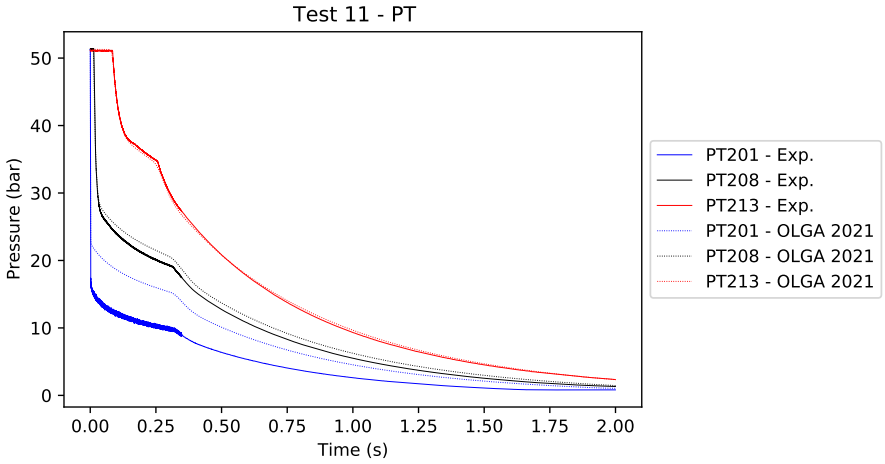

Figure 5.16.: Test 11 - Validation of experimental data vs OLGA model (II).

Pressure trends have been analyzed for validation purpose and results from Test 3 and Test 4 are presented. Indeed, this cases have been selected as representative among all the available described in Table 5.2. Test 3 has been conducted starting

from a gas-phase condition while Test 4 present a liquid/dense-phase condition at steady-state. The flowchart presented in 5.14 has been followed for the simulation and the Test 3 results from both version of OLGA 2020.2 and 2021.1 have been compared. For the validation, a representative set of 3 sensors have been selected, PT201, PT208 and PT213 respectively distant from the rupture disk 0.08 m, 4.79 m and 29.97 m (see Figure 5.3). According to the results presented in Figure 5.17 it can be noted how both the code accurately predict the pressure decrease for the sensors far from the orifice while the first sensor considered for the validation (PT201) presents a considerable overestimation in the first second.

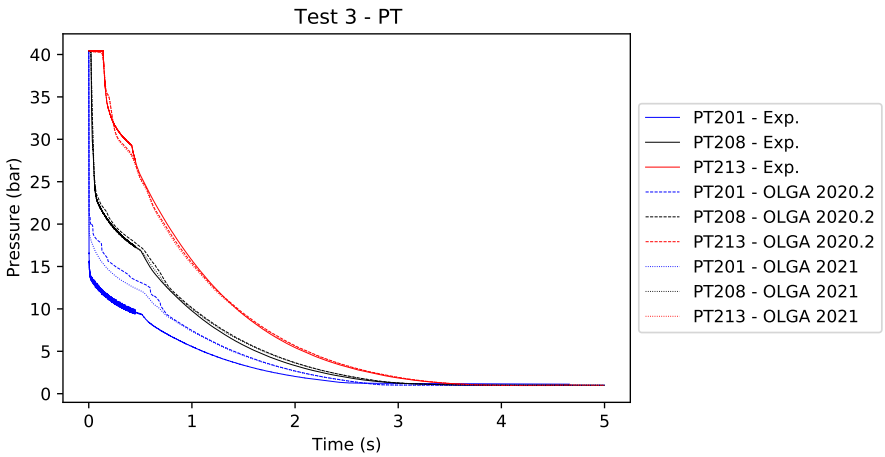

Figure 5.17.: Test 3 - Validation of pressure experimental data vs OLGA model 2020.1 and 2021.1 (I).

In Figure 5.18 a focus on the sensor in object with a comparison of the two release of the OLGA code considered is reported. The over-prediction of the simulation is present in both codes, however, it is clearly visible how the new release has a more stable and smooth prediction of the pressure drop. The behaviour of the pressure wave calculated by the OLGA 2021.1 at the same condition, report a better agreement with experimental data for all pressure sensors considered.

The same sensors have been analyzed for Test 4 and some consideration on the results can be drawn. A tuning factor of 0.3 for the mass-transfer (liquid-gas) has been utilized for Test 4 as a results from the sensitivity analysis on tuning factors. In Figure 5.19 the results of the numerical simulation have been reported and compared with the experimental data for the sensors PT201, PT208 and PT213. The performances of the 2020.2 again has been improved and some numerical instabilities are not present in the 2021.1 release (see Figure 5.20 for focus). However, an general under-estimation of the pressure is reported for Test 4 for both codes analyzed. Indeed, the pressure decrease more rapidly in the simulation, this is due to the inaccurate prediction of the phase-change between liquid and gas. In experimental data it has been observed that the transition between liquid and gas for CO_2 is slower if compared to simulation. This is mainly due to the homogeneous equilibrium

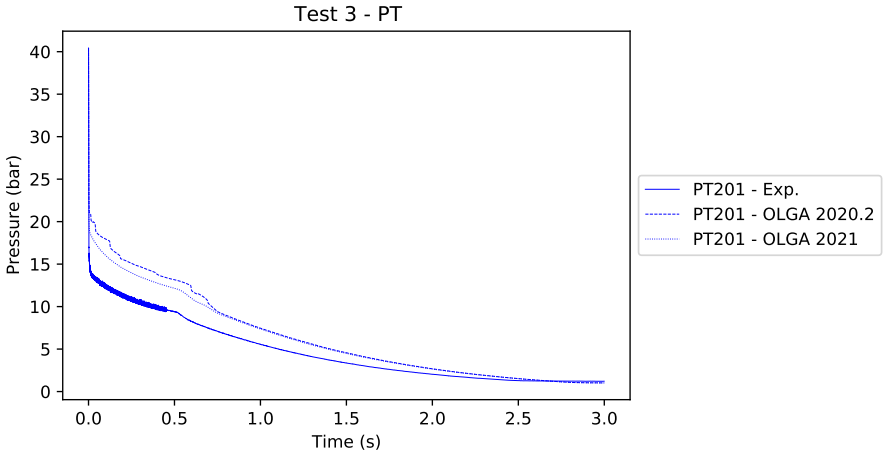

Figure 5.18.: Test 3 - Validation of pressure experimental data vs OLGA model 2020.1 and 2021.1 (II).

method (HEM) assumption that is present in most of the simulators. The HEM does not take into account the phase-slip between phases, that seems to be responsible for the delayed pressure drop in the transition from liquid to gas for dense CO_2. Another possible explanation is the position in which the sensors have been placed, indeed, the formation of two-phase flow can led to anomalies in term of pressure data acquired.

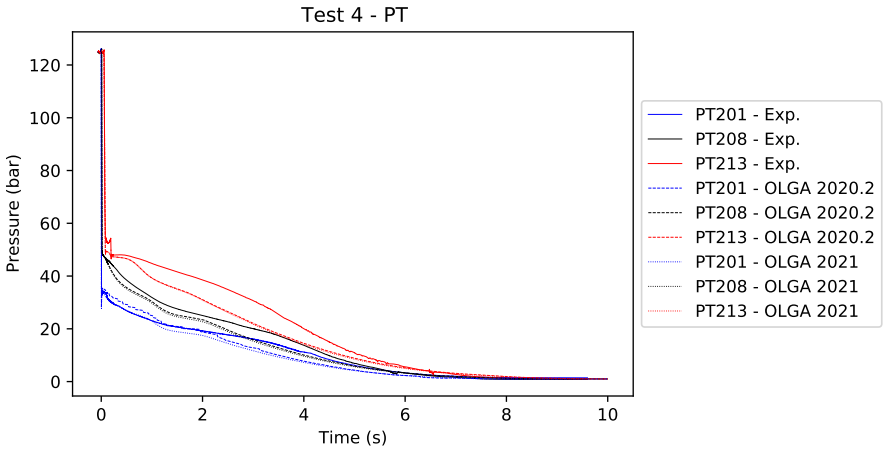

Figure 5.19.: Test 4 - Validation of pressure experimental data vs OLGA model 2020.1 and 2021.1 (I).

In Figure 5.20 a focus on the first second of the depressurization has been reported. It can ben observed how the pressure is slightly under-estimated for the first second, especially for the sensor PT208 and PT213 while for the PT201, the agreement of the results from the 2021.1 simulations are considerably better compared to the 2020.2 results. For PT213 it can be observed a sharp edge around 0.2 s, this can be a result of a back-pressure wave coming from the sudden closure of the hydraulic valve system

at the opposite side rupture disk section. This is obviously not predicted by the simulation since it has been considered a sudden opening of the valve that simulate the rupture disk, but on the other hand the opposite side of the pipe is numerically described as a closed node from the beginning. Another possible explanation is the sudden vaporization of a liquid pool nearby the sensor that drastically reduced the pressure read in a small amount of time. This phenomena have been also observed for Test 6 and 8.

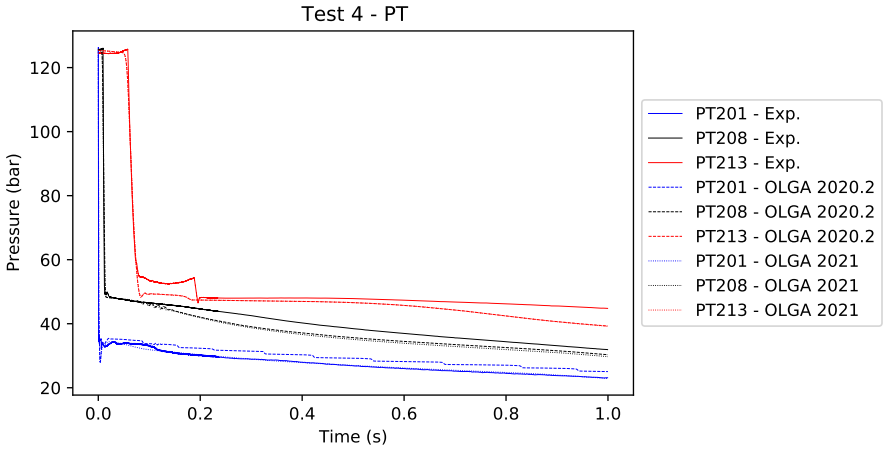

Figure 5.20.: Test 4 - Validation of pressure experimental data vs OLGA model 2020.1 and 2021.1 (II).

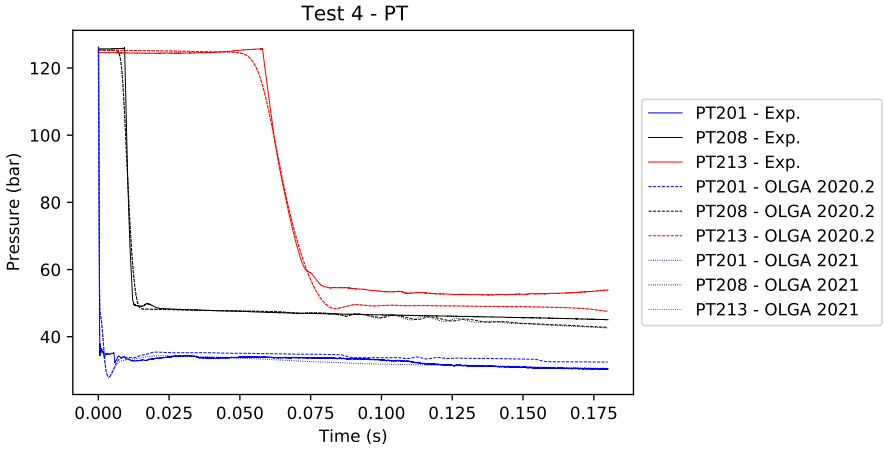

Figure 5.21.: Test 4 - Validation of pressure experimental data vs OLGA model 2020.1 and 2021.1 (III).

In Figure 5.21 a closest look at the first 0.18 s is proposed to analyse the OLGA capability to predict the sudden depressurization from the first instants. An integration time of $1 \cdot 10^{-6}$ has been imposed in the transient simulation in order to capture the phenomena. Simulation for both the code utilized have been performed under the same conditions. The results obtained are very similar especially for

the sensors PT201 and PT208, where the depressurization is well predicted in the first decimal of seconds with the exception of minor instabilities that led to a lower pressure prediction in the very first milliseconds. The better stability of the OLGA 2021.1 is evident for the PT201 results if compared with 2020.2 (see Figure 5.20). In Test 4, the largest deviation between prediction and experimental data has been registered for the PT213. However, the convergence to a steady-state condition has been reached for both code and experimental data after around 8 seconds from the rupture disk opening.
A similar method has been adopted for the comparison of the experimental data with the numerical results for the temperature sensors. Temperature experimental data has been collected and already presented in some parts based on the work of Munkejord et al. [19] in Subsection 5.2.1. As per pressure data analyzed, some sensors have been selected among the all available for the estimation of the main differences in temperature prediction and validate the simulation results. A large number of temperature sensors were available from the rig (see Figure 5.3), for the validation, the sensors TT201, TT206, TT207, TT261 and TT271 have been considered. The selection has been made based on the sensors location, in particular the distance from the rupture disk which is reported in Table 5.5. All the sensors considered are positioned horizontally at half height from the bottom of the pipe (right side or left side), with the only exception of the temperature sensors TT261 and TT271 which are positioned at the bottom of the pipe.

Table 5.5.: Locations of PT (pressure), TT (fluid temperature) sensors, defined as the distance from rupture disk.

Nominal location at 25°C (m)	PT sensor	TT sensor
0.08	PT201	TT201
1.599	PT206	TT206
3.198	PT207	TT207
4.798	PT208	TT208
29.986	PT213	TT213
46.085	-	TT261
61.28	-	TT271

In order to compare the results from different representative cases, Test 3 and Test 6 has been selected for the temperature results analysis. Both the test have been conducted at the same conditions and the temperature results have been extracted from the same simulation performed for the pressure results already presented. In Figure 5.22 the results from the TT201, the one closest to the rupture disk are reported. It should be noted how the numerical simulations of both code under-predict the minimum temperature and the recovery appear delayed.

In Figure 5.23 the same behaviour is observed where the sensors TT206 and TT207 have been included. At the same location, the pressure trend were under-predicted,

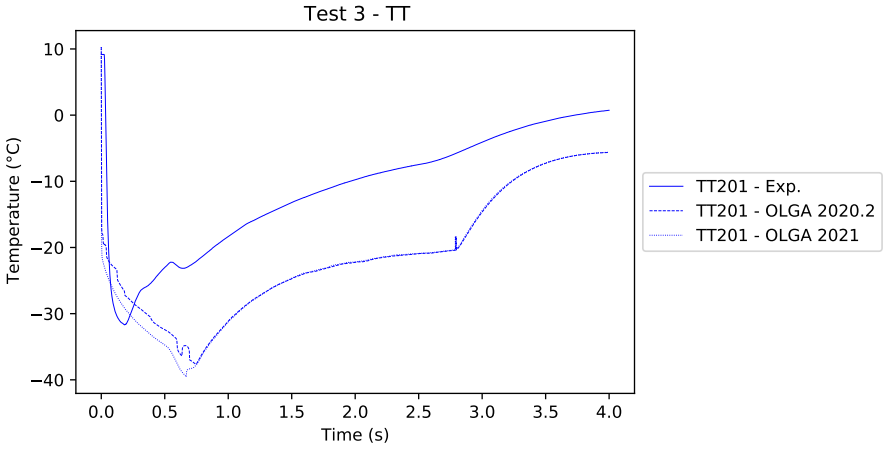

Figure 5.22.: Test 3 - Validation of temperature experimental data vs OLGA model 2020.1 and 2021.1 (I).

meaning that the depressurization occurs faster than the simulation is capable to handle in the first seconds in term of pressure drop. However, the temperature drop predicted by the simulations is slightly over-estimate, indeed the minimum temperature reached is lower than the observed in experimental data.

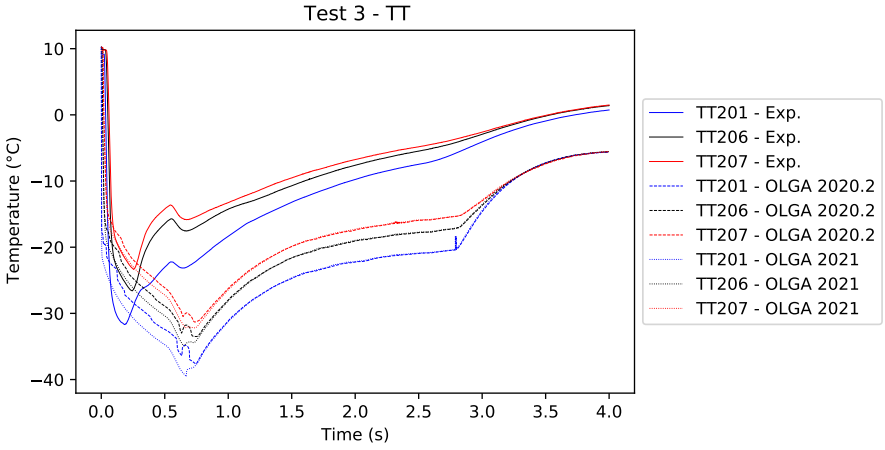

Figure 5.23.: Test 3 - Validation of temperature experimental data vs OLGA model 2020.1 and 2021.1 (II).

In Table 5.6 the minimum values of temperature predicted by the simulator for both the releases considered has been reported as well as the experimental minimum temperature detected by the sensors. The absolute deviation (%) from the experimental data is also reported and a general over-estimation of the temperature has been registered with the only exception of the TT261 sensor. In sensor TT271 the largest deviation has been observed, where the temperature in the simulation decreased to the minimum value of -79.56°C, the possibility of solid formation in this case is a wrong results from simulation. On the other hand the experimental

results showed how the minimum temperature registered was around -21°C, this large deviation can be attributed to an instability of the code in the position far from the outlet point or a too much sparser grid in that location, indeed since the outlet of the test facility was the main focus, the optimization of CPU-time led to a denser grid around the release end of the pipe.

Table 5.6.: Test 3 - Minimum Temperature comparison for experimental data and simulation results.

TT sensor	T_{min} (exp)	T_{min} (2020.2)	T_{min} (2021.1)	2020.2 dev. (%)	2021.1 dev. (%)
TT201	-31.69	-37.62	-39.55	18.71%	24.80%
TT206	-26.59	-33.50	-34.93	25.99%	31.37%
TT207	-23.36	-31.30	-32.18	33.99%	37.76%
TT261	-43.06	-38.04	-40.34	-11.66%	-6.32%
TT271	-21.42	-79.44	-79.56	270.87%	271.43%

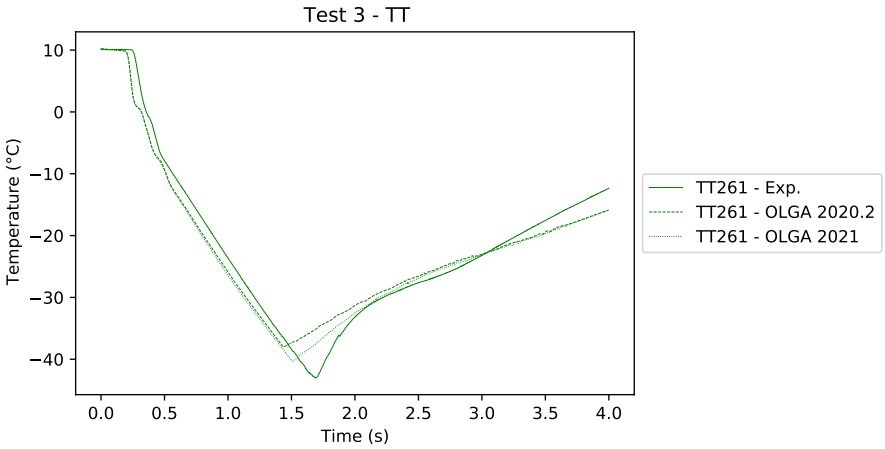

Figure 5.24.: Test 3 - Validation of temperature experimental data vs OLGA model 2020.1 and 2021.1 for sensor PT261.

Temperature results for the Test 4, 6 and 8 have been analyzed and major deviations and instabilities have been found. Indeed, the results is not unexpected since the temperature calculation of CO_2 crossing the liquid-gas phase are a matter of study. An useful comparison with experimental data is reported in order to understand the lack and main bias of the simulation results. Test 6 has been selected for this analysis, both simulator release have been used even more instabilities have been found for the 2020.2 code. As reported in Figure 5.25, the results of 2021.1 code follow the trend already presented for Test 3 with an over-estimation (lower temperature predicted) and a slow and delayed recovery. Moreover, code 2020.2 reports major instabilities as it is clearly visible from t = 6.5 s. It should be considered, however, that the depressurization process at that time, it is already completed and the

pipe is almost empty, therefore the temperature results during the recovery are not relevant. The most important data that it is notably interesting due to brittle fracture implication and solid formation is the minimum temperature. In Figure 5.25 the results for sensor PT201 are reported, it can be noted that the 2021.1 code reports a slightly lower temperature (-68.81 °C) if compared to 2020.2 code (-67.70 °C), and experimental data (-54.84 °C). However, as better highlighted in Figure 5.26 with the results from sensor TT216, the stability of the temperature trend prediction has been substantially increased in 2021.1 code. Indeed, a major instability have been registered in temperature prediction for TT261 in the first seconds while the red curve plotted for 2021.1 show no instabilities. The lower temperature prediction for both codes has been registered for all sensors, while a difference of few degrees (within 2) occurred between the 2021.1 and 2020.2 code (see Table 5.7 for detail of Test 6 results). Looking closely to the results for Test 6, it can be noted how the temperature far from the nozzle (rupture disk) is well predicted while the major deviations have been registered close to the release section. A possible explanation of this is related to the rapid phase transition from liquid to gas in the first section of the nozzle that is not well predicted by the OLGA model, indeed, a temperature difference up to 13.97 °C occurred for the minimum temperature at TT201 which is the closest to the rupture disk. This is in line with the results from the other test and the background already discussed regarding the phase slip and the HEM, indeed the OLGA code predict a lower temperature than the one recorded from experiments. The temperature decay in real cases is not as fast as the one predicted by OLGA, also, the minimum temperature reached is higher for the analysed cases.

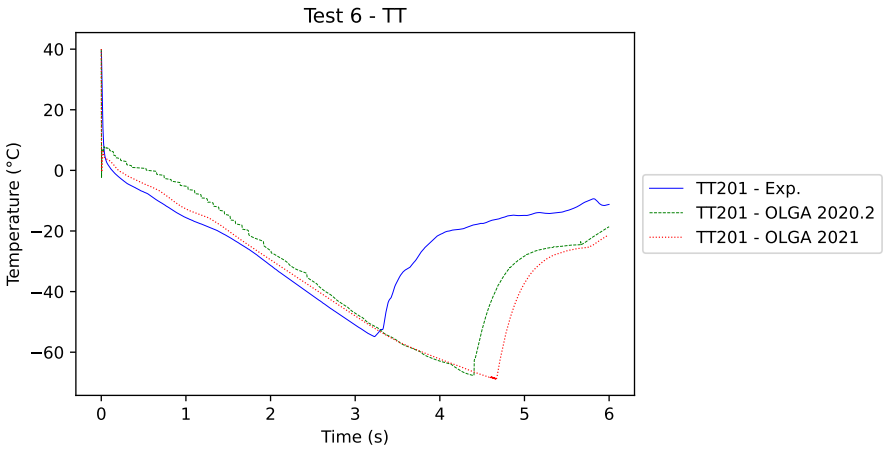

Figure 5.25.: Test 6 - Validation of temperature experimental data vs OLGA model 2020.1 and 2021.1 (I).

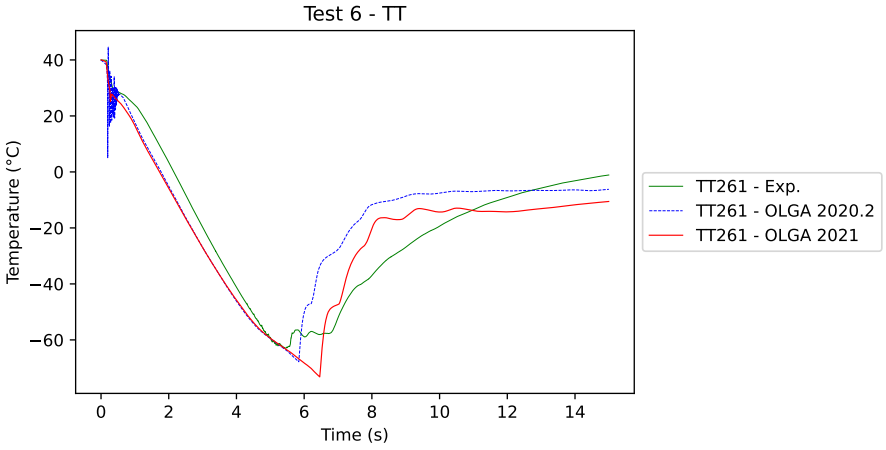

Figure 5.26.: Test 6 - Validation of temperature experimental data vs OLGA model 2020.1 and 2021.1 (II).

Table 5.7.: Test 6 - Minimum Temperature comparison for experimental data and simulation results.

TT sensor	T_{min} (exp)	T_{min} (2020.2)	T_{min} (2021.1)
TT201	-54.84	-67.70	-68.81
TT206	-48.41	-64.83	-66.83
TT207	-46.15	-63.19	-65.41
TT261	-62.93	-67.81	-68.17
TT271	-68.72	-69.13	-67.92

5.3. Vertical flow

5.3.1. DeFACTO facility setup

The Demonstration of Flow Assurance for CO_2 Transport Operations (DeFACTO) project was initiated by Equinor (Statoil at the time) as a CLIMIT Demo in 2013. In 2016, SINTEF Energy took over the project management, while Equinor remained project owner, and Total (now Total Energies) joined as project partner. The project's main goal was to design, build, and commission an experimental facility for measuring relevant flow data for transport and injection of CO_2. During the project, an advanced facility has been constructed and commissioned at Gløshaugen in Trondheim, and an experimental campaign has been carried out.
It should be noted that, since the DeFACTO project and facility details are covered by a Non-Disclosure-Agreement (NDA) signed during the experimental campaign period by the Ph.D candidate, only a limited, non-strategic amount of informations have been reported in this sections.

Figure 5.27.: Vertical section of the DeFACTO facility in Gløshaugen,Trondheim.

The DeFacto infrastructure comprises an extended horizontal flow circuit integrated with a vertical flow loop, indeed it is connected to the horizontal facility ECCSEL ERIC already described in Subsection 5.2.1. DeFACTO's 139 meters long horizontal flow loop enables the circulation of CO_2 with tightly controlled parameters (temperature, pressure, gas to liquid ratio). The vertical section supports the circulation of CO_2 through an 87 meters deep U-tube loop. The crane with the vertical section over the ground of DeFACTO is reported in Figure 5.27. The U-loop consists of two vertical tubes of different diameters. It is instrumented with over 60 high-precision fast-response pressure and temperature sensors, allowing the measurement of pressure waves with a high degree of accuracy. Each tube in the U-loop can be isolated and pressurised or depressurised individually, allowing a high level of flexibility to the rig. The data collected help understanding when and how the CO_2 freezes under depressurisation, cavitation phenomena, two-phase and transient flow behaviour, and ultimately assist engineers in the design of safer and more efficient CO_2 transport and storage systems. Experiments that can be performed through DeFACTO both with pure-CO_2 and with impurities (N_2, up to 20% CH_4):

- Both single and two phase flow
- Steady state flow at different p-T conditions and gas to liquid ratios

- Transient conditions:
  - Shut in and first fill
  - Depressurisations
  - Blowouts
  - Fluid hammers
- Estimation of heat transfer coefficient under controlled conditions.
- Reservoir backflow

Some information regarding the design, included in datasheet that are publicly available are reported hereafter. The U tube is composed by two legs, the largest has an internal diameter (ID) of 32 mm while the smallest an internal diameter (ID) of 16 mm. The maximum allowable opearating pressure (MAOP) of the rig is 160 bar (16 MPa), process temperature from -60 °C to +60 °C while the temperature in the hole can be controlled between -5 °C and 35 °C, finally the design flow is 10 kg/min (0.2 kg/s).

5.3.2. Experimental activity

The experimental activities described in this section have been conducted as a result of a collaboration between SINTEF Energy Research and NTNU for the project SIGNIFY. The Ph.D candidate spent two months at the facility located in Trondheim (NO) in order to join the SINTEF-NTNU teams for the experimental campaign.
The project SIGNIFY focuses on the verification and validation of data collected from sensor. The main objective of SIGNIFY is to develop methodologies (and assess their performance) for preventing corrupted data to be processed by the digital twin (with focus on safety-critical applications) and avoid erroneous action planning whose consequences range from performance degradation to lack of security and risk of danger.
Project SIGNIFY application to DeFACTO required several operations in order to obtain reliable data from sensors. Indeed, the accuracy of acquired data is crucial in the process of model tuning for a digital twin, moreover, if safety of people and operation is involved, care should be taken during data quality evaluation. In this work, temperature, pressure and flow sensors were the specific sensor available on the system to be used to capture data for evaluating a novel sensor anomaly detection, identification and accommodation framework. Practical work for the project included the creation of a clean and accurate data set. This newly calibrated data set can then be tampered with to create a second data set with synthesized sensor faults, and be a reference for a third data set containing sensor fault introduced in reality at the test rig. The work will include physical sensor calibration related work at the test rig, and post-processing techniques of the generated sensor data.
Digital twins are a new field in the digital transformation which allows virtual

monitoring and prediction of a range of different applications based on real sensor measurements in real-time. The capability of a system to detect (detect a faulty condition for a sensor), isolate (identifying the faulty or several faulty sensors out of a large network of sensor) and accommodate (replacing the faulty data with some other trusted data) is a matter of study included in the modelling part of this project. Machine learning technique has been proposed for the purpose in this project, and the importance of high-accuracy and reliability data for this applications is well known. Indeed, a machine learning algorithm is strongly dependent to the training dataset, therefore, the accuracy of the measurements in the training phase should be high as well as the reliability. Some work related to this project have beeen already conducted by Darvishi et al. [204] and the fundamental of the machine learning approach for the project SIGNIFY has been presented.
The purpose of the experimental work has been defined with the partners of the project, the activities can be resumed in three main points:

- Rig maintenance
- Calibration
- Data analysis

The first operations conducted were related to the rig maintenance, this included ordinary activities and non-ordinary issues. Among the overall activities performed it is included the replacement of filters, battery of the flow meter, leak detection and calibration of equipment and sensors. The most important operation was the calibration of the reference sensors, four Keller PA-33X reference sensors are mounted on different sections on the DeFACTO facility, namely two on the large leg and two on the smaller one. These sensor are used a reference for the calibration of the other sensors since they are more precise. In Figure 5.28a is a picture of one of the reference sensor Keller PA-33X mounted on the DeFACTO rig.

Since an anomaly in the atmospheric pressure has been identified in the reference sensors (namely 0.7 bar instead of 1 bar), a re-calibration was required. The overall operation of calibration lasted more than a week and required several steps. The main non-restricted aspects of the procedure and the results are reported. The calibration has been performed using a dead-weight, the machine is the fundamental digital pressure standard type 26000 M and is made by the company Desgranges et Huot. Several pressure levels were required from 10 to 160 bar in order to tune the calibration coefficient and recalibrate the sensors. Nitrogen has been utilized as a pressurized gas since it is not dangerous and its properties match the requirements at every pressure level tested. The software CCS30 has been utilized for the data acquisition and the calibration.

(a) Reference sensor Keller PA-33X mounted on the rig.

(b) Display for the UNIK5000 sensor.

Figure 5.28.: Sensors on the DeFACTO rig.

5.3.3. Data analysis

Once the calibration has been completed and the sensor mounted again on the rig, the monitoring system has been started up. Once the system was pressurized the acquisition of measurements from the sensors started too. The control panel for the management of the parameters and equipment consisted in a Lab-View interface situated on the roof of the building, next to the top of the facility.
To develop a easy-to-use data analysis tool, several python codes have been developed in order to simultaneously extract and analyse data from sensors. Data from the sensors are logged trough a National Instrument acquisition similar to the one described for the horizontal section in Section 5.2.1 of this chapter. Data can be then stored in multiple hard-disk in a *.cvs* format. Since huge amount of data and months of data can be easily stored in the system, a reliable and flexible tool to extract and analyse data was required.
The development of the code was divided in separate sections that operate specific calculation or operations, then only the processed data useful to the next section are exported and managed. This was very useful to speed up calculation and data extraction especially when dealing with lot of data, i.e. involving months of continuous logging. The structure of the code as reported in Figure 5.29, can handle few tasks wisely.

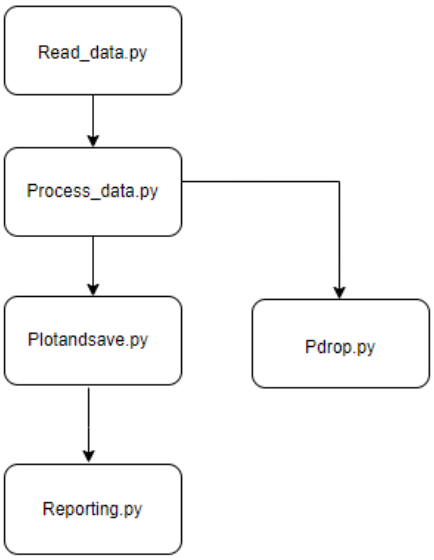

Figure 5.29.: Data analyser flow-diagram.

First step of the data analysis is the read and import data from the Lab-View output file, this task has been developed trough the creation of *data-frame* in a python pandas environment. This operation was useful to speed up the reading process and pass the created data-frame to the processing data script. The data processing has been developed with the flexibility to select a moving window in term of time-series, indeed a specific analysis on a transient phenomena can require the focus on specific few seconds of an event. This operation of *time-filtering* was also coupled with the possibility to sample the raw data to a sparser time-series. The sampling processing has been included with the setting of a single variable called *sampling-time*. With this feature, the monitoring of very slow processes such as hours of data logging, can be managed faster thanks to the reduction of the frequency between one measurement and the following one (i.e. 1 temperature value every 5 minutes instead of 1 value every 5 seconds). An example of the output passed trough a filtering and sampling operation is reported in Figure 5.30, where raw data from sensor TT-S5004 5.30a has been filtered from 45.14 min to end and sampled every 5 min 5.30b.

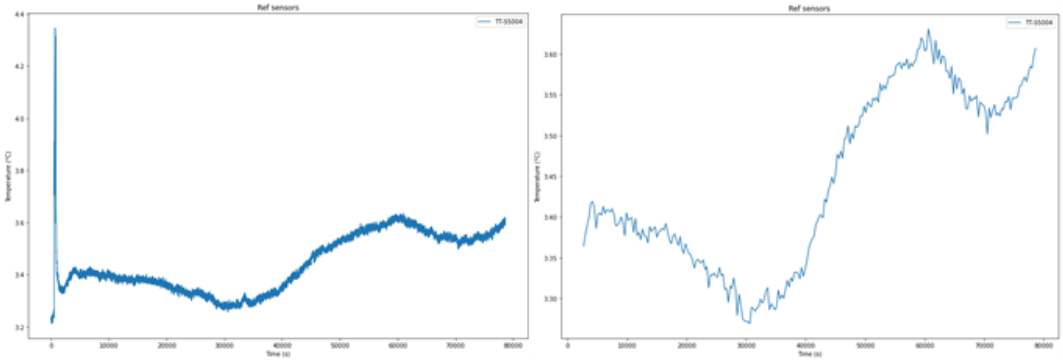

(a) Raw data from sensor TT-S5004.

(b) Filtered and sampled data from sensor TT-S5004.

Figure 5.30.: Filtering and sampling of sensors output.

The data processing has been developed with the utilization of dictionaries in python, this was the fastest way to perform multiple similar calculation on data-frames. Data analysis on the filtered and sampled data from the raw log are also analysed in this section of the code. The mean, standard deviation, slope, intercept and the R^2 are calculated for each time-series for every sensor output. The slope of the processed output was calculated in term of bar/min for the pressure sensors, kg/min^2 for flow sensors, while for temperature sensors was $°C/min$. The processed data according to the diagram in Figure 5.29 can be passed to the *Pdrop* function or the *Plotandsave* script. This selection can be done by the user and allow the possibility to switch trough two function depending on the desired output. The function *Pdrop* calculates the pressure drop for specific sensors identified among the all sensors available. The reference sensors are automatically selected for the analysis. The pressure difference between two selected point in time is calculated and the slope is calculated. This was also useful during the maintenance phase to identify the presence of leaks and try to quantify the entity of the leaking gas volume. An example of the output that can be obtained with this function is reported in Figure 5.31. In the case presented for the sensor PT-L5004, there was an evident pressure drop since the system was pressurized and closed. Indeed, after around 21 hours, the pressure drop from 31.165 bar to 24.703 bar, the estimate pressure drop rate was around 0.31 bar/h calculated as:

$$P_{drop} = \frac{\Delta P}{\Delta t} \tag{5.13}$$

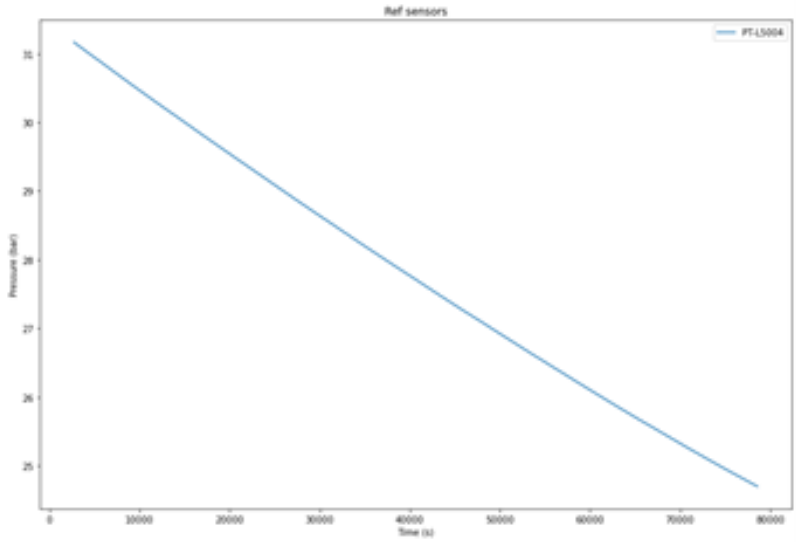

Figure 5.31.: Pressure drop registered for PT-L5004.

Going back to the process data function, if the pressure drop as been already assessed and are not object of specific interest, the next step is the *plotandsave* and *reporting* operations. This function are related to the editing and the arrangement of the previously calculated information into a well-organized report in *.pdf* format. The report is auto-generated and saved in the computer with all the relevant information and the figures generated by the code. Each page include specific analysis report for a group of sensors: flow meter sensor, outlet temperature sensors for CO_2, pipe surface temperature sensors for CO_2, tempearature in the well of the heating medium, pressure of the CO_2 in the well and temperature of the CO_2 in the well. An example of the auto-generated page for the CO_2 pressure in the well is reported in Appendix C.
The analysis of the data can be useful to obtain information and to better understand the behaviour of transient phenomena of vertical CO_2 flows, moreover the accurate measurement of pressure and temperature can be utilized for the estimation of density and to understand when the fluid appears to be in the two-phase region. The development of a digital twin of the plant as well as the improvement of the SIGNIFY project are considered for ongoing and future further research.

5.4. Expansion wave calculation

During the pre-commissioning of a pipeline, the quality of the material employed is strictly controlled. The possible formation of defect during the casting of metals and carbon-steel are taken into account from manufacturers. However, the presence of a defect cannot be completely avoided. Indeed, many internal and external factors can contribute to the development of defects especially after the production of the pipe sections. These defects can be due to outside forces, such as: corrosion,

operators mistakes, environmental conditions. During the service period, the defect can increase its length, both under the effects of the thermal stresses and stress induced by variations of operative conditions. Fractures occur when the stresses acting on a defect overcome the fracture initiation tolerance and reach the critical size, depending on pipeline geometry, material properties and operating conditions. The fracture in a metallic material can be of two different types: brittle or ductile. To avoid the brittle fracture of a pipe, the accurate selection of the material and the vendor can be an efficient solution. Indeed, during the years, lot of steel manufacturer have improved their capability to overcome to this problem. Brittle fracture can be avoided with an high toughness of the material, once the pipe is commissioned, the material engineer designer indicates the minimum required toughness for the pipe to be used in the project.
However, ductile fracture remains an issue that is harder to avoid, especially for challenging services such as CO_2-rich pipeline or when dealing with high-vapour pressure fluids in general. The ductile fractures can not be prevented in any case, but if it occurs it is possible to limit its propagation. The ductile fracture control analysis ensures that the fracture remains confined, i.e. it does not propagate along the pipe. In the unlucky event of ductile fracture, it can propagates through pipe sections and it length can extended up to several miles (see Figure 5.32).

Figure 5.32.: Ductile fracture propagation [20].

A solution to the fracture propagation control was found for the first time by "The Battelle Memorial Memorial Institute" in 1993. They proposed the so called "two-curves model", a multi-physic model based on the comparison of two curves,

one curve dependent by the pipe and the other dependent by the fluid at operative conditions. The two curves involved in the two-curve method are the velocity of propagation of a fracture to the internal pipe pressure, and the expansion wave velocity in the fluid to the internal pressure. The residual pressure acting on the crack tip of the pipeline represents the energy source governing the propagation of the fracture. The pressure profile is given by the expansion wave, which propagates along the pipeline during the fracture [108]. CO_2 pipelines are notably susceptible to propagating ductile fractures because the CO_2 is transported in the dense phase. Indeed, it is a high vapour pressure liquid. At high pressures, supercritical CO_2 behaves as a liquid, and has a liquid-like density, but it yields a very large volume of gas when its pressure is lowered. The rupture of a pipeline due to large propagation of ductile fracture, as previously discussed in Chapter 3 can pose risks to human and nearby wildlife. In the Oil & Gas industry the study of decompression and rapid expansion of gases/hydrocarbons, is a well established operation. The study of running ductile fractures for high-vapour pressure (HVP) fluids has been studied both numerically and experimentally trough burst tests and rupture induced tests. During the development of CO_2 pipelines in the U.S. the behaviour of running ductile fracture has been studied, crack arrestors have been utilized for the limitation of the propagation (i.e. every 300 m). However, it should be noted that in the U.S. case, only pure-CO_2 was involved and transported via pipeline. As discussed in the previous chapters, in the near future, CCS project will require more flexibility in the management of CO_2 in order to abate costs. The cost reduction and the safe operation requirements are strongly impacted by the prevention of incidents (see 3.4) and the management of CO_2-rich mixtures. In Chapter 4 has been demonstrated how the presence of little amount of other chemical compounds can led to wrong VLE and density predictions. Thus, the calculation of expansion waves is strongly impacted by the prediction of the thermo-physical properties. In this section the propagation of ductile fracture has been analysed and a novel calculation tool is presented for the prediction of the expansion wave curve. Several equations of state have been tested since their impact on the properties prediction can not be neglected (see Chapter 4).

5.4.1. Literature review

The ductile fracture phenomena has been investigated during the year both for hydrocarbons and CO_2-rich mixtures. Indeed, the ductile fracture was first experienced in pipelines transporting natural gas. The problem also rose during the transportation of nearly pure-CO_2, while the presence of impurities has increased the impact on the ductile fracture propagation risk that should be properly assessed during the pipeline design. Running fractures are considered one of the most dangerous catastrophic mode of failure of high-pressure transportation pipelines [205]. High strength steels used for pipeline construction must have specifications, ensuring that any possible

defect in the pipeline will not lead to failure due to a brittle fracture. Nevertheless a ductile fracture of the pipeline cannot be easily prevented with the technologies currently available. Thus, a fractures can initiate at any service stress level, if defects occur into the pipe. Fracture initiation is associated with the critical through wall (axial) length of a defect which will result in a rupture, and is dependent upon the pipe geometry, material properties and operating stress. Fracture propagation occurs when a failure results in rupture and then the energy released by the fluid is greater than the resistance of the steel to running fractures [20]. In order to reduce the risks of the pipeline running fractures, the pipeline material, diameter and wall thickness, as well as mitigation measures (e.g. placement of the pipeline crack arrestors and using emergency isolation valves) are carefully considered in the design relying on predictions using mathematical models of fracture propagation and arrest [205]. Axially oriented defects tend to dominate, as the pipeline hoop stress is generally the largest contributor to the combined stress of a pipeline. Circumferential defects require the longitudinal stresses to exceed the hoop stress and are typically associated with additional loading of the pipeline due to environmental conditions or outside forces. These situations can impose a longitudinal force on the pipeline that when combined with any existing bending and longitudinal stress could cause stresses sufficiently higher than the hoop stress such that a circumferentially oriented defect could become critical [108]. The strategies to control the development of a long running fracture can be classified into two categories: prevention strategies and limitation approaches.

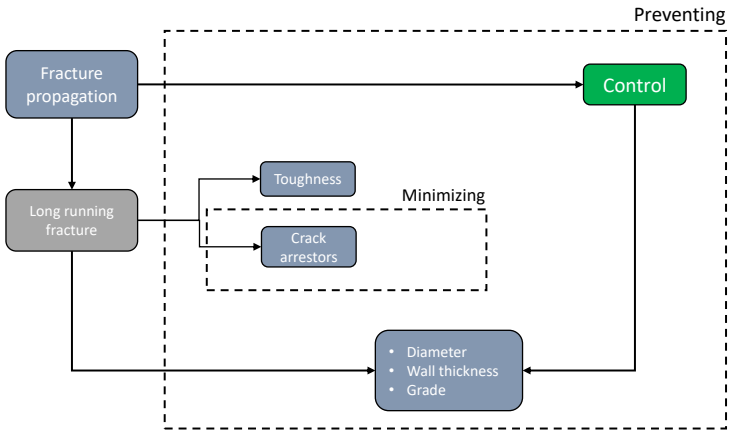

Figure 5.33.: Long running fracture propagation control strategies.

In Figure 5.33 a scheme of the main factors involved of the control strategies. The strategies of prevention include the accurate material selection of the pipe wall in term of steel grade, thickness and toughness. Crack arrestors has been classified in a sub-category of minimization, indeed they are designed as a safety structural tool that is capable to arrest the fracture by limiting the propagation. Literature reports the utilization of crack arrestors for CO_2 pipelines in the U.S. as the one reported in Figure 5.34 installed at a defined distance.

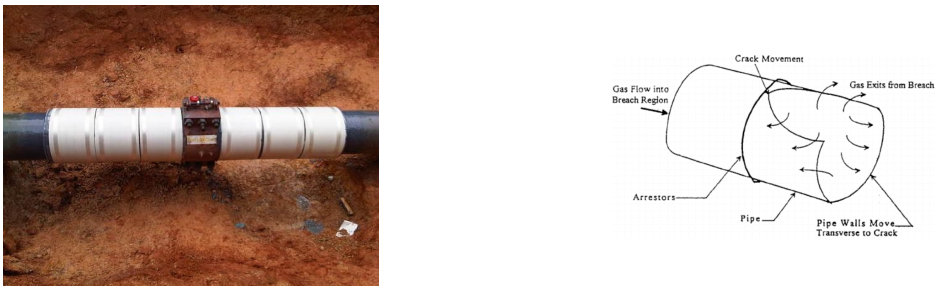

(a) Crack arrestor installed.

(b) Crack arrestor background.

Figure 5.34.: Crack arrestor for the limitation of fracture propagation [21].

In order to select the right properties for the materials involved during the design of a CO_2 pipeline, the prediction of the consequences of a possible rupture shold be investigated properly. In literature, several works have been published, with different approaches, to address the effect of a rapid decompression on the pipe wall. These aspects impact the selection of the pipe steel grade and thickness as well as the toughness required. The most popular approach reported in literature was the coupling of CFD simulations, or semi-empirical parameters, with finite elements method (FEM) tecniques to calculate deformations on the pipe wall. Talemi et al. [206] presented a hybrid fluid-structure interaction model that couple the results of a one-dimensional CFD model with a FEM model. The work, specifically designed for buried CO_2 pipelines, can assess the risk of brittle fracture. A similar approach has been presented by Aursand et al. [207] where a homogeneous equilibrium model, coupled with the Span-Wagner EoS has been utilized including the possibility to account for a solid phase. The results of coupling CFD models with FEM have been validated with good agreement with respect of fracture propagation velocity, however the non-direct applicability of the methods utilized for the natural gas has been confirmed [208]. Liu et al. [22] presented a multi-phase CFD model using GERG-2008 and included some 'source terms' for mass transfer and latent heat in order to model the non-equilibrium liquid/vapour transition. However, this methods are usually realized from custom made simulations, with very high-efforts in term of computational costs, as reported also in Chapter 3 for the simulation of

accidental releases. Furthermore, the development of simplified methods that can give reasonably accurate results with low computational costs and time, are often a viable solution. However, as noted from Cooper et al. [20] an additional correction on the measured CVN impact energy and on the saturation pressure is required when dealing with dense-phase CO_2 pipelines. Nonetheless, this is an issue regarding the measurement and the interpretation of the CVN results and should not impact the expansion wave curve calculated for the fluid when applying the BTCM, but only the "material" curve.

5.4.2. Thermodynamic and calculation model

The Battelle two-curve method is the most acknowledged method to estimate the fracture propagation and arrest. The method has been developed by the Battelle Memorial Institute and it is a multi-physics model that couple the model of the velocity propagation of a ductile fracture and the model of the velocity of the expansion wave in the pipe, both functions of internal pipe pressure. The energy required for the fracture to propagate is provided by the internal pipe pressure acting on the crack tip. Given a certain material, temperature and geometry, it is possible to correlate the propagation velocity of a ductile fracture to the internal pipe pressure. During a decompression, if the expansion wave velocity is higher than the crack propagation velocity ($U_{wave} > U_{crack}$), the fracture will remain confined. Otherwise, if the expansion wave is lower or equal to the crack propagation velocity ($U_{wave} < U_{crack}$), the residual pressure will provide the required energy for the crack to propagate.

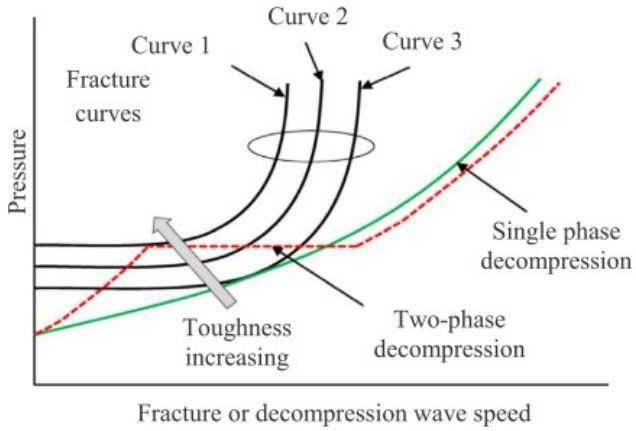

Figure 5.35.: Battelle two-curves method [22].

In Figure 5.35 an application of the Battelle two-curve method (BTCM) is reported.

It can be observed how the curves 1, 2 and 3 correspond to different materials based on their properties. It is emphatized how the different type of fluids can show different behaviour during the decompression and consequently the expansion wave velocity curve trend. Indeed, a single-phase fluid such as natural gas, shows a smooth curve that intercept the material curve in a lower pressure point if compared to a two-phase decompression. For a two-phase decompression, it is typical to observe the "plateau zone" that correspond to the phase transition from liquid phase to two-phase gas-liquid and then from two-phase to gas phase. This behaviour during the decompression has been also discussed in Chapter 4 when dealing with impurities and the calculation of density. The impact of impurities, also reported in Chapter 2 has a strong impact on the VLE and so the plateau zone appearance during the calculation of the expansion wave curve.

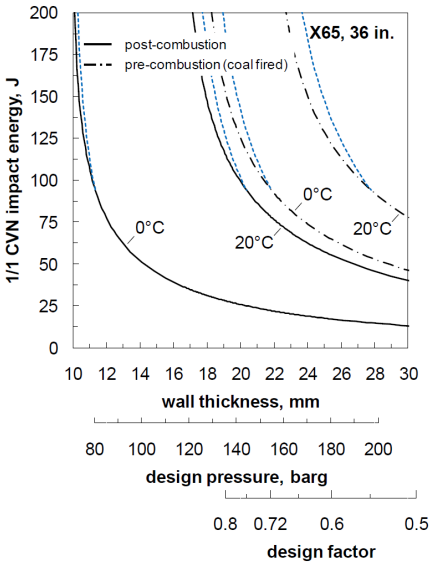

Figure 5.36.: The effect of wall thickness, design pressure and design factor on the full-size CVN impact energy required to arrest a running ductile fracture [22].

Since the intercept of the two-curve method (BTCM) is very different from a single-phase to a two-phase decompression, the considerations regarding the pressure and the toughness required from the Charpy-V notch test are different. As noted by Cooper et al. [20] the methods for determining the toughness requirements to arrest a propagating ductile fracture are semi-empirical, and have not been validated for application to dense phase CO_2 pipelines. Indeed, when developing a facture control plan for a carbon dioxide pipeline, the limiting condition corresponds to the minimum operating pressure and the maximum operating temperature, for natural gas is the opposite. In Figure 5.36 it is reported how the material requirement in term of toughness can vary with other parameters such as wall thickness, design pressure and design factor. Few observation can be outlined for a CO_2-rich mixture:

- The increase of the saturation pressure will increase the toughness required to arrest a running ductile fracture.

- Increasing the initial temperature will increase the arrest toughness.

- Increasing the concentration of H_2, CO, O_2, N_2, Ar or CH_4 will increase the arrest toughness.

The semi-empirical method defined by the Battelle Institute, requires as input the curve related to material property that can be obtained from the manufacturer trough the Charpy-V notch test and the expansion wave velocity curve. The calculation of the expansion wave rely on the correct estimation of the properties of the fluid during the decompression. For single-phase fluids the decompression calculation is simpler to calculate since there is no phase-transition, thus also the sound velocity is simpler to calculate. During the years, several calculation tools have been developed for the expansion wave velocity calculation. Among all the available in literature, the most acknowledged are:

- GASDECOM: uses the BWRS EoS with modified constants to optimise the estimations of light hydrocarbons gas mixtures decompression [209].

- DECAY: it is a code similar to GASDECOM, which adopts the PR EoS to evaluate the decompression of single-phase in a pipe undergoing fracture propagation [210].

- Decomwave: it uses combined EoSs (PR, SRK, BWRS) to evaluate the decompression behaviour of hydrocarbon gas mixtures [211].

- PRDECOM: it uses PR EoS and calculate the sound velocity with the Nichita method [212] in the two-phase zone [108].

An example of decompression where the appearance of a second phase is noticed is reported in Figure 5.37. The phase envelope in diagram p-T is reported, while the decompression curve is described as the intercept 5.37a. At the pressure in correspondence to the dew curve crossing, it can be observed the sudden change in density and consequent drop in the expansion wave velocity. When the fluid enters in the 'two-phase' region, usually the sound velocity shows a strong reduction, this is reflected in a slower expansion wave velocity, as showed in Figure 5.37b. The mixture considered for the example contains: CO_2 (0.8 mol), N_2 (0.1 mol), Ar (0.1 mol).

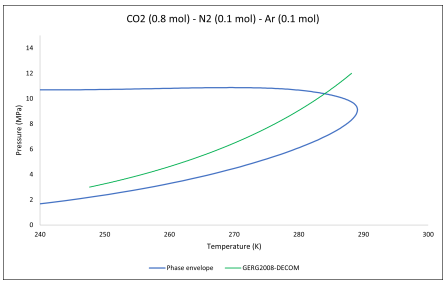

(a) Isentropic decompression prediction calculated by CO2RIDER and phase envelope (REFPROP 10.0) for a CO_2-rich mixture.

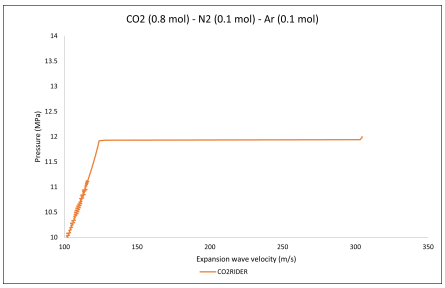

(b) Expansion wave velocity calcualted by CO2RIDER for a CO_2-rich mixture.

Figure 5.37.: Decompression prediction and expansion wave calculation of a CO_2-rich mixture.

A novel tool for the calculation of expansion wave is presented, the main objective of CO2RIDER (CO2-RIchDEcompRession) project was to develop a quick and reliable software, with a built in graphic user interface, for the simulation of the expansion wave of CO_2-rich mixtures. The model presented has been developed trough several assumptions: the multi-flash approach proposed by Dall'Acqua et al. [108] has been improved trough the utilization of the REFPROP 10.0 engine [196] coupled with a novel custom MATLAB algorithm, the sound velocity has been calculated with the method presented by Picard [213]. The method assumes that the process is isentropic and the flow is one-dimensional. The isentropic assumption was proven by Picard [213], who showed that non-isentropic effects will generally not be of concern for pipe sizes above approximately 508 mm OD. The code is divided in few sections, each section perform simple operations or iterates some instructions, in Figure 5.38 a scheme of the calculation method is reported.

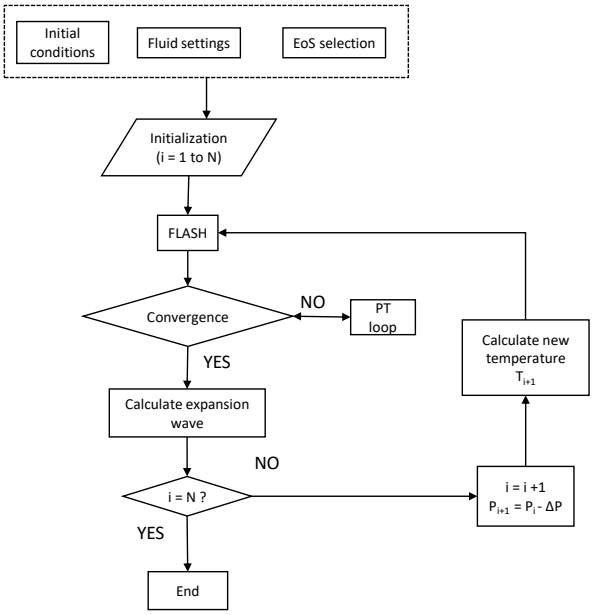

Figure 5.38.: Scheme of the calculation model.

In order to calculate the expansion wave velocity, the calculation model requires the following input variables to calculate the thermo-physical properties during the decompression:

- fluid mixture molar composition, (z_i)
- initial fluid pressure, $\mathrm{P_{start}}$
- initial fluid temperature, $\mathrm{T_{start}}$

The model calculates the expansion wave velocity for different pressure levels, starting from the initial conditions. The pressure step ΔP can be chosen arbitrarily by the user, in such way the decompression path is defined as:

$$P_{i+1} = P_i - \Delta P. \tag{5.14}$$

According to the scheme reported in Figure 5.38, the code can be divided in several sections:

- Setting-up
- Initialization
- Results plot and save

In the first phase, all the settings relevant to the utilization of the code, and the simulation start-up should have been defined. The composition of the mixture should be defined in term of molar composition and chemical compounds. The code can manage all the 147 pure fluids included in REFPROP 10.0 and mixtures up to 10 components. The capability of the code include the theoretical possibility to simulate the decompression behaviour of any type of hydrocarbon mixtures, however the optimization on the convergence for CO2RIDER have been designed for CO_2-rich mixtures.
The possibility to select a specific equation of state for the calculation among the ones available has been included in the Graphic User Interface of the code, indeed the EoS available are: the Peng-Robinson (with Peneloux volume correction), the AGA8, GERG-2008, Peng-Robinson and finally the REFPROP method. The REFPROP "Default" method implements three models for the thermodynamic properties of pure fluids: equations of state explicit in Helmholtz energy, the modified Benedict-Webb-Rubin equation of state, and an extended corresponding states (ECS) model [196]. Mixture calculations employ a model that applies mixing rules to the Helmholtz energy of the mixture components, as already described in Chapter 4.
The initialization of the calculation is made defining the starting conditions of the mixture, such as pressure P_{start} and temperature T_{start}. The pressure step ΔP is also required, if not selected by the user is automatically set to 0.01 MPa. The code calculates then the VLE and properties at the initial pressure and temperature such as: density (ρ), entropy (S) and quality (q). Once the entropy is calculated, the iso-entropic decompression calculation proceed for the next pressure step with convergence check at every iteration. If a non-convergence is detected by the limiters, a PT loop start to find the closest value of temperature that led to quasi-isoentropic results. A deviation is calculated as the difference between the current value of entropy and the starting one (see Equation (5.15)). The threshold is fixed to an error of 5% but can be changed by the user. When the condition is verified the PT loop breaks and the regular calculation proceeds.

$$S_{dev} = \frac{S_{start} - S_i}{S_{start}} \tag{5.15}$$

During the failure, the fluid starts to flow outward from the opening area. The fluid velocity changes along the pipeline due to the traveling expansion wave. The local fluid velocity is calculated by the compatibility equation, as reported by Picard [213].

$$u = -\int_{P_{start}}^{P} \frac{dP}{\rho c} \tag{5.16}$$

where P is the local pressure and c is the speed of sound at zero frequency travelling in fluid at same conditions. Supposing the rupture at the right end of the pipe, the minus sign of the Equation (5.16) would change with a positive sign. For an isentropic flow $dP = c^2 d\rho$, so it is possible to reduced Equation (5.16) to its differential form:

$$du = c_i \frac{d\rho}{\rho_i} \tag{5.17}$$

where, the subscript i represents the i-th step, described by the state (P_i, T_i). For discrete differences the Equation (5.17) becomes:

$$\Delta u = c_i \frac{\Delta\rho}{\rho_i} \tag{5.18}$$

where $\Delta\rho = \rho_i - \rho_{i+1}$. The local fluid velocity is calculated for each pressure decrement, by

$$u_{i+1} = u_i + \Delta u \tag{5.19}$$

The assumption of a null initial fluid velocity, $u_0 = 0$, does not affect significantly the result. Generally, in gas pipeline, the fluid has a maximum velocity of 15 m/s, which is far lower than the sound velocity, so assuming a null initial fluid velocity would introduce a small error in the prediction of the expansion wave velocity. For each pressure step i corresponds a velocity of the expansion wave. Once known the sound velocity of the fluid and the local fluid velocity it is possible to calculate the expansion wave velocity, as:

$$\omega_i = c_i - u_i \tag{5.20}$$

Passing from a single phase to a two-phase system (vapour-liquid), the sound velocity decreases dramatically when the second phase appears and the flow keeps as a homogeneous dispersion. Speed of sound in two-phase fluid is object of research also in this days, several authors performed experimental measurements and proposed their models across the years. Flatten [214] and Lund [215], Castier [216] and Nichita [212] among many others, proposed different approaches and method for the calculation of speed of sound. The method proposde by Nichita [212] and utilized by Dall'acqua et al. [108] has been tested during the work, but no relevant improvement on the results has been noted nor the code slowdown. REFPROP engine do not allow calculation of sound velocity in two-phase zone, thus a methodology for the sound velocity calculation is utilized. CO2RIDER utilizes the method presented by Picard, the sound velocity is calculated as finite difference, both in the single-phase and in two-phase. The speed of sound is calculated as:

$$\sqrt{\left(\frac{\Delta P}{\Delta\rho}\right)_S} \tag{5.21}$$

where:

$$\Delta\rho = \rho(P, T_1) - \rho(P - \Delta P, T_2) \tag{5.22}$$

where the temperature T_2 respect the isentropic condition $S(P, T_1) = S(P - \Delta P, T_2)$. The same calculation method for the speed of sound is implemented in the

decompression code called GASDECOM [209, 217].

5.4.3. Validation with experimental data

The accuracy of a simulation tool needs to be validated with experimental data and sometimes also compared with other software. The availability of experimental data for full-scale decompression tests involving natural gas or hydrocarbon is quite limited while for CO_2-rich mixtures is even lower. However, in this work, a comparison of CO2RIDER with experimentally measured expansion waves has been performed and reported in this section. The Northern Alberta Burst Tests were conducted at Foothills by Picard er al. [213], the so called NABT3 composition has been validated for natural gas composition while more focus has been reserved for CO_2-rich mixtures data. The tests performed at TransCanada PipeLines (TCPL) [218] has been utilized for the validation, moreover, other tests reported by Botros et al. in 2017 [219]. The composition of the mixture tested is reported in Table 5.8 while the initial condition of each test in Table 5.9. NABT3 and Test 4 involves a composition tested at the Trans Canada Pipeline Gas Dynamic Test Facility in Alberta, Canada [218, 220]. Test 2-3 and 11 refers to the work published by Botros et al. [219], while the tests from Test 5 through Test 10 were commissioned by the National Grid at GL Noble Denton's Spadeadam Test Site in Cumbria, UK [221].
The accuracy of CO2RIDER for the prediction of the expansion wave for the NABT3 case shows a good agreement with the experimental data. In Figure 5.39 a comparison between the experimental data and the model utilizing the GERG-2008 EoS for the determination of the properties. The first section of the decompression curve is predicted well, a slightly deviation is encountered in the phase-change zone, while the last part is reasonably well predicted. The accuracy of the code against CO_2-rich mixtures has been tested with different composition and different models, including GERG-2008, Default REFPROP method, and Peng-Robinson with Peneloux volume correction. In Figure 5.40 a comparison between the prediction of the CO2RIDER utilizing the PR(Peneloux) EoS and the GERG-2008 is reported against a scatter of the available experimental data. The accuracy of the GERG-2008 is undoubtedly superior in this specific case in the first part of the decompression. However, the description of the plateau looks very similar. Main differences rely in the correct prediction of the VLE as reported and widely discussed in Chapter 4.

	NABT3	Test 2	Test 3	Test 4	Test 5	Test 6	Test 7	Test 8	Test 9	Test 10	Test 11
CO_2	-	0.94028	0.96670	0.72600	0.95960	0.97380	0.91710	0.96190	0.93030	0.91030	0.96516
Ar	-	-	-	-	-	-	-	-	-	-	-
He	-	0.00025	-	-	-	-	-	-	-	-	0.00014
H_2	-	-	-	-	-	0.02620	0.04000	0.00900	0.00950	0.01150	-
O_2	-	0.00127	0.03330	-	-	-	-	0.00970	0.01870	0.01870	-
Methane	0.85350	-	-	0.27400	-	-	-	0.00910	0.02130	0.01950	0.03470
Ethane	0.08220	-	-	-	-	-	-	-	-	-	-
Propane	0.04340	-	-	-	-	-	-	-	-	-	-
Isobutane	0.00182	-	-	-	-	-	-	-	-	-	-
Butane	0.00278	-	-	-	-	-	-	-	-	-	-
Isopentane	0.00029	-	-	-	-	-	-	-	-	-	-
Pentane	0.00028	-	-	-	-	-	-	-	-	-	-
Hexane	0.00013	-	-	-	-	-	-	-	-	-	-
Nitrogen	0.01560	0.05820	-	-	0.04040	-	0.04290	0.01030	0.02020	0.04000	-

Table 5.8.: Tested fluids molar compositions.

	NABT3	Test 2	Test 3	Test 4	Test 5	Test 6	Test 7	Test 8	Test 9	Test 10	Test 11
Pressure (MPa)	8.8	14.828	14.561	28.568	14.04	14.1	14.06	14.02	14.02	14.95	14.78
Temperature (K)	269.65	309.05	308.24	313.65	292.85	293.05	292.95	293.15	293.05	283.15	309.45

Table 5.9.: Tested fluids initial conditions.

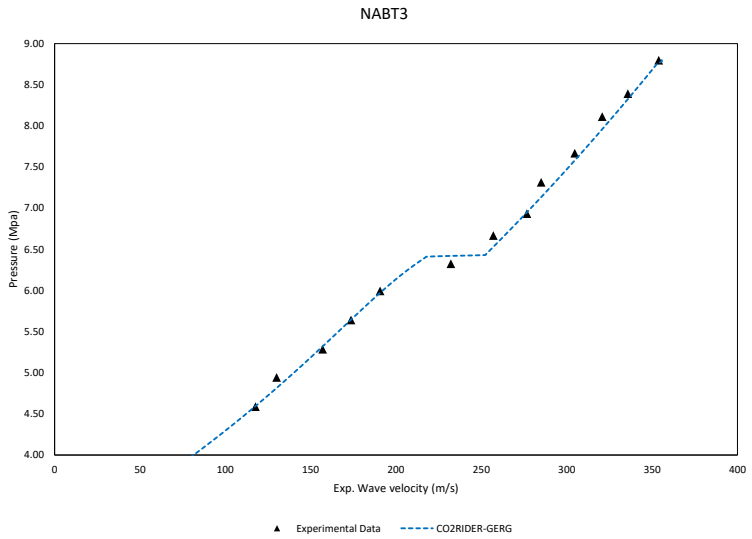

Figure 5.39.: Expansion wave velocity for the mixture NABT3. Comparison of CO2RIDER predictions against experimental data.

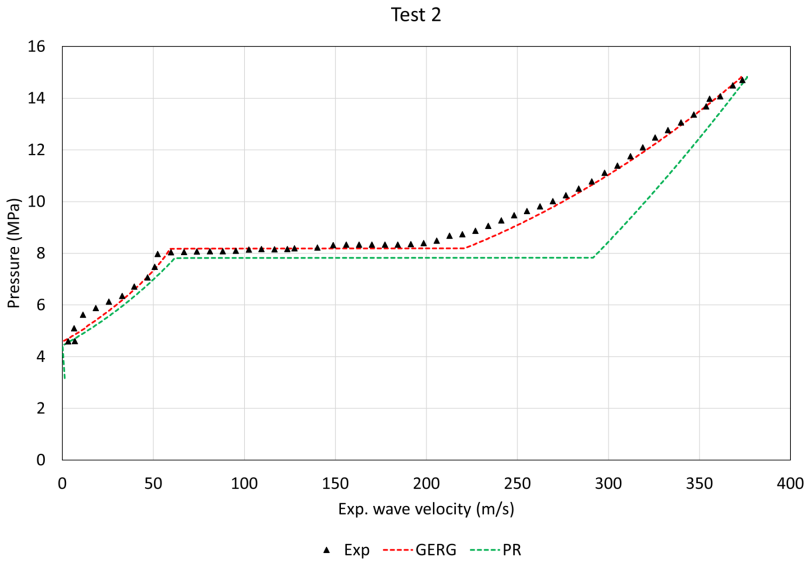

Figure 5.40.: Expansion wave velocity for the mixture Test 2. Comparison of CO2RIDER predictions with PR and GERG-2008 against experimental data.

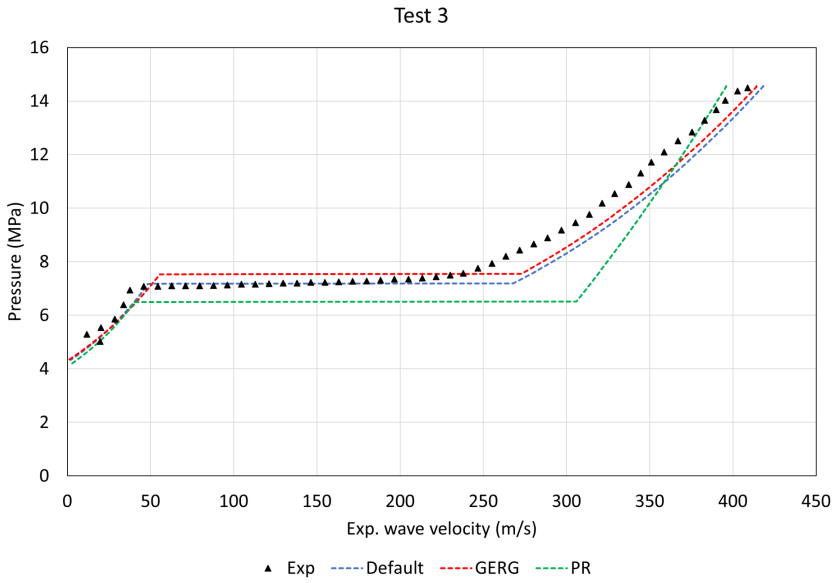

Figure 5.41.: Expansion wave velocity for the mixture Test 3. Comparison of CO2RIDER predictions with 3 EoSs against experimental data.

In Figure 5.41 a comparison between the 3 model available in CO2RIDER is proposed against the experimental data of the Test 3. The results show how the accuracy of GERG-2008 and REFPROP are superior in the first stages of the decompression. Nonetheless, the plateau description in the phase change zone show different aspects. The GERG-2008 appears slightly conservative in term of pressure, meaning that the plateau zone occurs before than the experimental data, while the REFPROP shows a closest accuracy. Peng-Robinson solution predict the curve with a little delay and appear to be under-conservative. Again the possible explanation of this rely on the differences in the VLE prediction. Test 4 5.42 and Test 11 5.43 confirm the superior accuracy of the GERG-2008 model for the prediction of the expansion wave.

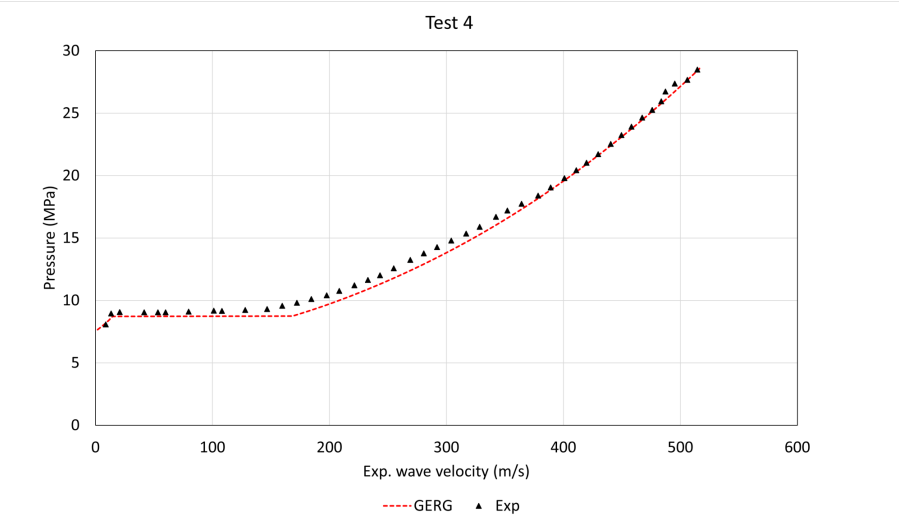

Figure 5.42.: Expansion wave velocity for the mixture Test 4. Comparison of CO2RIDER predictions against experimental data.

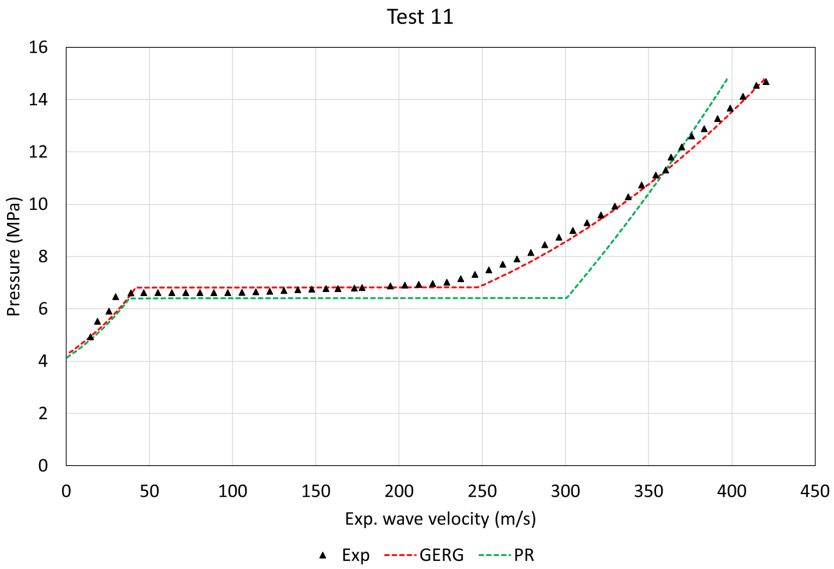

Figure 5.43.: Expansion wave velocity for the mixture Test 11. Comparison of CO2RIDER predictions against experimental data.

The results for Tests 5 5.44 and 8 5.45 show a better agreement for the PR model if compared with the GERG-2008. While the Test 6-7-9 has been compared directly

with the best performing method. Also in this cases a deviation between model and experimental data has been registered.

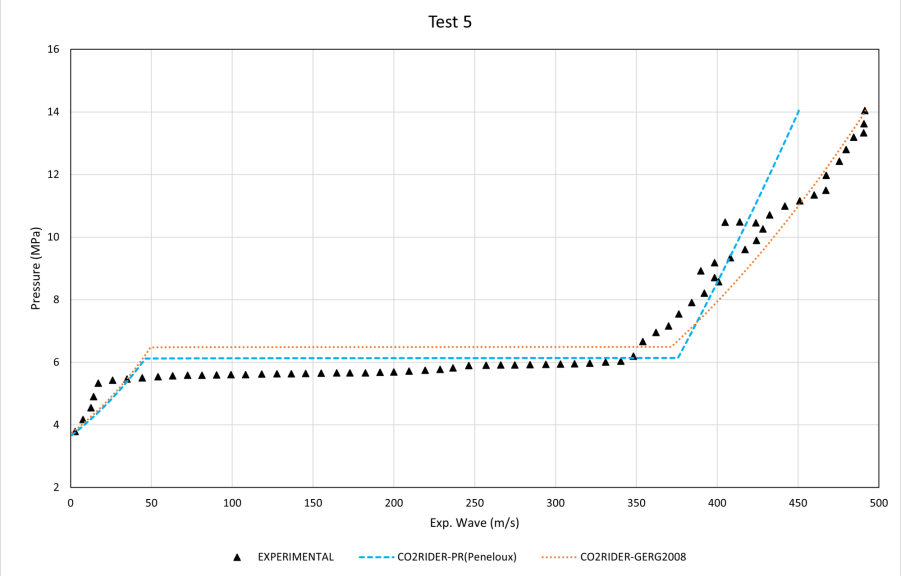

Figure 5.44.: Expansion wave velocity for the mixture Test 5. Comparison of CO2RIDER predictions against experimental data.

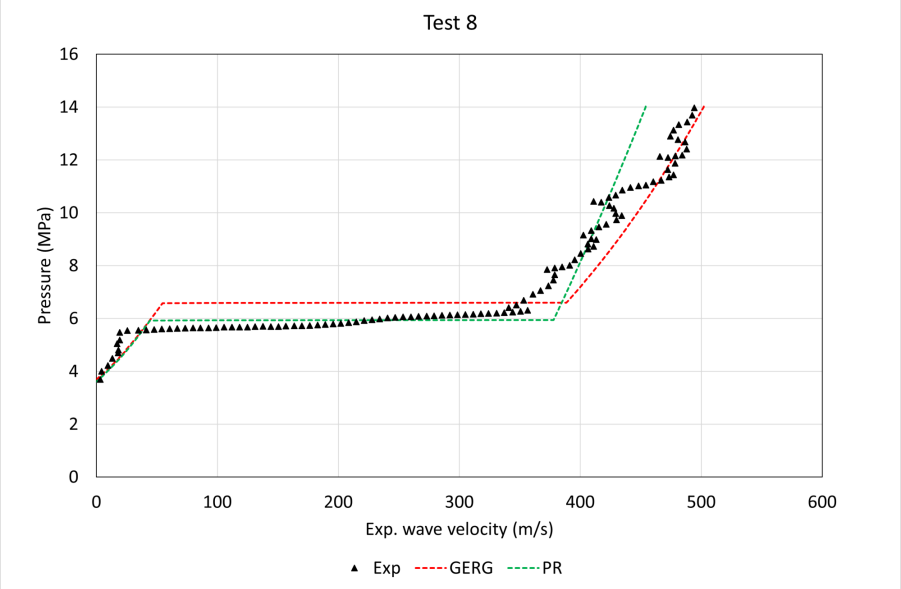

Figure 5.45.: Expansion wave velocity for the mixture Test 8. Comparison of CO2RIDER predictions against experimental data.

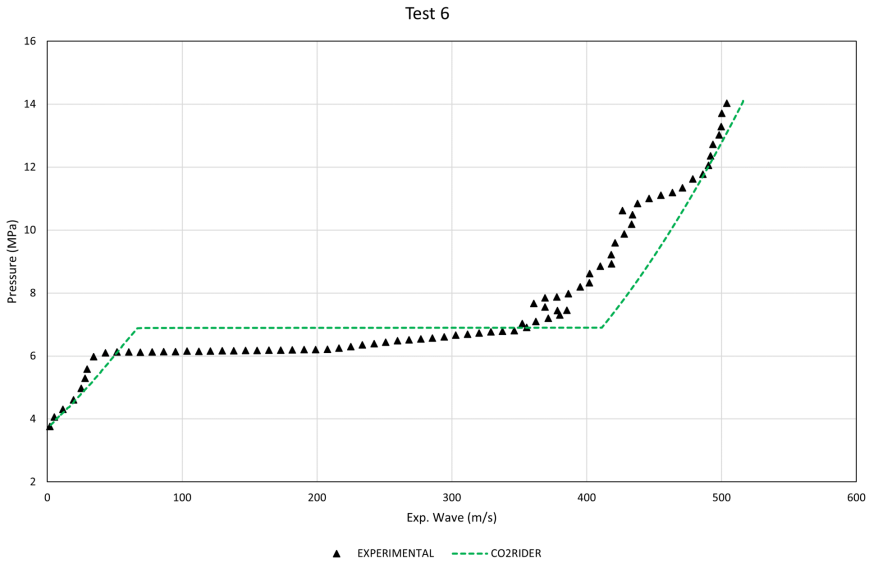

Figure 5.46.: Expansion wave velocity for the mixture Test 6. Comparison of CO2RIDER predictions against experimental data.

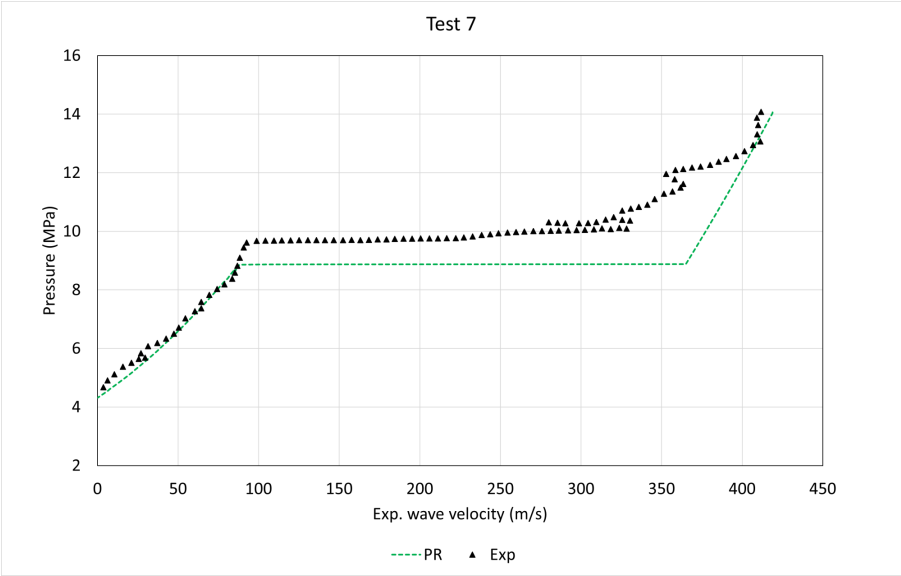

Figure 5.47.: Expansion wave velocity for the mixture Test 7. Comparison of CO2RIDER predictions against experimental data.

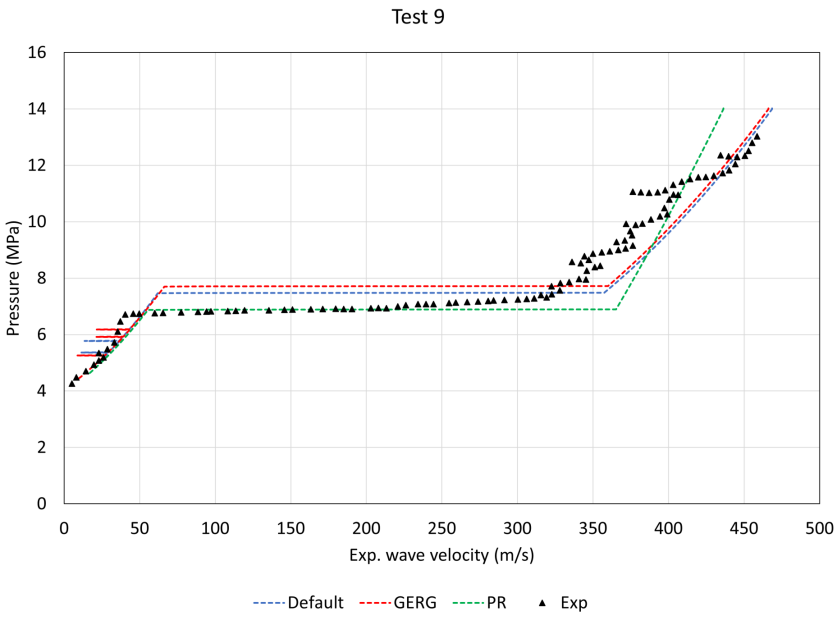

Figure 5.48.: Expansion wave velocity for the mixture Test 9. Comparison of CO2RIDER predictions against experimental data.

5.5. Conclusions

In this section the transient flow assurance of CO_2 has been investigate trough simulations and experimental work. The Chapter has been divided in three main sections, the horizontal depressurization, the vertical flow and the expansion wave calculation. Tool and methods has been proposed to advance simulations accuracy and emphasize the lack of accuracy of models in certain transient conditions. Horizontal transient flows have been analysed in this chapter with specific focus on depressurization scenarios. High-resolution experimental data have been collected from a leading laboratory in CO_2 processing and simulations. In order to validate the experimental data with predictions from simulations, a numerical model has been built. The model was defined in the OLGA environment and the most recent releases of the code have been tested against each other and also with experimental data. Several test have been compared starting from different initial conditions, including a gas phase test conducted with Nitrogen, gas phase test with CO_2 and finally dense phase or liquid CO_2. Pressure and temperature data from sensors and model in the same location have been compared and validated in order to identify the main differences. A grid refining as well as model tuning have been developed in order to reduce the instabilities and reach more accurate results. Several parameters have been modified in the default OLGA model in order to better converge the simulation, including integration coefficients, mass transfer tuning, heat transfer and valve models. Results have been presented and conclusions can be made. Pressure

was generally slightly under-estimated for most of the test especially in the first second of the depressurization and close to the release point. Generally, the time required to reach steady state condition (end of the depressurization) was comparable to the one registered to experimental data, however, the minimum pressure and the pressure drop trend is different. The temperature prediction on the other hand was also under predicted in term of minimum temperature, in some case the temperature difference was not negligible. The minimum temperature registered by the model in some cases highlight the possibility of solid phase formations while in the experimental test was not evident for every case. Finally, from the comparison of the OLGA code 2020.2 and 2021.1, based on the analysed data and the results obtained, it can be stated that a lot of numerical instabilities have been registered in 2020.2 if compared with the newest release 2021.1 both in term of pressure and temperature. However, the pressure and temperature prediction in term of minimum values was not always improved, indeed, in some cases a slightly worst behaviour have been registered. Despite that the deviation of was comparable to the results of 2020.2 with a substantial benefit gave by the instabilities reduction.

Vertical flows has been investigated experimentally, the work has been developed on the DeFACTO facility and some aspects have been reported in compliance with the NDA. The experimental campaign was mainly useful to acquire invaluable experience and knowledge in CO_2 management and processing in experimental setups. Operational maintenance and calibration of the equipment in the rig has been performed and a data extraction and processing tool has been developed. The DeFACTO reporter has been coded in python environment and it can easily manage many hours of data from the experimental rig as well as perform analysis and processing of the data. The capability to automatically produce a .pdf report of the data can be considered as a useful tool for the data analysis and improved the potential of the facility to capture the vertical flow behaviour in single and two-phase experiments.

The running ductile propagation phenomena has been investigated and a novel simulation tool for the calculation of the expansion wave has been presented. The importance of the correct estimation of the expansion wave has been explained and the two-method curve developed by the Battelle Institute has been utilized. A literature review of the available models and the work published on the topic is also reported. Based on the considerations regarding the VLE and density prediction of the different equations of state, an evaluation of their impact has been investigated. Indeed, as reported in Chapter 4, the density prediction can have an error between 1.32 and 3.18 %, while the VLE over-prediction up to 4.5 % can be envisaged. Based on the equation involved on the calculation of the speed of sound and consequently the expansion wave velocity (see from (5.16) to (5.20)), the impact of the equations of state errors cannot be ignored.

A new tool called CO2RIDER for the simulation of the decompression behaviour and the calculation of the expansion wave has been established and a validation against experimental data has been reported. The possibility to switch between different

equations of state in the same tool has been included for comparison and flexibility purpose. The tool can manage up to 10 different components in a single mixture, performances for natural gas mixture and CO_2-rich mixtures has been validated. The results obtained with the CO2RIDER are generally in good agreement with the experimental data, few observation can be outlined:

- Simulation performed with GERG-2008 shows a better agreement in the first part of the depressurization and in most cases a conservative over estimation of the plateau
- Peng-Robinson with Peneloux volume correction simulations shows different behaviour, but generally a slightly under-estimation of the plateau and a large deviation in the first part of the expansion wave
- Default method REFPROP has a similar behaviour of the GERG-2008 even if the plateau zone was predicted differently in some cases

The accurate prediction of the plateau of PR when the first part was clearly different from the experimental data, suggest that the PR has a lower accuracy in density prediction for the liquid/dense phase of CO_2-rich mixtures. This aspects can led to an observation: the non-accurate prediction of the density and the VLE of PR can led to a fictious well-predicted pleateau due to co-occurence of errors. This because with the same method of calculation, GERG-2008 showed better performances during the first part of the curve (single-liquid phase).
Finally, the accuracy of the CO2RIDER has been established and validated trough the experimental data available. A generally good agreemnent has been found for all the tested mixture, however, some test were predicted better from an EoS insted of another. This can be overcomed, by the accurate calculation of the deviation in term of VLE and density prediction by performing a sample of the mixture and tune the parameter to the better fitting equation of state. The deviation of some EoS has been calculated in Chapter 4, and seems to be dependent on the presence of certain component in the mixture. Thus, for a first estimation of which EoS can led to a more accurate results, if experimental data is not available, a similar analysis can be conducted.

Appendix A.

VLE EoS Validation Results

In this appendix all the results plots obtained from the VLE analysis conducted as reported in Chapter 4.

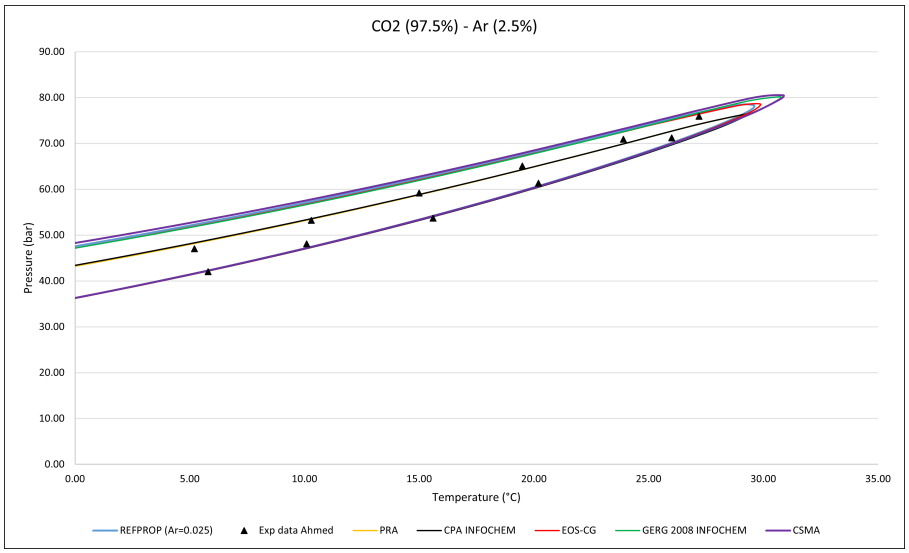

Figure A.1.: VLE experimental data from Ahmad et al. [23] vs models. (I)

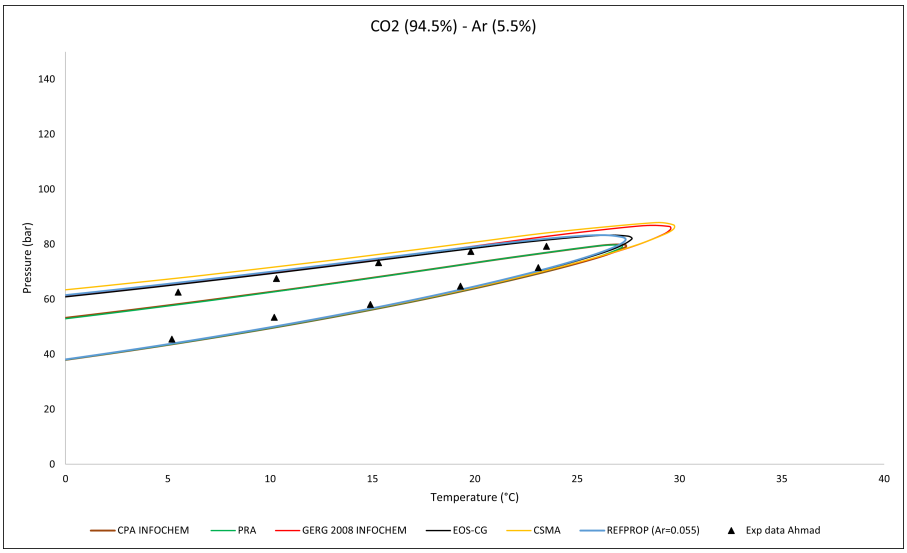

Figure A.2.: VLE experimental data from Ahmad et al. [23] vs models. (II)

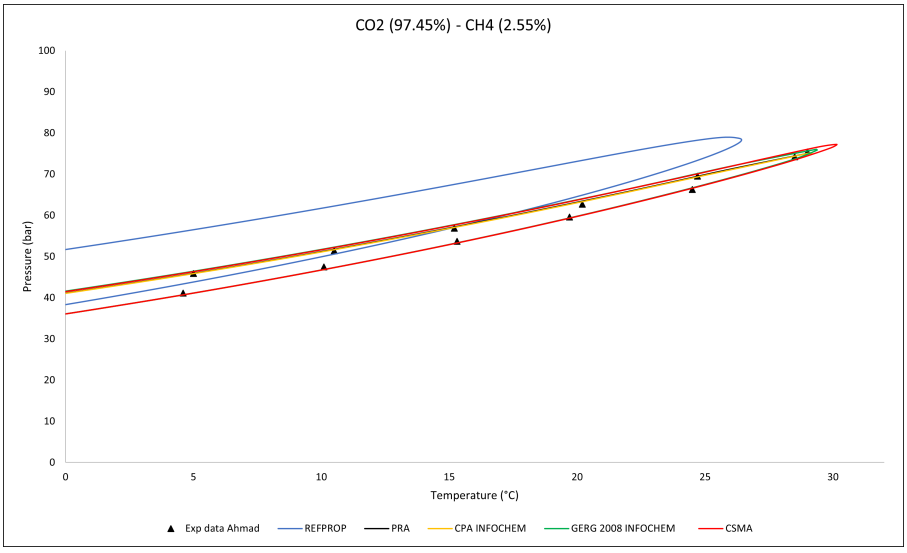

Figure A.3.: VLE experimental data from Ahmad et al. [23] vs models. (III)

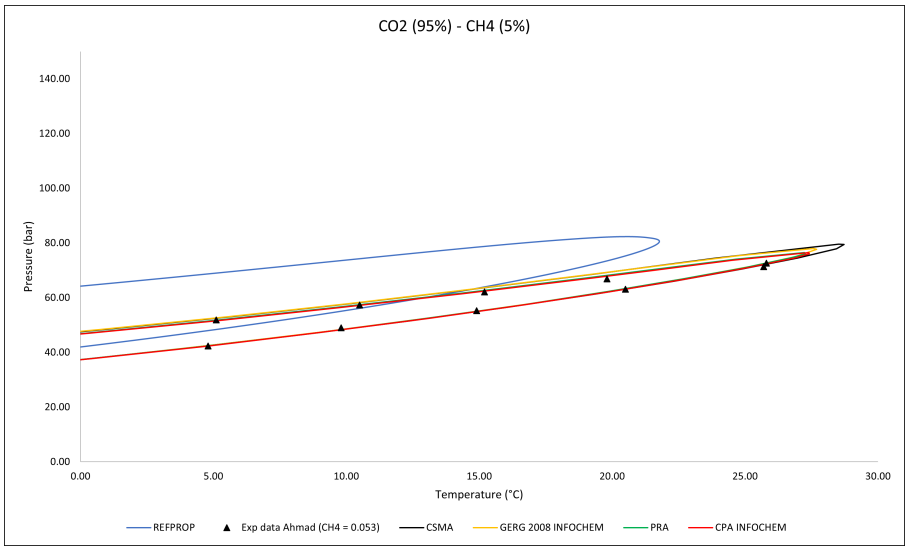

Figure A.4.: VLE experimental data from Ahmad et al. [23] vs models. (IV)

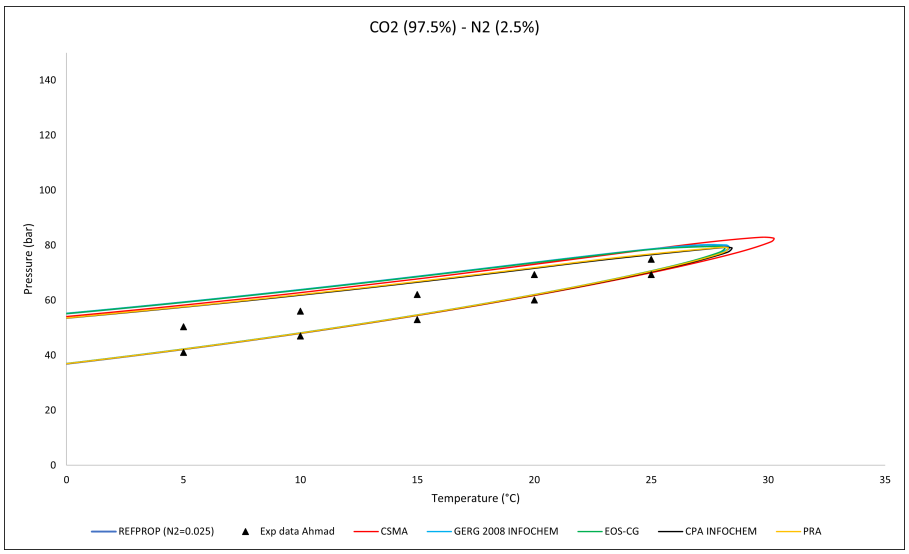

Figure A.5.: VLE experimental data from Ahmad et al. [23] vs models. (V)

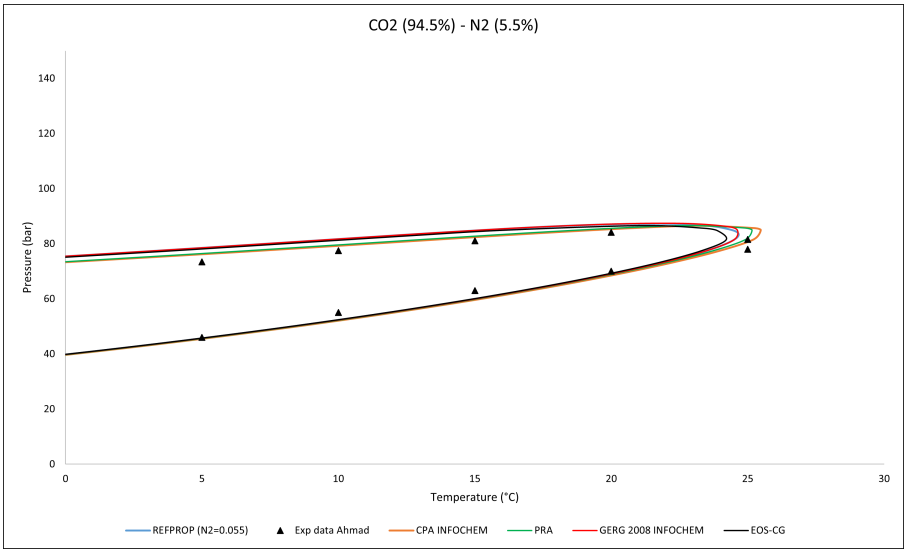

Figure A.6.: VLE experimental data from Ahmad et al. [23] vs models. (VI)

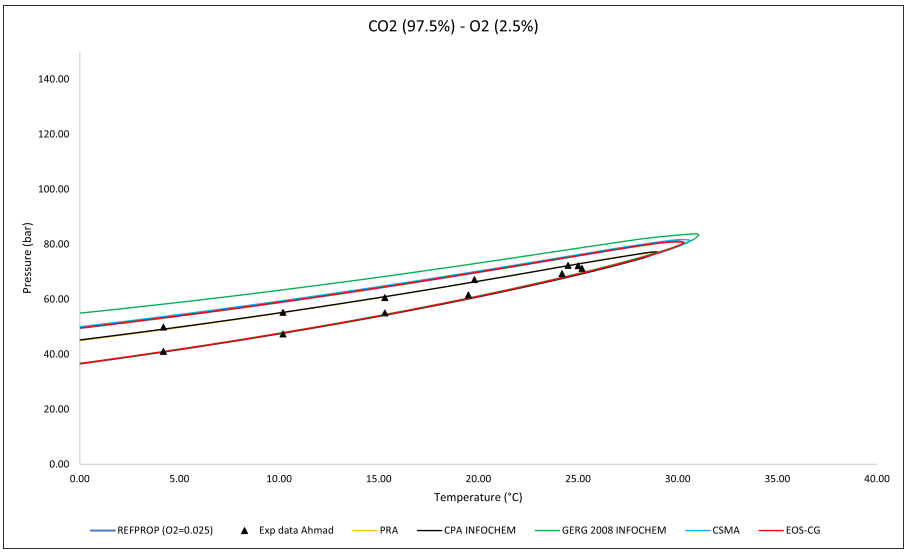

Figure A.7.: VLE experimental data from Ahmad et al. [23] vs models. (VII)

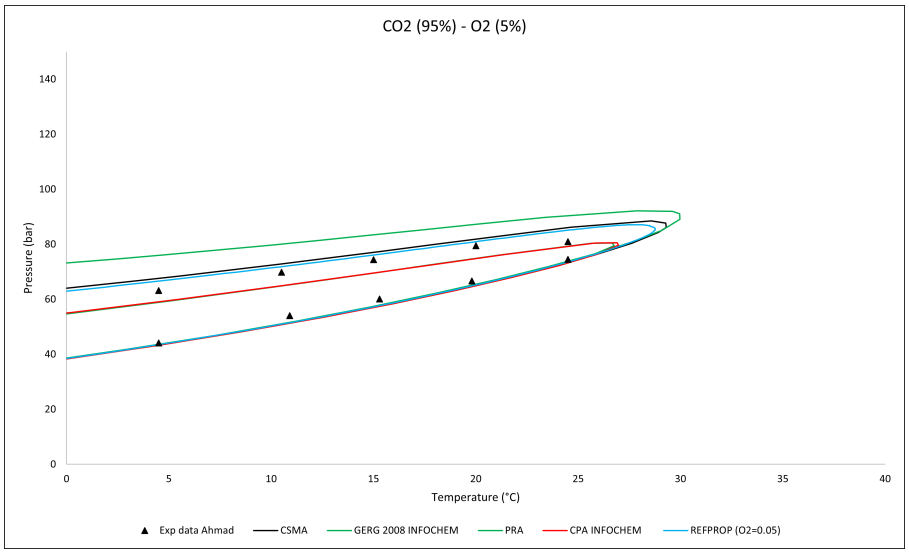

Figure A.8.: VLE experimental data from Ahmad et al. [23] vs models. (VIII)

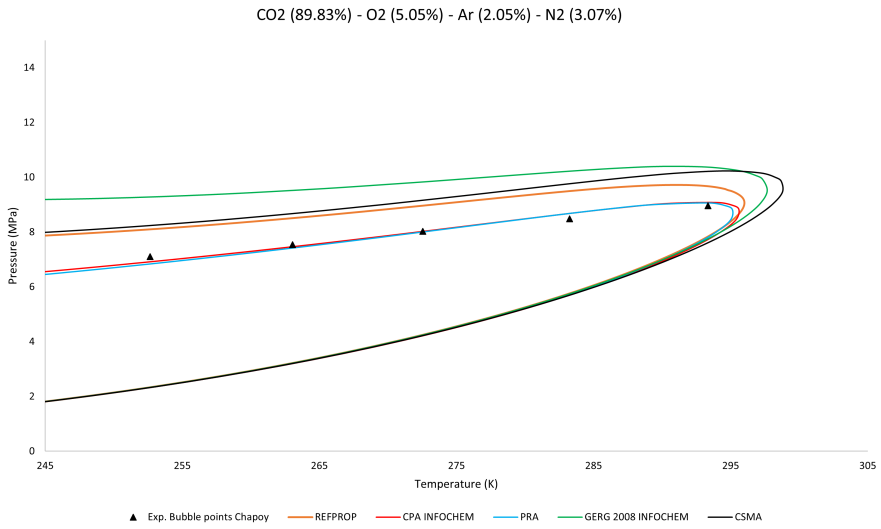

Figure A.9.: VLE experimental data from Chapoy et al. [15] vs models.

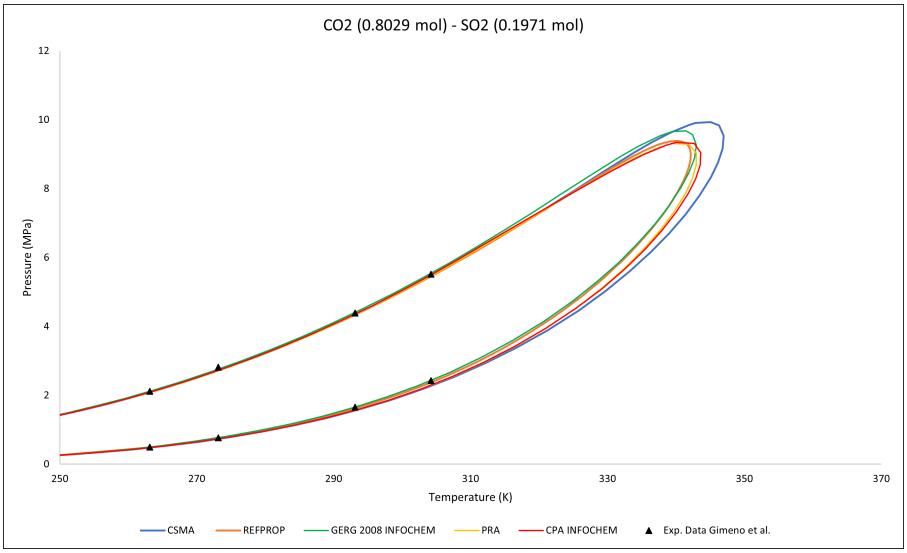

Figure A.10.: VLE experimental data from Gimeno et al. [16] vs models. (I)

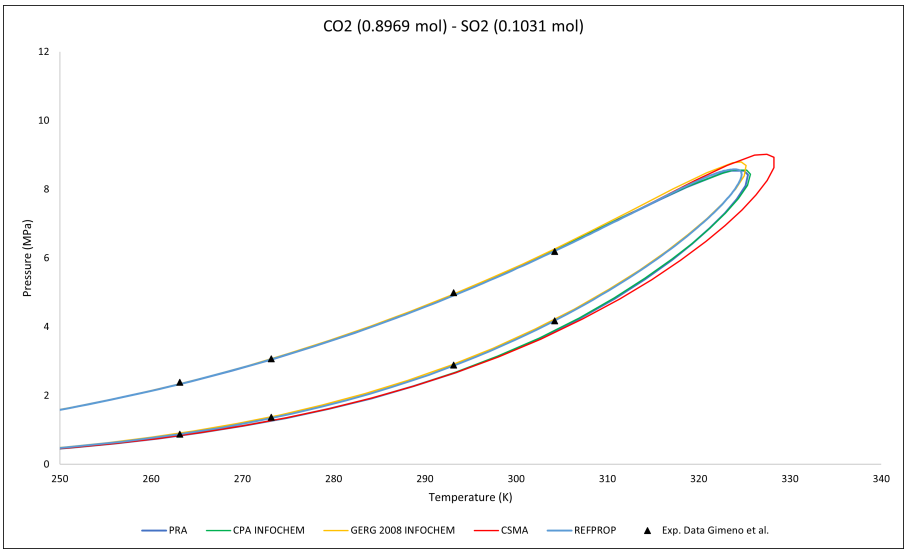

Figure A.11.: VLE experimental data from Gimeno et al. [16] vs models. (II)

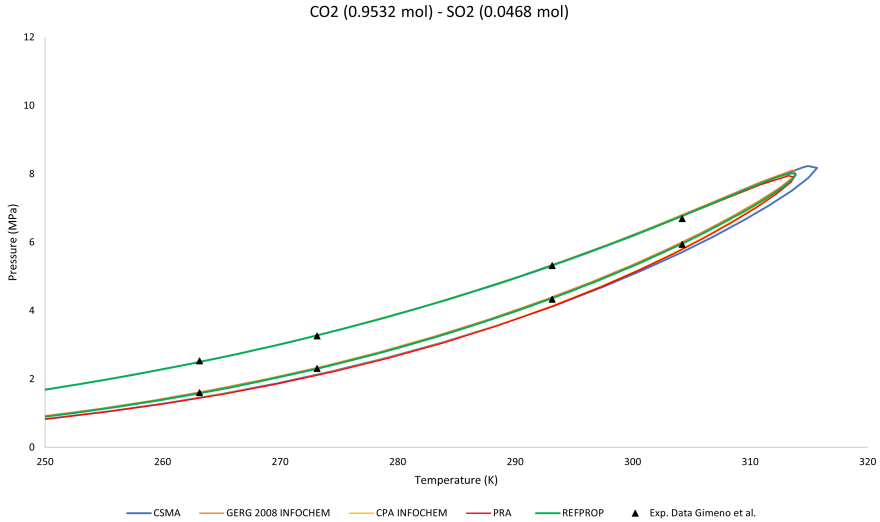

Figure A.12.: VLE experimental data from Gimeno et al. [16] vs models. (III)

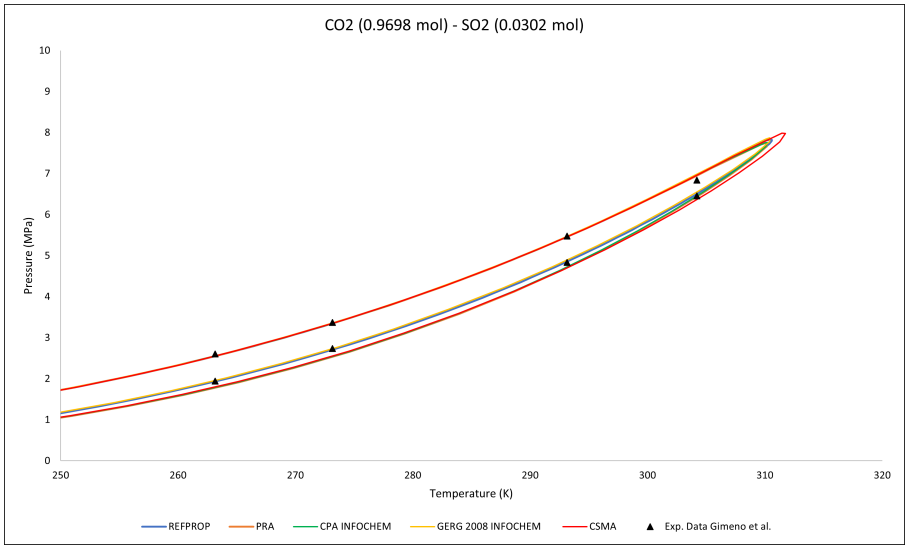

Figure A.13.: VLE experimental data from Gimeno et al. [16] vs models. (IV)

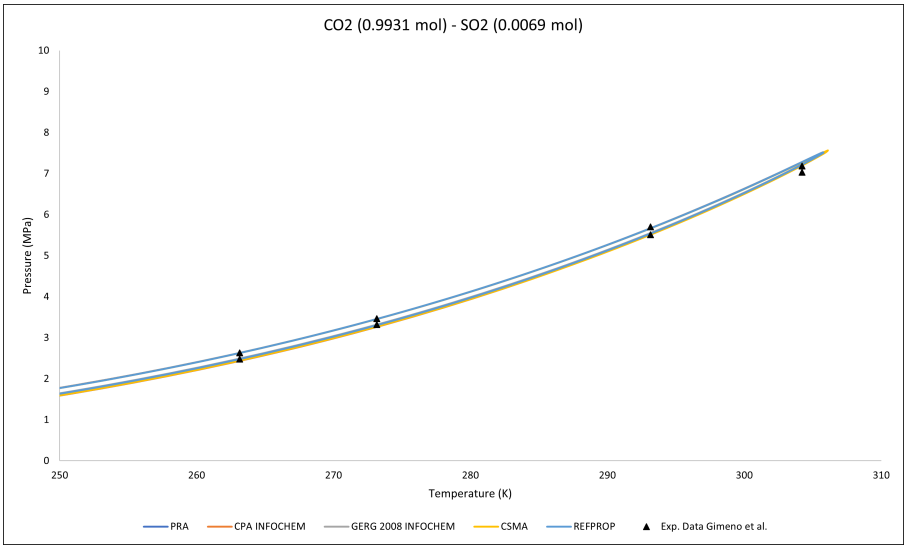

Figure A.14.: VLE experimental data from Gimeno et al. [16] vs models. (V)

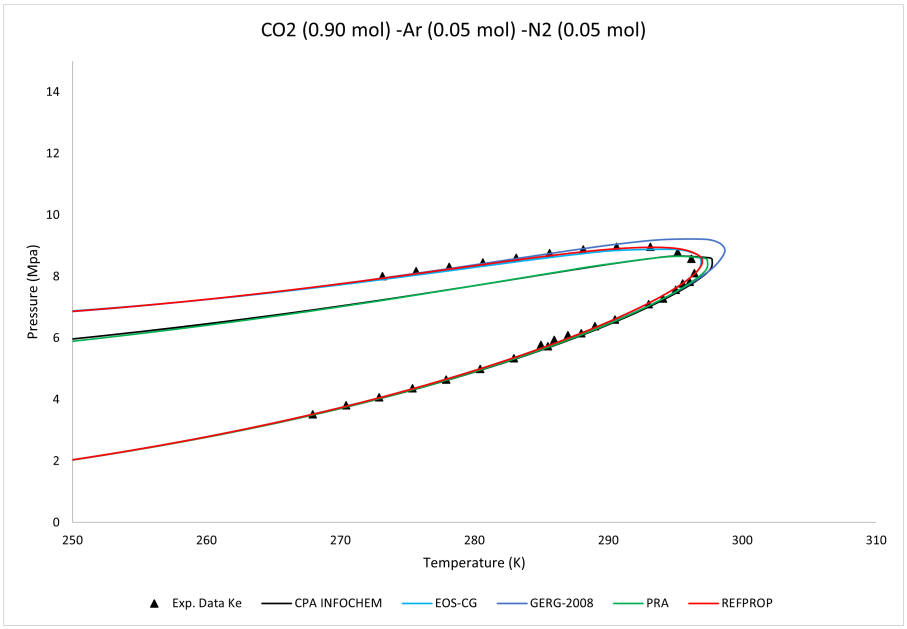

Figure A.15.: VLE experimental data from Ke et al. [24] vs models. (I)

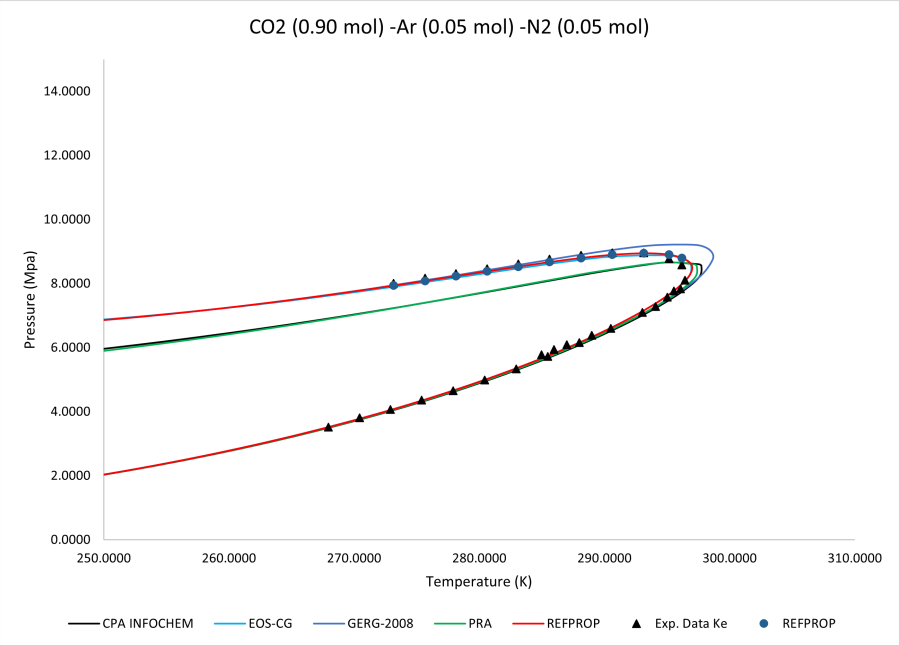

Figure A.16.: VLE experimental data from Ke et al. [16] vs models. (II)

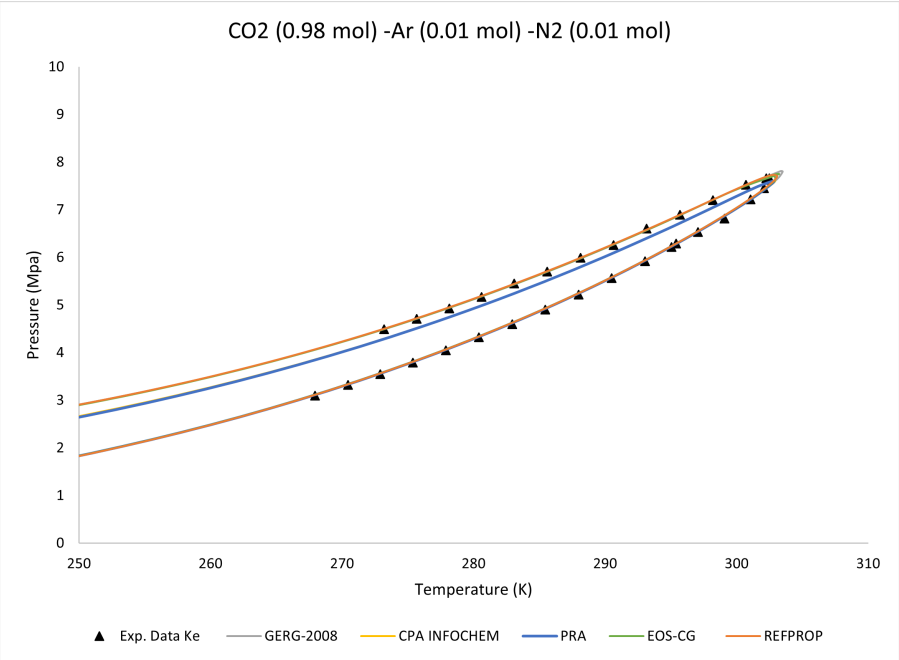

Figure A.17.: VLE experimental data from Ke et al. [16] vs models. (III)

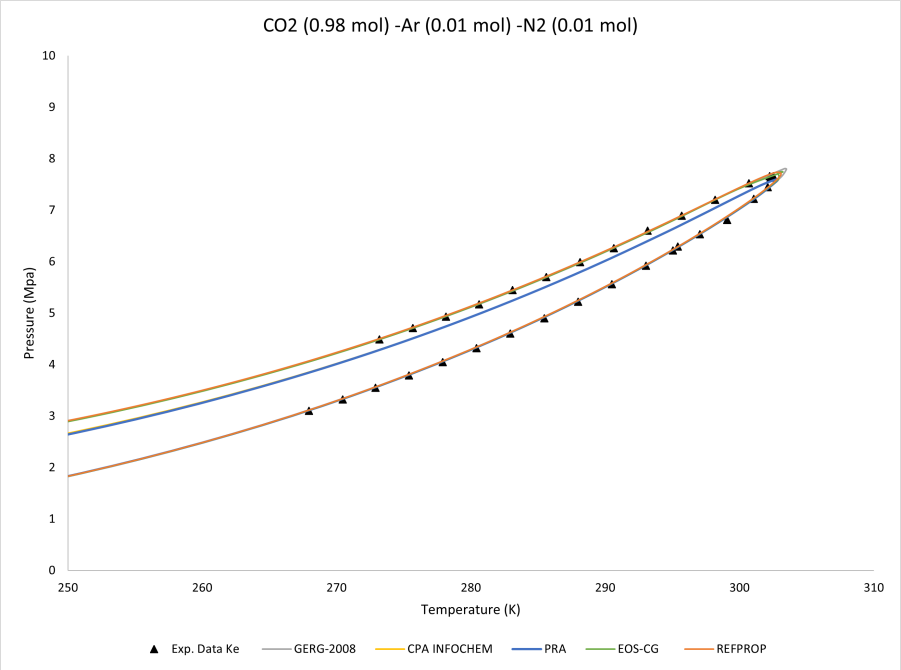

Figure A.18.: VLE experimental data from Ke et al. [16] vs models. (IV)

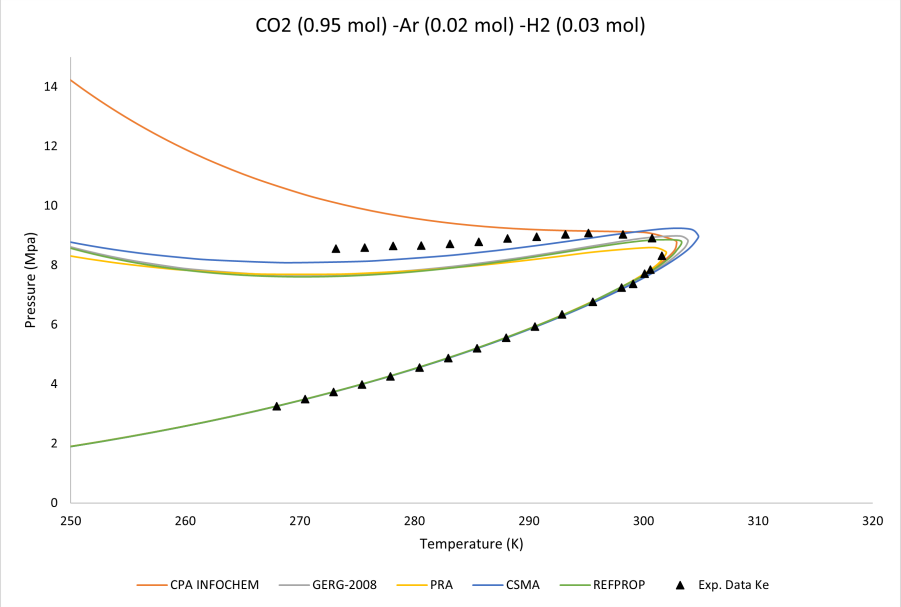

Figure A.19.: VLE experimental data from Ke et al. [16] vs models. (V)

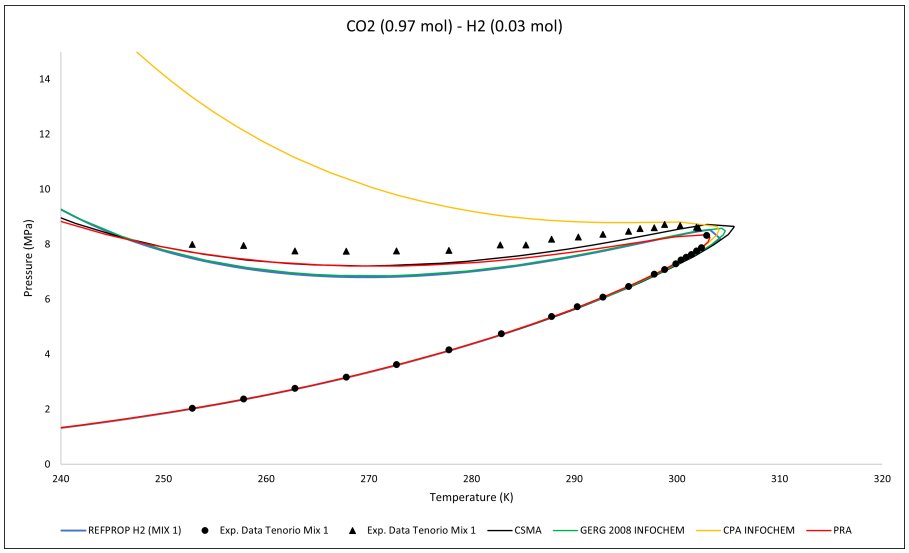

Figure A.20.: VLE experimental data from Tenorio et al. [14] vs models. (I)

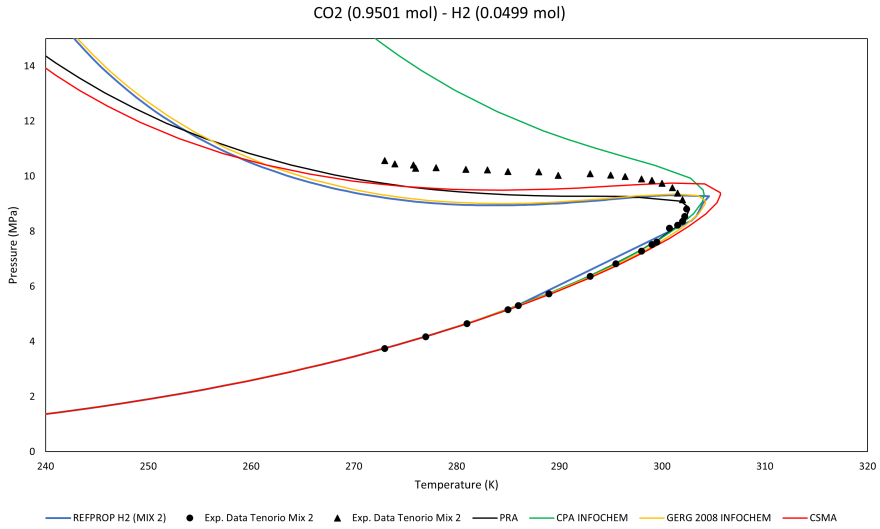

Figure A.21.: VLE experimental data from Tenorio et al. [14] vs models. (II)

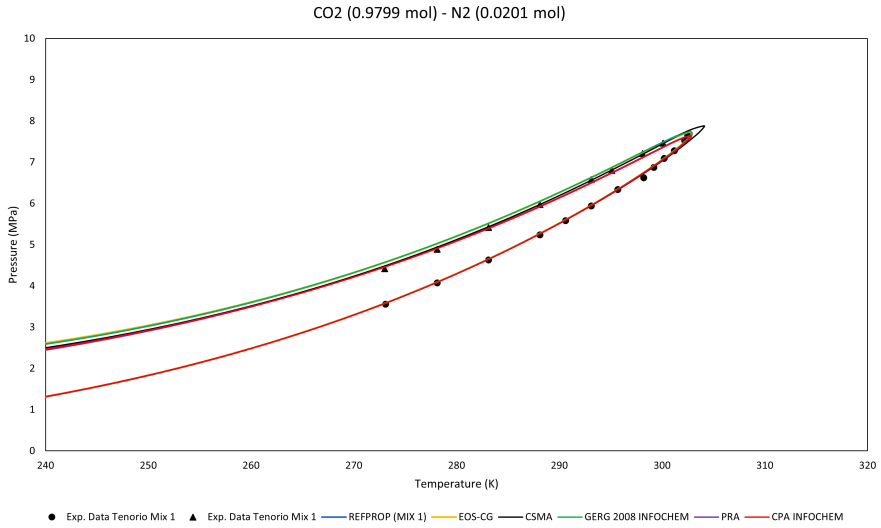

Figure A.22.: VLE experimental data from Tenorio et al. [14] vs models. (III)

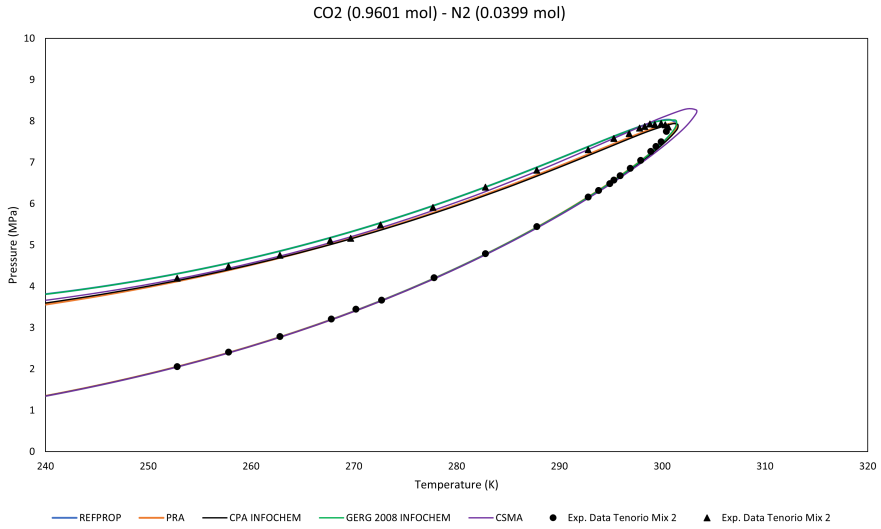

Figure A.23.: VLE experimental data from Tenorio et al. [14] vs models. (IV)

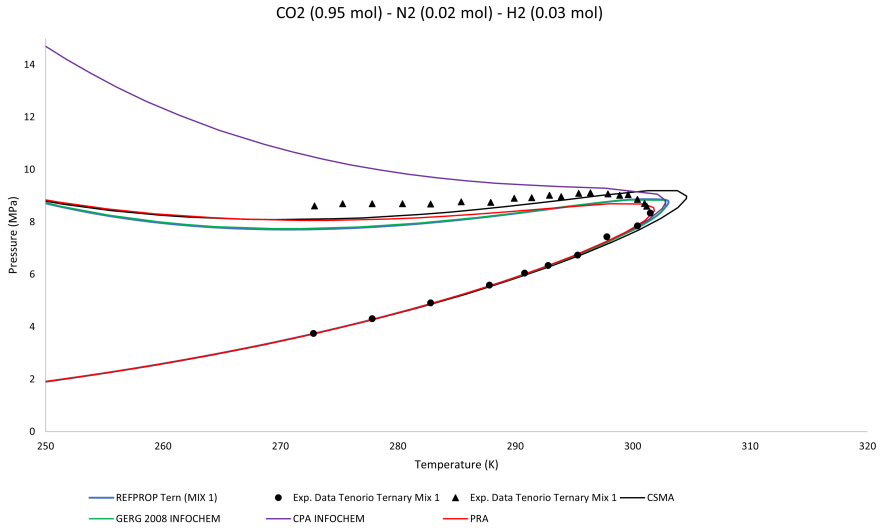

Figure A.24.: VLE experimental data from Tenorio et al. [14] vs models. (V)

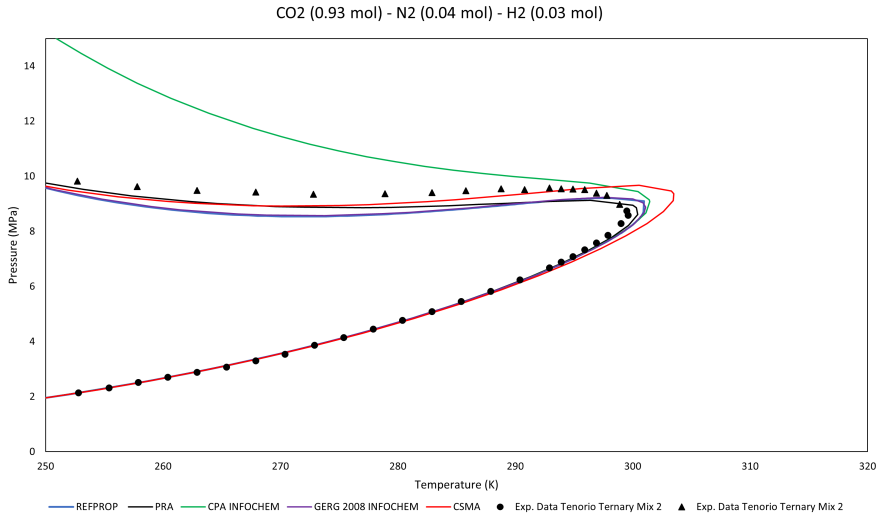

Figure A.25.: VLE experimental data from Tenorio et al. [14] vs models. (VI)

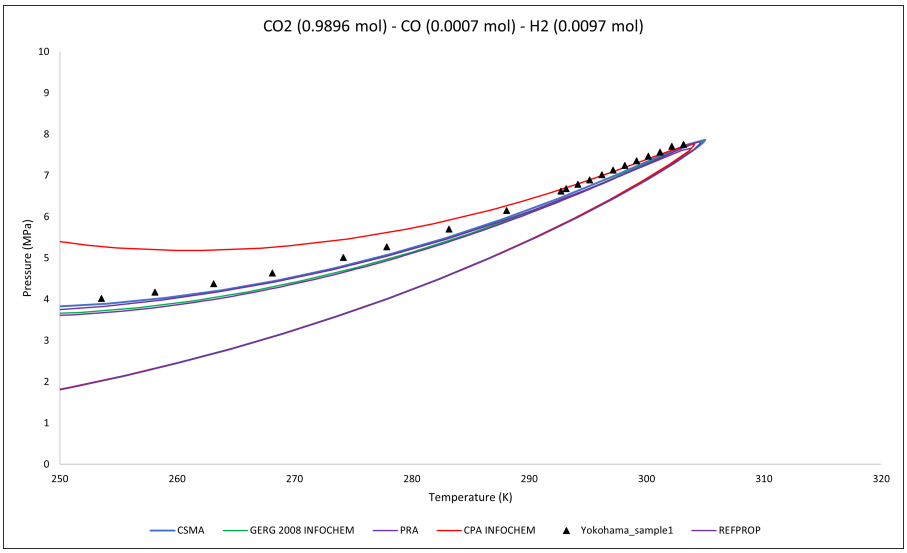

Figure A.26.: VLE experimental data from Yokohama et al. [13] vs models. (I)

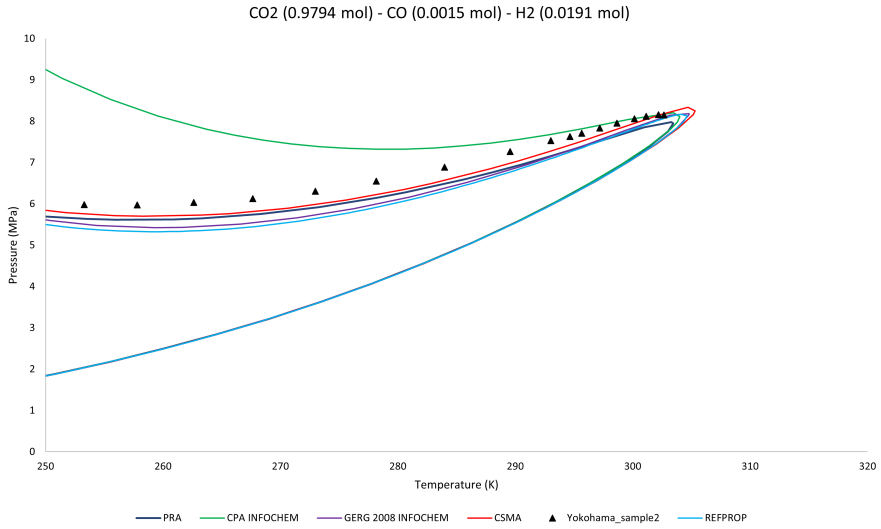

Figure A.27.: VLE experimental data from Yokohama et al. [13] vs models. (II)

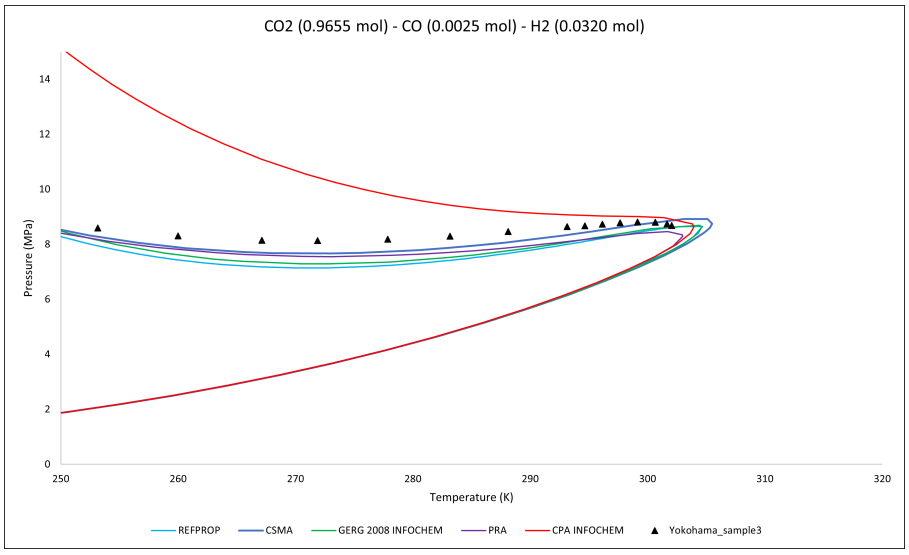

Figure A.28.: VLE experimental data from Yokohama et al. [13] vs models. (III)

Appendix B.

Density data points utilized for validation

In this appendix all the results plots obtained from the density analysis conducted as reported in Chapter 4.

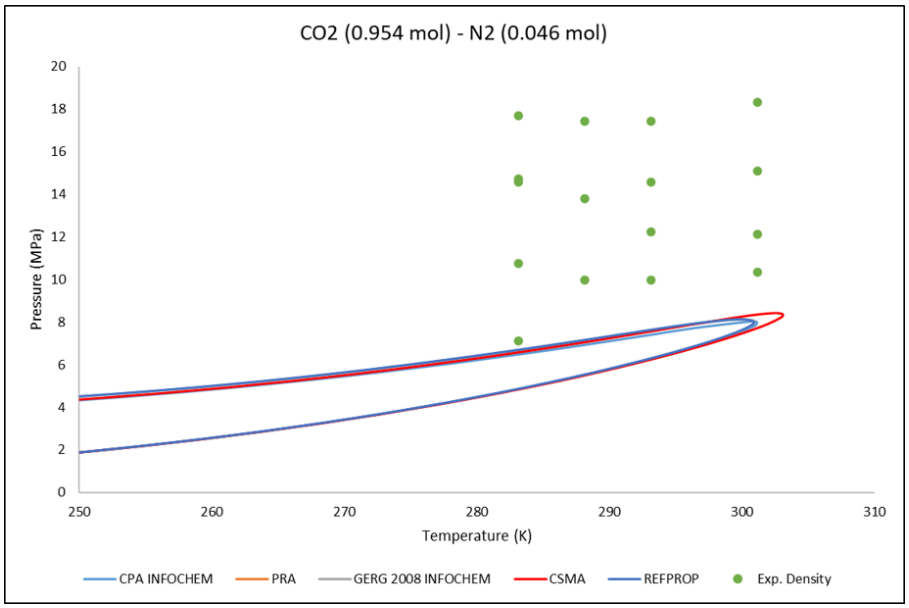

Figure B.1.: Density experimental data from Al-Siyabi [4] vs models. (I)

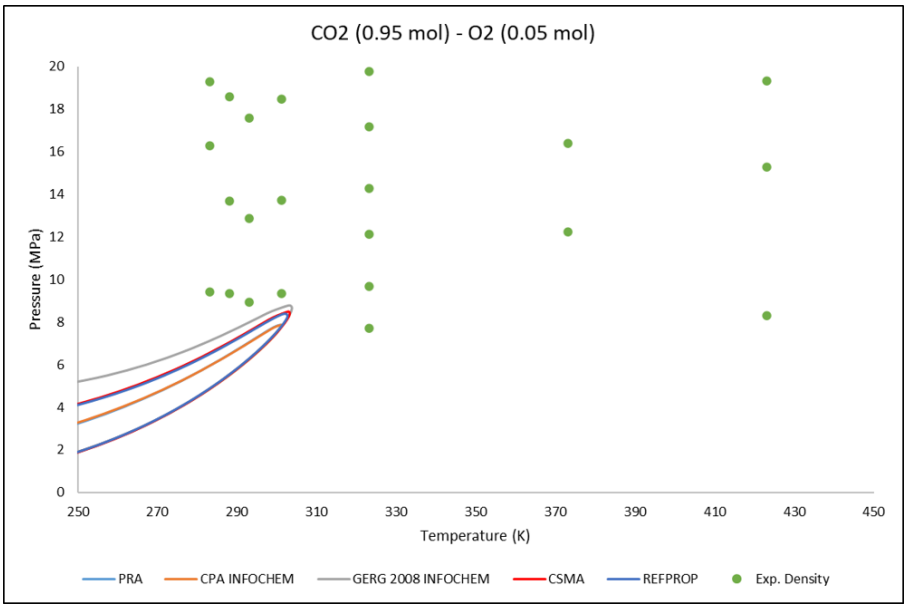

Figure B.2.: Density experimental data from Al-Siyabi [4] vs models. (II)

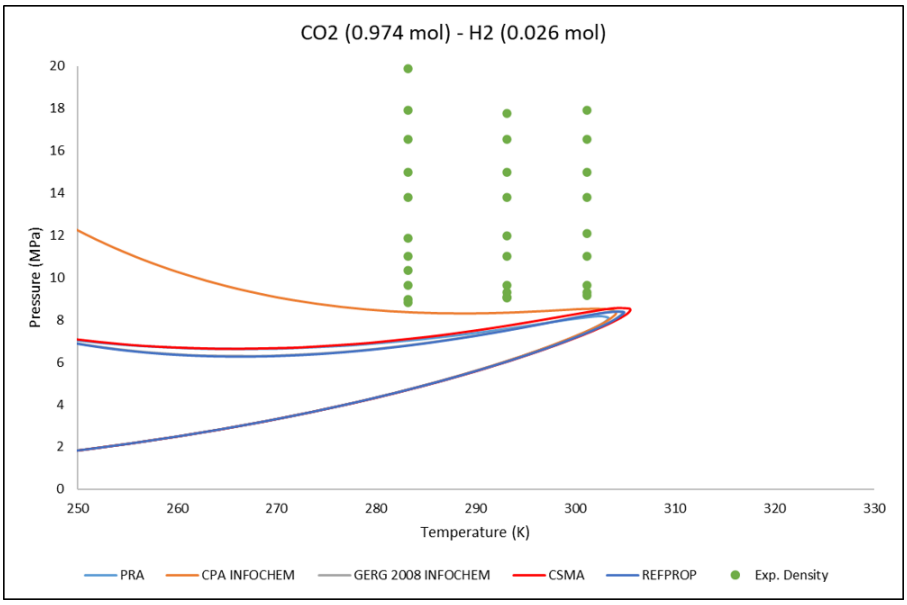

Figure B.3.: Density experimental data from Al-Siyabi [4] vs models. (III)

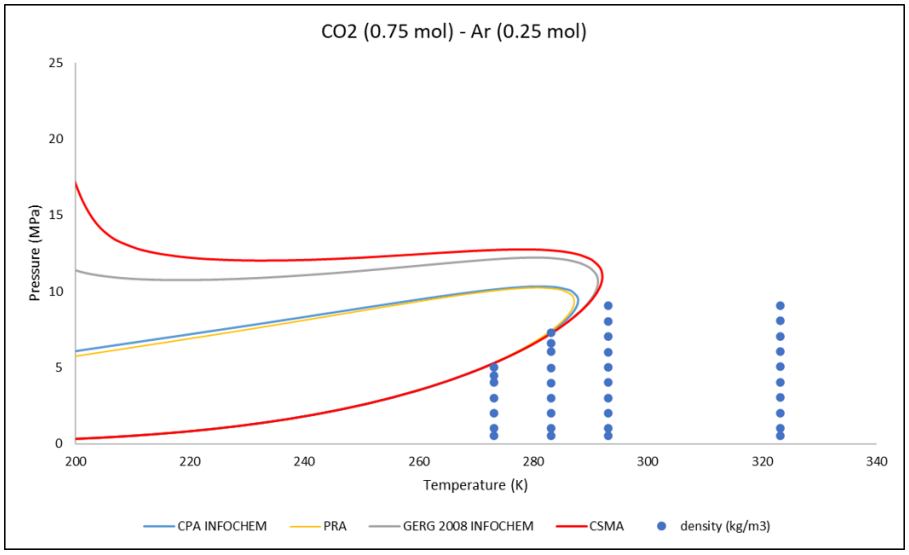

Figure B.4.: Density experimental data from Ben Souissi et al. [25] vs models. (I)

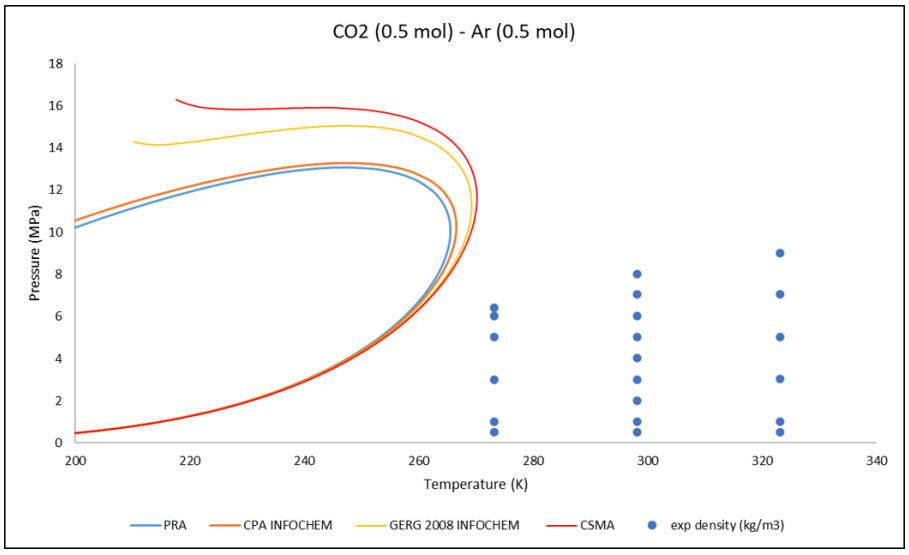

Figure B.5.: Density experimental data from Ben Souissi et al. [25] vs models. (II)

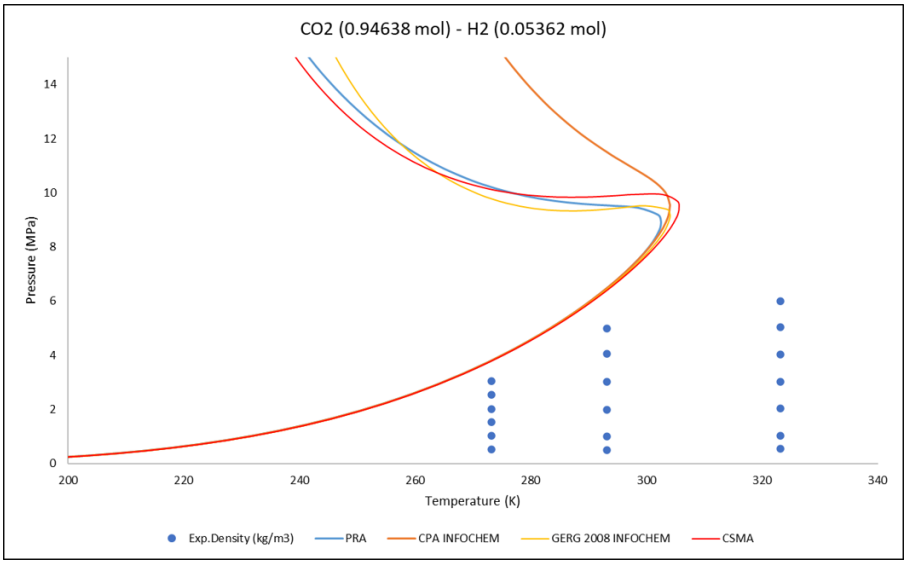

Figure B.6.: Density experimental data from Ben Souissi et al. [26] vs models. (III)

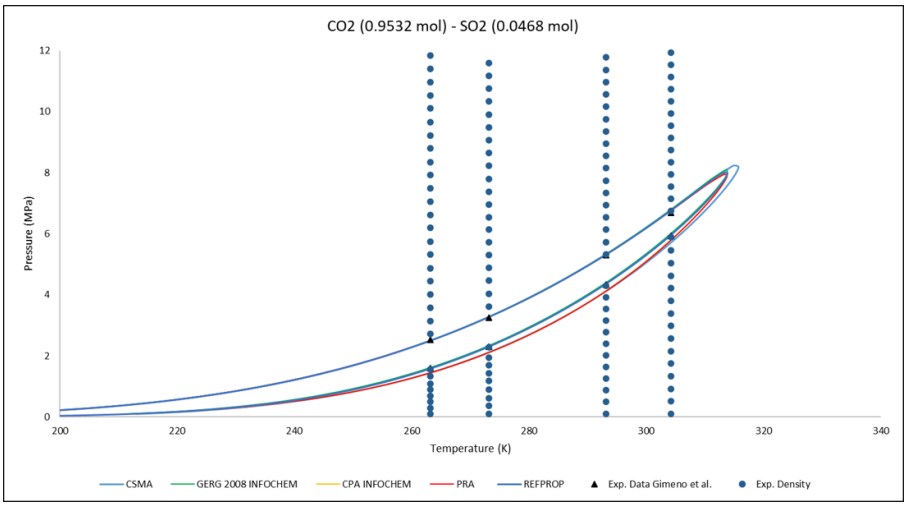

Figure B.7.: Density experimental data from Gimeno et al. [16] vs models. (I)

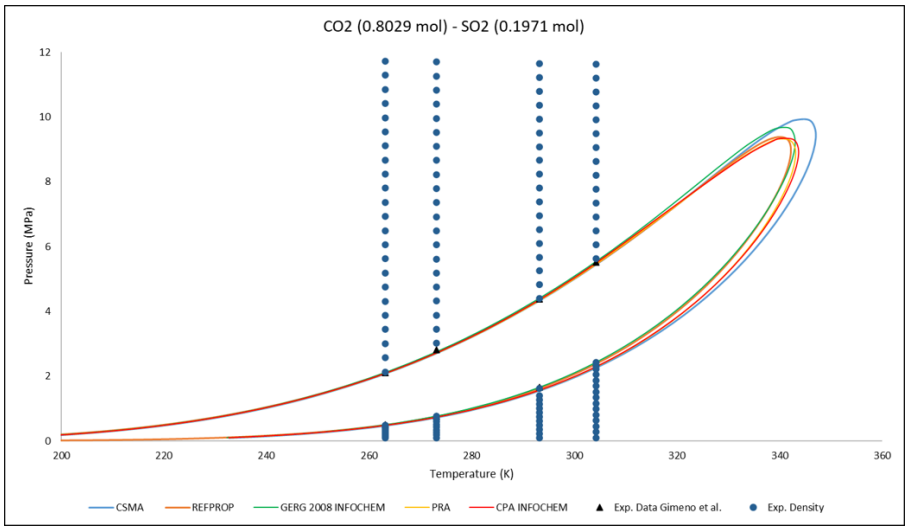

Figure B.8.: Density experimental data from Gimeno et al. [16] vs models. (II)

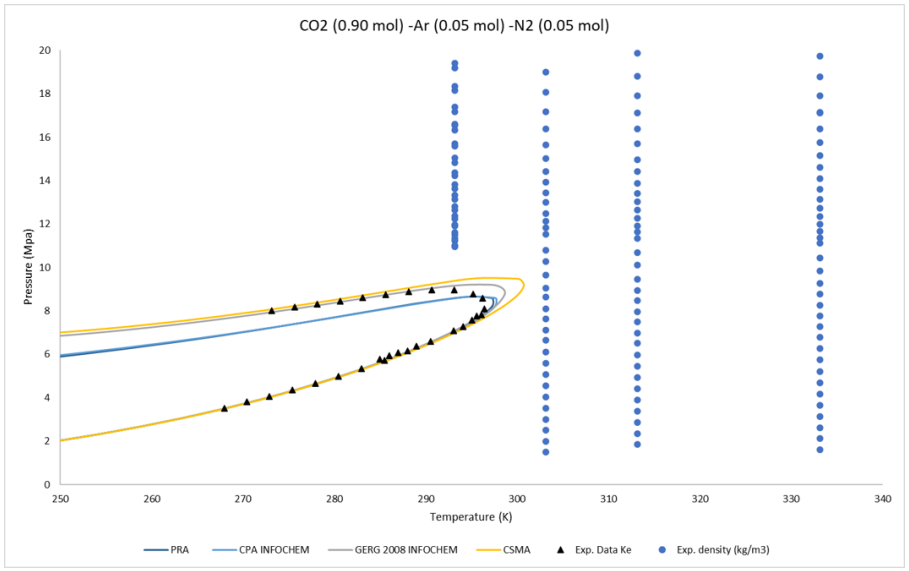

Figure B.9.: Density experimental data from Ke et al. [24] vs models. (I)

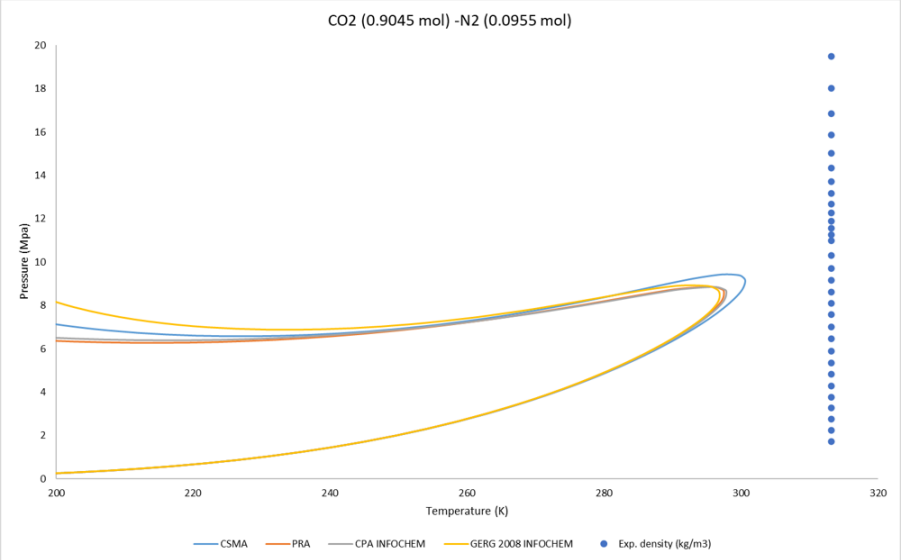

Figure B.10.: Density experimental data from Ke et al. [24] vs models. (II)

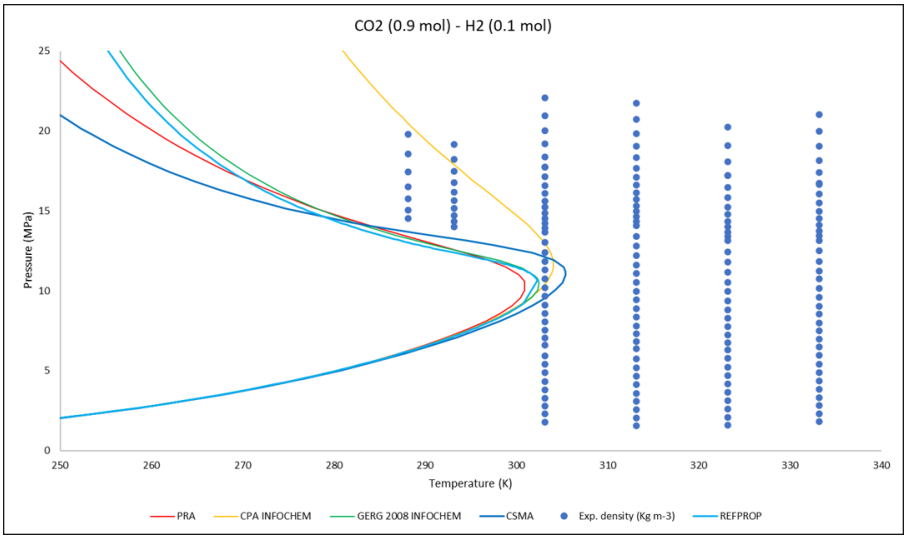

Figure B.11.: Density experimental data from Sanchez-Vicente et al. [17] vs models. (I)

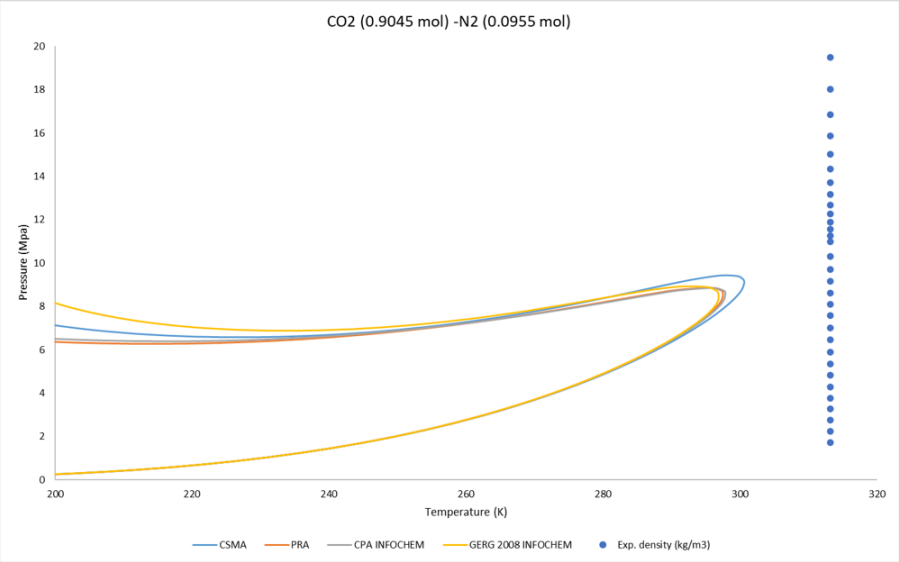

Figure B.12.: Density experimental data from Sanchez-Vicente et al. [17] vs models. (II)

Appendix C.

DeFACTO auto-reporter

SINTEF

DeFACTO datalog Report

CO2 pressure in the well

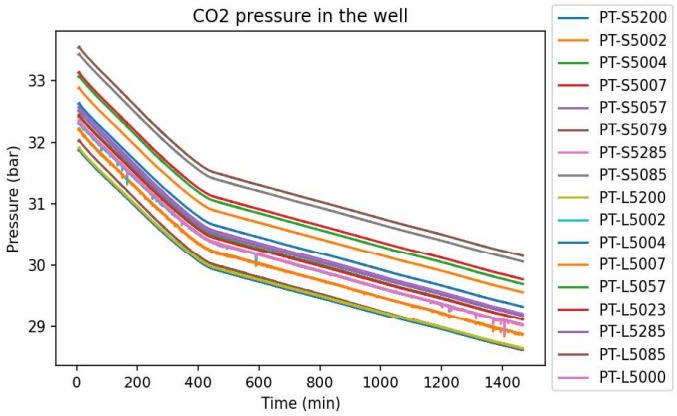

Sensor	Mean (bar)	Std. dev	Slope (bar/min)	Intercept (bar)	R^2
PT-S5200	29.739	0.8432	-0.0019	31.148592	0.9131
PT-S5002	30.0249	0.8644	-0.002	31.467436	0.9148
PT-S5004	30.2762	0.8653	-0.002	31.721486	0.9164
PT-S5007	30.2554	0.8587	-0.0019	31.686687	0.9126
PT-S5057	30.3698	0.8739	-0.002	31.826363	0.9125
PT-S5079	29.8081	0.8807	-0.002	31.277276	0.914
PT-S5285	30.3288	0.8624	-0.002	31.773964	0.9127
PT-S5085	31.2159	0.8769	-0.002	32.67727	0.9123
PT-L5085	31.3173	0.8813	-0.002	32.785957	0.9122
PT-L5285	30.3221	0.8637	-0.002	31.767413	0.9126
PT-L5057	30.8551	0.8762	-0.002	32.31548	0.9125
PT-L5023	30.9233	0.8706	-0.002	32.374207	0.9122
PT-L5007	30.7017	0.8606	-0.0019	32.136266	0.9127
PT-L5004	30.464	0.8574	-0.0019	31.893623	0.9133
PT-L5002	30.1686	0.8565	-0.0019	31.599048	0.9162
PT-L5200	29.7664	0.8443	-0.0019	31.178526	0.9132
PT-L5000	30.176	0.8664	-0.002	31.622523	0.9157

Page 9/10

Figure C.1.: Example of the auto-generated report for DeFACTO facility.

Bibliography

[1] Our World in Data, "Kaya Identity Prospects."

[2] Mauna Loa Observatory/NOAA, "Mauna Loa Observatory - CO2 Tracker," 2022.

[3] Global CCS Institute, "Brief for Policymakers: CCS - Targeting Climate Change," 2020.

[4] I. Al-Siyabi, "Effect of impurities on CO₂ stream properties," *PhD Thesis. Heriot-Watt University*, no. February, pp. 1–182, 2013.

[5] A. Chapoy, R. Burgass, B. Tohidi, and I. Alsiyabi, "Hydrate and phase behavior modeling in CO2-rich pipelines," *Journal of Chemical & Engineering Data*, vol. 60, no. 2, pp. 447–453, 2015.

[6] C. Sun, J. Sun, S. Liu, and Y. Wang, "Effect of water content on the corrosion behavior of X65 pipeline steel in supercritical CO2-H2O-O2-H2S-SO2 environment as relevant to CCS application," *Corrosion Science*, vol. 137, pp. 151–162, 2018.

[7] ISO, "ISO. (2009). ISO GUIDE 73: 2009" Risk Management-Vocabulary"."," tech. rep., 2009.

[8] DNV-GL, "DNV-GL CO2RISKMAN - Guidance Level 4," no. January, 2013.

[9] M. Vitali, C. Zuliani, F. Corvaro, B. Marchetti, A. Terenzi, and F. Tallone, "Risks and Safety of CO2 Transport via Pipeline: A Review of Risk Analysis and Modeling Approaches for Accidental Releases," *Energies*, vol. 14, no. 15, p. 4601, 2021.

[10] M. Ahmad, B. Lowesmith, G. De Koeijer, S. Nilsen, H. Tonda, C. Spinelli, R. Cooper, S. Clausen, R. Mendes, and O. Florisson, "COSHER joint industry project: Large scale pipeline rupture tests to study CO2 release and dispersion," *International Journal of Greenhouse Gas Control*, vol. 37, pp. 340–353, 6 2015.

[11] X. Liu, A. Godbole, C. Lu, G. Michal, and V. Linton, "Investigation of the consequence of high-pressure CO2 pipeline failure through experimental and numerical studies," *Applied Energy*, vol. 250, no. May, pp. 32–47, 2019.

[12] S. F. Westman, H. G. Stang, S. W. Løvseth, A. Austegard, I. Snustad, S. T. Størset, and I. S. Ertesvåg, "Vapor-liquid equilibrium data for the carbon dioxide and nitrogen (CO2 + N2) system at the temperatures 223, 270, 298 and 303 K and pressures up to 18 MPa," *Fluid Phase Equilibria*, vol. 409, pp. 207–241, 2016.

[13] C. Yokoyama, K. Arai, S. Saito, and H. Mori, "Bubble-point pressures of the H2COCO2 system," *Fluid Phase Equilibria*, vol. 39, no. 1, pp. 101–110, 1988.

[14] M.-J. Tenorio, A. J. Parrott, J. A. Calladine, Y. Sanchez-Vicente, A. J. Cresswell, R. S. Graham, T. C. Drage, M. Poliakoff, J. Ke, and M. W. George, "Measurement of the vapour–liquid equilibrium of binary and ternary mixtures of CO2, N2 and H2, systems which are of relevance to CCS technology," *International Journal of Greenhouse Gas Control*, vol. 41, pp. 68–81, 2015.

[15] A. Chapoy, M. Nazeri, M. Kapateh, R. Burgass, C. Coquelet, and B. Tohidi, "Effect of impurities on thermophysical properties and phase behaviour of a CO2-rich system in CCS," *International Journal of Greenhouse Gas Control*, vol. 19, pp. 92–100, 2013.

[16] B. Gimeno, M. Artal, I. Velasco, J. Fernández, and S. T. Blanco, "Influence of SO2 on CO2 Transport by Pipeline for Carbon Capture and Storage Technology: Evaluation of CO2/SO2 Cocapture," *Energy and Fuels*, vol. 32, no. 8, pp. 8641–8657, 2018.

[17] Y. Sanchez-Vicente, T. C. Drage, M. Poliakoff, J. Ke, and M. W. George, "Densities of the carbon dioxide+hydrogen, a system of relevance to carbon capture and storage," *International Journal of Greenhouse Gas Control*, vol. 13, pp. 78–86, 2013.

[18] M. Darzi and C. Park, "Experimental Visualization and Numerical Simulation of Liquid-Gas Two-Phase Flows in a Horizontal Pipe," 11 2017.

[19] S. T. Munkejord, A. Austegard, H. Deng, M. Hammer, H. G. J. Stang, and S. W. Løvseth, "Depressurization of CO2 in a pipe: High-resolution pressure and temperature data and comparison with model predictions," *Energy*, vol. 211, p. 118560, 2020.

[20] R. Cooper and J. Barnett, "Fracture Propagation in Dense Phase CO 2 Pipelines from an Operator's Perspective," tech. rep., 2016.

[21] V. E. Onyebuchi, A. Kolios, D. P. Hanak, C. Biliyok, and V. Manovic, "A systematic review of key challenges of CO2 transport via pipelines," *Renewable and Sustainable Energy Reviews*, vol. 81, no. October, pp. 2563–2583, 2018.

[22] B. Liu, X. Liu, C. Lu, A. Godbole, G. Michal, and A. K. Tieu, "A CFD decompression model for CO2 mixture and the influence of non-equilibrium phase transition," *Applied Energy*, vol. 227, no. October 2017, pp. 516–524, 2018.

[23] M. Ahmad, J. Gernert, and E. Wilbers, "Effect of impurities in captured CO2 on liquid-vapor equilibrium," *Fluid Phase Equilibria*, vol. 363, pp. 149–155, 2014.

[24] J. Ke, N. Suleiman, Y. Sanchez-Vicente, T. S. Murphy, J. Rodriguez, A. Ramos, M. Poliakoff, and M. W. George, "The phase equilibrium and density studies of the ternary mixtures of CO2 + Ar + N2 and CO2 + Ar + H2, systems relevance to CCS technology," *International Journal of Greenhouse Gas Control*, vol. 56, pp. 55–66, 2017.

[25] M. A. Ben Souissi, M. Richter, X. Yang, R. Kleinrahm, and R. Span, "Vapor-phase (p, ρ, T, x) behavior and virial coefficients for the (argon + carbon dioxide) system," *Journal of Chemical and Engineering Data*, vol. 62, no. 1, pp. 362–369, 2017.

[26] M. A. Ben Souissi, R. Kleinrahm, X. Yang, and M. Richter, "Vapor-Phase (p, ρ, T, x) Behavior and Virial Coefficients for the Binary Mixture (0.05 Hydrogen + 0.95 Carbon Dioxide) over the Temperature Range from (273.15 to 323.15) K with Pressures up to 6 MPa," *Journal of Chemical and Engineering Data*, vol. 62, no. 9, pp. 2973–2981, 2017.

[27] H. Li, "Thermodynamic properties of CO2 mixtures and their applications in advanced power cycles with CO2 capture processes," 2008.

[28] E. De Visser, C. Hendriks, M. Barrio, M. J. Mølnvik, G. de Koeijer, S. Liljemark, and Y. Le Gallo, "Dynamis CO2 quality recommendations," *International journal of greenhouse gas control*, vol. 2, no. 4, pp. 478–484, 2008.

[29] E. Adu, Y. Zhang, and D. Liu, "Current situation of carbon dioxide capture, storage, and enhanced oil recovery in the oil and gas industry," *Canadian Journal of Chemical Engineering*, vol. 97, no. 5, pp. 1048–1076, 2019.

[30] Timothy Fout and Steve Herron, "Quality guidelines for Energy System Guidelines, CO2 Impurity design parameters," *NETL Quality guidelines for energy system studies*, no. August, 2013.

[31] P. Shirley and P. Myles, "Quality Guidelines for Energy System Studies: CO2 Impurity Design Parameters," tech. rep., 2019.

[32] A. Dugstad, M. Halseid, and B. Morland, "Testing of CO2 specifications with respect to corrosion and bulk phase reactions," *Energy Procedia*, vol. 63, pp. 2547–2556, 2014.

[33] A. Oosterkamp and J. Ramsen, "Report number Date Security level State-of-the-Art Overview of CO 2 Pipeline Transport with relevance to offshore pipelines," tech. rep., 2008.

[34] R. Martínez, I. Suárez, M. A. Zapatero, B. Saftic, I. Kolenkovic, M. Car, S. Persoglia, and F. Donda, "The EU GeoCapacity project—saline aquifers storage capacity in group south countries," *Energy Procedia*, vol. 1, no. 1, pp. 2733–2740, 2009.

[35] T. Harkin, I. Filby, H. Sick, D. Manderson, and R. Ashton, "Development of a CO2 Specification for a CCS Hub Network," *Energy Procedia*, vol. 114, pp. 6708–6720, 2017.

[36] DNV-GL, "CO2RISKMAN - Guidance on CCS CO2 Safety and Environment Major Accident Hazard Risk Management - Level 3," tech. rep., 2013.

[37] National Center for Biotechnology Information, "PubChem Compound Summary for CID 49792852," 2004.

[38] J. N. Knudsen, O. M. Bade, I. Askestad, O. Gorset, and T. Mejdell, "Pilot plant demonstration of CO2 capture from cement plant with advanced amine technology," *Energy Procedia*, vol. 63, no. October 2015, pp. 6464–6475, 2014.

[39] Y. Kaya, "Impact of carbon dioxide emission control on GNP growth: interpretation of proposed scenarios," *Intergovernmental Panel on Climate Change/Response Strategies Working Group, May*, 1989.

[40] P. R. Ehrlich and J. P. Holdren, "Impact of Population Growth: Complacency concerning this component of man's predicament is unjustified and counterproductive.," *Science*, vol. 171, no. 3977, pp. 1212–1217, 1971.

[41] P. H. M. Feron, "1 - Introduction," pp. 3–12, Woodhead Publishing, 2016.

[42] EPA, "Greenhouse Gas Emissions - United States Environmental Protection Agency (EPA)."

[43] S. Solomon, M. Manning, M. Marquis, and D. Qin, *Climate change 2007-the physical science basis: Working group I contribution to the fourth assessment report of the IPCC*, vol. 4. Cambridge university press, 2007.

[44] International Energy Agency, "Putting CO2 to Use," *Energy Report*, no. September, p. 86, 2019.

[45] S. R. Gíslason, H. Sigurdardóttir, E. S. Aradóttir, and E. H. Oelkers, "A brief history of CarbFix: Challenges and victories of the project's pilot phase," *Energy Procedia*, vol. 146, pp. 103–114, 2018.

[46] A. P. Simpson and A. E. Lutz, "Exergy analysis of hydrogen production via steam methane reforming," *International journal of hydrogen energy*, vol. 32, no. 18, pp. 4811–4820, 2007.

[47] L. Barelli, G. Bidini, F. Gallorini, and S. Servili, "Hydrogen production through sorption-enhanced steam methane reforming and membrane technology: a review," *Energy*, vol. 33, no. 4, pp. 554–570, 2008.

[48] IEA, "Energy Technology Perspectives 2020 - Special Report on Carbon Capture Utilisation and Storage," *Energy Technology Perspectives 2020 - Special Report on Carbon Capture Utilisation and Storage*, 2020.

[49] C. F. Heuberger, I. Staffell, N. Shah, and N. Mac Dowell, "Quantifying the value of CCS for the future electricity system," *Energy & Environmental Science*, vol. 9, no. 8, pp. 2497–2510, 2016.

[50] E. Cox, E. Spence, and N. Pidgeon, "Public perceptions of carbon dioxide removal in the United States and the United Kingdom," *Nature Climate Change*, vol. 10, no. 8, pp. 744–749, 2020.

[51] P. Viebahn and E. J. Chappin, *Scrutinising the gap between the expected and actual deployment of carbon capture and storage - A bibliometric analysis*, vol. 11. 2018.

[52] R. Allam, S. Martin, B. Forrest, J. Fetvedt, X. Lu, D. Freed, G. W. Brown, T. Sasaki, M. Itoh, and J. Manning, "Demonstration of the Allam Cycle: An Update on the Development Status of a High Efficiency Supercritical Carbon Dioxide Power Process Employing Full Carbon Capture," *Energy Procedia*, vol. 114, no. November 2016, pp. 5948–5966, 2017.

[53] European Commission, "EU Emission Trading System," 2022.

[54] "CCS Norway - The Longship Project."

[55] A. Witkowski, A. Rusin, M. Majkut, S. Rulik, and K. Stolecka, "Comprehensive analysis of pipeline transportation systems for CO 2 sequestration. Thermodynamics and safety problems," *Energy Conversion and Management*, vol. 76, pp. 665–673, 2013.

[56] F. Neele, J. Koornneef, J. P. Jakobsen, A. Brunsvold, and C. Eickhoff, "Toolbox of Effects of CO2 Impurities on CO2 Transport and Storage Systems," in *Energy Procedia*, vol. 114, pp. 6536–6542, Elsevier Ltd, 2017.

[57] A. K. Furre, O. Eiken, H. Alnes, J. N. Vevatne, and A. F. Kiær, "20 Years of Monitoring CO2-injection at Sleipner," *Energy Procedia*, vol. 114, no. November 2016, pp. 3916–3926, 2017.

[58] I. Duncan and H. Wang, "Evaluating the likelihood of pipeline failures for future offshore CO2 sequestration projects," *International Journal of Greenhouse Gas Control*, vol. 24, pp. 124–138, 2014.

[59] "PHMSA incident database."

[60] M. Vitali, F. Corvaro, B. Marchetti, and A. Terenzi, "Thermodynamic challenges for CO2 pipelines design: A critical review on the effects of impurities, water content, and low temperature," *International Journal of Greenhouse Gas Control*, vol. 114, p. 103605, 2022.

[61] B. Wetenhall, H. Aghajani, H. Chalmers, S. D. Benson, M. C. Ferrari, J. Li, J. M. Race, P. Singh, and J. Davison, "Impact of CO2 impurity on CO2 compression, liquefaction and transportation," in *Energy Procedia*, vol. 63, pp. 2764–2778, Elsevier Ltd, 2014.

[62] H. Li, Wilhelmsen, Y. Lv, W. Wang, and J. Yan, "Viscosities, thermal conductivities and diffusion coefficients of CO2 mixtures: Review of experimental data and theoretical models," 9 2011.

[63] M. Anheden, A. Andersson, C. Bernstone, S. Eriksson, J. Yan, S. Liljemark, and C. Wall, "CO2 quality requirement for a system with CO2 capture, transport and storage," in *Greenhouse Gas Control Technologies 7*, pp. 2559–2564, Elsevier, 2005.

[64] M. Nazeri, A. Chapoy, R. Burgass, and B. Tohidi, "Measured densities and derived thermodynamic properties of CO2-rich mixtures in gas, liquid and supercritical phases from 273 K to 423 K and pressures up to 126 MPa," *Journal of Chemical Thermodynamics*, vol. 111, pp. 157–172, 2017.

[65] M. Nazeri, A. Chapoy, R. Burgass, and B. Tohidi, "Viscosity of CO2-rich mixtures from 243K to 423K at pressures up to 155MPa: New experimental viscosity data and modelling," *Journal of Chemical Thermodynamics*, vol. 118, pp. 100–114, 3 2018.

[66] M. Ahmad and S. Gersen, "Water solubility in CO2 mixtures: Experimental and modelling investigation," in *Energy Procedia*, vol. 63, pp. 2402–2411, Elsevier Ltd, 2014.

[67] S. Lasala, P. Chiesa, R. Privat, and J.-N. Jaubert, "VLE properties of CO2–Based binary systems containing N2, O2 and Ar: Experimental measurements and modelling results with advanced cubic equations of state," *Fluid Phase Equilibria*, vol. 428, pp. 18–31, 2016.

[68] S. W. Løvseth, A. Austegard, S. F. Westman, H. G. J. Stang, S. Herrig, T. Neumann, and R. Span, "Thermodynamics of the carbon dioxide plus argon

(CO2+ Ar) system: An improved reference mixture model and measurements of vapor-liquid, vapor-solid, liquid-solid and vapor-liquid-solid phase equilibrium data at the temperatures 213–299 K and pressures up ," *Fluid Phase Equilibria*, vol. 466, pp. 48–78, 2018.

[69] C. Coquelet, A. Valtz, and P. Arpentinier, "Thermodynamic study of binary and ternary systems containing CO2+ impurities in the context of CO2 transportation," *Fluid Phase Equilibria*, vol. 382, pp. 205–211, 2014.

[70] S. Camy, J.-J. Letourneau, and J.-S. Condoret, "Experimental study of high pressure phase equilibrium of (CO2+ NO2/N2O4) mixtures," *The Journal of Chemical Thermodynamics*, vol. 43, no. 12, pp. 1954–1960, 2011.

[71] S. P. Peletiri, I. M. Mujtaba, and N. Rahmanian, "Process simulation of impurity impacts on CO2 fluids flowing in pipelines," *Journal of Cleaner Production*, vol. 240, p. 118145, 2019.

[72] Y. Tan, W. Nookuea, H. Li, E. Thorin, L. Zhao, and J. Yan, "Property impacts on performance of CO2 pipeline transport," *Energy Procedia*, vol. 75, pp. 2261–2267, 2015.

[73] S. P. Peletiri, N. Rahmanian, and I. M. Mujtaba, "CO2 Pipeline design: A review," *Energies*, vol. 11, no. 9, 2018.

[74] M. D. Jensen, S. M. Schlasner, J. A. Sorensen, and J. A. Hamling, "Operational flexibility of CO2 transport and storage," in *Energy Procedia*, vol. 63, pp. 2715–2722, Elsevier Ltd, 2014.

[75] J. M. Race, B. Wetenhall, P. N. Seevam, and M. J. Downie, "Towards a CO 2 pipeline specification: defining tolerance limits for impurities.," *Journal of Pipeline Engineering*, vol. 11, no. 3, 2012.

[76] Craig. R. & Butler D., "Oil Sands CO2 Pipeline Network Study (2017)," tech. rep., Canada's Oil Sands Innovation Alliance., 2017.

[77] J. Brown, "On behalf of the CO2PIPETRANS Steering Committee and DNV GL, Best regards," tech. rep., 2014.

[78] DNV GL, "DNVGL-RP-F104 Design and operation of carbon dioxide pipelines," no. November, p. 76, 2017.

[79] S. Brown, J. Beck, H. Mahgerefteh, and E. S. Fraga, "Global sensitivity analysis of the impact of impurities on CO2 pipeline failure," *Reliability Engineering & System Safety*, vol. 115, pp. 43–54, 2013.

[80] K. S. Pedersen, P. L. Christensen, and J. A. Shaikh, *Phase behavior of petroleum reservoir fluids*. CRC press, 2014.

[81] G. P. Guidetti, G. L. Rigosi, and R. Marzola, "The use of polypropylene in pipeline coatings," *Progress in Organic Coatings*, vol. 27, no. 1-4, pp. 79–85, 1996.

[82] I. S. Cole, P. Corrigan, S. Sim, and N. Birbilis, "Corrosion of pipelines used for CO 2 transport in CCS: Is it a real problem?," 7 2011.

[83] M. F. Morks, P. Corrigan, N. Birbilis, and I. S. Cole, "A green MnMgZn phosphate coating for steel pipelines transporting CO2 rich fluids," *Surface and Coatings Technology*, vol. 210, pp. 183–189, 2012.

[84] M. F. Morks, N. F. Fahim, and I. S. Cole, "Environmental phosphate coating for corrosion prevention in CO2 pipelines," *Materials Letters*, vol. 94, pp. 95–99, 2013.

[85] A. Dugstad, M. Halseid, and B. Morland, "Effect of SO2 and NO2 on corrosion and solid formation in dense phase CO2 pipelines," *Energy Procedia*, vol. 37, pp. 2877–2887, 2013.

[86] A. Dugstad, B. Morland, and S. Clausen, "Corrosion of transport pipelines for CO2 - Effect of water ingress," in *Energy Procedia*, vol. 4, pp. 3063–3070, Elsevier Ltd, 2011.

[87] F. W. Schremp and G. R. Roberson, "Effect of supercritical carbon dioxide (CO2) on construction materials," *Society of Petroleum Engineers Journal*, vol. 15, no. 03, pp. 227–233, 1975.

[88] L. Buit, M. Ahmad, W. Mallon, and F. Hage, "CO2 EuroPipe study of the occurrence of free water in dense phase CO2 transport," *Energy Procedia*, vol. 4, pp. 3056–3062, 2011.

[89] ISO, "ISO 27914 : 2017 Standards Publication Carbon dioxide capture , transportation and geological storage," 2017.

[90] H. Salari, H. Hassanzadeh, S. Gerami, and J. Abedi, "On Estimating the Water Content of CO2 in Equilibrium With Formation Brine," *Petroleum Science and Technology*, vol. 29, pp. 2037–2051, 7 2011.

[91] J. J. Carroll, "The water content of acid gas and sour gas from 100 to 220 F and pressures to 10,000 Psia," in *81st Annual GPA Convention*, Dallas Texas, USA, 2002.

[92] Y. Xiang, Z. Wang, X. Yang, Z. Li, and W. Ni, "The upper limit of moisture content for supercritical CO2 pipeline transport," *The Journal of Supercritical Fluids*, vol. 67, pp. 14–21, 2012.

[93] F. E. Uilhoorn, "Evaluating the risk of hydrate formation in CO2 pipelines under transient operation," *International Journal of Greenhouse Gas Control*, vol. 14, pp. 177–182, 2013.

[94] S. Foltran, M. E. Vosper, N. B. Suleiman, A. Wriglesworth, J. Ke, T. C. Drage, M. Poliakoff, and M. W. George, "Understanding the solubility of water in carbon capture and storage mixtures: An FTIR spectroscopic study of H2O+ CO2+ N2 ternary mixtures," *International Journal of Greenhouse Gas Control*, vol. 35, pp. 131–137, 2015.

[95] Y. S. Choi and S. Nešić, "Determining the corrosive potential of CO2 transport pipeline in high pCO2-water environments," *International Journal of Greenhouse Gas Control*, vol. 5, pp. 788–797, 7 2011.

[96] Y.-S. Choi, S. Nesic, and D. Young, "Effect of impurities on the corrosion behavior of CO2 transmission pipeline steel in supercritical CO2 water environments," *Environmental science & technology*, vol. 44, no. 23, pp. 9233–9238, 2010.

[97] J. Sun, C. Sun, G. Zhang, X. Li, W. Zhao, T. Jiang, H. Liu, X. Cheng, and Y. Wang, "Effect of O2 and H2S impurities on the corrosion behavior of X65 steel in water-saturated supercritical CO2 system," *Corrosion Science*, vol. 107, pp. 31–40, 2016.

[98] W. He, O. Knudsen, and S. Diplas, "Corrosion of stainless steel 316L in simulated formation water environment with CO2-H2S-Cl-," *Corrosion Science*, vol. 51, no. 12, pp. 2811–2819, 2009.

[99] M. Halseid, A. Dugstad, and B. Morland, "Corrosion and bulk phase reactions in CO2 transport pipelines with impurities: review of recent published studies," *Energy Procedia*, vol. 63, pp. 2557–2569, 2014.

[100] S. Sim, I. S. Cole, Y. S. Choi, and N. Birbilis, "A review of the protection strategies against internal corrosion for the safe transport of supercritical CO2 via steel pipelines for CCS purposes," *International Journal of Greenhouse Gas Control*, vol. 29, pp. 185–199, 2014.

[101] Y. Hua, R. Barker, and A. Neville, "Effect of temperature on the critical water content for general and localised corrosion of X65 carbon steel in the transport of supercritical CO2," *International Journal of Greenhouse Gas Control*, vol. 31, pp. 48–60, 12 2014.

[102] Y. Hua, R. Barker, and A. Neville, "The influence of SO2 on the tolerable water content to avoid pipeline corrosion during the transportation of supercritical CO2," *International Journal of Greenhouse Gas Control*, vol. 37, pp. 412–423, 2015.

[103] R. Barker, Y. Hua, and A. Neville, "Internal corrosion of carbon steel pipelines for dense-phase CO2 transport in carbon capture and storage (CCS) – a review," *International Materials Reviews*, vol. 62, pp. 1–31, 1 2017.

[104] Shell U.K. Limited, "Peterhead CCS Project, Basic Design and Engineering Package.," tech. rep., 2016.

[105] VATTENFALL Europe Carbon Storage GmbH & Co., "CO2 Transport Pipeline (FEED Study).," tech. rep., 2011.

[106] White Rose CCS Project, "K26: Transport – Process Description, Technical Transport.," tech. rep., 2016.

[107] A. Terenzi, E. Bonato, and L. Maggiore, "Analysis of Depressurization of Onshore Pipeline Containing Flashing Liquid," in *PSIG Annual Meeting*, Pipeline Simulation Interest Group, 2016.

[108] D. Dall'Acqua, A. Terenzi, M. Leporini, V. D'Alessandro, G. Giacchetta, and B. Marchetti, "A new tool for modelling the decompression behaviour of CO 2 with impurities using the Peng-Robinson equation of state," *Applied Energy*, vol. 206, no. September, pp. 1432–1445, 2017.

[109] S. T. Munkejord and M. Hammer, "Depressurization of CO<inf>2</inf>-rich mixtures in pipes: Two-phase flow modelling and comparison with experiments," *International Journal of Greenhouse Gas Control*, vol. 37, pp. 398–411, 2015.

[110] S. T. Munkejord, M. Hammer, and S. W. Løvseth, "CO2 transport: Data and models - A review," 5 2016.

[111] X. Guo, S. Chen, X. Yan, X. Zhang, J. Yu, Y. Zhang, H. Mahgerefteh, S. Martynov, A. Collard, and S. Brown, "Flow characteristics and dispersion during the leakage of high pressure CO2 from an industrial scale pipeline," *International Journal of Greenhouse Gas Control*, vol. 73, no. 2, pp. 70–78, 2018.

[112] K. Li, X. Zhou, R. Tu, Q. Xie, J. Yi, and X. Jiang, "A study of small-scale CO2accidental release in near-field from a pressurized pipeline," in *Energy Procedia*, vol. 142, pp. 3234–3239, Elsevier Ltd, 2017.

[113] X. Guo, X. Yan, J. Yu, Y. Zhang, S. Chen, H. Mahgerefteh, S. Martynov, A. Collard, and C. Proust, "Under-expanded jets and dispersion in supercritical CO2 releases from a large-scale pipeline," *Applied Energy*, vol. 183, no. 2, pp. 1279–1291, 2016.

[114] Q. Cao, X. Yan, S. Liu, J. Yu, S. Chen, and Y. Zhang, "Temperature and phase evolution and density distribution in cross section and sound evolution during the release of dense CO2 from a large-scale pipeline," *International Journal of Greenhouse Gas Control*, vol. 96, p. 103011, 2020.

[115] S. Martynov, W. Zheng, H. Mahgerefteh, S. Brown, J. Hebrard, D. Jamois, and C. Proust, "Computational and Experimental Study of Solid-Phase Formation during the Decompression of High-Pressure CO2 Pipelines," *Industrial and Engineering Chemistry Research*, vol. 57, pp. 7054–7063, 5 2018.

[116] W. Zheng, H. Mahgerefteh, S. Martynov, and S. Brown, "Modeling of CO2 Decompression across the Triple Point," *Industrial and Engineering Chemistry Research*, vol. 56, pp. 10491–10499, 9 2017.

[117] J. D. Wells, A. A. A. Majid, J. L. Creek, E. D. Sloan, S. E. Borglin, T. J. Kneafsey, and C. A. Koh, "Water content of carbon dioxide at hydrate forming conditions," *Fuel*, vol. 279, p. 118430, 2020.

[118] R. Burgass, A. Chapoy, P. Duchet-Suchaux, and B. Tohidi, "Experimental water content measurements of carbon dioxide in equilibrium with hydrates at (223.15 to 263.15) K and (1.0 to 10.0) MPa," *The Journal of Chemical Thermodynamics*, vol. 69, pp. 1–5, 2014.

[119] Q. Xie, R. Tu, X. Jiang, K. Li, and X. Zhou, "The leakage behavior of supercritical CO2 flow in an experimental pipeline system," *Applied energy*, vol. 130, pp. 574–580, 2014.

[120] C. Vianello, P. Mocellin, and G. Maschioa, "Study of formation, sublimation and deposition of dry ice from carbon capture and storage pipelines," *CHEMICAL ENGINEERING*, vol. 36, 2014.

[121] P. Mocellin, C. Vianello, and G. Maschio, "Carbon capture and storage hazard investigation: numerical analysis of hazards related to dry ice bank sublimation following accidental carbon dioxide releases," *Chemical Engineering Transactions*, vol. 43, 2015.

[122] White Rose CCS Project, "K34: Flow Assurance, Technical Transport.," tech. rep., 2015.

[123] DNV-GL, "DNV-GL CO2RISKMAN - Guidance Level 1," no. January, 2013.

[124] "AIGA 068/10 – Carbon Dioxide - GLOBALLY HARMONISED DOCUMENT, Based on CGA G-6 (7th edition, 2009).," tech. rep., 2009.

[125] G. Kennedy, "WA Parish Post-Combustion CO2 Capture and Sequestration Demonstration Project Final Technical Report," tech. rep., 2020.

[126] J. A. Feliu, M. Manzulli, and M. A. Alós, "Determination of Dry-Ice Formation during the Depressurization of a CO," *Cutting-Edge Technology for Carbon Capture, Utilization, and Storage*, p. 135.

[127] D. Y. Leung, G. Caramanna, and M. M. Maroto-Valer, "An overview of current status of carbon dioxide capture and storage technologies," *Renewable and Sustainable Energy Reviews*, vol. 39, pp. 426–443, 2014.

[128] J. Gale and J. Davison, "Transmission of CO2-safety and economic considerations," *Energy*, vol. 29, no. 9-10, pp. 1319–1328, 2004.

[129] A. Aspelund, M. J. Mølnvik, and G. De Koeijer, "Ship transport of CO2: Technical solutions and analysis of costs, energy utilization, exergy efficiency and CO2 emissions," *Chemical Engineering Research and Design*, vol. 84, no. 9, pp. 847–855, 2006.

[130] H. Kruse and M. Tekiela, "Calculating the consequences of a CO2-pipeline rupture," *Energy Conversion and Management*, vol. 37, no. 6-8, pp. 1013–1018, 1996.

[131] Z. X. Zhang, G. X. Wang, P. Massarotto, and V. Rudolph, "Optimization of pipeline transport for CO2 sequestration," *Energy Conversion and Management*, vol. 47, no. 6, pp. 702–715, 2006.

[132] A. Lemontzoglou, G. Pantoleontos, A. G. Asimakopoulou, N. I. Tsongidis, and A. G. Konstandopoulos, "Analysis of CO2 transport including impurities for the optimization of point-to-point pipeline networks for integration into future solar fuel plants," *International Journal of Greenhouse Gas Control*, vol. 66, pp. 10–24, 11 2017.

[133] G. W. Kling, M. A. Clark, G. N. Wagner, H. R. Compton, A. M. Humphrey, J. D. Devine, W. C. Evans, J. P. Lockwood, M. L. Tuttle, and E. J. Koenigsberg, "The 1986 lake nyos gas disaster in cameroon, west Africa," *Science*, vol. 236, no. 4798, pp. 169–175, 1987.

[134] P. J. Baxter, M. Kapila, and D. Mfonfu, "Lake Nyos disaster, Cameroon, 1986: the medical effects of large scale emission of carbon dioxide?," *British Medical Journal*, vol. 298, no. 6685, pp. 1437–1441, 1989.

[135] R. Cooper and J. Barnett, "Pipelines for transporting CO2 in the UK," in *Energy Procedia*, vol. 63, pp. 2412–2431, Elsevier Ltd, 2014.

[136] P. Cleaver and K. Warhurst, "Routeing of Dense Phase CO2 Pipelines in the UK," 2012.

[137] C. Vianello, S. Macchietto, and G. Maschio, "Risk Assessment of CO 2 Pipeline Network for CCS-A UK Case Study," 2013.

[138] A. Mazzoldi, T. Hill, and J. J. Colls, "Assessing the risk for CO2 transportation within CCS projects, CFD modelling," *International Journal of Greenhouse Gas Control*, vol. 5, no. 4, pp. 816–825, 2011.

[139] A. McGillivray, J. L. Saw, D. Lisbona, M. Wardman, and M. Bilio, "A risk assessment methodology for high pressure CO2 pipelines using integral consequence modelling," *Process Safety and Environmental Protection*, vol. 92, no. 1, pp. 17–26, 2014.

[140] N. Paltrinieri, L. Breedveld, J. Wilday, and V. Cozzani, "Identification of hazards and environmental impact assessment for an integrated approach to emerging risks of CO2 capture installations," in *Energy Procedia*, vol. 37, pp. 2811–2818, Elsevier Ltd, 2013.

[141] N. Paltrinieri, J. Wilday, M. Wardman, and V. Cozzani, "Surface installations intended for Carbon Capture and Sequestration: Atypical accident scenarios and their identification," *Process Safety and Environmental Protection*, vol. 92, pp. 93–107, 1 2014.

[142] DNV-GL, "DNV-GL CO2RISKMAN - Guidance Level 2," no. January, 2013.

[143] DNV-GL, "DNV-GL CO2RISKMAN - Guidance Level 3," no. January, 2013.

[144] J. Wilday, J. L. Saw, M. Wardman, and M. Bilio, "The CO2PipeHaz Good Practice Guidelines for CO 2 pipeline safety," tech. rep.

[145] C. Vianello, S. MacChietto, and G. Maschio, "Conceptual models for co2 release and risk assessment: A review," *Chemical Engineering Transactions*, vol. 26, pp. 573–578, 2012.

[146] R. M. Woolley, M. Fairweather, C. J. Wareing, S. A. Falle, H. Mahgerefteh, S. Martynov, S. Brown, V. D. Narasimhamurthy, I. E. Storvik, L. Sælen, T. Skjold, I. G. Economou, D. M. Tsangaris, G. C. Boulougouris, N. Diamantonis, L. Cusco, M. Wardman, S. E. Gant, J. Wilday, Y. C. Zhang, S. Chen, C. Proust, J. Hebrard, and D. Jamois, "CO2PipeHaz: Quantitative hazard assessment for next generation CO2 pipelines," *Energy Procedia*, vol. 63, pp. 2510–2529, 2014.

[147] J. Koornneef, M. Spruijt, M. Molag, A. Ramirez, A. Faaij, and W. Turkenburg, "Uncertainties in risk assessment of CO2 pipelines," *Energy Procedia*, vol. 1, no. 1, pp. 1587–1594, 2009.

[148] International Energy Agency, "Special Report on Clean Energy Innovation: Accelerating technology progress for a sustainable future," *Energy Technology Perspectives 2020*, pp. 61–89, 2020.

[149] Energy Institute, "Technical guidance on hazard analysis for onshore carbon capture installations and onshore pipelines," *Energy Institute*, no. 1st, p. 125, 2010.

[150] Dijkshoorn; Kaman, "QRA CO2 transport," Tech. Rep. november, 2011.

[151] DSB, "Lloyd's Register: "Retningslinjer for kvantitative risikovurderinger for anlegg som håndterer farlig stoff. (Title translated: Guidelines for quantitative risk assessment for installations handling hazardous substances).," tech. rep., DSB, 2017.

[152] C. Lam and W. Zhou, "Statistical analyses of incidents on onshore gas transmission pipelines based on PHMSA database," *International Journal of Pressure Vessels and Piping*, vol. 145, pp. 29–40, 2016.

[153] H. Wang and I. J. Duncan, "Likelihood, causes, and consequences of focused leakage and rupture of US natural gas transmission pipelines," *Journal of loss prevention in the process industries*, vol. 30, pp. 177–187, 2014.

[154] M. Pursell, "Esperimental investigation of high-pressure liquid CO2 release behaviour," tech. rep., 2012.

[155] X. Guo, X. Yan, Y. Zheng, J. Yu, Y. Zhang, S. Chen, L. Chen, H. Mahgerefteh, S. Martynov, A. Collard, and S. Brown, "Under-expanded jets and dispersion in high pressure CO2releases from an industrial scale pipeline," *Energy*, vol. 119, pp. 53–66, 2017.

[156] X. Fan, Y. Wang, Y. Zhou, J. Chen, Y. Huang, and J. Wang, "Experimental study of supercritical CO2 leakage behavior from pressurized vessels," *Energy*, vol. 150, pp. 342–350, 5 2018.

[157] L. Teng, Y. Li, D. Zhang, X. Ye, S. Gu, C. Wang, and J. Wang, "Evolution and Size Distribution of Solid CO2 Particles in Supercritical CO2 Releases," *Industrial and Engineering Chemistry Research*, vol. 57, pp. 7655–7663, 6 2018.

[158] A. Godbole, X. Liu, G. Michal, B. Davis, C. Lu, K. Armstrong, and C. H. Medina, "Atmospheric Dispersion of CO2 following full-scale burst tests," tech. rep., 2018.

[159] C. M. Dixon, S. E. Gant, C. Obiorah, and M. Bilio, "Validation of Dispersion Models for High Pressure Carbon Dioxide Releases," tech. rep.

[160] L. Phillips, "Shell FRED Technical Guide. Updated for FRED 5.1.," tech. rep., 2007.

[161] HGSYSTEM, "Technical Reference Manual. Cap. 7. THE HEAVY GAS DISPERSION MODEL HEGADAS.," tech. rep.

[162] S. E. Gant, A. Kelsey, K. McNally, H. W. M. Witlox, and M. Bilio, "Methodology for global sensitivity analysis of consequence models," *Journal of Loss Prevention in the Process Industries*, vol. 26, no. 4, pp. 792–802, 2013.

[163] W. Seattle and D. C. Washington, "NATIONAL OCEANIC AND ATMOSPHERIC ADMINISTRATION Office of Response and Restoration Emergency Response Division The CAMEO ® Software System ALOHA ® USER'S MANUAL," no. February, 2007.

[164] T. Scpicer and J. Havens, "User's Guide For The DEGADIS 2.1," 1989.

[165] T. K. v. L. T. Defensie, "Methods for the calculation of physical effects: Due to releases of hazardous materials (liquids and gases)(" Yellow Book"),," 2005.

[166] TNO, "TNO Safety software EFFECTS," 2016.

[167] A. Mazzoldi, T. Hill, and J. J. Colls, "CFD and Gaussian atmospheric dispersion models: A comparison for leak from carbon dioxide transportation and storage facilities," *Atmospheric environment*, vol. 42, no. 34, pp. 8046–8054, 2008.

[168] S. R. Hanna and J. C. Chang, "Use of the Kit Fox field data to analyze dense gas dispersion modeling issues," *Atmospheric Environment*, vol. 35, no. 13, pp. 2231–2242, 2001.

[169] S. E. Gant, V. D. Narasimhamurthy, T. Skjold, D. Jamois, and C. Proust, "Evaluation of multi-phase atmospheric dispersion models for application to Carbon Capture and Storage," *Journal of Loss Prevention in the Process Industries*, vol. 32, pp. 286–298, 11 2014.

[170] H. W. Witlox, M. Harper, A. Oke, and J. Stene, "Phast validation of discharge and atmospheric dispersion for pressurised carbon dioxide releases," *Journal of Loss Prevention in the Process Industries*, vol. 30, no. 1, pp. 243–255, 2014.

[171] M. M. Knoope, I. M. Raben, A. Ramírez, M. P. Spruijt, and A. P. Faaij, "The influence of risk mitigation measures on the risks, costs and routing of CO2 pipelines," *International Journal of Greenhouse Gas Control*, vol. 29, pp. 104–124, 2014.

[172] J. Fiates, R. R. C. Santos, F. F. Neto, A. Z. Francesconi, V. Simoes, and S. S. Vianna, "An alternative CFD tool for gas dispersion modelling of heavy gas," *Journal of Loss Prevention in the Process Industries*, vol. 44, pp. 583–593, 2016.

[173] H. Witlox, "Data review-Shell C02 experiments 1 CO 2 discharge and dispersion Data review & Phast analysis for Shell experiments CO2PIPETRANS, Phase 2 (WP1)," tech. rep., 2012.

[174] J. Wen, A. Heidari, B. Xu, and H. Jie, "Dispersion of carbon dioxide from vertical vent and horizontal releases—A numerical study," *Proceedings of the Institution of Mechanical Engineers, Part E: Journal of Process Mechanical Engineering*, vol. 227, no. 2, pp. 125–139, 2013.

[175] A. Mack and M. P. Spruijt, "CFD dispersion investigation of CO2 worst case scenarios including terrain and release effects," in *Energy Procedia*, vol. 51, pp. 363–372, Elsevier Ltd, 2014.

[176] B. Liu, X. Liu, C. Lu, A. Godbole, G. Michal, and A. K. Tieu, "Computational fluid dynamics simulation of carbon dioxide dispersion in a complex environment," *Journal of Loss Prevention in the Process Industries*, vol. 40, pp. 419–432, 2016.

[177] X. Liu, A. Godbole, C. Lu, and G. Michal, "Investigation of terrain effects on the consequence distance of CO2 released from high-pressure pipelines," *International Journal of Greenhouse Gas Control*, vol. 66, pp. 264–275, 2017.

[178] A. Mazzoldi, D. Picard, P. G. Sriram, and C. M. Oldenburg, "Simulation-based estimates of safety distances for pipeline transportation of carbon dioxide," *Greenhouse Gases: Science and Technology*, vol. 3, no. 1, pp. 66–83, 2013.

[179] X. Liu, A. Godbole, C. Lu, G. Michal, and P. Venton, "Source strength and dispersion of CO2 releases from high-pressure pipelines: CFD model using real gas equation of state," *Applied Energy*, vol. 126, pp. 56–68, 2014.

[180] R. M. Woolley, M. Fairweather, C. J. Wareing, C. Proust, J. Hebrard, D. Jamois, V. D. Narasimhamurthy, I. E. Storvik, T. Skjold, S. Falle, S. Brown, H. Mahgerefteh, S. Martynov, S. E. Gant, D. M. Tsangaris, I. G. Economou, G. C. Boulougouris, and N. I. Diamantonis, "An integrated, multi-scale modelling approach for the simulation of multiphase dispersion from accidental CO2 pipeline releases in realistic terrain," *International Journal of Greenhouse Gas Control*, vol. 27, pp. 221–238, 2014.

[181] R. Span and W. Wagner, "A new equation of state for carbon dioxide covering the fluid region from the triple-point temperature to 1100 K at pressures up to 800 MPa," *Journal of physical and chemical reference data*, vol. 25, no. 6, pp. 1509–1596, 1996.

[182] A. Jager and R. Span, "Equation of state for solid carbon dioxide based on the Gibbs free energy," *Journal of Chemical & Engineering Data*, vol. 57, no. 2, pp. 590–597, 2012.

[183] A. G. Perez, C. Coquelet, P. Paricaud, and A. Chapoy, "Comparative study of vapour-liquid equilibrium and density modelling of mixtures related to carbon capture and storage with the SRK, PR, PC-SAFT and SAFT-VR Mie equations of state for industrial uses," *Fluid Phase Equilibria*, vol. 440, pp. 19–35, 2017.

[184] J. F. Ely, W. M. Haynes, and B. C. Bain, "Isochoric (p, Vm, T) measurements on CO2 and on (0.982CO2 + 0.018N2) from 250 to 330 K at pressures to 35

MPa," *The Journal of Chemical Thermodynamics*, vol. 21, no. 8, pp. 879–894, 1989.

[185] B. D. Abadio and P. J. McElroy, "(Pressure, amount-of-substance density, temperature) of {(1-x)CO2+xH2} using a direct method," 1993.

[186] Y. Arai, G. i. Kaminishi, and S. Saito, "The experimental determination of the p-v-t-x relations for the carbon dioxide-nitrogen and the carbon dioxide-methane systems," *JOURNAL of CHEMICAL ENGINEERING of JAPAN*, vol. 4, no. 2, pp. 113–122, 1971.

[187] M. L. Huber, "NIST Thermophysical properties of hydrocarbon mixtures database (SUPERTRAPP), version 3.2," 2007.

[188] Y.-X. Zuo and E. H. Stenby, "A linear gradient theory model for calculating interfacial tensions of mixtures," *Journal of Colloid and Interface Science*, vol. 182, no. 1, pp. 126–132, 1996.

[189] D.-Y. Peng and D. B. Robinson, "A new two-constant equation of state," *Industrial & Engineering Chemistry Fundamentals*, vol. 15, no. 1, pp. 59–64, 1976.

[190] R. Stryjek and J. H. Vera, "PRSV: An improved Peng—Robinson equation of state for pure compounds and mixtures," *The canadian journal of chemical engineering*, vol. 64, no. 2, pp. 323–333, 1986.

[191] A. Péneloux, E. Rauzy, and R. Fréze, "A consistent correction for Redlich-Kwong-Soave volumes," *Fluid phase equilibria*, vol. 8, no. 1, pp. 7–23, 1982.

[192] Infochem/KBC Advanced Technologies ltd, "Multiflash 6.1 - User Guide," Tech. Rep. 0, Infochem/KBC Advanced Technologies ltd 42-50 Hersham Road Walton on Thames Surrey KT12 1RZ UK, 2015.

[193] G. M. Kontogeorgis, M. L. Michelsen, G. K. Folas, S. Derawi, N. Von Solms, and E. H. Stenby, "Ten Years with the CPA (Cubic-Plus-Association) equation of state. Part 1. Pure compounds and self-associating systems," *Industrial and Engineering Chemistry Research*, vol. 45, no. 14, pp. 4855–4868, 2006.

[194] L. C. Dos Santos, S. S. Abunahman, F. W. Tavares, V. R. Ruiz Ahón, and G. M. Kontogeorgis, "Cubic Plus Association Equation of State for Flow Assurance Projects," *Industrial and Engineering Chemistry Research*, vol. 54, no. 26, pp. 6812–6824, 2015.

[195] G. M. Kontogeorgis, E. C. Voutsas, I. V. Yakoumis, and D. P. Tassios, "An equation of state for associating fluids," *Industrial and Engineering Chemistry Research*, vol. 35, no. 11, pp. 4310–4318, 1996.

[196] E. W. Lemmon, I. H. Bell, M. L. Huber, and M. O. McLinden, "NIST Standard Reference Database 23: Reference Fluid Thermodynamic and Transport Properties-REFPROP, Version 10.0, National Institute of Standards and Technology," *Standard Reference Data Program, Gaithersburg*, 2018.

[197] M. L. Huber, "Models for viscosity, thermal conductivity, and surface tension of selected pure fluids as implemented in REFPROP v10. 0," 2018.

[198] M. Jaeschke, A. Benito, A. Fredheim, J.-M. Henault, B. Viglietti, P. v. Wesenbeeck, H. J. Pannemann, R. Klimeck, O. Kunz, and W. Wagner, "GERG Project: Wide-range reference equation of state for natural gases," *GAS UND WASSERFACH GAS ERDGAS*, vol. 144, no. 7/8, p. 430, 2003.

[199] O. Kunz, R. Klimeck, W. Wagner, and M. Jaeschke, "The GERG-2004 wide-range equation of state for natural gases and other mixtures," 2007.

[200] O. Kunz and W. Wagner, "The GERG-2008 wide-range equation of state for natural gases and other mixtures: an expansion of GERG-2004," *Journal of chemical & engineering data*, vol. 57, no. 11, pp. 3032–3091, 2012.

[201] L. Sun and J. F. Ely, "A corresponding states model for generalized engineering equations of state," *International Journal of Thermophysics*, vol. 26, no. 3, pp. 705–728, 2005.

[202] K. H. Bendiksen, D. Malnes, R. Moe, I. Brandt, P. Fuchs, and H. Linga, "Two-phase flow research at SINTEF and IFE: some experimental results and a demonstration of the dynamic two-phase flow simulator OLGA," 1986.

[203] K. H. Bendiksen, D. Maines, R. Moe, and S. Nuland, "The dynamic two-fluid model OLGA: Theory and application," *SPE production engineering*, vol. 6, no. 02, pp. 171–180, 1991.

[204] H. Darvishi, D. Ciuonzo, E. R. Eide, and P. S. Rossi, "Sensor-fault detection, isolation and accommodation for digital twins via modular data-driven architecture," *IEEE Sensors Journal*, vol. 21, no. 4, pp. 4827–4838, 2020.

[205] S. B. Martynov, R. H. Talemi, S. Brown, and H. Mahgerefteh, "Assessment of Fracture Propagation in Pipelines Transporting Impure CO2 Streams," *Energy Procedia*, vol. 114, no. November 2016, pp. 6685–6697, 2017.

[206] R. H. Talemi, S. Brownb, S. Martynov, and H. Mahgereftehb, "Assessment of brittle fractures in CO 2 transportation pipelines: A hybrid fluid-structure interaction model," *Procedia Structural Integrity*, vol. 2, pp. 2439–2446, 2016.

[207] E. Aursand, S. Dumoulin, M. Hammer, H. I. Lange, A. Morin, S. T. Munkejord, and H. O. Nordhagen, "Fracture propagation control in CO2 pipelines:

Validation of a coupled fluid-structure model," *Engineering Structures*, vol. 123, pp. 192–212, 2016.

[208] H. O. Nordhagen, S. T. Munkejord, M. Hammer, G. Gruben, M. Fourmeau, and S. Dumoulin, "A fracture-propagation-control model for pipelines transporting CO2-rich mixtures including a new method for material-model calibration," *Engineering Structures*, vol. 143, pp. 245–260, 2017.

[209] R. Eiber, T. Bubenik, and W. Maxey, *Fracture control technology for natural gas pipelines*. 1993.

[210] D. G. Jones and D. W. Gough, "Rich gas decompression behaviour in pipelines," in *AGA-EPRG Linepipe Research Seminar IV, BRITISH GAS, Duisburg*, 1981.

[211] W. Qiu, J. Gong, and J. Zhao, "A study on natural gas decompression behavior," *Petroleum Science and Technology*, vol. 29, no. 1, pp. 29–38, 2011.

[212] D. V. Nichita, P. Khalid, and D. Broseta, "Calculation of isentropic compressibility and sound velocity in two-phase fluids," *Fluid Phase Equilibria*, vol. 291, no. 1, pp. 95–102, 2010.

[213] D. J. Picard and P. R. Bishnoi, "The importance of real-fluid behavior and nonisentropic effects in modeling decompression characteristics of pipeline fluids for application in ductile fracture propagation analysis," *The Canadian Journal of Chemical Engineering*, vol. 66, no. 1, pp. 3–12, 1988.

[214] T. Flåtten and H. Lund, "Relaxation two-phase flow models and the subcharacteristic condition," *Mathematical Models and Methods in Applied Sciences*, vol. 21, no. 12, pp. 2379–2407, 2011.

[215] H. Lund, "A hierarchy of relaxation models for two-phase flow," *SIAM Journal on Applied Mathematics*, vol. 72, no. 6, pp. 1713–1741, 2012.

[216] M. Castier, "Thermodynamic speed of sound in multiphase systems," *Fluid phase equilibria*, vol. 306, no. 2, pp. 204–211, 2011.

[217] A. Cosham and R. J. Eiber, "Fracture propagation of CO2 pipelines," *Energy*, no. 049, pp. 115–124, 2003.

[218] K. K. Botros, J. Geerligs, J. Zhou, and A. Glover, "Measurements of flow parameters and decompression wave speed following rupture of rich gas pipelines, and comparison with GASDECOM," *International Journal of Pressure Vessels and Piping*, vol. 84, no. 6, pp. 358–367, 2007.

[219] K. K. Botros, J. Geerligs, B. Rothwell, and T. Robinson, "Measurements of Decompression Wave Speed in Binary Mixtures of Carbon Dioxide and Impurities," *Journal of Pressure Vessel Technology, Transactions of the ASME*, vol. 139, no. 2, pp. 1–11, 2017.

[220] K. K. Botros, J. Geerligs, L. Carlson, and M. Reed, "Experimental validation of GASDECOM for High Heating Value Processed Gas mixtures (58 MJ/m3) by specialized shock tube," *International Journal of Pressure Vessels and Piping*, vol. 107, pp. 20–26, 2013.

[221] A. Cosham, D. G. Jones, K. Armstrong, D. Allason, and J. Barnett, "The decompression behaviour of carbon dioxide in the dense phase," in *International Pipeline Conference*, vol. 45141, pp. 447–464, American Society of Mechanical Engineers, 2012.